ASSESSMENT OF A PROTOTYPE ENERGY-DISSIPATING ORTHOSIS FOR THE MEASUREMENT AND MANAGEMENT OF UPPER EXTREMITY INTENTION TREMOR

by

Allison Suzanne Arnold

S.B. in Mechanical Engineering
Massachusetts Institute of Technology, 1990

SUBMITTED TO THE DEPARTMENT OF
MECHANICAL ENGINEERING IN PARTIAL FULFILLMENT OF
THE REQUIREMENTS FOR THE DEGREE OF

MASTER OF SCIENCE

at the

MASSACHUSETTS INSTITUTE OF TECHNOLOGY

June 1992

Signature of Author _____
Department of Mechanical Engineering
May 29, 1992

Certified by _____
Michael J. Rosen
Thesis Supervisor

Accepted by _____
Ain A. Sonin
Chairman, Department Committee on Graduate Studies

ASSESSMENT OF A PROTOTYPE ENERGY-DISSIPATING ORTHOSIS FOR THE MEASUREMENT AND MANAGEMENT OF UPPER EXTREMITY INTENTION TREMOR

by

Allison Suzanne Arnold

Submitted to the Department of Mechanical Engineering on May 29, 1992
in partial fulfillment of the requirements for the degree of
Master of Science in Mechanical Engineering

Abstract

The purpose of this study was to assess the effectiveness of the MIT CEDO 1, a Controlled Energy-Dissipating Orthosis developed at the MIT Newman Laboratory for Biomechanics and Human Rehabilitation, both as a prototype orthosis for assisting tremor-disabled individuals and as a research tool for quantifying tremor characteristics. Conventional neurological practice is generally unsuccessful in restoring independent upper extremity function to persons with debilitating pathological tremors. The CEDO 1 was built to determine whether an *alternative* approach to tremor management, namely the application of velocity-dependent resistive loads to tremorous limbs, is a feasible means of attenuating intention tremor without degrading purposeful movement. The CEDO 1 mounts to a wheelchair or table, permits the three degrees of freedom needed for "table-top" activities, and generates its resistive loads by means of computer-controlled magnetic particle brakes whose torques are transmitted to the user's forearm via a stiff low-inertia linkage.

In this investigation, six tremor-disabled and six able-bodied subjects were given computer-mediated pursuit tracking tasks in one or two degrees of freedom to verify that damping loads applied by the CEDO 1 do suppress upper-extremity intention tremor without degrading purposeful movement. Experiments were also done to determine the range of damping loads needed in a tremor-suppressing orthosis, whether non-linear (velocity-squared) loads offer advantages over linear (viscous) loads, whether the inertia of the orthosis affects users' tremors, and to what extent other experimental factors must be considered when measuring tremor characteristics or evaluating tremor-suppressing orthoses. Subjectively, all disabled subjects offered positive remarks on the effect of damping. Objectively, data from five of the six disabled subjects, processed using spectral analysis techniques, demonstrated that linear and non-linear viscous loads *can* reduce subjects' tremors by statistically significant amounts (p-values < 0.001) without degrading purposeful tracking. These and other results have allowed design specifications for tremor-suppressing orthoses to be refined, and plans for the CEDO 2 -- a functionally improved version of the CEDO 1 -- are underway.

Thesis Supervisor: Dr. Michael J. Rosen
Title: Principal Research Scientist

Acknowledgements

I would like to acknowledge those individuals who, through their guidance, assistance, and support, have helped me complete my graduate degree. First, I would like to thank Dr. Michael Rosen for enthusiastically serving as my graduate advisor and mentor at MIT and Dr. Mindy Aisen for serving as my clinical advisor and consultant at the Burke Rehabilitation Center. I would also like to thank the members of the tremor group -- Chen-An Chen, Karen Palmer, Jack Kotovsky, Jolanda Hendriks, and Jeff Snyder; my faithful UROPer Winnie Leung; individuals in the Newman Laboratory, especially Zoher Karu, Michael Goldfarb, Judy Schreidell, Pat McCosco, Marie Stuppard, Norman Berube, Ralph Burgess, and Prof. Will Durfee; the staff of the Burke Rehabilitation Center, particularly Dr. Steve Price and the occupational therapists; and finally Dr. Jorge Romero at the Brigham and Women's Hospital for valuable assistance and suggestions. Chen-An Chen deserves a special thanks for being my "research partner" during our stay at Burke and for being such a terrific friend. Next, I would like to acknowledge with deep appreciation those who provided the moral support -- my family, my close buddies Honor and Chris Passow, my roommate Chee Chia, and my friends on the MIT gymnastics team and at the Beacon Hill Baptist Fellowship -- and those who provided the financial support -- Mr. Cecil Green, the Tau Beta Pi Association, and the National Science Foundation -- that enabled me to succeed at MIT. Finally, and most of all, I would like to thank those individuals who willingly participated in my experiments, who taught me more about tremor than I could ever learn from a book, and who provided not just the raw data but also the primary motivation for this thesis.

-- Allison S. Arnold

This work was supported in part by the Burke Rehabilitation Center of White Plains, NY and by fellowships sponsored by Cecil and Ida Green, the Tau Beta Pi Association, and the National Science Foundation.

Table of Contents

List of Figures

Chapter 5 *page*

Chapter 5 (continued) *page*

Chapter 5 (continued) *page*

Appendix B

List of Tables

Chapter 1
Introduction

1.1 Objective

1.1.1 Significance of the Problem

Pathological tremor is an involuntary rhythmic oscillation of the limbs, head, trunk, or other part of the body superimposed on purposeful movement. A recent survey of 20 neurologists, physiatrists, and other movement disorder specialists, distributed and compiled by a member of the MIT tremor group specifically to learn more about the U.S. population disabled by tremor and the effectiveness of current treatment methods, suggests that pathological tremor impairs an estimated one million Americans today [Chen 1991].

For members of this population and for their families, physicians, and other providers, pathological tremor is a significant problem for two main reasons. First, because tremor interferes with voluntary movement, it is frustrating, embarrassing, and often disabling. In its mildest form, pathological tremor impedes activities of daily living and hinders social function. In more severe cases, however, tremor occurs with sufficient amplitude to obscure all underlying voluntary activity. For the large fraction (65 to 70 percent) of tremor-disabled individuals who have tremor in their shoulders, elbows, wrists, or hands, independent function is difficult or impossible [Elble & Koller 1990, Chen 1991].

Perhaps even more troubling is the fact that the underlying physiology of pathological tremor is not well understood and that existing methods of diagnosis and treatment are largely ineffective. Tremors are currently classified according to the physiological state in which they occur, i.e. resting, postural, or action tremor, and by the presumed etiology or site of the lesion responsible for the oscillation, i.e. Parkinsonian tremor, cerebellar tremor, and rubral tremor [Stein & Oguztoreli 1978, Findley 1987]. However, descriptive terms are used ambiguously [Findley & Capildeo 1984], and errors in diagnosis are common, particularly among the elderly [Salisachs and Findley 1984]. No clinical tremor assessment scale has been universally

accepted, and most specialists agree that existing assessment scales are imprecise, subjective, and generally inadequate [Findley & Capildeo 1984, Elble & Koller 1990, Chen 1991]. Although attempts have been made to differentiate tremors by their response to pharmacological agents, only Parkinsonian tremor can be distinguished reliably [Fahn 1984].

Pathological tremor is particularly difficult to diagnose because consistent relationships between tremor etiologies, underlying mechanisms, and visible tremor characteristics have not been found. In the U.S., approximately 30 percent of the tremor population suffers from multiple sclerosis, 29 percent from essential tremor, and 22 percent from Parkinson's Disease. Others develop tremor as a result of a head injury, stroke, or tumor causing damage to the spino-cerebellar and mid-brain centers that interact to coordinate movement [Elble & Koller 1990, Chen 1991]. Tremor may also accompany other movement disorders in ailments such as Friedreich's Ataxia and Cerebral Palsy [Rondot et al 1978]. A description of neurological disorders which cause tremor is provided in Appendix A.

The most effective treatment available today for tremor-disabled individuals is medication used on a trial-and-error basis [Rondot et al 1978, Shahini & Young 1978]. Because clinicians cannot reliably predict an individual's response to a particular drug, it is standard procedure for clinicians to prescribe, in the order of decreasing expected effectiveness, the drugs known to reduce tremor. When a drug fails to provide relief, the dosage is altered or the next drug on the list is prescribed. Even when a drug does reduce tremor, its benefits must outweigh its undesirable side effects and potential for addiction before it is prescribed on a long-term basis [Aisen et al 1991]. Common side effects of tremor medications include sedation, weight gain, nausea, diarrhea, rash, impotence, and depression [Elble & Koller 1990].

A frequent conclusion in the clinical tremor literature is that a complete understanding of the physiological mechanisms that drive pathological tremor is necessary to support the search for more effective treatments [Fahn 1984, Legg 1984, Findley 1987]. Until such treatments are found, there is a desperate need for better assessment and diagnosis schemes to facilitate the prescription of available drugs, and, for individuals for whom drugs are ineffective or side

effects are intolerable, there is a special need for assistive devices and interfaces that will enable persons with pathological tremor to lead more independent and productive lives.

1.1.2 Purpose of the Project

The purpose of this project was to assess the effectiveness of the MIT CEDO 1 -- a Controlled Energy-Dissipating Orthosis developed at the MIT Newman Laboratory for Biomechanics and Human Rehabilitation -- both as a research tool for quantifying tremor characteristics and as a prototype orthosis for assisting tremor-disabled individuals. The first tremor experiments done at MIT in the 1970's tested the hypotheses that the application of peripheral mechanical loads to the limbs of persons with tremor can suppress their tremors in a clinically useful way and can perhaps provide insight into the underlying mechanisms which generate their movement disorders. After successfully demonstrating that viscous loads do suppress wrist tremor in one-degree-of-freedom (1-dof) experiments [Dunfee 1979, Adelstein 1981, Rosen & Adelstein 1981], members of the MIT tremor group began designing and building special-purpose devices capable of measuring tremor in multiple degrees of freedom while simulating a variety of loads including inertia, elasticity, damping, rigid walls, force perturbations, and combinations of the above. Work was also begun on the design of tremor-suppressing orthotics and assistive interfaces. To date, five devices have been completed: the CEDO 1, a 3-dof wheelchair-mounted restraint system meant to enable tremor-disabled individuals to do a particular set of daily activities independently [Baiges 1989, Baiges & Rosen 1989, Rosen et al 1992]; the Adelstein Manipulandum, a 2-dof "virtual environment" joystick for conducting experiments on human motor control [Adelstein et al 1987, Adelstein 1989]; the MED (Modulated Energy Dissipation) Manipulator, a 6-dof computer-controlled energy dissipating manipulandum similar to the CEDO for measuring tremor and assessing the effects of viscous loading during functional whole-arm movements [Maxwell 1990]; the C-SCAT (Computer-based System for Clinical Assessment of Tremor), a 1-dof computer-controlled manipulandum designed to help neurologists diagnose movement disorders and

prescribe drugs more effectively [Brongo 1990, Brongo & Rosen 1991]; and the MIT Damped Joystick, an assistive interface for powered wheelchairs and other 2-dof electrical and electronic systems [Rosen et al 1979, Beringhause et al 1989, Hendriks et al 1991]. The present focus of the MIT tremor group is to use these devices in experiments to quantify tremor characteristics, to develop models of tremor mechanisms based on experimental findings, and to establish guidelines for the design and development of improved assistive orthotics and special-purpose research equipment. The study described in this thesis, then, comprises one subset of the investigations currently underway.

Preliminary experiments with five tremor-disabled subjects have demonstrated that the CEDO 1's viscous damping does suppress upper-extremity intention tremor [Baiges 1989]. The specific objectives of this study were to:

1. verify, for a larger subject population, the preliminary finding that the CEDO 1's viscous damping loads do suppress upper-extremity pathological intention tremor.
2. establish guidelines for pursuit tracking experiments and methods for interpreting tremor power spectra that are applicable to 2-dof upper-extremity tremor measurements and more generally by extending the methods used previously for 1-dof wrist tremor measurements [Adelstein 1981].
3. assess the repeatability of upper extremity tremor measurements and subject performance on 2-dof pursuit tracking tasks from trial to trial within a test session and from day to day over two or more test sessions.
4. assess the uniformity of upper extremity tremor measurements and subject performance on 2-dof pursuit tracking tasks from subject to subject and from etiology to etiology.
5. begin exploring answers to questions such as:
    a). How much damping is necessary or desirable in an assistive orthosis for tremor-disabled individuals?

b). How do the effects of linear damping loads compare with those of non-linear damping loads?

c). How do inertial loads and damped inertial loads affect measured upper extremity tremor characteristics and subject performance during 2-dof pursuit tracking tasks?

d). Does a relationship exist between the voluntary force an individual is required to exert during a pursuit tracking task and the measured characteristics of his or her tremor?

Although the CEDO 1 device was used in this investigation, the experimental methods and data analysis techniques developed in this study are applicable to other studies involving other apparatus. The intended contribution of this thesis, in pursuing these objectives, was to guide the planning of future experimental protocol and to aid the development of improved assistive orthotics.

The remainder of this chapter reviews related studies in which mechanical loads were applied to the limbs of either able-bodied or tremor-disabled persons for the purposes of tremor mechanism modeling, tremor classification, or tremor management. Chapter 2 describes the CEDO 1 hardware and software and explains the methods used to calibrate and characterize the system; Chapter 3 outlines the experimental protocol and describes a typical test session; and Chapter 4 explains the techniques used for data analysis and tremor quantification. Finally, Chapter 5 presents the experimental results and Chapter 6 lists recommendations for future work.

1.2 Classification and Modification of Tremor Using External Loads

Mechanical loads have been applied to the limbs of able-bodied and tremor-disabled individuals for three different purposes. Beginning in the 1940's, inertial and elastic loads were applied to persons' limbs to experimentally verify models of hypothesized tremor mechanisms. After discovering that not all tremors respond to applied loads in the same

manner, researchers have more recently proposed measuring how pathological tremors respond to various loads to facilitate tremor classification and drug prescription. Engineers have also begun designing and building damping devices like the CEDO 1 to help tremor-disabled individuals function more independently.

1.2.1 The Use of Loading for Tremor Mechanism Modeling

There are, to date, three broad classes of hypothesized tremor mechanisms: biomechanical resonances, in which the limb oscillates at a tremor frequency related to its lumped passive mechanical properties and is forced by muscle noise that originates in a background of random motor unit firing or by cardioballistic oscillations [Bishop et al 1948, Robsen 1959, Randall & Stiles 1964, Stiles & Randall 1967, Brumlik & Yap 1970, Joyce & Rack 1974, Vilis & Hore 1977]; reflex loop instabilities, in which neuromuscular transmission delays reduce the phase margin of both segmental and transcortical reflex arcs, causing oscillation [Marsden et al 1969, Lippold 1970, 1971, Young & Hagbarth 1980, Burne 1987, Flament & Hore 1988]; and central nervous system (CNS) oscillators, in which autonomous sources in the CNS drive the affected muscle groups to oscillate at fixed frequencies, regardless of peripheral factors [Joffroy & Lammare 1971, Elble & Randall 1976, Jankovic & Fahn 1980, Elble 1986, Adelstein et al 1987, Elble et al 1987]. Most investigators agree by now that all of these hypothesized tremor mechanisms (and perhaps others) play a role in generating at least one type of tremor and that normal physiological tremors as well as pathological tremors are influenced by a combination of mechanisms which may interact in different proportions depending on metabolic factors, anxiety, pathology, and the mechanical situation in which the limb is involved.

Experimental evidence for these hypothesized tremor mechanisms has stemmed mainly from 1-dof studies of physiological tremor, the "normal" oscillation present in both able-bodied and disabled persons. Researchers now concur that physiological tremor has two distinct components. The most prominent component is produced by underdamped limb mechanics

and stretch reflexes in which the oscillation frequency is determined by the mass and the stiffness of the limb. Evidence for this component of physiological tremor includes Bishop et al's observation in 1948 that oscillation frequency increases with increases in muscle tension (implying increases in limb stiffness); Robsen's observation in 1959 that oscillation frequency increases with the application of elastic loads; Randall and Stiles's observation in 1974 that physiological tremor resembles the die-away oscillation of a body segment in response to a sharp mechanical tap and that the oscillation frequency is inversely proportional to the square root of the lumped sum of the body segment inertia and any externally-added masses; Joyce and Rack's observation in 1974 that the frequency of oscillation at the elbow is proportional to the square root of the equivalent spring stiffness of the arm over much of the elbow's range of movement; and Jankovic and Fahn's observation in 1980 that physiological tremor persists after deafferentation and therefore does not depend solely on reflex phenomena. This physiological tremor component is not associated with a particular pattern of myoelectric (EMG) activity in controlling muscles except when fatigue causes reflex modulation of motoneuron firing [Gottlieb & Lippold 1983, Elble 1986].

The second component of physiological tremor, in contrast, has amplitude and frequency characteristics that are unaffected by peripheral mechanical loads or limb temperature. This invariance and the correlation between this tremor component and synchronous EMG activity in controlling muscles suggests that some type of CNS or reflex oscillator is responsible [Elble 1986, Findley 1987]. Evidence for a neuronal component of physiological tremor includes Marsden et al's observation in 1969 that desensitizing muscle spindles through ischaemia diminishes a component of physiological tremor; Lippold's observations in 1970 and 1971 that an 8-12 Hz tremor is present throughout the body in postural maintenance situations in addition to biomechanical resonance oscillations; and Young and Hagbarth's observation in 1980 that when a subject makes a Jendrassik maneuver known to reinforce the segmental stretch reflex, i.e. the subject makes a tight fist with his or her contralateral hand without increasing the force output of the wrist being tested, his or her physiological tremor is enhanced. The precise

anatomical location of the 8-12 Hz neuronal oscillator in the nervous system, however, has not been found [Elble & Koller 1990].

Although the mechanisms of physiological tremor are fairly well understood, the mechanisms of pathological tremors remain largely unknown for several reasons. First, much of the experimental work to date has emphasized physiological tremor. Second, few consistent relationships between tremor etiologies, underlying pathology, and visible tremor characteristics have been found. Finally, experiments to date have not always enabled investigators to distinguish among various hypothesized mechanisms, nor have they allowed investigators to determine which mechanisms actually *generate* tremor and which mechanisms merely *influence* tremor.

Distinguishing reflex phenomena from biomechanical resonance and CNS factors, in particular, has posed numerous challenges. Because the dynamics of reflex oscillations are influenced by mechanical loads, peripheral reflex tremors are expected to exhibit frequency characteristics which are similar to biomechanical resonance tremors. This explains why Stiles introduced the term "mechanical-reflex" tremor in 1980, lumping biomechanical resonance and reflex mechanisms into one category. However, under conditions of low inertia and high reflex gain, reflex pathways can theoretically exhibit oscillations at frequencies that are relatively independent of limb mechanics, a characteristic also expected for CNS oscillators [Stein and Oguztoreli 1976]. Or, alternatively, CNS oscillators may be so strongly coupled to stretch reflexes by sensory afferent pathways that the amplitude and frequency of CNS-generated oscillations are, in fact, affected by mechanical loading or by augmenting or suppressing sensory feedback [Elble & Koller 1990].

Studies done on Cebus monkeys with experimentally-induced pathological tremor have provided some evidence that all three of the hypothesized tremor mechanisms may influence pathological tremor. For instance, Joffroy and Lammare in 1971 detected a relationship between postural tremor induced by cerebellar lesions in a deafferented monkey and activity at points in its sensory-motor cortex and postulated the existence of a CNS oscillator. In another

study, Vilis and Hore reported in 1980 that when tremor was induced by cooling the cerebellar nuclei in monkeys, the tremor frequency increased with the addition of spring loads and decreased with the addition of mass loads; the tremor amplitude decreased with an increase in viscous resistance; and the tremor phase changed with the application of randomly timed perturbations as predicted by a biomechanical resonance model. Finally in 1988, Flament and Hore noticed in monkeys with cerebellar dysfunction that limb oscillations were more irregular and lower in frequency when the monkeys were given isometric tasks than when the monkeys were given isotonic tasks, and they postulated that reflexes in proprioceptive loops were actively modulating the monkeys' intention tremors. It is unclear, however, whether the results of studies of experimentally-induced tremor in monkeys are applicable to studies of pathological tremor in humans.

In humans, contradictory results from limb loading experiments and EMG recordings have led researchers to believe that pathological tremor must result from the interaction of multiple tremor mechanisms. The "coupled stretch reflex and central oscillator theory" proposed by Elble, Higgins, and Moody in 1987, for example, combines CNS and peripheral reflex hypotheses. These researchers found that when the wrists of able-bodied subjects were mechanically perturbed, oscillations were induced at a frequency determined by the biomechanical properties of the limb, and when the oscillations were of sufficient amplitude, stretch reflexes acted to regulate this frequency in time with the disturbances. They also found that when the wrists of essential tremor patients were mechanically perturbed, oscillations were present *in addition to* the reflex-modulated oscillations which were *not* affected by the disturbances. To explain these findings, Elble et al postulated that interactions occur between coupled CNS and stretch reflex oscillators to generate tremor and that the resulting oscillations depend on the relative strengths of the oscillators, the relative frequencies of the oscillators, and the degree of coupling between the oscillators. This hypothesis may explain Adelstein's observation in 1981 that intention tremor in some individuals consists of two components, both of which are present during displacement tracking tasks but only one of which is present

during isometric tasks, and it also suggests why Marsden proposed that essential tremors be further categorized into two types. "Type I" essential tremor, as classified by Marsden, is behaviorally indistinguishable from enhanced physiological tremor, has a frequency of 8-12 Hz, and is due to an increased gain of the stretch reflex. "Type II" essential tremor has a lower frequency and a larger amplitude than Type I tremor and depends upon oscillation from within the central nervous system [as cited in Calzetti et al 1987].

Some investigators, in addition to running experiments, are now using computer simulation techniques to predict how tremors respond to mechanical loads and to model how different tremor mechanisms might interact. Thus far, single-dof models have been developed which ascribe tremor characteristics such as frequency peaks and load responses to one or more of the three hypothesized mechanisms. Specifically, Lohnberg's linear model simulates possible mechanisms of Parkinson tremor [1978], Zahalak and Cannon's model predicts the frequency and amplitude of physiological tremor in individual subjects [1983], and Fukumoto's model demonstrates how Parkinsonian tremor frequency changes with peripheral loading [1986]. Perhaps computer models and supporting experimental evidence will, in the future, eliminate the confusion which currently exists regarding the mechanisms of tremor generation.

1.2.2 The Use of Loading for Tremor Diagnosis

Because some evidence exists which suggests that persons with varying tremor etiologies respond differently to applied mechanical loads, researchers have proposed quantifying how pathological tremors respond to loads to facilitate tremor classification and drug prescription [Adelstein et al 1987, Homberg et al 1987; Brongo & Rosen 1991]. In a study by Adelstein et al in 1987, two types of wrist tremor experiments were used to distinguish persons with intention tremor from persons with essential tremor. In one set of experiments, subjects were given isometric torque tracking tests in which the gain between a wrist torque transducer and a visual display screen was systematically altered. In a second set of experiments, subjects were given free-movement displacement tracking tests in which varying amounts of inertia were

added to the subjects' hands. Adelstein found that all subjects exhibited two tremor peaks -- a large 2-7 Hz peak and a small 8-12 Hz peak. However, the response of the low frequency peak to experimental conditions differed for the two groups of subjects. In subjects with intention tremor, in both types of tests, the force amplitude of the low frequency tremor peak did not vary as subjects' increased their voluntary force. In subjects with essential tremor, in contrast, the force amplitude of the low frequency tremor peak increased in the isometric tests as subjects increased their voluntary force, and the frequency of the low frequency tremor peak decreased in the displacement tracking tests as inertial loads were added.

In another set of experiments by Homberg et al in 1987, inertial loads did not differentiate between persons with varying etiologies but, to a certain extent, EMG recordings did. When Homberg strapped weights to the dorsum of the hands of fifteen subjects with essential tremor and five subjects with Parkinson's Disease, he found that the tremor frequencies of both essential tremor subjects and Parkinson's Disease subjects were invariant regardless of the load applied. Measures of EMG activity in Parkinson's Disease subjects, however, always showed a reciprocating pattern of agonist and antagonist activity while measures of EMG activity in essential tremor subjects sometimes showed a synchronous pattern and sometimes showed a reciprocating pattern.

At MIT, the CSCAT device mentioned in Section 1.1.2 has been designed to more rigorously test the hypothesis that tremors with distinct pathologies can be differentiated by imposing controlled mechanical loads to the limbs of tremor-disabled patients as they perform specific tasks. Objective measures of load response are expected to reveal differences among tremors which would not appear under conventional assessment, and tremor classifications based on such measures are expected to predict drug effectiveness once the necessary experimental correlations have been established [Brongo & Rosen, 1991].

1.2.3 The Use of Loading for Tremor Management

Rosen et al have demonstrated that people with abnormal intention tremor are disabled not because they lack useful levels of volitional control or adequate muscular strength, but because the magnitudes of their superimposed pathological oscillations approach the magnitudes of their purposeful actions [1976, 1979, 1981]. This suggests that if an orthosis was designed to suppress high frequency tremor while allowing low frequency voluntary movement, acting essentially as a low-pass filter, it might enable individuals with tremor to perform some daily tasks independently. The theoretical and experimental rationale for managing pathological tremor with orthotics, particularly orthotics which incorporate damping loads, are presented below.

Theoretical Basis:

For any of the three hypothesized tremor mechanisms defined in Section 1.2.1, one can argue qualitatively that the application of damping loads to tremorous limbs will result in selective attenuation of tremor relative to voluntary movement. If, for example, an individual's tremor is caused by biomechanical resonance, then the addition of damping "in parallel" with the anatomical inertia of the limb and the elasticity of the muscles will increase the damping ratio of the system and will thereby diminish the amplitude of the resonant tremor peak. If an individual's tremor is driven by an oscillatory reference signal from the CNS, then a damper to ground (the proximal limb segment) presents a 1/s load to the force measured at the limb and and attenuates tremor relative to slower purposeful movement frequencies by 20 dB per decade of frequency difference. Finally, if an individual's tremor is generated by an autonomous reflex oscillation, the "physical plant" driven by the closed-loop neural system is a series element in that loop. If damping appropriately alters the dynamics of the plant, it could effectively reduce the tendency to oscillate.

Experimental Basis:

The rationale for incorporating damping loads in assistive orthotics to manage pathological tremor is further supported by experimental evidence. In addition to studies done by the MIT tremor group [Dunfee 1979, Adelstein 1981, Rosen & Adelstein 1981], two other research groups have used a viscously-damped single-dof manipulandum to study how mechanical properties of the manipulandum affect the performance of subjects with wrist tremor during target tracking tasks [Morrice et al 1987, Sanes et al 1988]. In Morrice et al's study, four subjects with unilateral cerebellar lesions were presented with a visual display of a target moving horizontally in an unpredictable pattern at velocities of 0-30 degrees/sec. The subjects, using a manipulandum connected to a torque motor, tracked the target while the investigators, using position and velocity feedback, altered the viscous resistance or stiffness of the manipulandum. When subjects performed the tracking task with their affected arm, their "errors", defined as the cumulative difference between the signals representing wrist position and target position, were significantly higher (p-values < 0.005) than when they performed the task with their clinically unaffected arm. Increasing the manipulandum's viscosity improved tracking accuracy for subjects' affected arms but not for their clinically unaffected arms, and increasing the manipulandum's stiffness produced no consistent change in error scores.

In a similar study by Sanes et al, five subjects with 3-5 Hz upper extremity postural and intention tremors were shown a visual display containing a position cursor and a target cursor while their hands were placed between two padded plates of a handle attached to the axle of a DC torque motor. Subjects were instructed to align their cursor with the target and hold it for 1.5 to 2.5 seconds, after which a bell would sound and the target would jump to a new location. Movements were opposed or assisted by a constant load between 0.64 Nm opposing extension and 0.64 Nm opposing flexion; an inertial load of either 250, 500, or 1000 grams attached to the handle; or a viscous load between 0 and 0.00039 Nm/degree/sec. The investigators found that the lightest viscous loads suppressed tremor, measured as total distance travelled, by 38-56 percent compared to the no-load tremor and that the heaviest

viscous loads reduced tremor by an additional 2-23 percent. They also found that in three of the five subjects, inertial loads applied to the torque handle decreased the tremor in a non-linear and non-regular fashion and that constant loads requiring wrist flexion decreased postural tremor while constant loads requiring wrist extension increased postural tremor.

The concept of using fixed-base orthotics to modify the performance of the human arm is not new. *Active* multi-dof experimental orthotics such as the Case Western Reserve University "Arm Aid", a 5-dof exoskeletal robot meant to manipulate a paralyzed or partially paralyzed human arm [Corell & Wijnschenk 1964]; the Rancho Los Amigos Hospital "Electric Arm", a similar device which was actually developed into a commercial product [Nickel 1964, Karchak & Allen 1968]; man amplifiers, devices meant to amplify the load capability of the human body [reviewed by Kazerooni 1989]; and teleoperators, robotic devices whose motion is controlled by an operator at a distance [for example Fornof & Thornton 1973, Vykukal et al 1973], received considerable attention two to three decades ago. While these systems were uniformly too complex in design, too demanding of the user, and cosmetically too obtrusive to be successful as orthotic devices for tremor-disabled people in daily activities, other *passive* orthotics have been developed and are currently being used. For example, splints and other orthotic devices like the "Mobile Arm Support" or "Ball Bearing Feeder" are commonly used in rehabilitation medicine to provide low-friction arm support for people with deltoid muscle paresis or paralysis [see, for example, product literature from Jaeco Orthopedic Specialties or Ali-Med, Inc.]. Moreover, Michaelis Engineering of Southampton, England has recently developed and is commercially marketing two viscous-loading assistive devices -- a feeding aid called the "Neater Eater" and a computer mouse Tremor Reducing Apparatus called the "MouseTRAp" -- specifically for tremor-disabled individuals [Michaelis 1988].

The success of such devices demonstrate that taking an "orthotic" approach to tremor management is feasible and worthwhile. The task remains, however, to incorporate damping into more orthoses that are functional, affordable, and cosmetically acceptable.

Chapter 2
The CEDO 1 System

2.1 Overview of the CEDO 1 System

The MIT CEDO 1, pictured in Figure 2-1, is a 3-dof computer-controlled energy-dissipating orthosis which generates resistive loads by means of magnetic particle brakes whose torques are transmitted to the user's forearm via a stiff low-inertia linkage. The CEDO 1 was designed primarily as a prototype assistive device for persons disabled by tremor, meant to be evaluated by its potential users in abstract and functional tasks, and intended to be modified over time as design specifications are refined and improved designs are generated. The CEDO 1 is also a research tool for measuring some of the characteristics of tremor and for validating the hypothesis that velocity-dependent resistive loads can suppress intention tremor in more than one degree of freedom without unacceptably attenuating voluntary movement.

The main components of the CEDO 1 system are shown schematically in Figure 2-2. The user's forearm is secured to the CEDO via a rigid plastic cuff and velcro straps. Potentiometers mounted at the three orthosis axes measure the user's position, and differentiator circuits housed in an electronics box determine the user's velocity. These analog position and velocity signals are converted to digital signals via an analog-to-digital (A/D) converter, and the digital signals, in turn, are fed to a computer. To make the CEDO behave as a damper, a computer program reads the position and velocity information and calculates the brake torques needed to generate a resistive force proportional to the user's velocity. Finally, the computer's digital torque instructions are converted to analog signals via a digital-to-analog (D/A) converter, and the analog signals are sent to brake-driver circuits which generate the current to activate the brakes.

Figure 2-1. The MIT CEDO 1 in use.
(Photo courtesy of Donna Coveny, MIT News Office.)

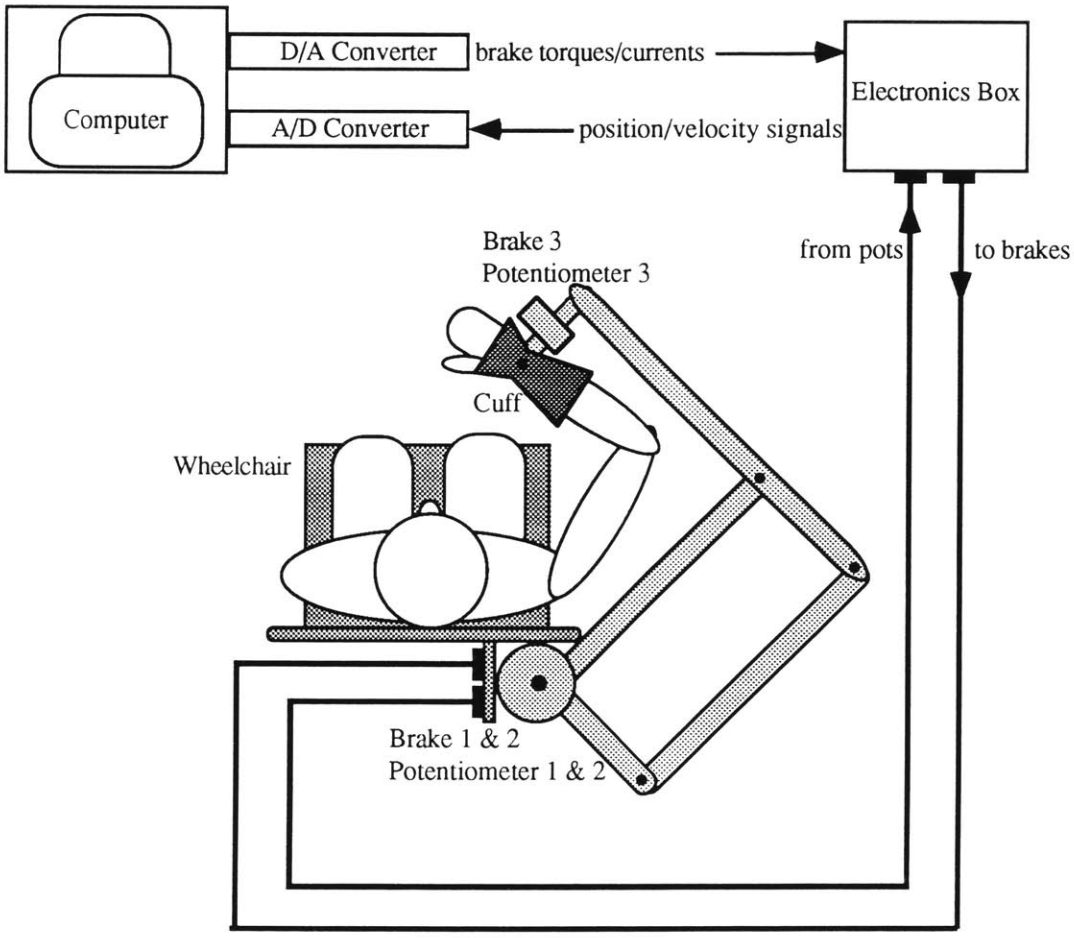

Figure 2-2. Schematic of the CEDO 1 system.

The first part of this chapter lists the features and limitations of the current CEDO system. The second part describes the CEDO 1 hardware and software, and the third explains the steps that were taken to calibrate, characterize, and model the system.

2.1.1 Design Features

Safety, compatibility, flexibility, and economy, in addition to tremor reduction effectiveness, are the goals S.M candidate Ivan Baiges deemed most important when he designed the CEDO 1 system and the CEDO's main features reflect these goals. For maximum safety, for instance, the CEDO 1 is equipped with magnetic particle brakes rather than motors or other actuators at each of its three axes. The passive, energy-dissipating particle brakes resist motion rather than produce it, so the device *cannot* move unless it is moved by the user.

For functional and anatomical compatibility, the CEDO 1 linkage is designed to resemble the widely-used Ball Bearing Feeder assistive device. Because its intended purpose is to reduce tremor in the performance of desktop and tabletop tasks, i.e."desk work", reading, and eating, its configuration consists of three rotational joints, two of which parallel the geometry of the arm and allow movement in the horizontal plane, and a third which permits the user to tilt his/her forearm about a horizontal axis perpendicular to the long axis of the forearm as shown in Figure 2-3. The CEDO 1 also allows the user to pivot his/her forearm in the horizontal plane about an axis perpendicular to the forearm.

For maximum flexibility as a research tool, the CEDO 1 is controlled by a personal computer. By making simple revisions to the control software or its input, a wide variety of damping coefficients and velocity-dependent resistive loads can be tried.

Finally, to minimize cost, the CEDO 1 is built with commonplace materials and components -- its links and supports are machined out of standard aluminum alloy; its off-the-shelf particle brakes are controlled without force feedback; and its three axes are equipped with precision potentiometers rather than other more expensive sensors [Baiges 1989, Rosen et al 1992]. A discussion of general design criteria for tremor-suppressing orthoses and an

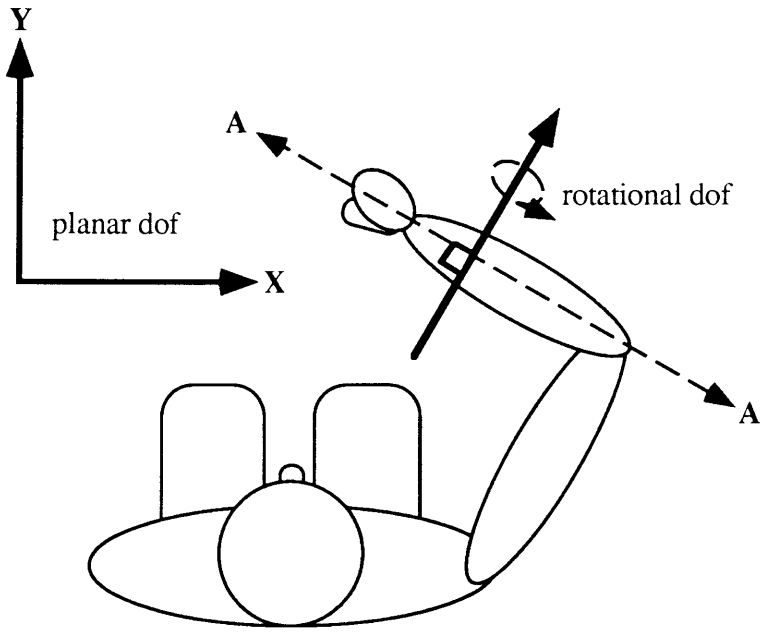

Figure 2-3. CEDO 1 degrees of freedom. The first and second degrees of freedom allow planar movement while the third allows rotational movement about a horizontal axis perpendicular to A-A, the long axis of the forearm.

evaluation of the CEDO 1 in light of these criteria can be found in the paper by Rosen et al [1992].

2.1.2 Design Limitations and Future Goals

The current CEDO orthosis is an experimental prototype, not a commercial product. One purpose of this investigation was to determine which CEDO features should be retained and which CEDO features should be revised in future models to increase its appeal as an assistive device or its effectiveness as a research tool. For example, the bulky aluminum links, chosen for their light weight and low cost, could be replaced by smaller, stiffer composites to reduce the device's size. Or, if experiments indicate that damping in the third degree of freedom (into and out of the horizontal plane) does not contribute significantly to the device's overall effectiveness, the third particle brake could be eliminated to reduce the CEDO's endpoint inertia and decrease its overall cost. Finally, although the prototype CEDO is mounted on a wheelchair, it obtains control signals from a personal computer and power from a standard wall outlet and thus cannot be moved during use. A future wheelchair-mounted system might incorporate a microprocessor or laptop computer for control and rechargeable batteries for power, or it might use mechanical dampers in place of the computer-controlled particle brakes for resistance. Alternatively, a future desktop-mounted system may be designed to support the user's arm from above rather than from below and from the front or side rather than from behind to facilitate eating and other desktop activities.

2.2 Description of Hardware

Since much of the CEDO 1 hardware is described in detail in Baiges' S.M. thesis, this section describes just the main CEDO components in brief, emphasizing revisions that have been made since 1989 to prepare the device for clinical experimentation.

2.2.1 Mechanical Hardware

Links:

The geometry and dimensions of the CEDO 1 linkage are shown in Figure 2-4. As mentioned in Section 2.1.1, the geometry of the CEDO 1 resembles that of the commercially available Ball Bearing Feeder assistive device and was chosen in part because of its proven compatibility with a wide range of desktop and tabletop tasks. The links are machined from 6061-T6 aluminum, selected for reasons of availability, low cost, and ease of fabrication. The outer diameter and wall thickness of the links are 1.5 inches and 0.13 inches, respectively, designed to meet stiffness criteria for transmitting damping loads in the horizontal direction and for imposing "rigid" restraint in the vertical direction. The design specifications, statics analysis, and dynamics analysis used to determine link dimensions are provided in Baiges' thesis and are discussed further in Section 2.4.3.

Brakes:

The CEDO 1 is equipped with three magnetic particle brakes, chosen for reasons of safety, economy, ease of control, ease of maintenance, high power-to-weight ratio, and proven reliability in past Newman Laboratory projects. The two large brakes at axes 1 and 2, Placid Industries, Inc. model B150P-06, have a maximum voltage of 6 volts, a maximum current of 1.8 amps, a rated power of 11 watts, an electrical resistance of 3 ohms, a de-energized drag of 30 oz-in, an unforced (i.e. without the use of speed-up circuitry) response time of 130 ms, and a continuous torque rating of 150 lbf-in. The small brake at axis 3, Placid Industries, Inc. model B15P-24, has a maximum voltage of 24 volts, a maximum current of 250 mA, a rated power of 6 watts, an electrical resistance of 105 ohms, a de-energized drag of 5 oz-in, an unforced response time of 25 ms, and a continuous torque rating of 15 lbf-in.

Magnetic particle brakes engage mechanically without movement of mechanical parts. To generate a resistive torque, the output disc-shaft assembly is centered in a gap filled with a fine, dry, stainless steel powder. This powder flows freely until current is applied to a stationary

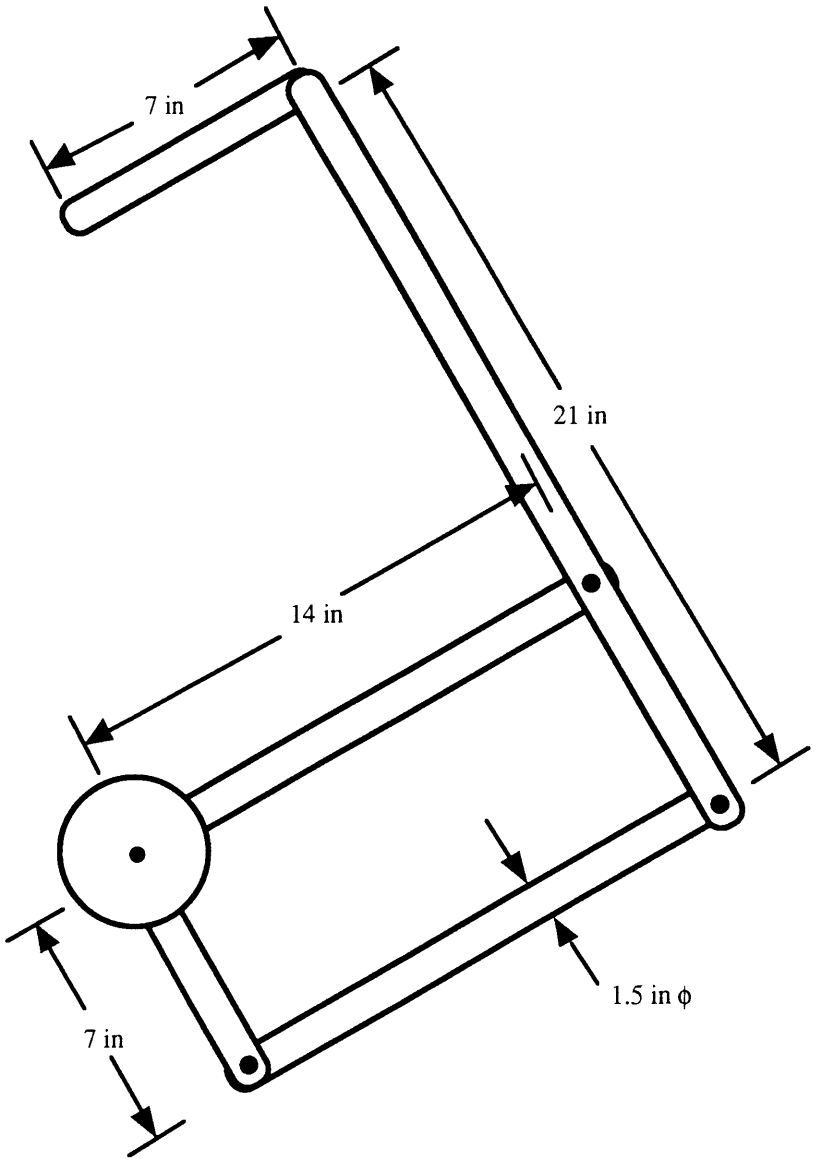

Figure 2-4. Geometry and dimensions of the CEDO 1 linkage.

coil, inducing a magnetic field. The induced magnetic field causes the powder particles to form chains along the magnetic field lines, and these chains link the disc to the housing. An output torque is thus produced which is proportional to the induced magnetic field and to the applied input current.

Flexure-Bearing Brake Mounts:

The brake mounts, pictured in Figure 2-5, are flexure bearings meant to accommodate small runout of the brake shafts (i.e. deviations from straightness). Since the bearings in the brakes are insufficient to transmit the expected radial loads to ground, the joints which couple the proximal CEDO links to the brake shafts incorporate pairs of tapered roller bearings in addition to the bearings in the brakes and, as a consequence, prohibit the brakes from being rigidly mounted to ground. The short segments of welding rod, shown in the figure, bend elastically as needed to accommodate the (barely perceptible) wobble of the brakes while providing the stiffness in compression and tension required to transmit reaction torques from the brakes to the links. This design is an improved version of Baiges' original brake mount design and was incorporated in 1990 by Newman Laboratory graduate student Sheila Eglowstein with an idea contributed by Research Engineer Ralph Burgess.

Limb Coupling:

The cuff and dovetail joint pictured in Figure 2-6 transmit the CEDO's resistive loads to the user's forearm and prevent both wrist flexion/extension and forearm pronation/supination. Three different-sized cuffs, Ali-Med Wrist-Hand Orthosis Models #5842, 5844, and 5846, were purchased to comfortably accommodate a range of participants for the short-term CEDO 1 experiments (although custom-fabricated cuffs may eventually be needed for long-term functional use). Although the cuff is somewhat flexible, measurement errors associated with the compliance of the cuff are probably small compared to those associated with the compliance of the user's skin and underlying tissue. The dove-tail joint, one of Eglowstein's

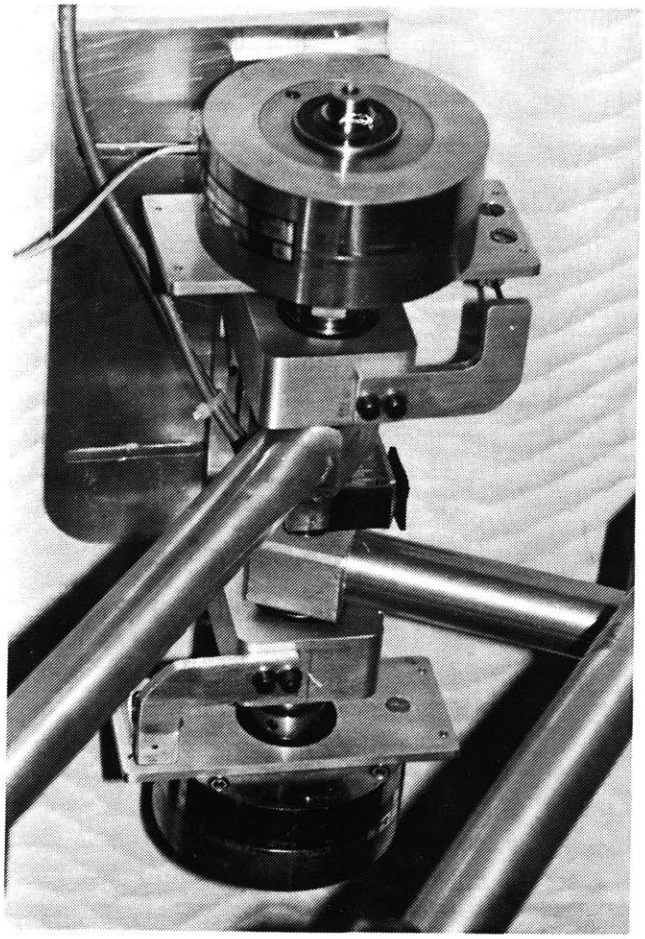

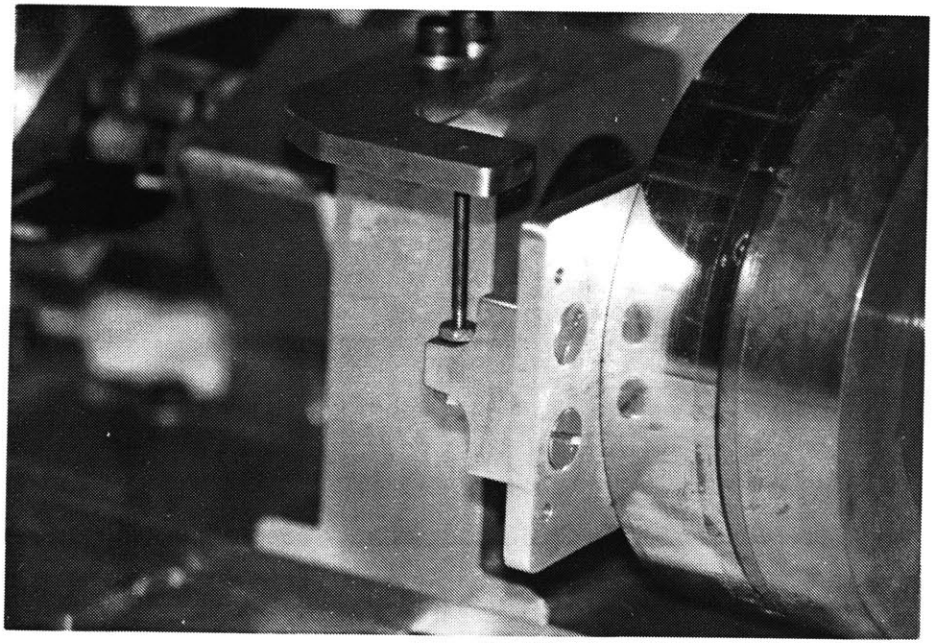

Figure 2-5. The CEDO I brakes and flexure-bearing brake mounts.

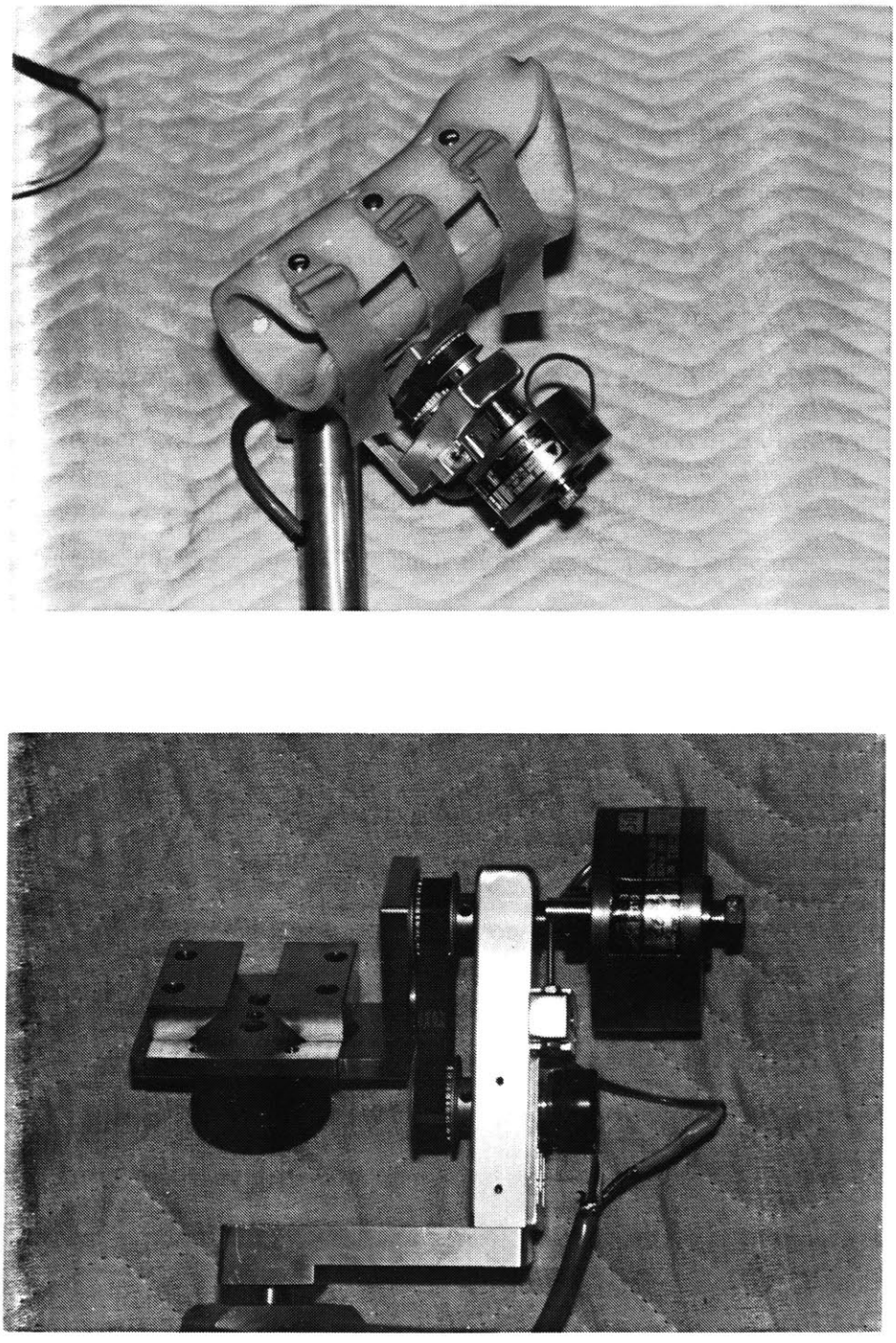

Figure 2-6. The CEDO I forearm cuff and dovetail joint.

contributions, allows the attachment between the cuff and the CEDO 1 linkage to be easily adjusted between a point very close to the wrist to a point more proximal on the user's forearm.

Wheelchair:

The original CEDO 1 system was mounted on a large general-purpose experimental chair designed by doctoral candidate Scott Maxwell and built by Project Technician Norman Berube. Another of Eglowstein's contributions to the CEDO project was to re-mount the CEDO 1 linkage on a standard wheelchair. The wheelchair-mounted system is more portable than the chair-mounted system and, because it is less bulky, is more appealing to clinicians and participants. In fact, one tremor-disabled person who participated in Baiges' preliminary set of experiments did not recognize the wheelchair-mounted CEDO as the same device when he participated in this investigation. (While chair-mounting may not be the most sensible for a final product, it certainly conveyed the impression of a viable commercial product better than the original setup.)

One problem with the wheelchair-mounted CEDO, however, is that the base upon which the brakes are mounted is positioned further behind the user when mounted on the wheelchair than when mounted on the general-purpose experimental chair. This places the CEDO more frequently in its nearly fully-extended state and, consequently, reduces the range of movement directions for which the CEDO is force-velocity colinear. That is, for certain linkage geometries determined by the angle between the proximal CEDO links, the passive CEDO system cannot produce a resistive force that is colinear to the endpoint velocity vector and thus cannot simulate viscous damping. A mathematical derivation of the CEDO's non-colinearity properties can be found in Baiges' thesis. A geometric explanation is presented below for clarity and illustration.

Figure 2-7 shows a simplified sketch of the CEDO 1 with the angle Θ at an indeterminate angle greater than 90 degrees. In all parts of Figures 2-7 and 2-8, the line between the base joint and the CEDO endpoint is drawn parallel to the long axis of the page to emphasize that the

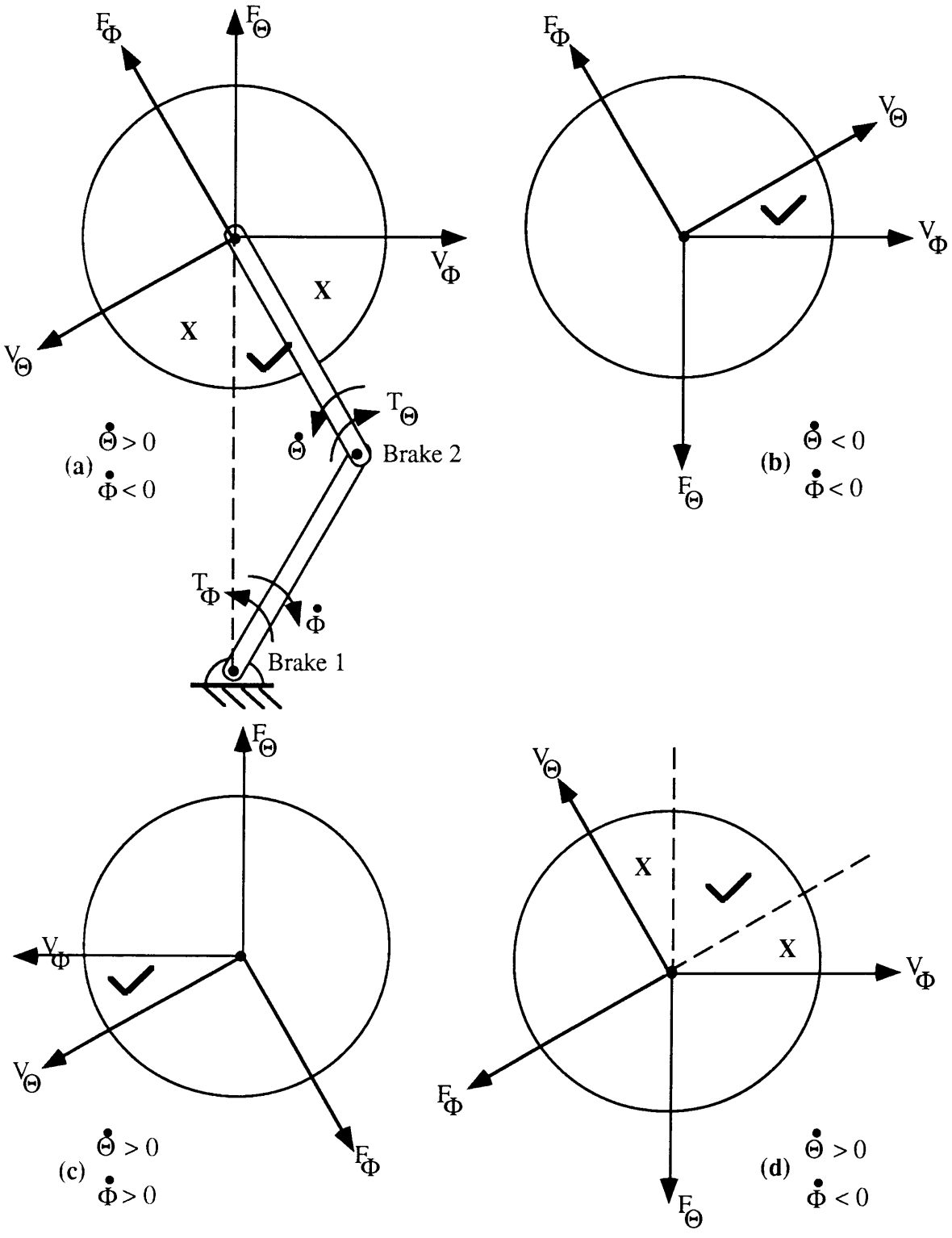

Figure 2-7. Force and velocity contributions from the two joints for the four combinations of angular velocity directions.

base angle Φ (i.e. the rotational position of the whole orthosis) is irrelevant; it simply rotates the sectors of colinearity and non-colinearity derived in this analysis.

In Figure 2-7(a), the sign of Θ-dot is arbitrarily chosen to be positive (orthosis elbow flexing) and the sign of Φ-dot is chosen to be negative (proximal link rotating clockwise). The purely resistive torques T_Θ and T_Φ generated by the brakes at the joints act in directions *opposite* to Θ-dot and Φ-dot as shown in the figure. The two velocity vectors V_Θ and V_Φ, drawn at the CEDO endpoint, represent the local endpoint velocities resulting from pure rotation at one joint or the other. The two force vectors F_Θ and F_Φ represent the forces generated at the endpoint as a result of each of these one-joint rotations and are drawn in the directions in which they impinge on the user's limb.

The directions of F_Θ and F_Φ bear explanation. F_Θ is aligned with the orthosis axis, i.e. the line joining the CEDO endpoint and the base joint. The force generated by a torque at Θ with the Φ brake off *must* be in this direction because a component in any other direction would require a moment about the base joint. By the same reasoning, F_Φ must be aligned with the distal link since a component in any other direction would imply the existence of a moment at the elbow joint, a moment which is impossible without torque at the elbow. Note that these arguments are completely general and do not depend in any way on the values of Θ or Φ.

The force the user feels, given the specified rotational directions, must lie within the angular sector defined by the extensions of F_Θ and F_Φ. Its actual direction depends only upon the relationship between the damping constants of the two brakes. The critical observation is that the range of net force directions at the endpoint is narrower than the range of possible movement directions which result from the same combination of joint rotations. This implies that whenever the endpoint movement direction falls outside the zone indicated with a check, the resistive force vector cannot be aligned with the endpoint velocity vector.

Parts (b), (c), and (d) of Figure 2-7 repeat this analysis for the three other combinations of rotations, and parts (a) and (b) of Figure 2-8 present colinearity circles for two extreme CEDO configurations to illustrate that the distance from the base joint to the endpoint has a dramatic

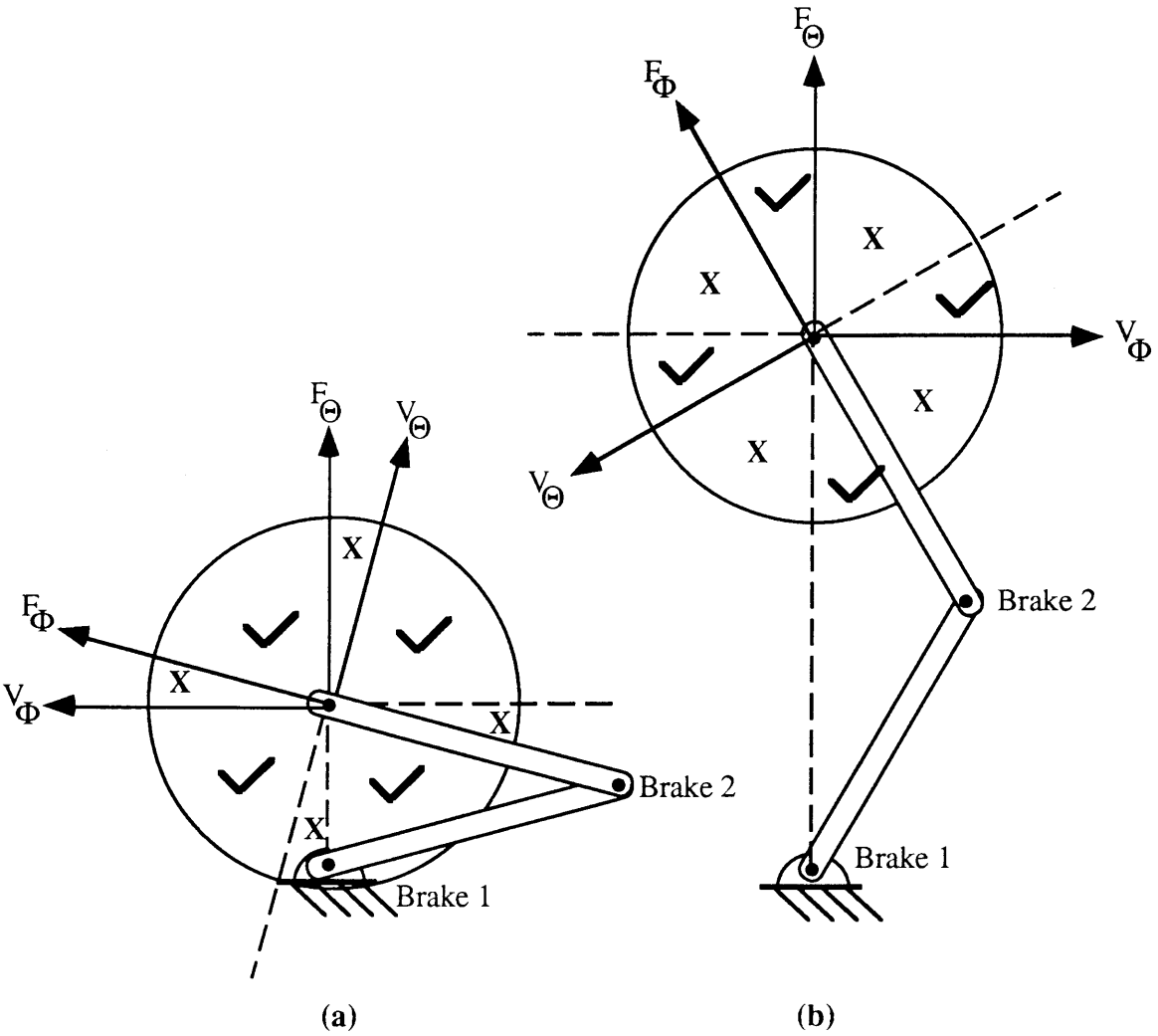

Figure 2-8. Non-colinearity diagrams for very flexed and very extended CEDO configurations.

effect on the relative sizes of the colinear and non-colinear zones. Although Baiges reported in his thesis that the non-colinear regions were unnoticeable in the original CEDO 1, these regions are certainly noticeable in the wheelchair-mounted device.

2.2.2 Electronic Hardware

Because the original CEDO 1 electronic hardware was not intact, the electronics box, the power supply, the analog circuitry, and all connectors were re-designed, fabricated, and/or purchased for this study. Circuit diagrams and descriptions of the revised CEDO 1 circuits are given below. Layout diagrams and connector pinouts are provided in Appendix B, and an electronics components parts list is included in Appendix C.

Position Sensors:

Bourns model 6637 conductive plastic precision potentiometers measure the rotational position of the three CEDO brake shafts. These 5 kΩ, single turn potentiometers have a ± 1 percent linearity tolerance over a 340 ± 3 degree range, a shaft diameter of 0.125 inches, and a housing diameter of 0.875 inches. The potentiometers for axes 1 and 2 are shown in Figure 2-9(a).

Electronics Box:

The CEDO 1 electronics box is pictured in Figure 2-9(b). This enclosure houses the power supply, the position/velocity circuitry, and the brake driver circuitry. It also routes signals between the computer and the orthosis.

Power Supply:

A Computer Products, Inc. model NFS110-7602 AC/DC switching power supply was purchased to power the position/velocity circuit, the brake driver circuit, the potentiometers, and the brakes. This 110 watt universal input supply provides output voltages and maximum

(a)

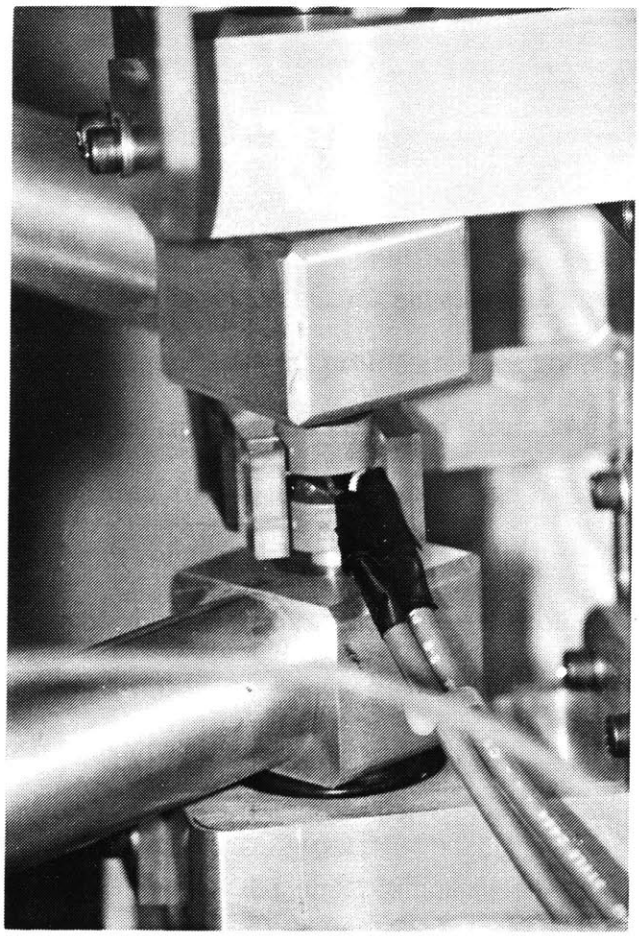

(b)

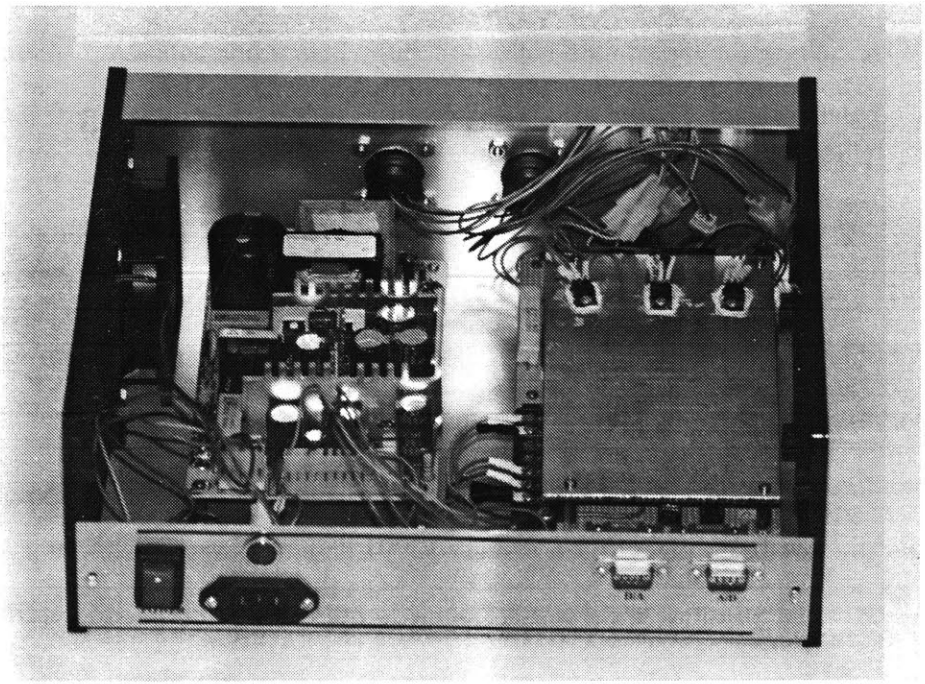

Figure 2-9. The CEDO I electronics, showing (a) the precision potentiometers for axes 1 and 2 and (b) the electronics box housing the power supply and the analog circuitry.

currents of +5.1 V at 10 A, +24 V at 4.5 A, +12 V at 5 A, and -12 V at 1 A. The supply has a fuse for overvoltage protection and an integral filter to reduce line conducted noise.

Position/Velocity Circuitry:

The position/velocity circuitry provides an analog measure of position and velocity for each CEDO axis. As illustrated in Figure 2-10, the position of each brake shaft is transduced by a 5 kΩ potentiometer and fed to an amplifier circuit and an RC differentiator circuit. In the amplifier circuit, operational amplifier U_2 and resistors R_3 and R_4 are wired in an inverting configuration to scale the input voltage range to 10 volts while resistor R_5, a 5 kΩ trimpot, is used to shift this voltage range to the ± 5 volts required by the computer. In the differentiator circuit, operational amplifier U_1, resistors R_1 and R_2, and capacitors C_1 and C_2 form a differentiator with transfer function:

$$\frac{V_{out}}{V_{in}} = - \frac{R_2C_1s}{(R_2C_2s + 1)(R_1C_1s + 1)} \qquad (2\text{-}1)$$

to yield a measure of axis velocity from the input position signal. Because the transfer function has two poles, input signals below the $1/R_2C_2$ corner frequency (13 Hz for axes 1 and 2; 8 Hz for axis 3) are differentiated and scaled while unwanted high frequency signals above the $1/R_1C_1$ corner frequency (18 Hz for axes 1 and 2; 9 Hz for axis 3) are attenuated.

Brake-Driver Circuitry:

The brake-driver circuitry generates the current needed to activate the three brakes. Baiges' original brake-driver circuits invoked voltage-to-current amplifier pulse-width modulation (PWM). Although the PWM circuits were inexpensive and reliable, Maxwell, initially using similar circuitry in the MED Manipulator device, discovered that they were nonlinear, noisy, and in general, unsatisfactory [Maxwell 1990]. The new CEDO brake-driver circuits, like Maxwell's revised MED Manipulator circuits, incorporate linear amplifiers to eliminate the noise and nonlinear conditions.

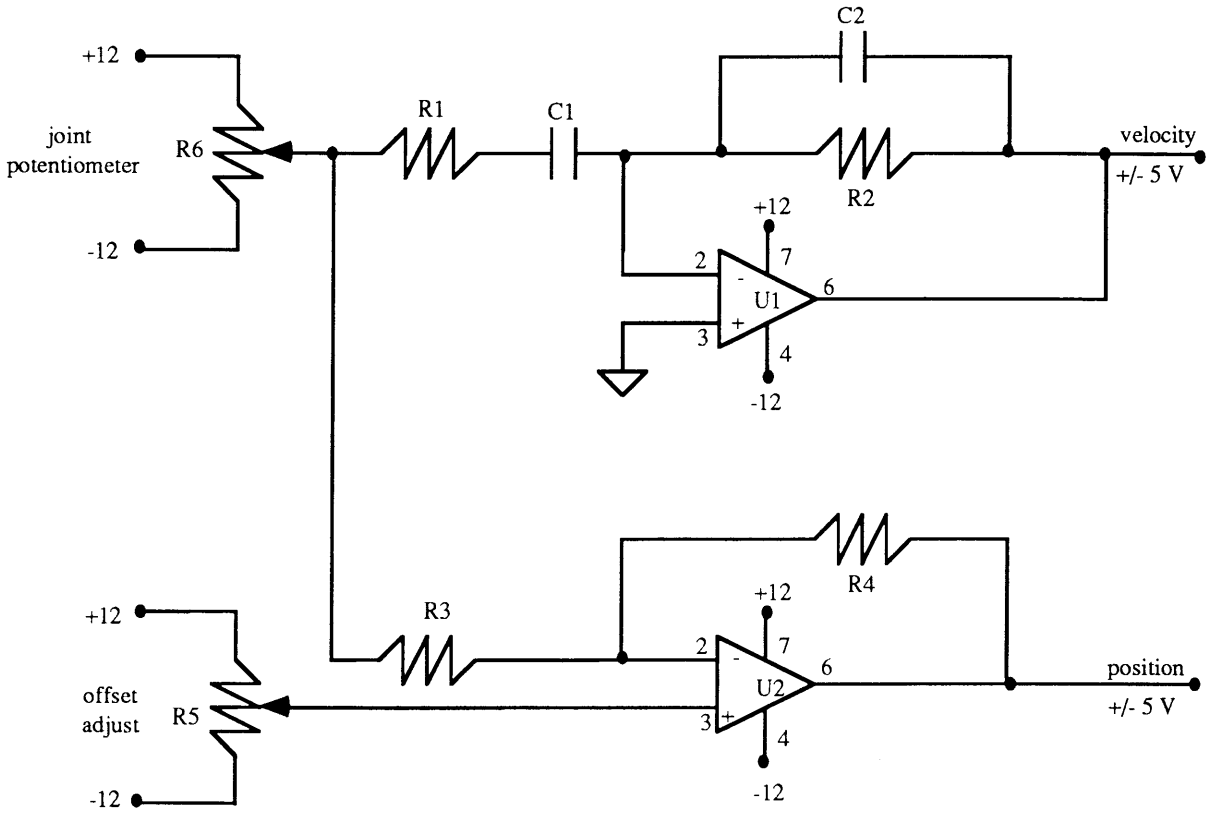

Figure 2-10. Schematic of the CEDO 1 position/velocity circuitry.

Table 2-1. Components of the CEDO 1 position/velocity circuits.

Component	*Axis 1 (upper axis)*	*Axis 2 (lower axis)*	*Axis 3*
R_1	12 kΩ	12 kΩ	180 kΩ
R_2	330 kΩ	330 kΩ	1.5 MΩ
R_3	180 kΩ	180 kΩ	200 kΩ
R_4	200 kΩ	200 kΩ	180 kΩ
R_5	5 kΩ	5 kΩ	5 kΩ
R_6	5 kΩ	5 kΩ	5 kΩ
C_1	1 μF	1 μF	0.1 μF
C_2	0.027 μF	0.027 μF	0.015 μF
U_1	LM741	LM741	LM741
U_2	LM741	LM741	LM741

The basic brake-driver circuit, illustrated in Figure 2-11, is a voltage-controlled current source. A 0-5 volt signal from the D/A converter, corresponding to the desired brake torque for one of the three brakes, is routed through an op-amp buffer and a voltage divider before being input to operational amplifier U_2. When this input signal is positive, transistors Q_1 and Q_2 are on and current is forced to flow from the +24 volt source through the brake to the current-sink resistor R_6. The amount of current in the brake is determined by the voltage across R_6, approximately equal to the non-inverting input of U_2 divided by the value of R_6. At the maximum (5 volt) input from the computer, the large brakes draw 1.5 A and produce 150 lbf-in of torque each while the small brake draws 200 mA and produces 15 lbf-in of torque.

Resistors R_3 and R_4 and capacitor C_1 shown in Figure 2-11 form a lead compensator of the form:

$$\frac{V_{out}}{V_{in}} = \left(\frac{R_4}{R_3+R_4}\right)\left(\frac{R_3C_1s+1}{\frac{R_3R_4}{R_3+R_4}C_1s+1}\right) = \alpha\left(\frac{Ts+1}{\alpha Ts+1}\right) \tag{2-2}$$

and compensate for the time response of the brakes. Because a certain amount of time is required to generate current in a coil of wire, a certain amount of time is required for a magnetic particle brake to respond to changes in input. If the brake is modeled as an inductor in series with a resistor, then this response time can be modeled as a first order time delay which depends on the magnitude of the voltage across the coil:

$$V_L = L\left(\frac{dI_L}{dt}\right) = \frac{L}{R}\left(\frac{dV_{in}}{dt}\right) \tag{2-3}$$

Without the compensator, when the CEDO position data were sampled at 60 Hz (a frequency high enough to avoid aliasing of the tremor components and to obtain adequate frequency resolution for data analysis), the large brakes took significantly longer to respond than the 16.7 ms period available between samples. This time delay lead subjectively to a "lumpy" damping simulation because when the velocity of a link was increased, the resistive torque did not increase immediately proportional to the velocity. When the brakes did respond, the resistance slowed the movement, which in turn reduced the resistance, which in turn allowed

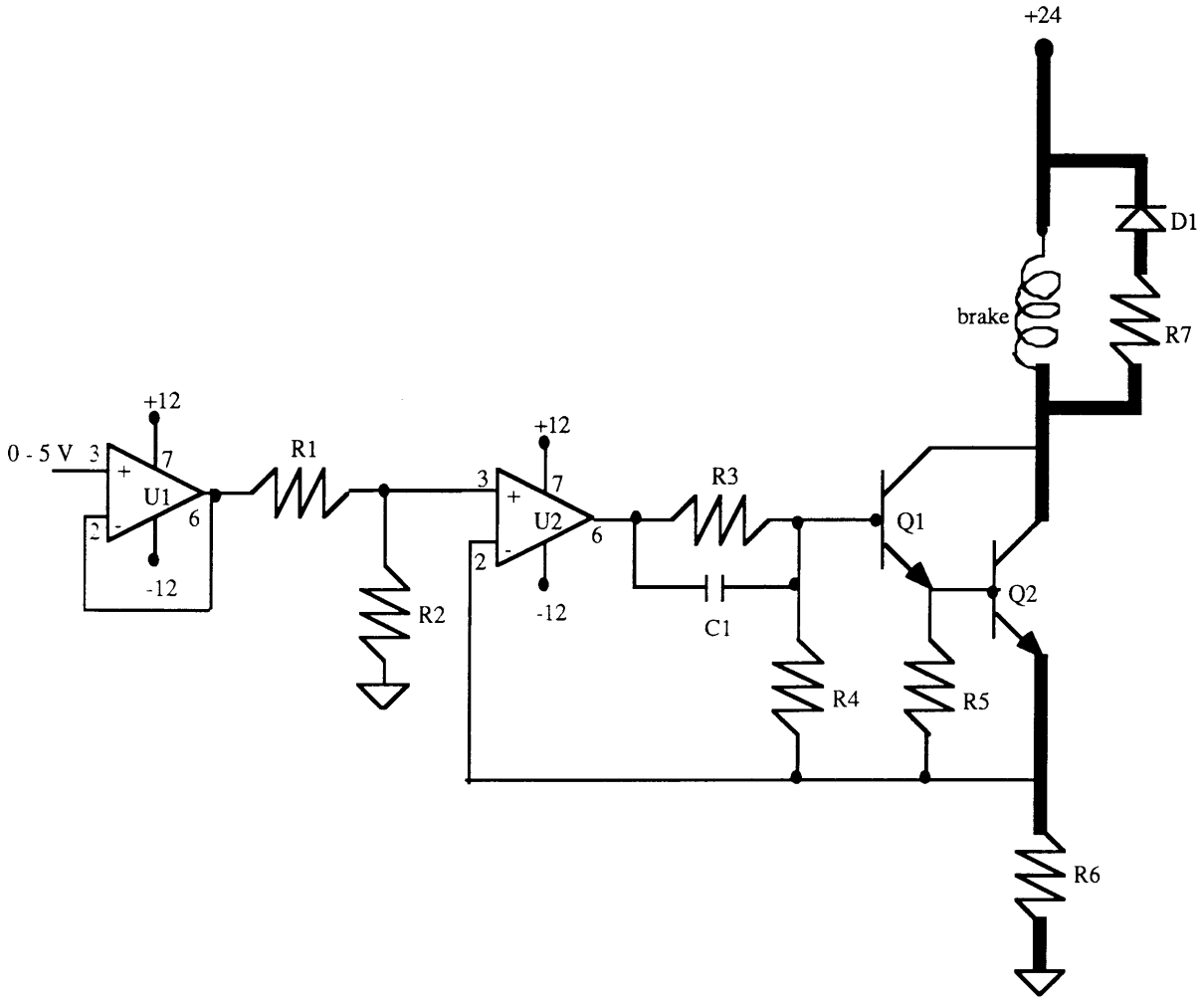

Figure 2-11. Schematic of the CEDO 1 brake driver circuitry.

Table 2-2. Components of the CEDO 1 brake driver circuits.

Component	*Axis 1 (upper axis)*	*Axis 2 (lower axis)*	*Axis 3*
R_1	3.3 kΩ	3.3 kΩ	5.1 kΩ
R_2	5.1 kΩ	5.1 kΩ	3.3 kΩ
R_3	3.9 kΩ	3.9 kΩ	3.9 kΩ
R_4	1 kΩ	1 kΩ	1 kΩ
R_5	10 kΩ	10 kΩ	10 kΩ
R_6	2 Ω	2 Ω	10 Ω
R_7	2 Ω	2 Ω	10 Ω
C_1	100 pF	100 pF	-
D_1	1N4001	1N4001	1N4001
U_1	LM741	LM741	LM741
U_2	LM741	LM741	LM741
Q_1	2N3904	2N3904	2N3904
Q_2	TIP 41B	TIP 41B	TIP 31B

the link to be moved quicker again resulting in an almost oscillatory behavior. (For further information on magnetic particle brake modeling, see Dunfee 1979 or Adelstein 1981.)

Because the brakes were difficult to model quantitatively, values for R_3, R_4, and C_1 were chosen essentially by trial and error. R_3 and R_4 were selected first to provide 41 degrees of phase lead, the maximum phase lead obtainable without adding another amplifier to the circuit. Then C_1, which determines the frequency range at which the phase lead occurs, was chosen by trying a variety of capacitors in the 10 pF to 500 pF range and selecting the one which subjectively provided the smoothest viscous simulation and which objectively resulted in the shortest time delay. The compensator improved the performance of the two large brakes immensely by reducing the rise time of the voltage across the brake to 35 ms. The compensator did not improve the performance of the small brake, whose measured rise time was approximately 80 ms regardless of capacitor values. In future designs a higher supply voltage should be used to reduce the response times of all brakes and of the small brake in particular.

While compensator substantially shortened the large brakes' rise times, it did not effectively shorten the decay times (approximately 200 ms for a step input of -4 volts). A final modification to the circuit involved placing resistor R_7 in series with the fly-back diode D_1, as illustrated in Figure 2-11, to further reduce the time needed for the current in each brake coil to decay. Although additional steps could have been taken to reduce the brakes' response times, the CEDO subjectively felt fine for low to moderately-high damping coefficients and it was assumed that during tracking tasks the brakes would not be required to step from zero to maximum torque or from maximum torque to zero in times much shorter than these compensated response times.

2.3 Description of Software

The CEDO 1 system software includes data collection and control programs (described in Section 2.3.2), calibration programs (described in Sections 2.4.1 and 2.4.2), and data analysis

programs (described in Chapter 4). Like the electronic hardware, the original CEDO 1 software required extensive revision before any experiments could be performed. All control and calibration programs were written in C and compiled using the Microsoft® C Optimizing Compiler Version 5.0 for the MS-DOS® operating system. All data analysis programs were written for use with either the MATLAB® commercial software for numeric computation or the S-PLUS® interactive software for statistics. A list describing all CEDO 1 programs is included in Appendix D, and instructions for running the CEDO 1 are included in Appendix E.

2.3.1 The Computer

The CEDO 1 control software was developed on a Leading Edge model D2 AT-compatible computer owned by the MIT tremor group. This computer is configured with 640 kilobytes of memory, an 8 MHz clock, an 80287 math coprocessor, an EGA enhanced graphics display adaptor, a Data Translation DT2814 A/D converter, a MetraByte DAS-8 A/D converter, and a MetraByte DDA-06 D/A converter. The Data Translation DT2814 A/D converter has 16 single-ended analog input channels with 12-bit resolution and is used to convert the analog position and velocity signals into the digital signals required by the computer. The MetraByte DDA-06 D/A converter has 6 analog output channels with 12-bit resolution and is used to convert the computer's digital brake current commands into the analog voltages required by the brake driver circuitry. The MetraByte DAS-8 A/D board has an Intel 8254 programmable interval timer and is used to generate the 60 Hz control signal.

Many of the clinical experiments in this study were performed with a Northgate 386 computer configured with 1024 kilobytes of memory, a 30 MHz clock, and the same A/D and D/A boards as MIT's 286 computer, owned by the Burke Rehabilitation Center of White Plains, NY. Since the 386 computer was equipped with a color monitor, a faster clock, and more memory than the 286 computer, it was better suited for the pursuit tracking experiments and data collection.

2.3.2 The CEDO 1 Control Algorithm

The CEDO's damping action is controlled through software. A flow chart for the CEDO 1 control algorithm is shown in Figure 2-12, and each component of the chart is discussed in detail below.

Step 1. Enter Calibration Data:

The first step in the CEDO control algorithm is to read from files the position and velocity calibration data, the screen scale factor data, the damping coefficient data, the target data, and the velocity voltage offset data. The position and velocity calibration files contain the conversion factors needed to convert digital positions and velocities in units of least significant bits (LSBs) into actual angular positions and velocities in units of radians and radians/sec. The screen scale factor file contains data used to scale the CEDO workspace to the screen during the pursuit tracking tasks. The damping coefficient file contains the desired damping coefficients in units of lbf/in/s, lbf/rad/s, lbf/(in/s)^2, and lbf/(rad/s)^2. The target file contains the x and y target data used for the pursuit tracking tasks in units of pixels. Finally, the velocity voltage offset file contains digital velocity data in LSBs, recorded with the CEDO held stationary, which are subtracted from angular velocity readings to improve accuracy.

Step 2. Initialize Timer:

All CEDO 1 control programs depend on the MetraByte DAS-8 A/D converter and timer board to generate a 60 Hz control cycle. The timer initialization step consists of loading the proper mode into clocks one and two, loading the proper count into clocks one and two, disabling the interrupts, and clearing the polling bit. To set the interrupt polling bit every 1/60th of a second, the board is configured so that the clock 2 output cascades into the clock 1 input and the clock 1 output connects to the interrupt input pin [Maxwell 1990].

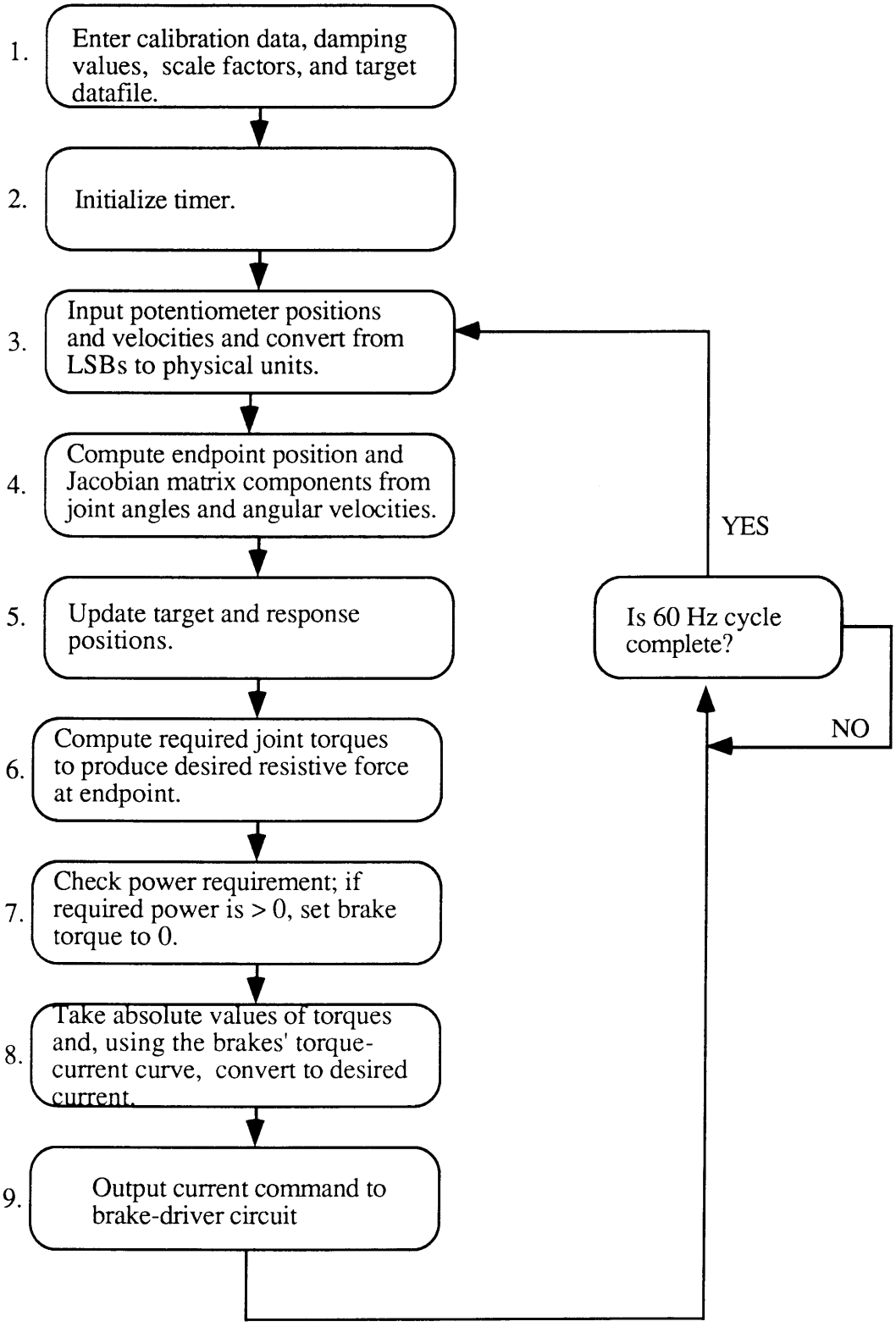

Figure 2-12. Schematic of the basic CEDO 1 control algorithm.

Step 3. Input Potentiometer Positions and Velocities:

Position and velocity signals from the position/velocity circuits are digitized via the Data Translations 2814 A/D board. Calibration data are then used to convert the digitized data into physical units.

Step 4. Compute Endpoint Position and Jacobian Matrix:

The CEDO 1 measures *joint positions* and computes *joint velocities* via the differentiator circuitry. However, to display the response cursor in pursuit tracking tasks the *endpoint position* is needed and to generate an endpoint force proportional to endpoint velocity the *endpoint velocity* is needed. The purpose of Step 4 in the control algorithm is to obtain the endpoint data from the measured joint positions, the computed joint velocities, and the CEDO linkage geometry shown in Figure 2-13. First, the CEDO endpoint position relative to the CEDO "home position", defined as the position at which θ_1, θ_2, and θ_3 are all zero (θ_3 is the rotational angle of the third degree of freedom not shown in the figure), is found from the CEDO geometry:

$$p_x = -\frac{2}{3}d_1\sin(\theta_1) + d_5(1-\cos(\theta_1)) - d_3(1-\cos(\theta_2)) \tag{2-4}$$

$$p_y = -\frac{2}{3}d_1(1-\cos(\theta_1)) - d_5\sin(\theta_1) + d_3\sin(\theta_2) \tag{2-5}$$

Next, Equations 2-4 and 2-5 are differentiated with respect to time to obtain a relationship between the endpoint linear velocity and the known joint angular velocities ω_1 and ω_2:

$$v_x = \left[d_5\sin(\theta_1) - \frac{2}{3}d_1\cos(\theta_1)\right]\omega_1 - \left[d_3\sin(\theta_2)\right]\omega_2 \tag{2-6}$$

$$v_y = \left[-\frac{2}{3}d_1\sin(\theta_1) - d_5\cos(\theta_1)\right]\omega_1 + \left[d_3\cos(\theta_2)\right]\omega_2 \tag{2-7}$$

Finally, Equations 2-6 and 2-7 are put into matrix form. If V is the vector of endpoint velocities, F is the vector of endpoint forces, W is the vector of joint angular velocities, T is the vector of joint torques, and J is the Jacobian matrix whose elements are the coefficients in Equations 2-6 and 2-7:

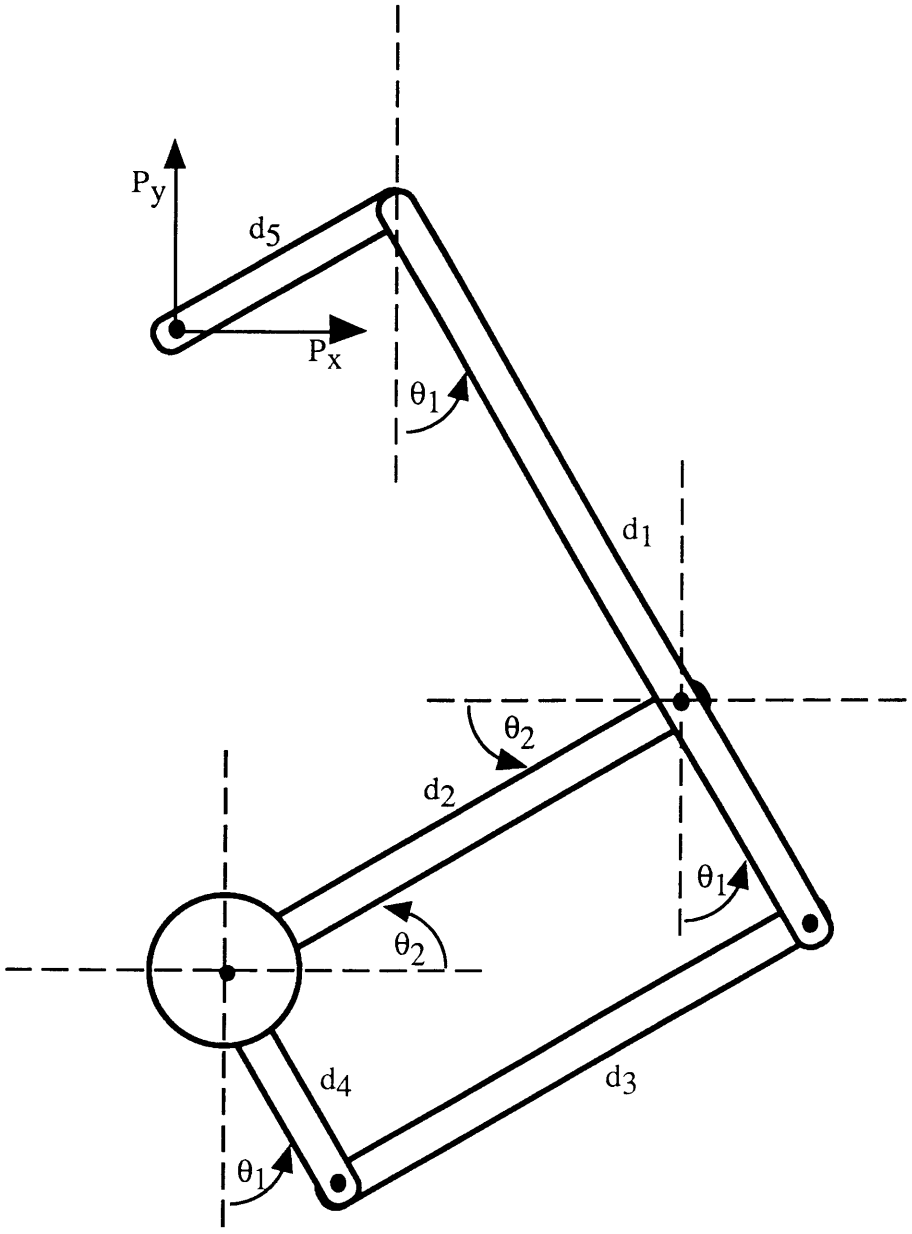

Figure 2-13. Important linkage geometry for computing the CEDO 1 endpoint position.

$$J = \begin{bmatrix} d_5\sin(\theta_1) - \frac{2}{3}d_1\cos(\theta_1) & -d_3\sin(\theta_2) \\ -\frac{2}{3}d_1\sin(\theta_1) - d_5\cos(\theta_1) & -d_3\cos(\theta_2) \end{bmatrix} \quad (2\text{-}8)$$

then the relationship between endpoint space and joint space is represented by:

$$\vec{V} = \mathbf{J}\vec{W} \quad (2\text{-}9)$$

$$\vec{T} = \mathbf{J}^t\vec{W} \quad (2\text{-}10)$$

Step 5. Update Target and Response Positions:

In programs involving a pursuit tracking task, the target and response positions are updated in Step 5. The target location is obtained from the target datafile and the response location is obtained from the actual CEDO endpoint position, computed in Equations 2-4 and 2-5, converted from units of inches to units of screen pixels using the screen scale factor data. The pursuit tracking task is discussed further in Section 3.2.3.

Step 6. Compute Required Joint Torques:

Once the Jacobian matrix and endpoint velocity components are found from Equations 2-8 and 2-9, the joint torques required to generate an endpoint force proportional to the endpoint velocity or to the square of the endpoint velocity are computed. For linear viscous damping, the endpoint resistive force vector should be colinear to the endpoint velocity vector and proportional to its magnitude:

$$\vec{F} \parallel \vec{V} \quad (2\text{-}11)$$

$$|F| = -c|V| \quad (2\text{-}12)$$

These requirements, along with Equations 2-8, 2-9, and 2-10, determine the CEDO joint torque vector required for linear damping:

$$\vec{T} = \mathbf{J}^t\vec{F} = \mathbf{J}^t(-c\vec{V}) = -\mathbf{J}^tc\mathbf{J}\vec{W} \quad (2\text{-}13)$$

$$\begin{bmatrix} T_1 \\ T_2 \end{bmatrix} = -c \begin{bmatrix} (j_{11}^2 + j_{21}^2)\,\omega_1 + (j_{11}j_{12} + j_{21}j_{22})\,\omega_2 \\ (j_{11}j_{12} + j_{21}j_{22})\,\omega_1 + (j_{12}^2 + j_{22}^2)\,\omega_2 \end{bmatrix} \quad (2\text{-}14)$$

For non-linear velocity-squared or "turbulent" damping, the endpoint resistive force vector should be colinear to the endpoint velocity vector and proportional to the square of its magnitude:

$$\vec{F} \parallel \vec{V} \tag{2-15}$$

$$|F| = -c\,|V|^2 \tag{2-16}$$

These requirements, along with Equations 2-8, 2-9, and 2-10 determine the CEDO joint torque vector required for non-linear damping:

$$\vec{T} = \mathbf{J}^t\vec{F} = \mathbf{J}^t(-c|V|\vec{V}) = -\mathbf{J}^t c|V|\mathbf{J}\vec{W} \tag{2-17}$$

$$\begin{bmatrix} T_1 \\ T_2 \end{bmatrix} = -c\sqrt{V_1^2+V_2^2}\begin{bmatrix} (j_{11}^2 + j_{21}^2)\,\omega_1 + (j_{11}j_{12} + j_{21}j_{22})\,\omega_2 \\ (j_{11}j_{12} + j_{21}j_{22})\,\omega_1 + (j_{12}^2 + j_{22}^2)\,\omega_2 \end{bmatrix} \tag{2-18}$$

Because the CEDO third degree of freedom is a single rotational joint, obtaining the torque required at axis 3 is less complicated than obtaining the torque required at axes 1 and 2. For both linear and non-linear damping, the raw angular velocity data for the third axis is converted to radians/sec and is then used directly to determine the required torque:

$$T_3 = -b\,\omega_3 \quad \text{(linear)} \tag{2-19}$$

$$T_3 = -b\,|\omega_3|\,\omega_3 \quad \text{(non-linear)} \tag{2-20}$$

Step 7. Check Power Requirements:

In the transformation between joint coordinates and endpoint coordinates, CEDO axes 1 and 2 are not completely de-coupled. One unfortunate result of this fact is that for certain linkage configurations, positive power is required to produce an endpoint force that is colinear to the endpoint velocity. Since the CEDO 1 is equipped with energy-dissipating brakes, not motors, it cannot meet the positive power requirement and therefore cannot simulate viscous damping for certain velocities and certain CEDO linkage configurations as explained above in Section 2.2.1. The purpose of Step 7 in the CEDO control algorithm is to check the sign of the required power at each joint as computed in Step 6. If positive power is "required" at a joint, the brake torque at that joint is set to 0.

Step 8. Convert Torques to Currents:

In Step 8, the brakes' torque-current curves are used to determine the brake current needed to generate the joint torques computed in Steps 6 and 7. These curves were obtained by fitting second-order polynomial equations to torque-current data from the brake manufacturer's specification sheets for the small and large brakes as discussed later in Section 2.4.5. The desired current values are then converted from units of amperes to units of LSBs.

Step 9. Output Current Command to Brake Driver Circuit:

In Step 9, analog signals representing the desired current for each brake are sent via the MetraByte DAS-8 D/A converter to the brake-driver circuitry. The computer then waits until the interrupt polling bit is set, signalling the completion of the clock cycle, before returning to Step 1 to repeat the loop. The control algorithm continues until a set number of loops have been completed or until the user presses a key on the keyboard to terminate the program.

2.4 System Calibration and Characterization

Before collecting clinical data, the following six procedures were developed to calibrate and characterize the CEDO 1 system and to insure that all hardware and software were working properly:

1. calibration procedures were developed to convert angular position and angular velocity from units of computer bits to radians and radians/sec;
2. the stiffness and inertia of the linkage was estimated to verify that the CEDO 1 meets Baiges' original static and dynamic design specifications;
3. the velocity circuitry cut-off frequencies were measured to verify that the position signals are indeed being differentiated;
4. the brakes' static torque-current curves were measured to make sure they match the curves supplied by the manufacturer;

5. data were collected to verify that the CEDO 1 endpoint force is proportional to the endpoint velocity during linear damping simulations and proportional to the square of the endpoint velocity during non-linear damping simulations; and
6. a model of the CEDO 1 was developed to estimate the force required by the user at the CEDO endpoint with and without the CEDO's damping loads.

2.4.1 Position Calibration

Software program PCALC was written to guide the CEDO angular position calibration procedure. This program asks the user to position the CEDO, one axis at a time, in a particular configuration with respect to the CEDO home position. (Generally a protractor taped into position is used to locate axes 1 and 2 while a Wedge Innovations digital level is used to locate axis 3.) For each known configuration, the input voltage from the position/velocity circuitry and A/D converter is read. Finally, after 9 readings, the linear least-squares relationship between actual position in radians and voltage input in LSBs is computed. This procedure is done separately for each axis so that one, two, or all axes can be re-calibrated in a given session as necessary. The CEDO 1 must be re-calibrated any time the links are disassembled, the potentiometers are re-positioned, or the trimpots in the electronics box are re-adjusted. The slopes, intercepts, correlation coefficients, and ranges of rotation (referenced to the CEDO home position for each axis) for a typical calibration session are presented in Table 2-3.

Table 2-3. CEDO 1 angular position calibration data and ranges for each axis.

CEDO Axis	*Intercept (radians)*	*Slope (radians/LSB)*	*Correlation Coefficient*	*Range (degrees)*
Axis 1	-1.044	0.000557	.9995	-45 to +70
Axis 2	-.9693	0.000528	.9975	-55 to +65
Axis 3	-1.105	0.000643	.9997	-60 to +85

2.4.2 Velocity Calibration

The CEDO 1 angular velocity calibration procedure does not require the user to move the CEDO axes at known angular velocities. Rather, the velocity conversion factor b_2 is computed from the the position conversion factor b_1 and the electronics gains G_p and G_d for each CEDO axis:

$$b_2 = \frac{b_1 G_p}{G_d} \tag{2-21}$$

where b_1, b_2, G_p, and G_d are defined in the position/velocity circuit block diagram in Figure 2-14. To derive this expression, let P_a be the voltage at point A representing position, P_b be the voltage at point B representing position, V_c be the voltage at point C representing velocity, V_d be the digital signal at point D representing velocity, P_{phys} be the actual CEDO axis position in physical units of radians, and V_{phys} be the actual CEDO axis velocity in physical units of radians/second. Then, from Figure 2-14, the following relationship is obtained:

$$V_c = G_d \frac{d}{dt}(P_a) = G_d \frac{d}{dt}\left(\frac{P_a}{G_p}\right) = \frac{G_d}{G_p}\frac{d}{dt}\left(\frac{P_{phys}}{b_1}\right) \tag{2-22}$$

Next, using Equation 2-22 and the fact that V_{phys} is the derivative of P_{phys}, an expression for V_{phys} can be derived in terms of the angular velocity V_c:

$$V_{phys} = \frac{dP_{phys}}{dt} = \frac{b_1 G_p}{G_d} V_c \tag{2-23}$$

Finally, when V_c is converted from an analog signal to a digital signal via the A/D converter, the desired conversion factor b_2 is obtained:

$$V_{phys} = \left(\frac{b_1 G_p}{G_d}\right) V_d = b_2 V_d \tag{2-24}$$

The position conversion factor b_1 in Equation 2-24 is simply the slope of the best-fit line determined from the PCALC program. The electronics gains G_p and G_d depend on resistor and capacitor values in the circuitry and are measured experimentally by inputting sine waves

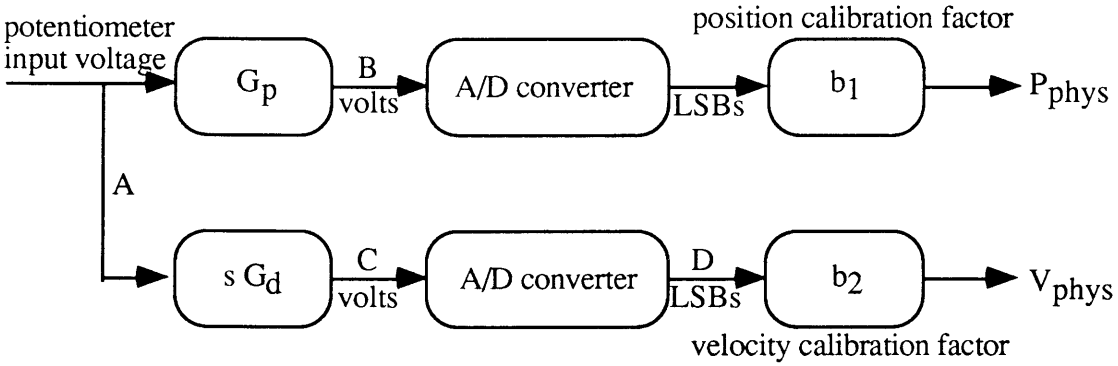

Figure 2-14. Block diagram for deriving the CEDO 1 angular velocity calibration gains.

with known amplitudes and frequencies into the circuit, measuring the output position signals and velocity signals on an oscilloscope, and computing the following ratios:

$$G_p = \frac{\text{position output amplitude}}{\text{input amplitude}} \tag{2-25}$$

$$G_d = \frac{\text{max velocity output amplitude}}{\text{input amplitude} \times 2\pi \text{ (input frequency)}} \tag{2-26}$$

For this particular study, five sine waves with amplitudes between 0-5 volts and frequencies between 0-4 Hz were input to each position/velocity circuit, the outputs were monitored on an oscilloscope, and the resulting G_p and G_d were averaged. Typical G_p, G_d, and b_2 values for each axis are listed in Table 2-4. Because b_2 must be changed whenever b_1 is changed, CEDO software program VCALC was written to compute the velocity conversion factors from the electronics gains and the position gains and must be run whenever PCALC is run. G_p and G_d should be re-entered into the VCALC program whenever any resistor or capacitor value in the position/velocity circuitry is changed.

In addition to calibration parameters, velocity offsets are used in all control programs. The program OFFSETC measures the voltage from the velocity circuitry with the CEDO held stationary. Any voltage drifts which occur in the system are measured and subtracted from the actual angular velocity readings to improve accuracy.

Table 2-4. CEDO 1 angular velocity calibration data for each axis.

CEDO Axis	*Gp*	*Gd*	*b2*
Axis 1	1.178	.3340	.000557
Axis 2	1.178	.3934	.000528
Axis 3	.9377	.1435	.000643

2.4.3 Verification of Static and Dynamic Design Specifications

Although Baiges designed the CEDO 1 based on static and dynamic analyses of its behavior, he did not experimentally measure its stiffness in the horizontal and vertical directions after it was built to verify that his design specifications were indeed met. Making such measurements is an important part of characterizing the system because if the linkage is designed or machined improperly, the inertia and elasticity that it interposes between the user and the brakes could cause the CEDO 1 to resonate or to deflect inappropriately.

The CEDO 1 can be modeled dynamically in 1-dof lumped-parameter form as a grounded dashpot in series with a spring and a mass. In the context of this model, as explained in Baiges' thesis, the mass and the stiffness of the linkage are constrained by two concerns. First, the minimum value of $\sqrt{km}/2$, i.e. half of the square root of the product of the effective endpoint mass and spring constant, must be greater than the maximum damping constant to prevent the possibility of resonance. Further, the resonant frequency $\sqrt{k/m}$ should be kept well above the expected tremor frequencies. This imposes the standard engineering problem of minimizing mass while maximizing stiffness.

Verifying that the CEDO's horizontal stiffness and effective mass meet this dynamic requirement involved several steps. Since the CEDO's horizontal compliance stems primarily from links 1, 3, and 4 (the transmission links) and is greatest with θ_1 and θ_2 equal to 0 degrees (yielding a 90 degree angle between the proximal links), measurements were taken for this worst-case configuration only. The CEDO 1 was disassembled from the wheelchair and clamped to a flat rigid surface, link 4 was clamped to fix θ_1 at 0 degrees, a spring scale was used to apply forces between 4 and 24 lbf at the endpoint, and a dial indicator with a resolution of 0.001 inches was used to measure the endpoint deflection. The approximate horizontal stiffness of the linkage -- **230 lbf/in or 40000 N/m** -- was then obtained from the slope of the deflection vs force plot shown in Figure 2-15.

To estimate the effective endpoint mass of the linkage in the same configuration, the inertia of the linkage about the brakes' axis of rotation was calculated from a model of the CEDO 1

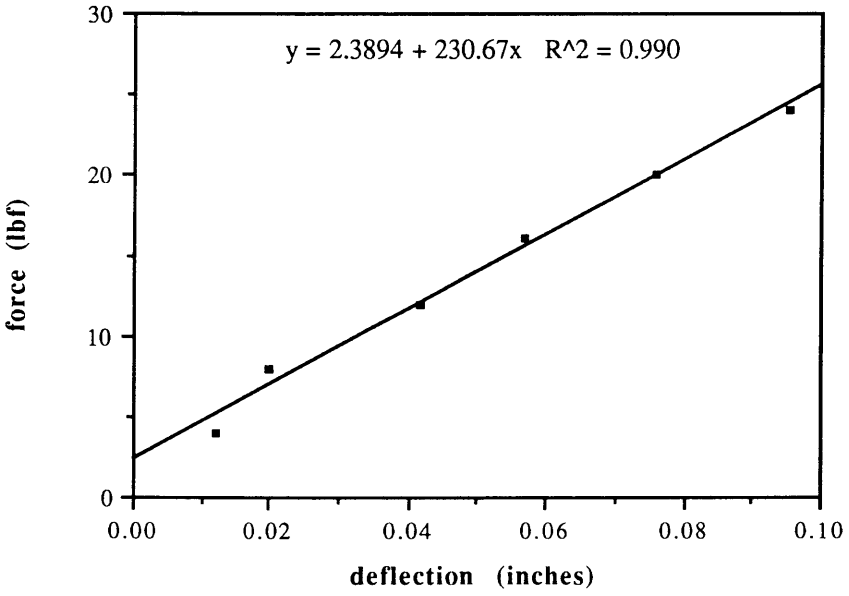

Figure 2-15. Deflection vs force plot for determining the horizontal stiffness of the CEDO 1 linkage.

(this calculation is discussed further in Section 2.4.7), and this value was divided by the square of the distance between the endpoint and the axis of rotation to obtain a mass estimate of **4.1 kg.** Using these values for k and m and a maximum damping constant of 90 N/m/s, the presumption that the CEDO 1 meets Baiges' original dynamic criterion is verified:

$$90 \text{ N/(m/s)} < 200 \text{ N/(m/s)} \quad \Rightarrow \quad c < \frac{1}{2}\sqrt{km} \tag{2-27}$$

In the vertical direction in which the orthosis must serve as a "rigid" restraint, the stiffness of the linkage must not only prevent resonance, but must also prevent disconcerting downward deflection and bounce of the orthosis endpoint under the weight and time-varying muscle forces of the user's arm. After conducting ad hoc experiments and consulting the anthropometrics literature [for example, Van Cott & Kinkaid 1972], Baiges specified a maximum downward deflection of 0.2 inches under a maximum downward load of 50 lbs assuming that this much movement would be imperceptible to the user and would be comparable to the compression of the user's skin and soft tissue. The link dimensions were then determined based on a static model of the linkage geometry using appropriate material properties.

The actual vertical deflection of the linkage was measured using the spring scale and dial indicator with the CEDO 1 in its most extended configuration and with the angle between the proximal CEDO links at 90 degrees. The resulting deflection vs force plots, shown in Figure 2-16, indicate that the CEDO 1 does *not* meet Baiges static criteria defined above, i.e. a 40 lbf load produces a deflection of 0.5 inches with the orthosis in its most extended configuration and a deflection of 0.3 inches with the angle between the proximal links at 90 degrees. The additional deflection measured in the vertical direction most likely stems from play in the bearings and joints which were not accounted for in Baiges' static model. Although the CEDO fails to meet Baiges' original static design criteria, it's vertical deflection is subjectively imperceptible under the lighter loads typically applied by tremor-disabled users.

(a)

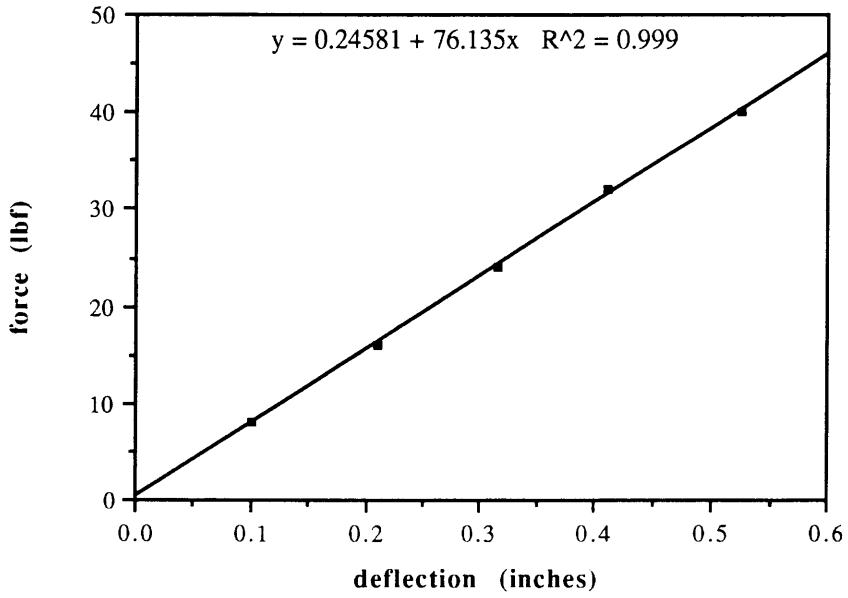

(b)

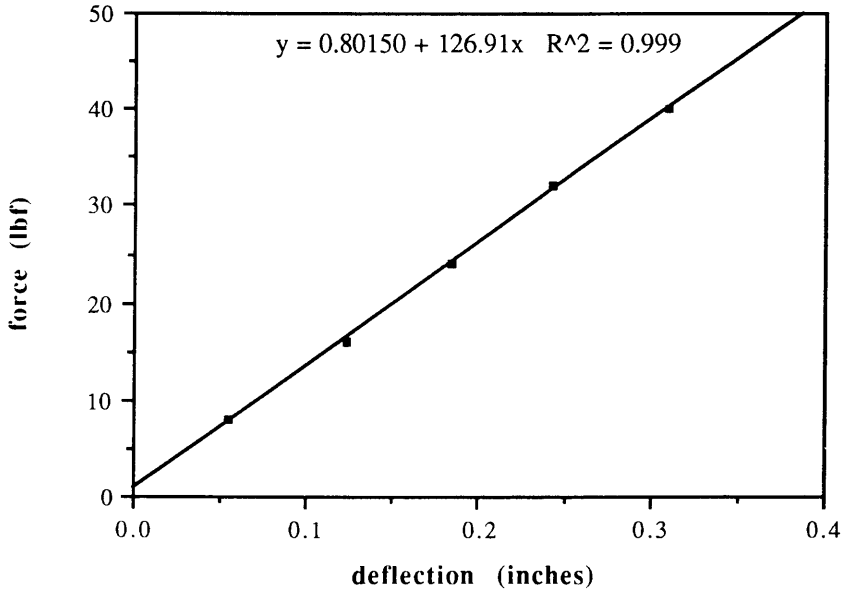

Figure 2-16. Deflection vs force plots for determining the vertical stiffness of the CEDO 1 linkage with (a) the linkage fully extended and (b) the angle between the proximal links at 90 degrees.

2.4.4 *Verification of Velocity Circuitry Cut-Off Frequencies*

As shown previously in Equation 2-1 of Section 2.2.2, the transfer function for the velocity circuitry has two poles so that input signals below the $1/R_2C_2$ corner frequency (13 Hz for axes 1 and 2; 8 Hz for axis 3) are differentiated and scaled while unwanted high frequency signals above the $1/R_1C_1$ corner frequency (18 Hz for axes 1 and 2; 9 Hz for axis 3) are attenuated. These corner frequency values were confirmed experimentally by applying sine waves of known amplitudes and frequencies to each circuit from a function generator, monitoring the resulting output voltages on an oscilloscope, and plotting the ratio of output voltage to input voltage in decibels versus frequency. These bode magnitude plots, shown in Figure 2-17, verify that the roll-off frequencies, determined by the poles of the system, have the expected values and are appropriately placed above the expected pathological tremor frequencies.

2.4.5 *Verification of Torque-Current Curves for the Brakes*

The static torque-current curves provided by the manufacturer (Placid Industries, Inc.) for the large and small brakes are shown in Figure 2-18 and the second-order polynomials which best fit these curves and which are used in the CEDO 1 control algorithm are given below:

$$i_L = 0.0293 + 0.0183\ t_L - 0.0000464\ t_L^2 \qquad (2\text{-}28)$$

$$i_S = 6.83 + 22.26\ t_S - 0.428\ t_S^2 \qquad (2\text{-}29)$$

In these equations, i_L and t_L are the current (amps) and torque (lbf-in) for the large brakes and i_S and t_S are the current (mA) and torque (lbf-in) for the small brake. These torque-current curves were verified experimentally by partially disassembling the CEDO, attaching wires to the CEDO links coupled directly to the shafts of brakes 2 and 3, running each wire over a pulley, attaching known masses (ranging from 10 grams to 3500 grams) to the free end of each wire, and monitoring the brake current needed to balance the torques acting on each link. For each mass, the brake current was increased until the brake torque just balanced the known

(a)

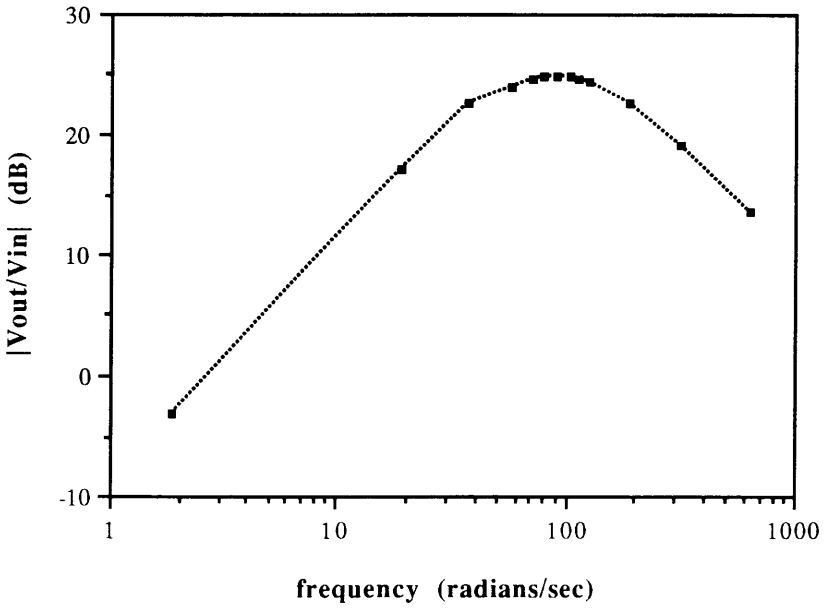

(b)

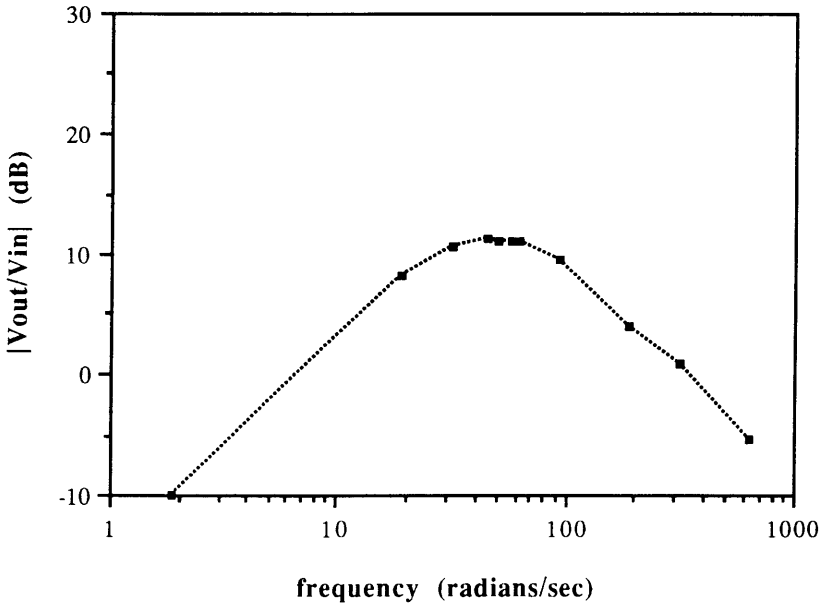

Figure 2-17. Experimentally-obtained Bode magnitude plots for the differentiator circuits for (a) axes 1 and 2 and (b) axis 3.

(a)

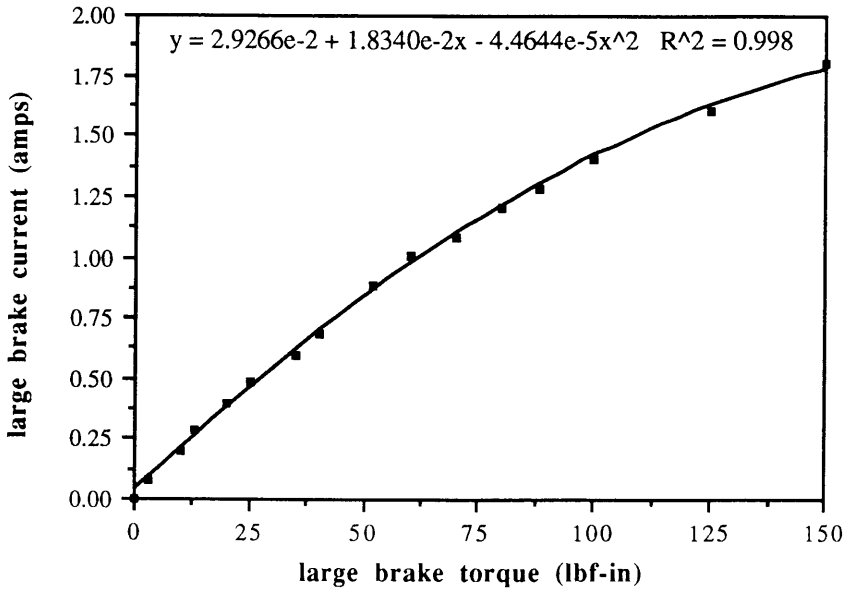

(b)

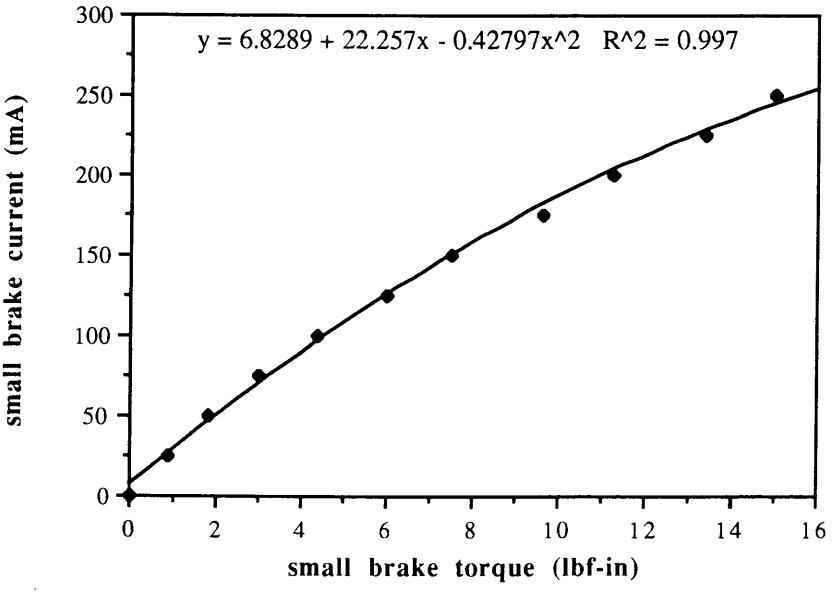

Figure 2-18. Torque-current curves for (a) the large brakes and (b) the small brake from data provided by the manufacturer.

torque from gravity acting on the mass. Masses were first incremented and then decremented to assess hysteresis effects. The resulting experimentally-obtained torque-current curves for the large and small brakes are shown in Figure 2-19. For both brakes, the measured torque-current curves are approximately linear and resemble the curves provided by the manufacturer. Apparently some magnetic hysteresis does occur as less current is needed to produce a given torque for a step down in torque than for a step up in torque.

2.4.6 Verification of Linear and Non-linear Damping Loads

Before using the CEDO 1 in experiments, data were collected to confirm that the CEDO's control algorithm simulates linear viscous damping or non-linear turbulent damping in the horizontal plane. Because the CEDO 1 is not equipped with a force transducer, a Measurement Systems, Inc. isometric joystick was taped securely to the CEDO endpoint to provide a measure of the x and y components of endpoint force. Then, while controlling the CEDO at a known damping level, the CEDO endpoint was moved at various velocities in the workspace via the joystick handle. The CEDO joint positions and angular velocities were recorded, and from this data the endpoint velocities were computed. Finally, the measured endpoint force was plotted versus the endpoint velocity for viscous damping and versus the square of the endpoint velocity for turbulent damping. Results for one linear and one non-linear damping coefficient are shown in Figures 2-20 and 2-21, respectively. Qualitatively the plots show the sort of deviation from straight lines expected from the presence of an inertial component to the load and from the fact that some of the data was taken in zones in which the kinematics prevent force and velocity from being colinear (see Section 2.2.1). The average slopes of the plots, determined by linear regression, do match the selected damping constants with reasonable accuracy. Available linear damping coefficients for the CEDO 1 range from 0 to 90 N/m/s (0 to 0.5 lbf/in/s) for the large brakes and 0 to 1 N-m/rad/s (0 to 8 lbf-in/rad/s) for the small brake. Available non-linear damping coefficients range from 0 to 210 $N/(m/s)^2$ (0 to 0.03 $lbf/(in/s)^2$) for the large brakes and 0 to 0.17 $N\text{-}m/(rad/s)^2$ (0 to 1.5 $lbf\text{-}in/(rad/s)^2$) for the small brake.

(a)

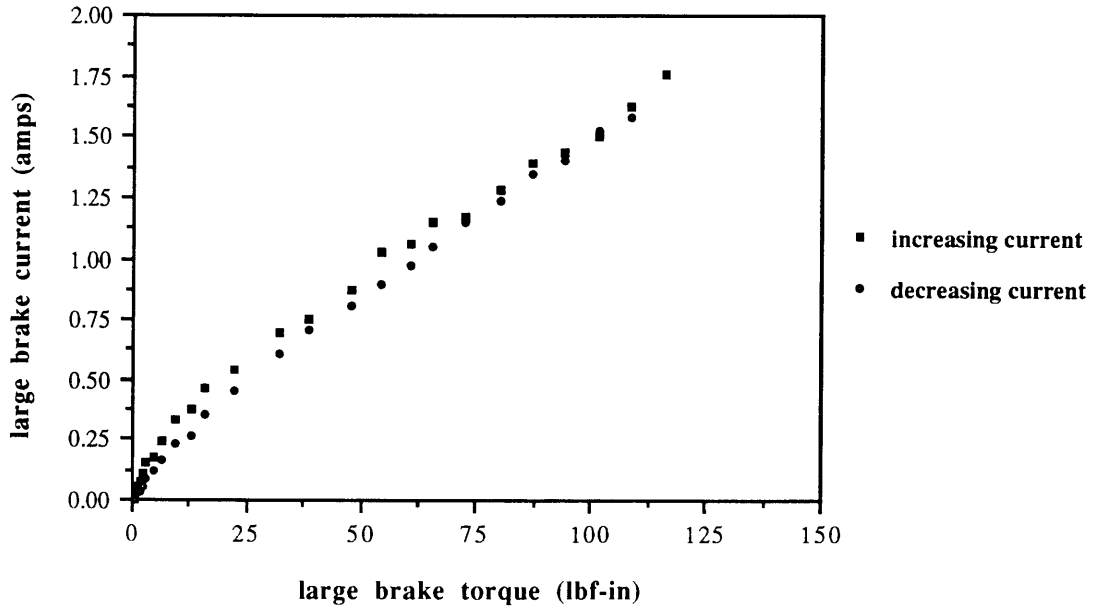

(b)

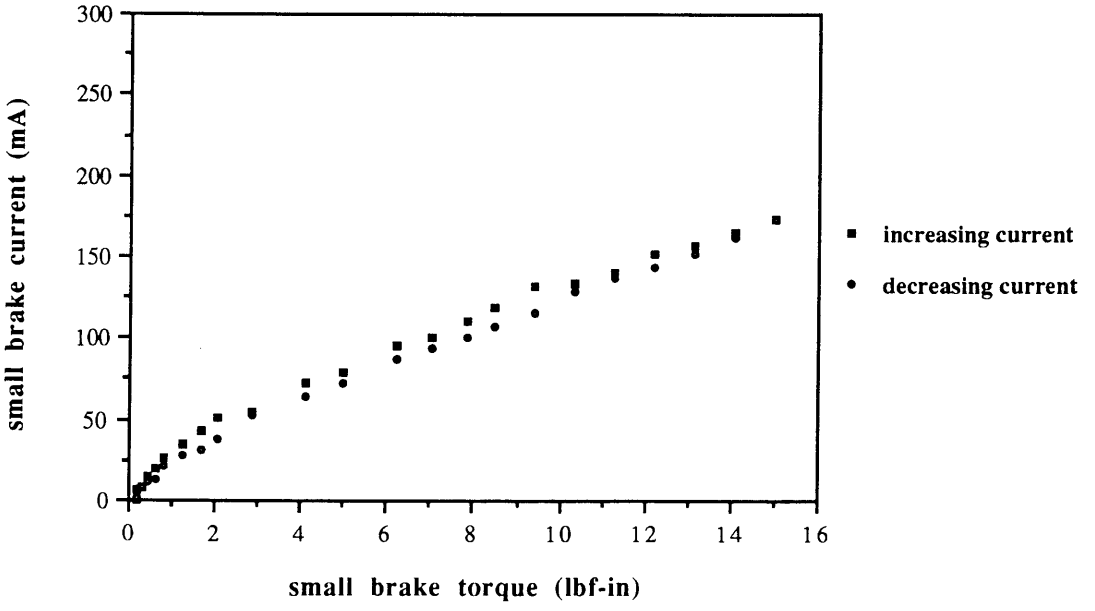

Figure 2-19. Torque-current curves for (a) the large brakes and (b) the small brake from data obtained experimentally.

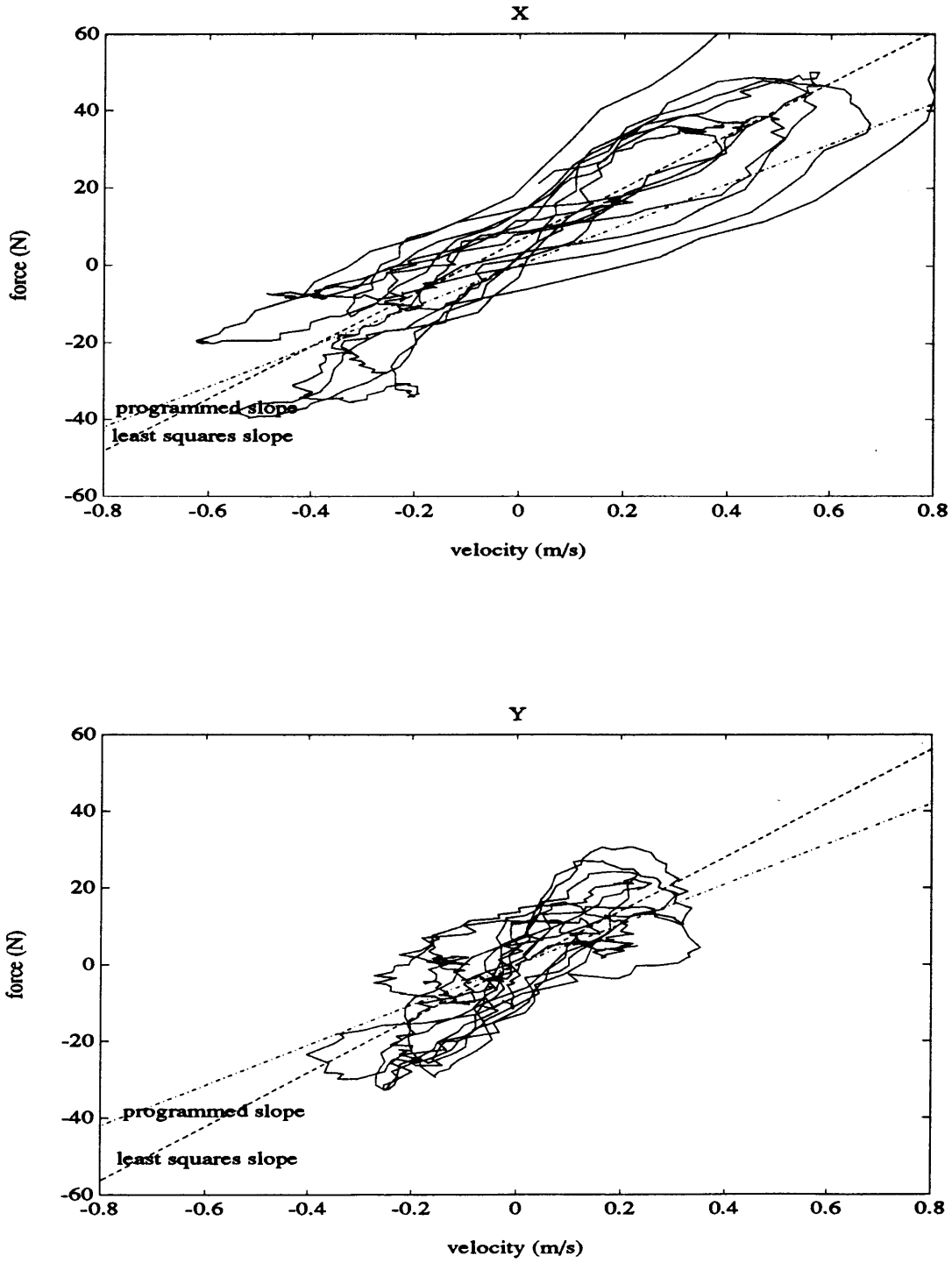

Figure 2-20. Verification of linear damping for a damping coefficient of 55 N/m/s.

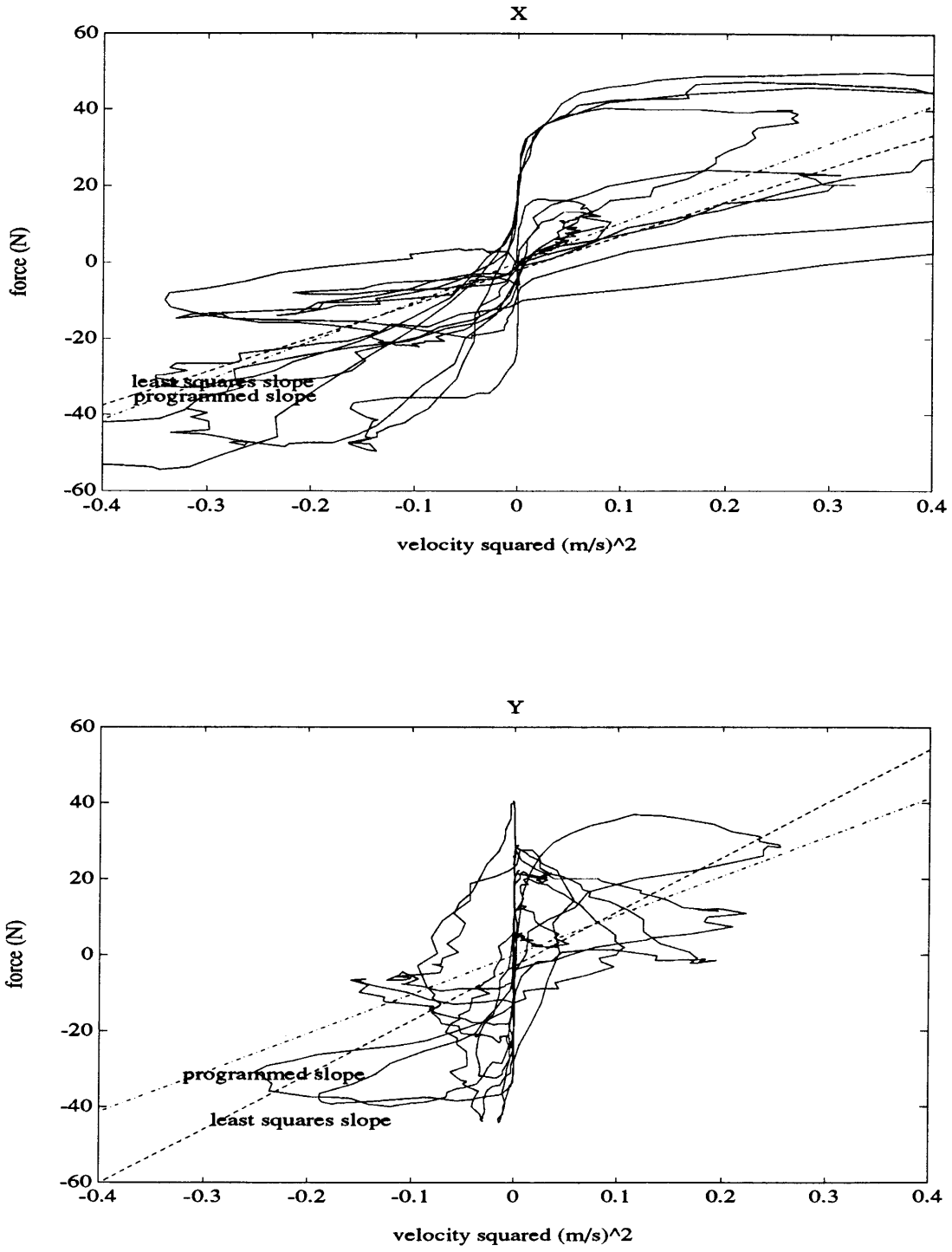

Figure 2-21. Verification of non-linear damping for a damping coefficient of 105 N/(m/s)^2.

2.4.7 Estimation of User Force Requirements

Determining the forces that the user exerts during an experimental trial to overcome the CEDO's inertia and any additional damping or inertial loads is also important part of characterizing the system. Since the CEDO 1 is not equipped with an endpoint force transducer, and since the isometric joystick referred to in Section 2.4.6 could not be used during an experimental trial, a dynamic model was derived to estimate what the user's force must have been as a function of time given records of the CEDO joint positions and joint angular velocities from an experimental trial. The components of the CEDO device which contribute to its dynamic behavior and which are included in the model are the inertias of the five links, the inertias of the four joints, and the inertia of any externally-applied (for experimental purposes) mass at the endpoint. Endpoint forces which are included in the model are the forces from the user and the forces from the linear and non-linear damping loads. All friction and compliance from the orthosis and limb coupler is ignored. Notation for this analysis is shown in Figure 2-22. Detailed geometry and calculations are provided in Appendix F.

The equation of motion for the CEDO 1 model is obtained by balancing torques about reference point O. That is, the sum of the torques about O from the externally-applied forces must balance the rate of change of angular momentum of the CEDO links and joints:

$$\Sigma\tau_O = (\tau_{linear} + \tau_{nonlinear} + \tau_{user})_O = \left(\frac{d\vec{H}}{dt}\right)_O \qquad (2\text{-}30)$$

The damping torques about point O, τ_{linear} and $\tau_{nonlinear}$, are each the sum of two torque components (one component from each degree of freedom θ_1 and θ_2) and are calculated from the Jacobian matrix and the joint velocity time records as expressed previously in Equations 2-14 and 2-18. The applied torque about point O, τ_{user}, is the quantity to be solved for and can be used to compute the user's applied endpoint force, F_{user}, as a function of time:

$$F_{user} = \mathbf{J}\ \tau_{user} \qquad (2\text{-}31)$$

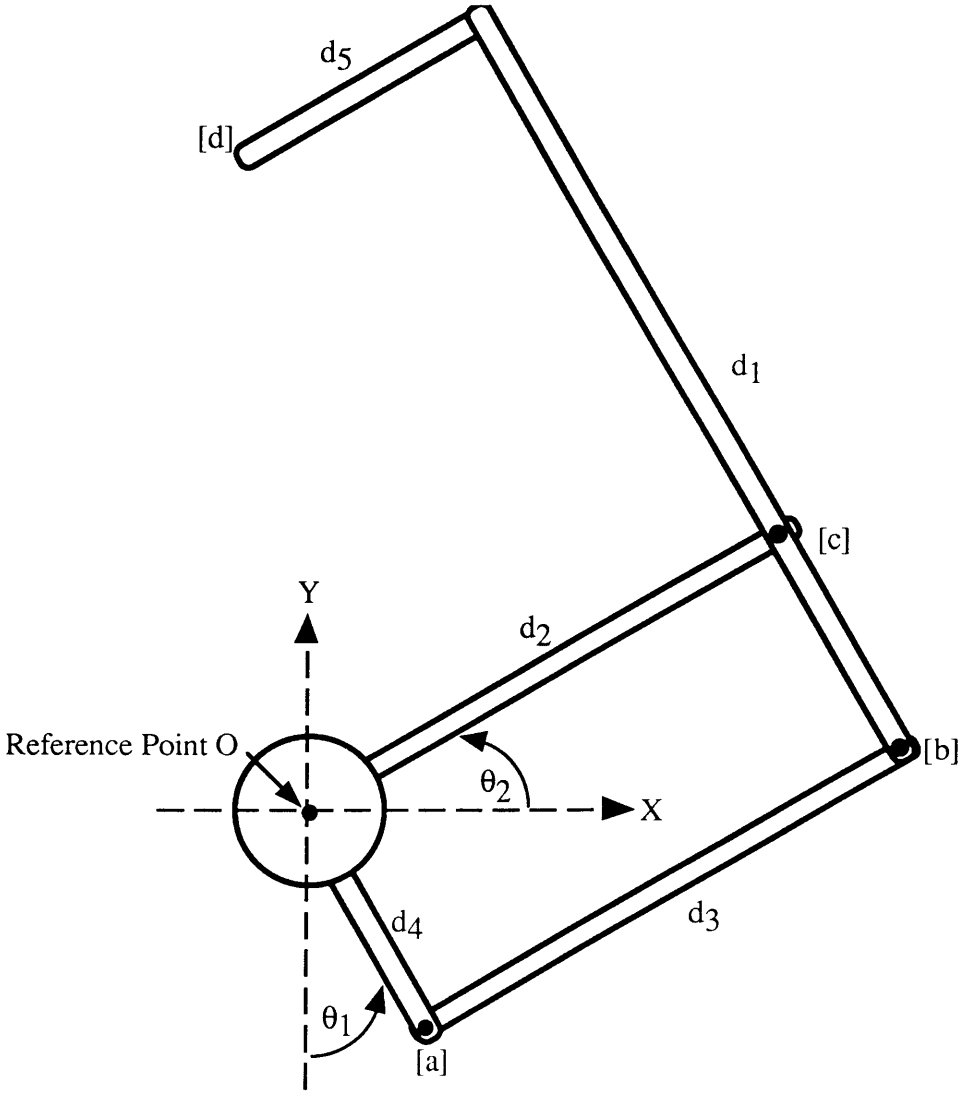

Figure 2-22. Links, joints, and coordinates used in the CEDO model.

H_o is the total angular momentum of the system about point O and is obtained from summing the angular momentum of the five links, the four joints, and the externally-applied mass.

Although computing τ_{linear} and $\tau_{nonlinear}$ from Equations 2-14 and 2-18 is relatively straightforward, determining the rate of change of H_o is more complicated. The inertias of the five links, the four CEDO joints, and the applied mass all contribute to H_o, and the angular momentum of each must be computed from:

$$\vec{h}_o = \vec{h}_c + \vec{r}_c \times m\vec{v}_c \tag{2-32}$$

where h_c is the angular momentum of the component about its centroid, r_c is the position vector from point O to the component's centroid, m is the mass of the component, and v_c is the velocity of the component's centroid. For the five links, h_c is obtained from:

$$\vec{h}_c = I_c \vec{\omega}_c \tag{2-33}$$

where I_c is the moment of inertia of the link about its centroid and ω_c is the angular velocity of the link about its centroid. Assuming the links are hollow cylinders, I_c is calculated from:

$$I_c = \frac{m_{link}}{12}\left[3(R^2 - r^2) + h^2\right] \tag{2-34}$$

where m_{link} is the mass of the link, R and r are the outer and inner diameters of the link, and h is the length of the link. The link mass m_{link} is estimated from the link volume V and the density of 6061 aluminum, ρ_a:

$$m_{link} = \rho_a V = \rho_a \pi (R^2 - r^2) h \tag{2-35}$$

Finally, the $r_c \times m_{link} v_c$ term in Equation 2-32 is calculated by expressing the position vector of each link in the x-y coordinate system of Figure 2-22, differentiating to obtain velocity, multiplying velocity by the mass obtained in Equation 2-35, and taking the cross-product:

$$\vec{r}_c \times m\vec{v}_c = m(r_x v_y - v_x r_y)\hat{z} \tag{2-36}$$

Values for ρ_a, R, r, h, m_{link}, and I_c, and expressions for r_c and v_c for each link are given in Appendix F. Because the four joints and the applied endpoint mass are assumed to act as point masses, their contributions to the system angular momentum H_o consist only of the $r_c \times m_{joint} v_c$ terms in Equation 2-32. For joints a, b, and c, m_{joint} is estimated by summing the

masses of the joint components -- two sets of roller bearings (measured), a steel shaft (estimated from the radius t, length s, and density ρ_s), and two aluminum plugs which couple the links to the shafts (estimated from the radii R and t, the lengths L and l, and density ρ_a):

$$m = m_{bearings} + \left(\rho_s \pi t^2 s\right)_{shaft} + \left(\rho_a \left[L^3 - \pi R^3 L\right]\right)_{plug1} + \left(\rho_a \left[l^3 - \pi t^3 l\right]\right)_{plug2} \qquad (2\text{-}37)$$

The mass of joint d, which includes particle brake 3, was measured using a balance scale after disassembling the joint from the CEDO. The $r_c \times m_{joint} v_c$ terms were then calculated by expressing the position vector of each joint in the x-y coordinate system of Figure 2-22, differentiating to obtain velocity, multiplying velocity by the mass of the joint, and taking the cross-product. Values for ρ_s, and m_{joint} and expressions for r_c and v_c for each joint are also given in Appendix F.

MATLAB program DYNAMICS was written to implement the above calculations. In the program, the linear and non-linear damping torques are calculated given the CEDO angular position and angular velocity data and the damping coefficients used for the trial. Then the angular momenta time records for each joint and link are computed from the CEDO angular position and angular velocity data, differentiated, and filtered using a second order Butterworth filter with cutoff frequency at 6 Hz. Finally τ_{user} is solved for from Equation 2-30 and F_{user} is solved for from Equation 2-31. Because singularity points occur in the user torque time records whenever the user's force vector is colinear to point O causing peaks in the numerical solution for F_{user} (i.e. the program attempts to divide by a zero moment arm), all such points are removed before finding the mean and median user force levels for a given trial. The DYNAMICS program was used to calculate the effective mass of the linkage for the analysis in Section 2.4.3, to estimate the contribution of the inertial force to the CEDO's total endpoint force, and to compare the forces from linear and non-linear damping trials with tremor and tracking performance scores to determine whether one damping scheme may require less force (and perhaps be less fatiguing) than the other while still providing similar beneficial effects.

Chapter 3
Protocol

3.1 Experimental Objectives

As stated in Chapter 1, the purpose of this study was to assess the effectiveness of the CEDO 1 both as a research tool for quantifying tremor characteristics and as a prototype orthosis for assisting tremor-disabled individuals. Because little experimentation had been done with the CEDO 1 prior to this investigation, the protocol was designed to answer as many questions about the CEDO 1 and its effects on tremor as possible and to determine which experimental factors influence these answers. Specific questions addressed in this study include:

1. Do the CEDO's linear and non-linear damping loads suppress upper-extremity pathological intention tremor? How much damping is necessary or desirable in an assistive orthosis for tremor-disabled individuals? Is one type of damping preferable to the other?
2. How consistent are measurements of upper extremity tremor, damping effects, and subject performance on 2-dof pursuit tracking tasks from trial to trial within a test session and from day to day over two or more test sessions?
3. How uniform are measurements of upper extremity tremor, damping effects, and subject performance on 2-dof pursuit tracking tasks from subject to subject and from etiology to etiology?
4. How do inertial loads and damped inertial loads affect measured upper extremity tremor and subject performance during 2-dof pursuit tracking tasks? How much inertia is desirable in a tremor-suppressing orthosis?
5. Does a relationship exist between the voluntary force an individual exerts during the pursuit tracking task and the measured characteristics of his or her tremor? If

tremor increases with voluntary force output, is there an optimum level of damping above which tremor actually worsens?

6. What experimental factors influence measured tremor and tracking performance? Are learning or fatigue effects noticeable? Does an individual's tremor or tracking performance vary with the position of his or her arm in the workspace or with the type of target being tracked?
7. Are the results from pursuit tracking experiments indicative of how a tremor-suppressing orthosis might enable an individual to perform activities of daily living?

By addressing these questions, it was hoped that the study would guide the planning of future experimental protocols and aid the development of improved assistive orthotics.

3.2 Experimental Methods

Researchers who work regularly with tremor-disabled individuals have reported that "tremor depends upon such variable factors as the precise position of the limbs in relation to the trunk, the patients' physiological state, the patients' drug, caffeine, or tobacco intake, the degree of general motor activity that has proceeded the testing of tremor, and even the personality of the examiner" [Potvin et al 1975]. These variables make designing an experimental protocol for tremor-disabled persons a challenge. In this investigation, attempts were made to keep environmental variables such as time of day, orientation of equipment, and position of the participant's workspace constant from session to session. Fatigue effects, in which a participant's performance is hindered at the end of a test session by fatigue or boredom, and learning effects, in which a participant's performance is improved at the end of a test session by practice or learning, were monitored by repeating the same trial condition near the beginning and end of each session. Trial conditions were randomized within sessions to eliminate the possibility of attributing changes in performance to specific trial conditions if in fact they might have been caused by fatigue or learning. Other participant-specific variables such as psychological state, energy level, and food and drug intake prior to testing were unable

to be controlled. By repeating trial conditions within a session and on different days, however, it was hoped that the averaged results would be less affected by variability in tremor measurements not attributable to the trial conditions.

3.2.1 The Experimental Protocol

The experimental protocol for this investigation is outlined in Table 3-1. As indicated, the protocol is comprised of four test sessions lasting 60 to 90 minutes each. Modifications to the protocol were made as needed to accommodate participants' schedules and abilities. Typically, participants completed one session per day for a period of four days. Participants who were not able to be tested on four days completed two sessions per day or completed a subset of the protocol. To insure that the body of data collected during a session included all trial conditions, trials within each session were grouped into identical sets. Within each set, trial conditions and tracking targets were randomized, and, to assess repeatability, two to four sets were collected per session. Thus, even if a participant became fatigued and had to stop during a session, at least one or two sets of data, with all trial conditions tested, was obtained. Each trial within a set was 30 seconds long. Participants were encouraged to rest between trials as necessary.

The goal of Session 1, as shown in Table 3-1, was to familiarize the participant with the CEDO and the pursuit tracking task. Practice trials were done at low and at high damping levels to determine the limiting levels at which the participant could be tested. If the participant had severe tremor, could he or she do the tracking task undamped without the risk of injury? If the participant had a high-frequency tremor, at what level of damping did the brakes begin to saturate? Trials were then done at one medium level of damping (chosen for each participant based on the results of the practice trials) with various tracking targets in order to determine the effect of target type and speed on tremor and tracking measurements. Other trials were done in which the scaling gain and bias between the participant's workspace and the screen was changed in order to measure the effect of limb position on tremor.

Table 3-1. Outline of the experimental protocol.

Session 1 *Purpose:* Familiarize the participant with the CEDO and tracking task;
Find the upper and lower limits on damping levels;
Explore effects of target type and speed on tracking performance;
Explore effects of limb position in the workspace.

Trials: a) Practice: 4-6 practice trials with various amounts of damping.

b) Targets: 6 target trials at a medium damping level, repeat 2x.

c) Positions: 3 screen scaling trials corresponding to the left, middle, and right areas of the workspace, repeat 3x.

Session 2 *Purpose:* Explore effects of linear and non-linear damping;
Assess the repeatability of results.

Trials: a) Non-damped condition, repeat 3x.

b) Linear damping for 5 different damping levels, repeat 3x.

c) Non-linear damping for 3 different damping levels, repeat 3x.

Session 3 *Purpose:* Explore effects of added inertia and damped inertia;
Assess the repeatability of results.

Trials: a) Non-damped condition, repeat 3x.

b) Linear damping at one medium level of damping, repeat 3x.

c) Mass (7.5 lbs), undamped, repeat 3x.

d) Mass (7.5 lbs) at the medium level of damping, repeat 3x.

e) Linear and non-linear damping from Session 2; repeat 1x.

Session 4 *Purpose:* Assess day-to-day repeatability of results.
Clinical assessment tasks.

Trials: a) Non-damped condition, repeat 1x.

b) Linear and non-linear damping from Session 2; repeat 1x.

c) Inertia and damped inertia from Session 3; repeat 1x.

d) Clinical assessment tasks (undamped, low, and high damping).

During Session 2, linear and non-linear damping trials were done to verify that the CEDO's damping suppresses tremor and to determine the range of damping needed in a tremor-suppressing orthosis. For the linear damping trials, damping levels of 0, 17, 34, 51, 68, and 85 N/m/s (0, 0.1, 0.2, 0.3, 0.4, and 0.5 lbf/in/s) were used for brakes 1 and 2 and proportional damping levels of 0, 0.17, 0.34, 0.51, 0.68, and 0.85 N/rad/s (0, 1.5, 3.0, 4.5, 6.0, and 7.5 lbf-in/rad/s) were used for brake 3. For the non-linear damping trials, damping levels of 0, 69, 138, and 207 $N/(m/s)^2$ (0, 0.01, 0.02, and 0.03 $lb/(in/s)^2$) were used for brakes 1 and 2 and proportional damping levels of 0, 0.055, 0.11, and 0.165 $N\text{-}m/(rad/s)^2$ (0, 0.5, 1.0, and 1.5 $lbf\text{-}in/(rad/s)^2$) were used for brake 3. Damping trials were generally done three times each to assess the repeatability of the results.

During Session 3, inertia trials and damped-inertia trials were done in which a 7.5 lb mass was strapped to the CEDO cuff at the participant's wrist. These trials were included in the study to investigate how the device's inertia affects the user's tremor. Are lightweight orthoses desirable, or does some amount of inertia help suppress tremor? The inertia trials were also done to help answer questions about functional tasks. For instance, occupational therapists sometimes apply wrist weights to the limbs of tremor-disabled individuals to "help" them perform functional tasks. How effective is this strategy? Activities of daily living frequently involve lifting and placing items. Does the application of inertia during the pursuit tracking trials make them more representative of daily activities?

In the final session, trial conditions from Sessions 1 and 2 were re-done to assess day-to-day repeatability. Any part of the protocol that had not been completed during the previous sessions was also done during Session 4. Lastly, participants were instructed to try functional tasks such as pointing and drawing with and without the CEDO's damping loads. Details on the pursuit tracking tasks and the clinical assessment tasks are provided in Sections 3.2.3 and 3.2.4, respectively.

3.2.2 A Typical Test Session

Although the length and content of the test sessions varied to a certain extent from participant to participant and from session to session, the equipment, instructions, and tracking tasks were similar for all participants and all sessions. Prior to an experimental session, the CEDO system was set up, tested, and re-calibrated if necessary. When the participant arrived, the purpose of the experiment was explained and the tracking task was demonstrated. The participant was then asked to sign an informed consent form in accordance with the rules of the *MIT Committee on the Use of Humans as Experimental Subjects* detailing the potential benefits and risks of the procedure. A sample of the informed consent form used for this study is included in Appendix G. The participant was then transferred to the CEDO wheelchair, his or her right arm fitted securely in the CEDO cuff, and the wheelchair positioned a distance of 29 to 32 inches from the computer screen at which the participant could see the screen comfortably. This wheelchair-screen distance (measured from the computer monitor to the participant's forehead) was recorded for each participant and was kept constant in subsequent sessions. To help the participant become accustomed to the CEDO's damping, program CONTROLC, which energizes the CEDO at various damping levels, was run. Then practice tracking tasks were done until the participant understood the mapping between the workspace and the computer screen and the investigator felt confident that further learning effects would be negligible. The last step before beginning the actual trials, when the participant was settled in the CEDO wheelchair, was to secure the participant to the chair with a velcro shoulder strap to minimize his or her trunk movement during the session.

The instructions given to participants regarding the test were simply to "follow the target as accurately as possible." Because the participants were unaccustomed to using their tremorous limb in tasks, they sometimes "cheated" by stabilizing their right arm with their left arm, locking their right arm at the elbow and attempting to use just shoulder and trunk motion to do the task, or waiting for the target marker to approach their response marker before trying to track the target. Participants would usually begin to cheat unconsciously, and they had to be

watched carefully and reminded frequently not to cheat and to use the same tracking strategies throughout the test. Between trials, participants were allowed to rest as long and as frequently as needed for comfort. Questions, comments, and suggestions from participants and those who accompanied them were encouraged. Participants could withdraw from the study at any time.

3.2.3 The Pursuit Tracking Tasks

Pursuit tracking tasks are useful tools for investigating the characteristics of pathological intention tremor for several reasons. First, pursuit tracking tasks are an effective means of inducing participants' intention tremors. Second, by requiring participants to follow pre-programmed targets, pursuit tracking tasks permit participants' voluntary movements to be distinguished from involuntary movements under the assumption that motions linearly related to the targets are voluntary and motions not linearly related to the targets are involuntary. Lastly, pursuit tracking tasks are easily programmed and modified on personal computers and are thus easily incorporated into experimental protocols.

The disadvantages of using pursuit tracking tasks are the restrictions they place on the selection of participants. Participants in an investigation must have the visual, perceptual, and cognitive abilities needed to complete the experimental task. They must be capable of learning the relationship between their workspace and the computer screen, and they must be capable of concentrating for the duration of the task The criteria used in selecting participants for this investigation are discussed further in Section 3.3.1.

The CEDO tracking task used in this investigation resembles a simple video game. During the experiment, the participant is instructed to view a computer screen. Two markers are shown on the screen, a "cross" or response marker which moves as the participant's arm moves, and a "box" which serves as the target and moves along a programmed trajectory. The participant is asked to move his or her limb so that the response marker follows the target marker as accurately as possible. In 2-dof tasks, the CEDO left-right degree of freedom in the

horizontal plane is mapped to the screen horizontal (x) axis and the CEDO front-back degree of freedom in the horizontal plane is mapped to the screen vertical (y) axis. In 1-dof tasks, the CEDO rotational degree of freedom in the vertical plane is mapped to the screen vertical (y) axis.

An important part of designing the CEDO tracking task was programming the target trajectory. Preliminary tracking experiments with the CEDO 1 showed that variables such as target speed, target type, workspace-screen scaling distance, and task length *may influence* an individual's tremor and tracking performance. Thus, care was taken when programming target trajectories for the final CEDO 1 protocol.

Selection of Target Speed and Target Type:

The speed and the type of target trajectories used in the CEDO 1 tracking experiments were determined by the capabilities of the disabled participants and the requirements of the data processing methods. With regard to target speed, the frequency content of all targets had to be high enough that participants' intention tremors were induced by the task, yet low enough that participants did not become frustrated by the task. Equally important, the target frequencies had to be sufficiently lower than the participants' tremor frequencies so that when analyzing the data in the frequency domain, tracking peaks and their harmonics did not overlap with tremor peaks in power spectral density plots. Similarly, with regard to target type, the trajectories of all targets had to be unpredictable enough that participants' did not learn the target trajectory, yet simple enough that participants were not discouraged by the task. The trajectories also had to be complex enough to prevent learning from trial to trial, but straightforward enough that participants felt comfortable with the task after only a few practice trials.

The speed and the type of targets chosen for this investigation differed from those used in previous MIT tremor group investigations. In his 1981 study of wrist tremor, Adelstein had participants track 1-dof sinusoidal targets with frequencies of 0.125, 0.25, 0.5, and 0.75 Hz [Adelstein 1981]. After discovering that the participants learned to track the rhythm of the

single sinusoids over time, however, Adelstein used random signals, low-pass filtered at 0.5 Hz, as targets in further experiments. In 2-dof tracking experiments, Baiges and Maxwell used pseudo-random targets in which the x and y target trajectories were each comprised of sums of sinusoids. Baiges summed seven sine waves with frequencies selected from the prime numbers between 3 and 41 divided by 100 to create the x and y trajectories for his targets [Baiges 1989], while Maxwell summed six sine waves with frequencies of 0.08, 0.12, 0.19, 0.27, 0.42, and 0.5 Hz to create the x and y trajectories for his targets [Maxwell 1990].

Unfortunately, Baiges had some difficulty distinguishing between peaks due to tremor and peaks due to tracking in power spectral density plots when processing his data in the frequency domain. The power spectral density of a random signal, described in detail in Chapter 4, represents the contribution of power at each frequency of the signal to the total power in the signal. By processing tremor records in the frequency domain, then, a measure of the power at tremor frequencies is obtained. If the signal being processed has only one frequency component, the power spectrum contains a single peak at that frequency as shown in Figure 3-1 for a unit amplitude 0.5 Hz sine wave. If the signal being processed has more than one frequency component, the power spectrum contains peaks at each of the component frequencies as shown in Figure 3-2 for a unit amplitude 0.5 Hz square wave. These peaks appear at the square wave's fundamental frequency and at the odd harmonics as predicted by its Fourier series representation:

$$\text{square wave} = \frac{4A}{\pi}\left(\sin\omega t + \frac{1}{3}\sin 3\omega t + \frac{1}{5}\sin 5\omega t + \ldots\right) = \frac{4A}{\pi}\sum_{n=1}^{\infty}\left[\frac{1}{2n-1}\sin(2n-1)\omega t\right] \quad (3\text{-}1)$$

When Baiges processed his data in the frequency domain, he found that the power spectral densities contained, in addition to the peaks expected at target frequencies and pathological tremor frequencies, unexpected peaks at frequencies *between* target and tremor frequencies. Although Baiges did not postulate the origin of these peaks in his thesis, preliminary experiments done for this study suggest that the unexpected peaks seen in his data

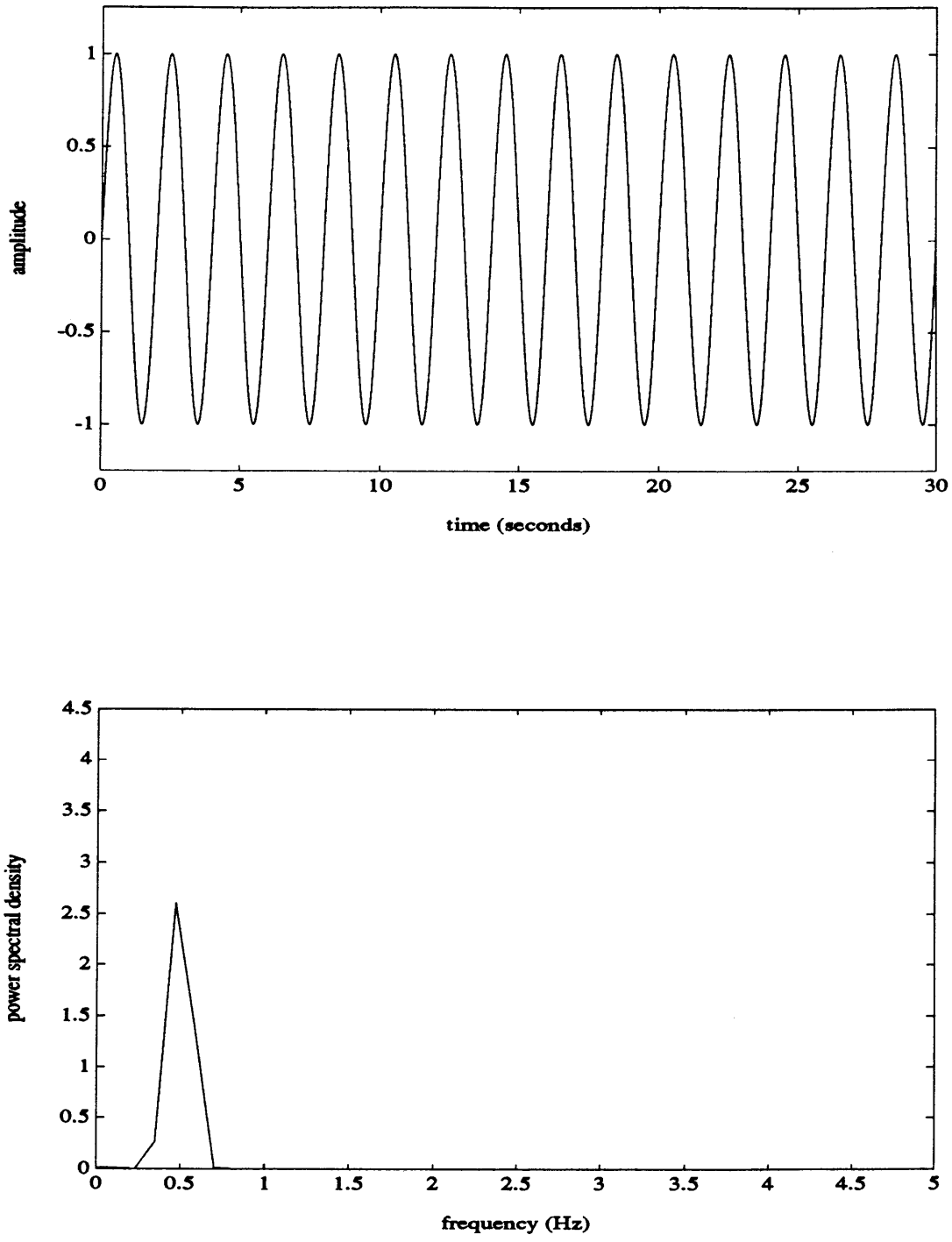

Figure 3-1. Unit amplitude 0.5 Hz sine wave and power spectral density plot.

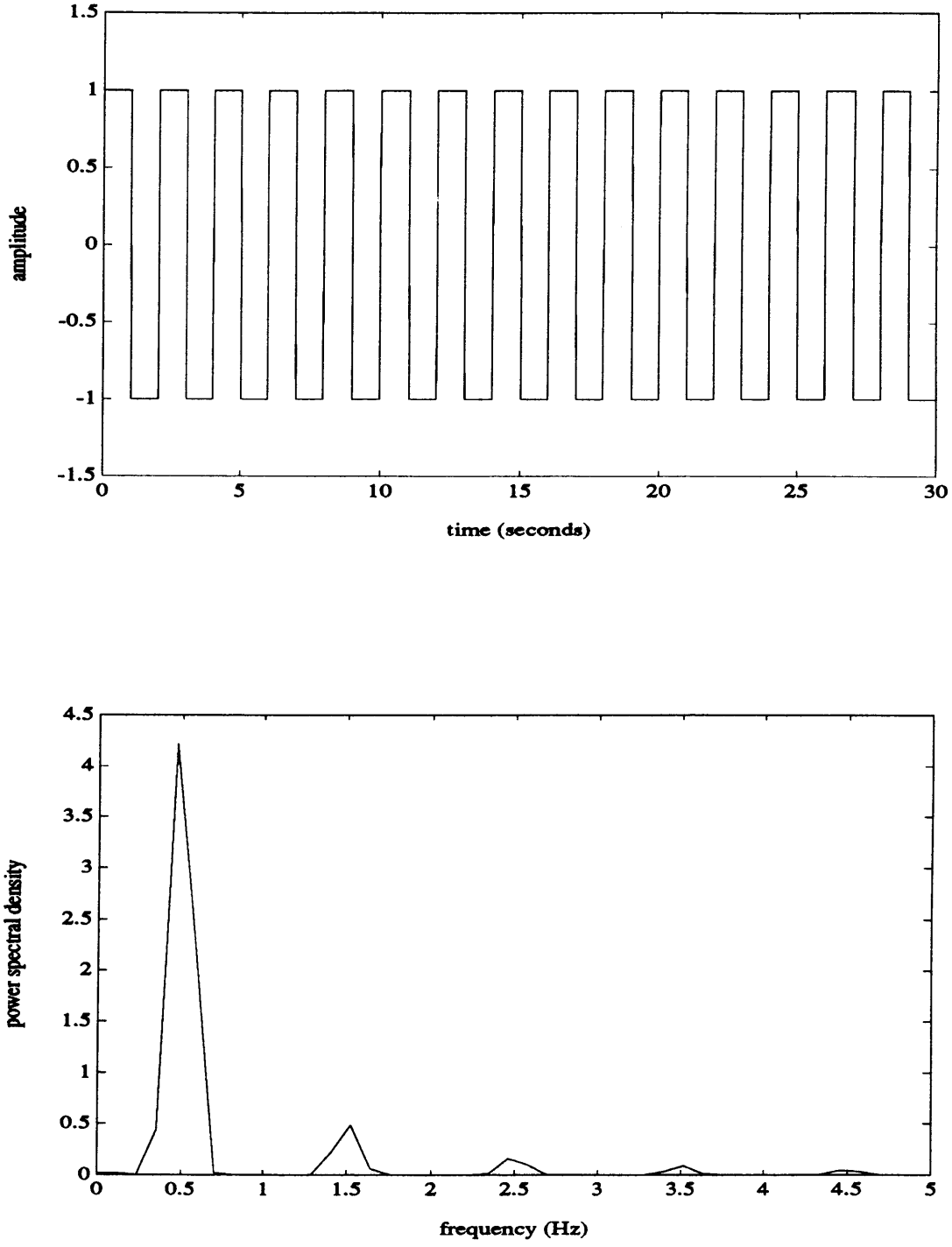

Figure 3-2. Unit amplitude 0.5 Hz square wave and power spectral density plot.

stem from tracking errors. That is, spectral peaks appear at harmonics of the target frequencies because humans do not track sine waves perfectly. If a sinusoidal target is approximated by a "square wave", with Fourier series representation given in Equation 3-1, or by a "triangle wave" with Fourier series representation given in Equation 3-2:

$$\Delta \text{ wave} = \frac{8A}{\pi^2}\left(\sin\omega t - \frac{1}{3}\sin 3\omega t + \frac{1}{5}\sin 5\omega t - \ldots\right) = \frac{8A}{\pi^2}\sum_{n=1}^{\infty}\left[\frac{(-1)^{n+1}}{(2n-1)^2}\sin(2n-1)\omega t\right] \quad (3\text{-}2)$$

then odd harmonics will appear in the power spectrum.

To verify that the peaks observed in the power spectra could be attributed to tracking errors, experiments were done by undergraduate research assistant Winnie Leung in which able-bodied subjects tracked 2-dof targets comprised of either single sine waves or sums of two sine waves of various frequencies. The results of the experiments for one "typical" subject tracking two different sinusoidal targets, showing tracking vs time plots and "residual" power spectral density plots in which the portion of the target spectra linearly related to the response spectra has been subtracted, are presented in Figures 3-3 and 3-4 (processing details are discussed further in Chapter 4). Although the data were not uniform enough across subjects to assert that all humans track sine waves like "square waves" or "triangle waves", and the limited resolution of the spectra combined with leakage effects (discussed further in Chapter 4) make it difficult to determine whether spectral peaks occur at specific harmonics of the target frequency, the data do suggest that low frequency peaks in the power spectra depend upon the frequency of the targets and can be attributed with reasonable certainty to tracking errors. Similar results were obtained in preliminary experiments with tremor-disabled individuals, implying that if tremor peaks are to be distinguished from tracking peaks in frequency domain analyses, target frequencies must be low enough to prevent peaks at approximately the third or fourth target harmonics from interfering with peaks at tremor frequencies. Since pathological tremor frequencies for the upper extremity range typically from 1.0 to 2.5 Hz, target frequencies for the CEDO tracking task were chosen to be less than 0.25 Hz.

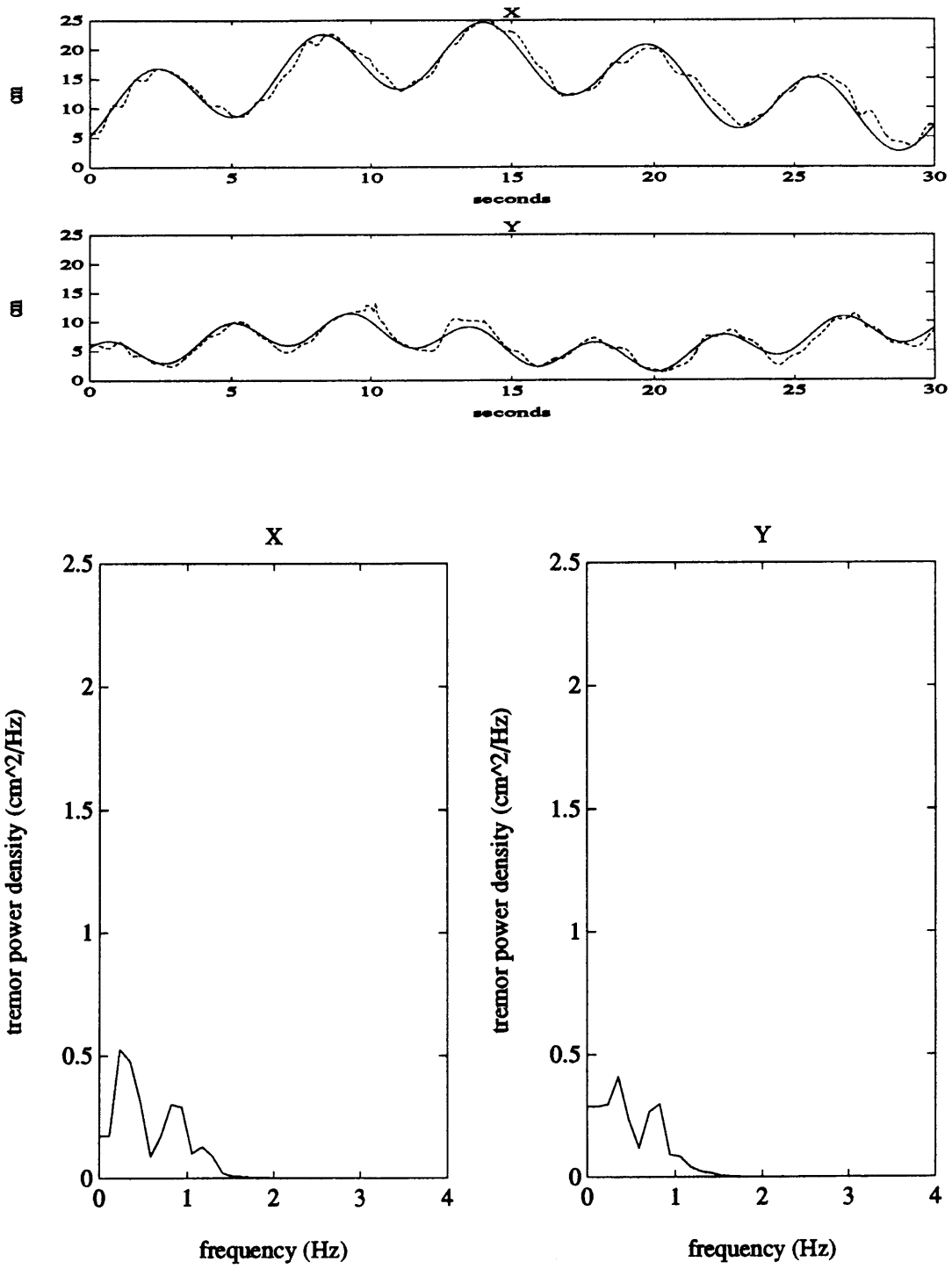

Figure 3-3. Time plots and residual power spectral density plots for one able-bodied subject tracking a sinusoidal target with frequencies of 0.03 and 0.17 Hz in x and 0.05 and 0.23 Hz in y.

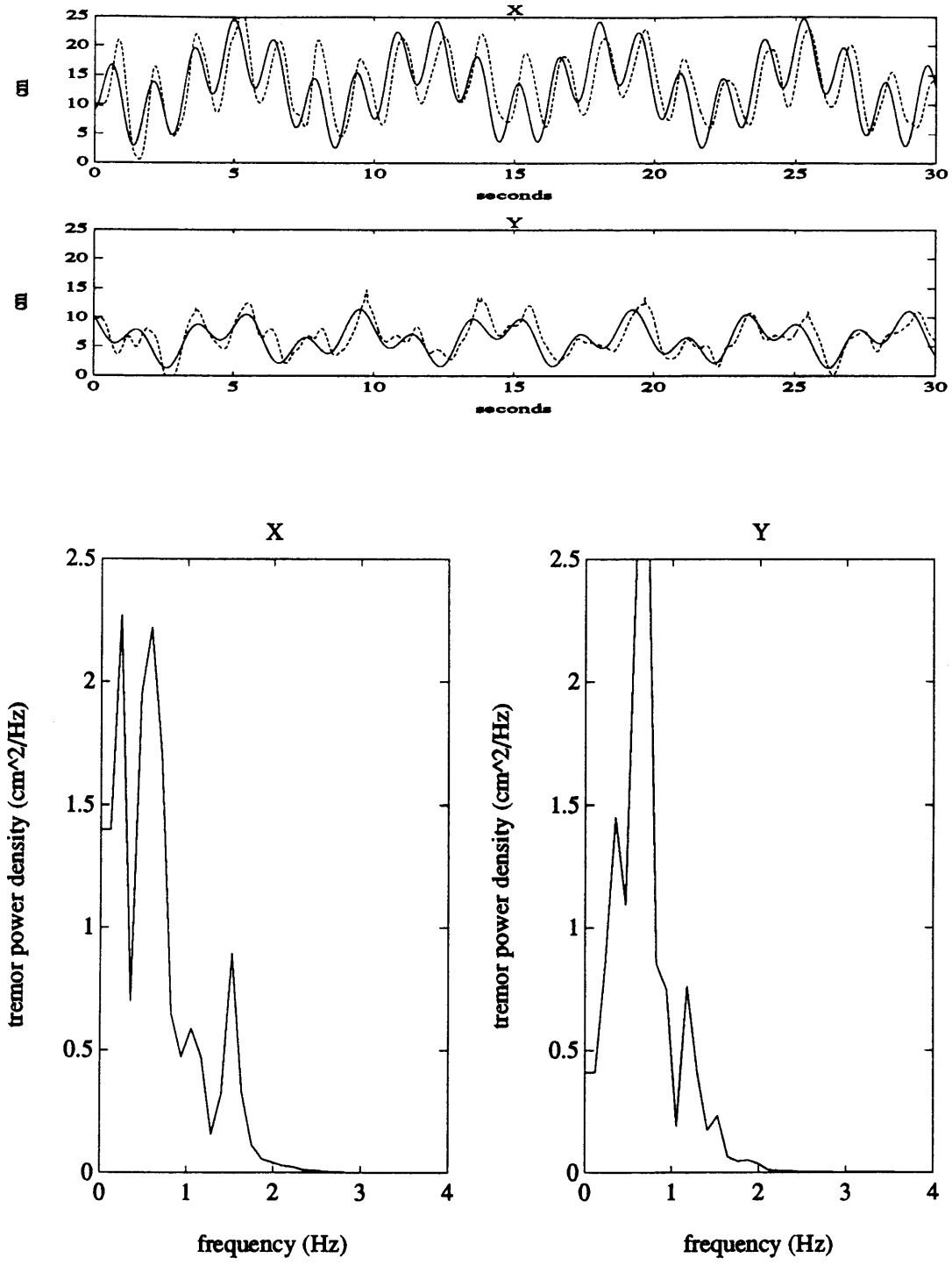

Figure 3-4. Time plots and residual power spectral density plots for the same able-bodied subject tracking a sinusoidal target with frequencies of 0.15 and 0.69 Hz in x and 0.21 and 0.51 Hz in y.

To further explore the role of the target in the pursuit tracking task, a portion of the experimental protocol was devoted to targets. In particular, six different target types (targets whose positions varied linearly, sinusoidally, or as a sum of sinusoids at various frequencies) were used in tracking tasks for some subjects during Session 1 to determine how target type and target speed affect tremor and tracking performance. Simple targets whose position varied linearly with time were used to verify that the low frequency peaks in the spectral plots presumed to be tracking harmonics disappear when tracking errors are not made. These targets were also used to determine whether simple, predictable targets induce intention tremor to the same extent as more unpredictable targets comprised of sums of sine waves. Sinusoidal targets, sums of two sinusoidal targets, and variations of sinusoidal targets were also tried. In some trials the frequencies of the sine waves were not kept constant during the trial but were varied continuously in an attempt to reduce or flatten the low-frequency spectra associated with tracking errors and to thereby accentuate the tremor peaks. Sums of only two sine waves were used, rather than six or seven, to more easily monitor the location of the low-frequency peaks.

The results of the Session 1 target experiments, discussed in greater detail in Chapter 5, suggest that target type and speed *can* affect tremor and tracking performance. Based on the experimental results for the first few participants, targets comprised of sums of two sine waves with continuously varying frequencies were used in subsequent sessions for all participants. Target frequencies in the x direction ranged from 0.05 to 0.25 Hz, and target frequencies in the y direction ranged from 0.07 to 0.19 Hz.

To generate the targets for the tracking experiments, program TARGETC was written. This program generates linear targets, targets comprised of single sine waves, and targets comprised of sums of two sine waves at slow (under 0.23 Hz), fast (under 0.46 Hz), and time-varying frequencies. For both the x and y trajectories of the sinusoidal targets, the program instructs the investigator to input the angle between 0 and 2π at which the sine wave is to begin, and the direction, positive or negative, in which the angle is to increment. Using this method, many targets with the same frequency content were generated by starting the x and y

target trajectories at different angles and incrementing the angles in different directions. This was important to prevent subjects from becoming familiar with the first few seconds of the target history.

Selection of Workspace-Screen Scaling Distances:

The mapping between the CEDO 1 workspace and the computer screen is another factor which can affect participants' tremors and tracking performances. Although the size of the screen and the number of pixels comprising the screen cannot be changed, the mapping between pixels on the screen and inches in the CEDO workspace can be changed in both the x and the y directions using CEDO program SCALEC. This program asks the user to position the CEDO endpoint at the far left corner of the desired workspace and at the near right corner of the desired workspace. The program records the coordinates of the CEDO endpoint at each corner relative to the CEDO home position, and the rectangular workspace defined by these coordinates is mapped to the four corners of the screen. Thus, the program defines not only the size of the CEDO workspace, but also the location of the CEDO workspace in global coordinates relative to the CEDO wheelchair.

To determine appropriate coordinates for scaling the workspace to the screen for participants in the CEDO 1 investigation, preliminary tests were done with four disabled participants and seven able-bodied participants in which the workspace for each participant was scaled to be as large as possible given the physical limits of the CEDO and the length of the participant's arm. Based on the coordinates of the workspaces used in the preliminary tests, a standard 8 inch by 6 inch workspace, within reach of all participants, was defined and used later in the CEDO 1 investigation for all subjects. Other, 5 inch by 4 inch workspaces positioned to the far left, middle, and far right of the CEDO home position were also defined and were used in Session 1 experiments to explore how workspace size and workspace location affect tremor and tracking performance. The workspaces used in the investigation,

defined by the coordinates of the CEDO endpoint relative to the CEDO home position (defined in Section 2.3.2 as the position at which θ_1, θ_2, and θ_3 are all zero), are given in Table 3-2.

Table 3-2. Workspaces used in the CEDO 1 investigation. The coordinates correspond to the position of the CEDO endpoint relative to the CEDO home position in units of inches.

CEDO region	*left coordinate (x)*	*right coordinate (x)*	*top coordinate (y)*	*bottom coordinate (y)*
standard 8x6"	-6	2	8	2
left 5x4"	-11	-6	10	6
middle 5x4"	-2.2	2.8	6	2
right 5x4"	0	5	9	5

Selection of Task Length:

To prevent fatigue effects from contaminating experimental data, the length of tracking tasks and rest periods was chosen with care. Adelstein, in 1-dof wrist tremor experiments, used tracking tasks that were five to six minutes long. His participants did one trial at each test condition, and they rested after each trial [Adelstein 1981]. Baiges and Maxwell, in contrast, used tracking tasks that were one minute long. Their participants did several trials at each test condition and rested only as needed during the experimental session [Baiges 1989, Maxwell 1990].

The primary advantage of using longer-duration tasks is that the resulting data are able to be processed in the frequency domain at high resolution. Because each data record contained over 8000 points in Adelstein's experiments, Adelstein was able to break each record into 1024-point segments, compute a Fast Fourier Transform (FFT) of each segment, and average the FFTs to obtain a frequency resolution of 0.05 Hz. The primary disadvantage of using longer-duration tasks, and the reason shorter trials were used in this investigation, is that some participants with severe intention tremor lack the mental and physical stamina to perform such a task, particularly an upper extremity 2-dof pursuit tracking task. In fact, preliminary

experiments done with disabled individuals in this study indicated that perhaps even one minute trials are too long for some subjects and that 30 second trials are better suited to participants' abilities. Thus, 30 second trials were used in this investigation. To gather enough data, two to four trials at each test condition were done per session, and test conditions were repeated on more than one session. Each data record contained 1800 points, and by splitting the records into 512-point segments for FFT processing, a frequency resolution of 0.117 Hz was obtained. Details on the data processing methods are provided in Chapter 4.

3.2.4 The Clinical Assessment Tasks

Some participants, in addition to the pursuit tracking tasks, were asked to try a variety of functional tasks with and without the CEDO's damping to obtain a basis for comparing the CEDO's quantitative measures of tremor and tracking performance to more traditional measures of tremor and functional disability. Numerous clinical rating scales have been used by neurologists to classify tremor, the majority of which use subjective rankings to quantify an individual's disability based on the amplitude of his or her tremor and on the ability of the individual to perform certain well-defined functional tasks. The standard clinical assessment form used by Dr. Mindy Aisen at the Burke Rehabilitation Center, shown in Appendix H, is a subset of the tremor rating scale proposed by Fahn et al [1988]. Functional tasks ranked in this assessment include writing one's name and date, drawing an "Archimedes spiral", pouring water between two cups, using a spoon to drink/eat "soup," and pointing to keys on a large keyboard.

Unfortunately, the functional tasks on the standard clinical assessment forms are difficult if not impossible to do when one's forearm is secured to the CEDO cuff and one's motion is restricted to the three degrees of freedom allowed by the CEDO linkage. Nearly all of the tasks on the standard clinical assessment forms require some amount of pronation, supination, wrist flexion, or finger prehension -- movements that are prohibited by the CEDO cuff. Moreover, the configuration of the CEDO linkage prevents its user from resting his or her forearm on a

tabletop and thus greatly hinders writing, drawing, and other tabletop activities. These observations do not imply that the CEDO 1 is a useless device; rather, they point out weaknesses in the current design and establish design goals to be addressed in future devices. The CEDO 1 is a prototype orthosis built to determine whether damping loads are feasible means of suppressing whole-arm intention tremor; it has not yet optimized for functional tasks.

Baiges also recognized that the CEDO's limitations make the standard clinical assessment tasks difficult, and he defined two other functional assessment tasks -- a hoop test and a keyboard test -- with which to evaluate the CEDO's effectiveness in his experiments [Baiges 1989]. In Baiges' hoop test, participants were required to capture a series of pegs with a hoop attached to the end of the orthosis, and they were scored based on the time they took to successfully capture 6 pegs. In Baiges' keyboard test, participants were required to strike keys on a large keyboard with a pointer attached to the end of the orthosis, and they were similarly scored based on the time they took to correctly strike a sequence of keys. Interestingly, his participants "scores" on the tests did not reflect their own subjective observations regarding the effectiveness of the damping in either test. Baiges predicted his participants would complete the tasks faster with damping. In actuality, however, they completed the tasks slower with damping because they had more control of their arms and consequently attempted to be more accurate [Baiges 1989].

Because Baiges' hoop tests and keyboard tests were inconclusive, three other functional tasks were tried in this investigation. The three tasks, defined in Appendix H and described briefly below, were taken from Fahn et al's clinical tremor scale [1988] and modified so that they could be preformed with the arm movements allowed by the CEDO:

1. *Tremor Amplitude*: In this task, the amplitude of the subject's tremor is estimated while his/her limb is at rest and relaxed, in a postural maintenance situation, and in action while alternatively touching the tip of his/her nose and the investigator's hand with his/her extended finger. This task is identical to one of the standard clinical

assessment tasks, and the subject's score is based on the amplitude of the tremor oscillations.

2. *Drawing Lines:* In this task the subject is asked to draw between two parallel lines separated by 0.5 cm, 1.0 cm or 2.0 cm using whole arm motions. Because the CEDO 1 prevents subjects from reaching the tabletop when gripping a regular pen, a "pen extender" was molded from Multiform thermoplastic material (Ali-Med Inc. catalog #4033, Dedham MA) for use in the drawing tasks. The pen extender has a T-grip handle and enables subjects to draw on a clipboard held below the CEDO linkage (approximately 8 inches below the CEDO cuff). Subjects are scored based on which of the three sets of parallel lines they successfully draw between (inside 0.5 cm bounds is normal; outside 2.0 cm bounds is severely disabled). The task is done in the vertical plane and in the horizontal plane in both the x and y directions.
3. *Drawing the Archimedes Spiral:* In this task the subject is asked to trace a version of the standard Archimedes spiral test using the pen extender and whole arm movements. Subjects are scored based on how well they stay between the lines of the spiral (no deviations from the path is normal; unable to complete the drawing is defined as "severely disabled").

Tasks were typically done at zero damping, a low level of damping, and a high level of damping to assess the effectiveness of the CEDO's damping loads.

Results from these functional assessment tasks are discussed in Chapter 5. While the clinical assessment did not provide nearly the kind of objective information about tremor and damping effects that the pursuit tracking tasks did, the assessment did provide some indication of how the CEDO 1 must be improved before it will be a functionally useful orthosis.

3.3 Participants

3.3.1 Criteria for Selecting Participants

The disabled individuals who participated in this study were selected from inpatient and outpatient populations at the Burke Rehabilitation Center in White Plains, NY and from hospitals, rehabilitation centers, and homes for the disabled in the Boston, MA and Concord, NH areas. All participants were diagnosed as having moderate to severe pathological cerebellar intention tremor due to multiple sclerosis, cerebellar injury, or cerebellar degeneration. (Further information on these and other neurological disorders which cause tremor is provided in Appendix A.) Since the CEDO 1 was built to measure whole-arm movements of the right upper extremity, participants were selected only if they exhibited intention tremor at the shoulder and/or elbow of their right arm. Participants also had to be free of cognitive or visual impairments that would hinder their performance on pursuit tracking tasks, and they had to demonstrate volitional movement. Further, participants had to have the necessary physical strength and mental stamina to complete a 30 to 60 minute test session, the mobility to be transferred to the CEDO wheelchair, and the willingness to cooperate for two to four sessions of testing.

3.3.2 Descriptions of Participants

Five participants met the criteria outlined in Section 3.3.1 and completed at least two sessions of the experimental protocol. These participants, in order of increasing tremor severity, are:

	Age	*Sex*	*Description*
Subject A	43	F	Subject A has a profound unilateral intention tremor and mild cognitive impairment due to chronic progressive MS. She is ambulatory with the use of a cane. Subject A is extremely cooperative but finds the tracking tasks frustrating because they "show off" her disability.

	Age	*Sex*	*Description*
Subject B	36	F	Subject B has severe intention tremor which affects her arms and trunk due to chronic progressive MS. She is confined to a wheelchair and transfers with help. Subject B fatigues quickly and depends upon others for assistance with nearly all activities of daily living. Although cooperative, Subject B finds the pursuit tracking tasks frustrating because of her inability to do them well.
Subject C	23	M	Subject C has severe intention tremor and ataxia in both arms as a result of a traumatic brain injury which occurred seven years ago. He ambulates and dresses himself with some assistance and successfully uses a computer with a trackball interface at home.
Subject D	38	F	Subject D has ataxic gait and cerebellar ataxia affecting only her right upper extremity due to cerebellar/cerebrovascular trauma. Her symptoms, which began approximately 15 years ago, include a high frequency low amplitude intention tremor and vary widely from day to day.
Subject E	40	M	Subject E has low-frequency, moderate intention tremor and ataxia affecting his hands and arms due to chronic progressive MS. He is confined to a wheelchair and transfers with help. Subject E does not mind participating in experiments because they make him "hopeful."

Subjects A, B, C, and E had participated in MIT tremor group experiments before and were familiar with the pursuit tracking tasks. In addition to these subjects, one individual completed a set of ten trials using the simplified 1-dof pursuit tracking task about the CEDO's third axis. He is:

	Age	*Sex*	*Description*
Subject F	60	M	Subject F has Shy-Drager Syndrome and, as a consequence, has a low-amplitude rest tremor in his shoulders and hands which is heightened by action. Because his voluntary movement is slow and his muscles fatigue quickly, Subject F only completed a set of ten 1-dof trials. He was unable do the 2-dof task. Subject F is confined to a wheelchair, has difficulty communicating vocally, and needs assistance for most activities of daily living.

In addition to the six tremor-disabled individuals, six able-bodied individuals were recruited from the student and staff population at MIT to serve as age and gender-matched control subjects. Each of the control subjects completed a set of 15 linear damping trials. The able-bodied "normal" participants are:

	Age	*Sex*	*Description*
Subject N_A	45	F	Able-bodied control for Subject A.
Subject N_B	36	F	Able-bodied control for Subject B.
Subject N_C	23	M	Able-bodied control for Subject C.
Subject N_D	38	F	Able-bodied control for Subject D.
Subject N_E	37	M	Able-bodied control for Subject E.
Subject N_F	53	M	Able-bodied control for Subject F.

Chapter 4
Data Analysis Techniques

4.1 Methods of Tremor Measurement

4.1.1 Methods of Tremor Recording

Numerous methods exist for measuring tremor, and the appropriateness of a particular method depends to a large extent upon how the measurement is used. Tremor data used by clinicians to diagnose ailments, assess disabilities, or monitor patients' progressions over time, for instance, may not need to be as precise as tremor data used by researchers to evaluate the effects of new drugs, design improved assistive devices, or test models of tremor mechanisms.

In hospitals and rehabilitation centers, tremor rating scales in which an individual's tremor is scored on the basis of his or her ability (or inability) to perform certain functional tasks are commonly used to quantify tremor severity and assess disability. Because they require no special equipment and no data processing, tremor rating scales are quick and easy to use. However, no tremor rating scale has been universally accepted, and existing scales are considered by most specialists to be imprecise, subjective, and for the most part, inadequate [Findley & Capildeo 1984, Elble & Koller 1990]. In an attempt to score drawing tasks on tremor rating scales more objectively, Elble et al have recently interfaced a commercially available digitizing tablet with a personal computer to analyze tremor induced by handwriting and drawing [Elble et al 1990].

Standard myoelectric (EMG) surface and needle electrodes have also been used to record characteristics of tremor. The EMG signal of a muscle represents the summation of motor unit action potentials, or electrical activity, generated by active motor units in the muscle. Thus, EMG recordings have been used by researchers to compare the firing patterns of motor units in able-bodied individuals to those in individuals with pathological tremor. EMG recordings have also been used to measure tremor frequency [Gottlieb & Lippold 1983, Sabra & Hallet 1984, Elble 1986, Findley 1988].

To completely quantify tremor characteristics in experimental investigations, multi-dof measurements are needed [Elble & Koller 1990]. However, most researchers have used and are still using uniaxial transducers to record tremor in one dimension across one joint [Randall & Stiles 1964, Fox & Randall 1970, Joyce & Rack 1974, Rietz & Stiles 1974, Vilis & Hore 1977, Gottlieb & Lippold 1983, Sabra & Hallet 1984, Elble 1986, Adelstein et al 1987, Calzetti et al 1987, Elble et al 1987, Flament & Hore 1987, Homberg et al 1987, Morrice et al 1987, Sanes et al 1988, Elek & Prochazka 1989, Elble & Koller 1990], and the resulting measure of tremor disability may be no more accurate than a carefully formulated rating scale [Elble & Koller 1990]. Commonly-used uniaxial transducers include goniometers, optical displacement transducers, and accelerometers. A few researchers, recognizing the need for more precise data, have obtained three dimensional measurements of tremor. In particular, Frost and Elble have each used triaxial accelerometry to measure low amplitude, high frequency hand tremors [Frost 1978, Elble 1990], and Will et al have used a VPL Data Glove and Polhemus tracking system to accurately measure both hand and finger tremors [Will et al 1990]. At the present time, however, no one has reported recording simultaneously both the translation and rotation of limbs or other parts of the body for the purpose of studying pathological tremor, nor has anyone reported measuring tremor at more than one joint at a time. Motion analysis systems in which computer-controlled video cameras or optoelectronic cameras are used to acquire the kinematics of an object in six dimensions are frequently employed for gait analysis and will perhaps be used in the future for recording more precisely the movement of tremor-disabled individuals.

In this study, the CEDO 1 device was used to measure movement at the user's wrist, restricted to the horizontal plane, resulting from whole-arm tremor. While the CEDO 1 does not measure tremor about the shoulder and elbow joints independently, it does measure motion at the wrist or "endpoint" of the limb -- the part of the limb which matters most functionally. The values recorded during data collection for this study, as functions of time, include the x and y position of the target and response markers in units of pixels, the angles and angular

velocities of each of the three CEDO brake axes in units of radians and radians/second, and the commanded brake torques for simulating damping in units of lbf-in.

4.1.2 Methods of Data Processing

Tremor data can be processed in either the time domain or the frequency domain. Time domain analyses yield plots of tremor amplitude versus time, plots of amplitude probability densities, or measures of accumulated tremor from integrating limb travel over time. Frequency domain analyses yield quantitative measures of tremor frequency and tremor power and are particularly useful for distinguishing voluntary movements from involuntary movements in pursuit tracking tasks.

In this investigation, pursuit tracking data were analyzed in both the time domain and the frequency domain to assess the effects of damping and inertial loads on tremor. Time domain records were examined to compare tremor and performance characteristics qualitatively from trial to trial, and power spectral densities were computed to obtain quantitative measures of tremor frequency, tremor power, and tracking fidelity.

4.2 Characterization of Tremor Data

Time history records of tremor, like time history records of many physical phenomena, are *random* or *non-deterministic* in that each experiment produces a unique record which is unlikely to be repeated and cannot accurately be predicted within reasonable experimental error. Methods for analyzing random data depend upon the data's time variance. Random data are *stationary* or *time-invariant* when average values of interest remain constant in time and contiguous segments of the same data record exhibit similar statistical properties. Usually every effort is made in practice to design experiments that will produce stationary data because the necessary analysis procedures for nonstationary data are substantially more difficult. Moreover, if random data are stationary, then the variance of spectral estimates can be reduced

by ensemble averaging when computing power spectral densities in the frequency domain [Bendat & Piersol 1980].

In this study, runs tests were done on selected data files from all participants to verify the stationarity of tremor time records. To execute the runs test, MATLAB script file RUNS was written. The RUNS program consists of six main steps:

1. The x and y response data from pursuit tracking tasks are loaded into the program and the overall linear trend is removed from each data record. (The stationarity of the tremor, not the DC trend, is of concern in this test. The linear trends are also removed before spectral analysis.)
2. The 1800-point x and y data records are divided into segments. The number of segments is a user-defined parameter that can sometimes influence the results of the test. A variety of segments were used, ranging from 20 segments of 90 points each to 60 segments of 30 points each, when testing the tremor data.
3. The mean μ, standard deviation σ, and mean square $\mu^2 + \sigma^2$ of each segment is computed.
4. The median of the segment mean squares is computed for the x segments and the y segments.
5. The sign of the mean square of each segment relative to the median is plotted versus segment number relative to the median as shown in Figure 4-1 for Subject A. The number of runs, or number of times the mean square fluctuates about the median, is counted.
6. A hypothesis test is formulated to assess stationarity in which the null hypothesis is that the data are stationary and the alternate hypothesis is that the data are not stationary. Under the null hypothesis, an equal number of segment mean squares are expected to lie on either side of the median, and the probable number of runs, attributed to random fluctuations in the data, is easily computed. The 95

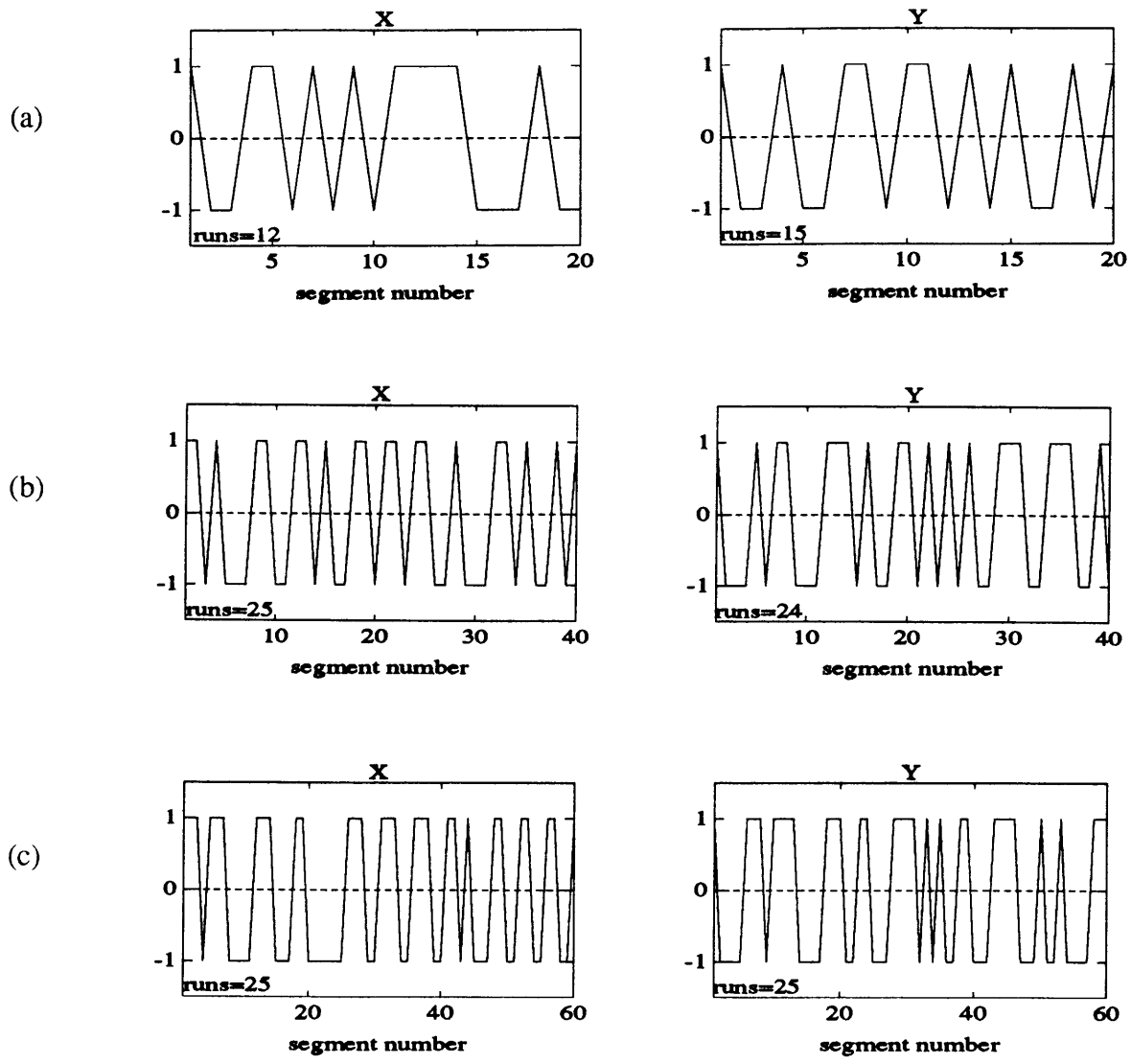

Figure 4-1. Results of typical tuns tests demonstrating stationarity of tremor data for (a) 20 segments, (b) 40 segments, and (c) 60 segments.

percent confidence interval for the number of runs is given in Table 4-1 for different numbers of segments.

A comparison of Figure 4-1 and Table 4-1 verifies that the data from Subject A are stationary at the $\alpha = 0.05$ level of significance regardless of the number of segments used in the test. These results are typical of the results obtained for all subjects except one (data from Subject E failed to pass the runs test using 20 segments but did pass the runs test using 40 and 60 segments). While the data are perhaps not "stationary in the strict sense" due to the sinusoidal tracking pattern, the data are "stationary in the wide sense" in that the expected segment mean square values are constant over the data record when computed from appropriate numbers of data points. The results of these tests are identical to the results obtained by Adelstein and justify the use of ensemble averaging for computing power spectral densities [Adelstein 1981, Oppenheim & Schafer 1989].

Table 4-1. The 95 percent confidence intervals for the number of runs R, under the null hypothesis, for different numbers of segments [Bendat & Piersol 1987].

Number of Segments	*Lower limit for R*	*Upper limit for R*
20	6	15
40	14	27
60	22	39

4.3 Fundamentals of Spectral Analysis

4.3.1 Fourier Transforms, Parseval's Theorem, and the Nyquist Criterion

Fourier Transforms and Parseval's Theorem for Continuous and Discrete Data:

Fourier transforms and Parseval's theorem are fundamental to the spectral analysis techniques used in this study and are reviewed briefly in this section. A continuous stationary random time record x(t) and its Fourier transform X(f) are related by the Fourier transform pair of equations:

$$X(f) = \int_{-\infty}^{+\infty} x(t)\, e^{-2\pi i f t}\, dt \tag{4-1}$$

$$x(t) = \int_{-\infty}^{+\infty} X(f)\, e^{2\pi i f t}\, df \tag{4-2}$$

and by Parseval's theorem, which states that the total power in a signal is the same whether it is computed in the time domain or in the frequency domain:

$$\text{Total Power} = \int_{-\infty}^{+\infty} |x(t)|^2\, dt = \int_{-\infty}^{+\infty} |X(f)|^2\, df \tag{4-3}$$

Often only discrete samples of x(t) are available. If a length T of x(t) is sampled N times at points Δt apart, then the discrete record x[t] is related to its discrete Fourier transform X[f] by the discrete Fourier transform (DFT) pair of equations:

$$X[k\Delta f] = \Delta t \sum_{n=0}^{N-1} x_n e^{-2\pi i \frac{kn}{N}} \tag{4-4}$$

$$x[n\Delta t] = \Delta f \sum_{k=0}^{N-1} X_k e^{2\pi i \frac{kn}{N}} \tag{4-5}$$

and by the discrete form of Parseval's theorem:

$$\text{Total Power} = \frac{1}{N} \sum_{k=0}^{N-1} |x_k|^2 = \frac{1}{N^2} \sum_{n=0}^{N-1} |X_n|^2 \tag{4-6}$$

In the discrete case, x[t] is defined only at times spaced Δt apart and X[f] is defined only at frequencies spaced Δf apart:

$$\Delta f = \frac{1}{T} = \frac{1}{N\Delta t} \tag{4-7}$$

The Nyquist Criterion:

The Nyquist criterion provides an important guideline for sampling. In general, a discrete signal x[t] is obtained from a continuous signal x(t) by sampling x(t) at a sampling frequency f_s equal to the reciprocal of the time between samples:

$$f_s = \frac{1}{\Delta t} \tag{4-8}$$

In order to retain all information carried by the continuous signal x(t) in the discrete samples x[t], f_s must satisfy the Nyquist criterion which states that f_s must be at least twice as large as the highest frequency component of x(t) to avoid aliasing. If any frequency component lies outside the range $\{-f_s/2, f_s/2\}$ in the continuous signal, then that component will be spuriously folded over, or aliased, into that range in the sampled signal [Bendat & Piersol 1980, Oppenheim & Schafer 1989].

4.3.2 Correlation and Power Spectral Density Functions

Auto- and Cross-Correlation Functions:

The correlation functions in the time domain and the power spectral density functions in the frequency domain are often employed to extract linear relationships between two or more sets of data. For random data, the autocorrelation function may be interpreted as a measure of how well future values of the data can be predicted based on past observations. If a signal reaches a certain value x at time t, it is likely to remain in the vicinity of x for times shortly following t. In other words, signal samples separated by short intervals are not, in general, independent from one another. The autocorrelation function characterizes these dependencies between samples and is defined for a stationary time record x(t) as:

$$R_{xx}(\tau) = \lim_{T\to\infty} \frac{1}{T} \int_0^T x(t)\, x(t+\tau)\, dt \tag{4-9}$$

The cross-correlation function, similarly, characterizes the dependencies between two different random signals and is defined for stationary time records x(t) and y(t) as:

$$R_{xy}(\tau) = \lim_{T\to\infty} \frac{1}{T} \int_0^T x(t)\, y(t+\tau)\, dt \tag{4-10}$$

Auto- and Cross-Spectral Density Functions:

The power spectral density functions are the Fourier transforms of the correlation functions. Thus, the autospectral density function of a stationary random time record x(t) is defined in the frequency domain by:

$$S_{xx}(f) = \int_{-\infty}^{\infty} R_{xx}(\tau)\, e^{-2\pi i f\tau}\, d\tau \tag{4-11}$$

and the cross-spectral density function of two stationary random time records x(t) and y(t) is defined by:

$$S_{xy}(f) = \int_{-\infty}^{\infty} R_{xy}(\tau)\, e^{-2\pi i f\tau}\, d\tau \tag{4-12}$$

These equations are defined over both positive and negative frequencies and are referred to as two-sided spectra. In practice it is more convenient to work with one-sided spectra defined over non-negative frequencies only:

$$G_{xx}(f) = 2S_{xx}(f), \quad f \geq 0 \tag{4-13}$$

$$G_{xy}(f) = 2S_{xy}(f), \quad f \geq 0 \tag{4-14}$$

The magnitude of the cross-spectrum density function is governed by the cross-spectrum inequality, a relationship between the cross-spectrum and the autospectra of two stationary random signals:

$$|G_{xy}(f)|^2 \leq G_{xx}(f)\, G_{yy}(f) \tag{4-15}$$

This inequality also defines the coherence function, a normalized measure of the degree to which one signal is linearly related to another signal as a function of frequency:

$$\gamma^2_{xy}(f) = \frac{|G_{xy}(f)|^2}{G_{xx}(f)\, G_{yy}(f)} \qquad 0 \le \gamma^2_{xy}(f) \le 1 \tag{4-16}$$

If x and y are unrelated, the coherence function equals 0. If x and y are perfectly linearly related, the coherence function equals 1.

The power spectral density functions can alternatively be derived by taking Fourier transforms of the original data records. If $X_k(f,T)$ and $Y_k(f,T)$ are the Fourier transforms of the kth segment of length T of stationary random time histories x(t) and y(t), then the one sided auto- and cross-spectral density functions are defined by:

$$G_{xx}(f) = \lim_{T\to\infty} \frac{2}{T} E[\,|X_k(f,T)|^2\,] \tag{4-17}$$

$$G_{xy}(f) = \lim_{T\to\infty} \frac{2}{T} E[X^*_k(f,T)\; Y_k(f,T)] \tag{4-18}$$

where the expected value operator E denotes an averaging operation over the k segments. As indicated by Equation 4-17, then, the autospectrum function may also be interpreted as a measure of the frequency distribution of the mean square value of the data [Bendat & Piersol 1980].

4.3.3 Power Spectrum Estimation

The Periodogram:

The autospectral density function was defined in Section 4.3.2 for continuous data. For discrete data, an estimate of the autospectral density function, called the periodogram, is obtained by taking an N-point sample of the data and using a Fast Fourier Transform (FFT) algorithm to compute its discrete Fourier transform. The one-sided periodogram estimate of the power spectrum is then defined at N/2+1 frequencies, with resolution f_s/N, by:

$$P_{xx}[f_0] = \frac{1}{N^2}|X_0|^2$$

$$P_{xx}[f_n] = \frac{1}{N^2}\left[\,|X_n|^2 + |X_{N-n}|^2\right], \quad n=1, 2, \ldots, \left(\frac{N}{2}-1\right)$$

$$P_{xx}[f_c] = \frac{1}{N^2}|X_{N/2}|^2 \tag{4-19}$$

where f_c is the cutoff frequency of the data, defined by the Nyquist criterion as half the sampling frequency f_s [Press et al 1988]. The periodogram estimate is usually normalized, by Parseval's theorem, so that the sum of the N/2 +1 values of P_{xx} is equal to the mean squared amplitude of the function x[t]:

$$\text{Total Power} = \frac{1}{N}\sum_{k=0}^{N-1}|x_k|^2 = \sum_{n=0}^{N-1}P_{xx}[f_n] \tag{4-20}$$

Variance of the Spectral Estimates:

Unfortunately, the periodogram as defined by Equation 4-19 is not a very good estimate of the autospectral density function. Because the periodogram is defined only at discrete frequencies, its amplitude at a particular frequency may appear larger than what it actually is due to leakage effects. More specifically, if the signal has a frequency component at some frequency f_1 and the closest available frequency in the periodogram is f_2, then the signal power at f_1 will appear at f_2 *and* at neighboring frequencies with the degree of leakage proportional to the difference between f_1 and f_2. The consequence of estimating the power spectrum from discrete data, then, is that the variance of the estimate at a particular frequency is equal to the square of its expected value at that frequency (i.e. the standard deviation of the estimate is equal to the estimate itself). Further, this result is independent of the number of data points N. If a longer run of data is sampled at the same sampling rate, the cutoff frequency is unchanged but finer frequency resolution is obtained within the Nyquist frequency range. If the same length of data is sampled with a finer sampling interval, the frequency resolution is unchanged but the Nyquist frequency range extends to a higher frequency. In neither case is the variance of any

one particular frequency's estimated power spectrum density decreased as a result of the additional samples [Press et al 1988, Elble 1990].

Methods to Reduce the Variance in the Spectral Estimates:

Fortunately, two steps can be taken during processing to reduce the variance of spectral estimates -- ensemble averaging and data windowing. Ensemble averaging involves partitioning the sampled data record into K segments of M points each. An M-point FFT and a periodogram is estimated for each segment, and the K periodograms are averaged at each frequency to obtain the power spectral density of the original data record. To obtain the smallest spectral variance per data point, the number of segments are chosen such that each segment overlaps the previous segment by one half of its length. This averaging procedure reduces the variance of the estimates by a factor of 9K/11 at the cost of attenuating the spectral peaks and reducing the frequency resolution [Press et al 1988, Elble 1990]. Multiplying each data segment by a smooth window function before computing its FFT also reduces the variance of the periodogram estimates by reducing the leakage effects inherent in the Fourier analyses of finite data records [Press et al 1988, Oppenheim & Schafer 1989].

The MATLAB *Spectrum* Function:

In this investigation, auto- and cross-spectral densities were computed with the Macintosh version of the *spectrum* function from the MATLAB Signal Processing Toolbox. The *spectrum* function uses the Welch method of power spectrum estimation and incorporates both ensemble averaging and data windowing to reduce the variance of the estimates. When using *spectrum*, the input (target) and output (response) data records are first divided into K segments overlapping by M/2 points. Then, because non-zero mean values appear as delta functions at the DC frequency f=0 in spectral density plots, the linear trend of each segment is removed to prevent leakage at frequencies near 0 [Bendat & Piersol 1980]. Successive segments of the detrended data are then multiplied by an M-point Hanning window:

$$\text{Hanning window } w[m] = \frac{1}{2}\left[1 - \cos\left(\frac{2\pi m}{M-1}\right)\right], \quad m=1, \ldots, M \tag{4-21}$$

and the windowed segments are transformed with an M-point FFT. Auto- and cross-spectral densities are computed from the FFT records for each segment, and the resulting spectra are ensemble averaged. Finally, the transfer function, defined as the ratio of the cross-spectral density function of the input and output to the autospectral density of the input, and the coherence function, defined in Equation 4-16, are computed and all results are output in matrix form. Because the spectral estimates obtained from the MATLAB function are in units of power, all spectra were divided by the frequency resolution to obtain the "equivalent" power spectral density in units of power/Hz before being plotted for presentation in Chapter 5.

4.4 Quantification of Tremor and Tracking Performance

Target and response position data from the CEDO pursuit tracking tasks were plotted first in the time domain to examine qualitatively the effects of linear and non-linear damping on tremor magnitude and tracking performance for each subject. Then, MATLAB spectral analysis program INSPECTOR was written to analyze the data in the frequency domain. Each 1800-point target and response time record was divided into 6 segments of 512 points each, overlapping by 256 points each. The autospectral densities of the target $P_{tt}[f]$ and response $P_{rr}[f]$, cross-spectral densities $P_{tr}[f]$, and coherence functions $\gamma^2_p[f]$ were then computed for the tremor position data using the MATLAB *spectrum* command. The target and response time records were also numerically differentiated to obtain velocity records, and the autospectral densities $V_{tt}[f]$ and $V_{rr}[f]$, cross-spectral densities V_{tr} [f], and coherence functions γ^2_v [f] were computed for the tremor velocity data to obtain spectra in which the low frequency tracking peaks were attenuated and the higher frequency tremor peaks were accentuated for comparison. (While Adelstein, Baiges, and Maxwell displayed position spectra in their theses, much of the tremor literature presents tremor records in the form of acceleration spectra obtained from accelerometer measurements which, because higher frequency peaks are accentuated, do have a somewhat different appearance.) Since the tremor time records were sampled at a frequency of

60 Hz (well above the pathological tremor frequencies), the tremor frequency records were defined up to the Nyquist cutoff frequency at 30 Hz and had a 0.117 Hz frequency resolution as determined by the sampling rate and the 512-point segment length:

$$\text{frequency resolution } \Delta f = \frac{f_s}{M} = \frac{60 \text{ Hz}}{512 \text{ points}} = 0.117 \text{ Hz} \tag{4-22}$$

4.2.1 Tremor Power Spectra

To distinguish between voluntary tracking movements and involuntary tremor movements in the frequency domain, portions of the position and velocity response spectra linearly related to the target spectra (i.e. portions of the response spectra that can be accounted for by performing linear operations on the target spectra at each frequency) were subtracted from the position and velocity response power spectra using the position and velocity coherence functions to obtain "tremor power spectra":

$$\text{tremor position spectrum } T_p = [1 - \gamma_p^2]\, P_{rr} \tag{4-23}$$

$$\text{tremor velocity spectrum } T_v = [1 - \gamma_v^2]\, V_{rr} \tag{4-24}$$

As an illustration, Figure 4-2 shows the "tremor position spectrum" computed for the square wave shown earlier in Figure 3-2 assuming the "target" is the sine wave shown earlier in Figure 3-1. Because power in the square wave spectrum at the harmonic frequencies can not be related linearly to power in the sine wave spectrum, peaks at these frequencies in Figure 3-2 also appear in Figure 4-2. Because power in the square wave spectrum at the fundamental frequency *is* related linearly to power in the sine wave spectrum, however, the peak at 0.5 Hz in Figure 3-2 does *not* appear in Figure 4-2.

For the tremor data in this study, tremor position and velocity spectra obtained from Equations 4-23 and 4-24 were averaged for all trials at a given damping level or trial condition from one or more sessions for each subject. The averaged spectra were then plotted versus frequency to examine qualitatively the trial-to-trial and day-to-day repeatability of results, the

(a)

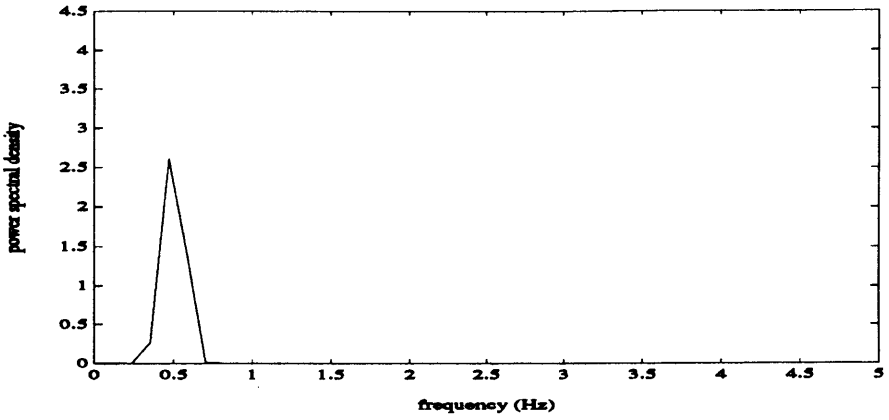

(b)

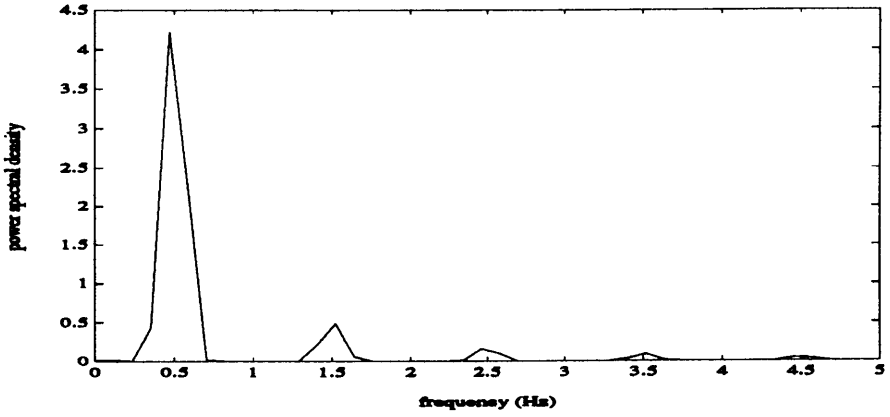

(c)

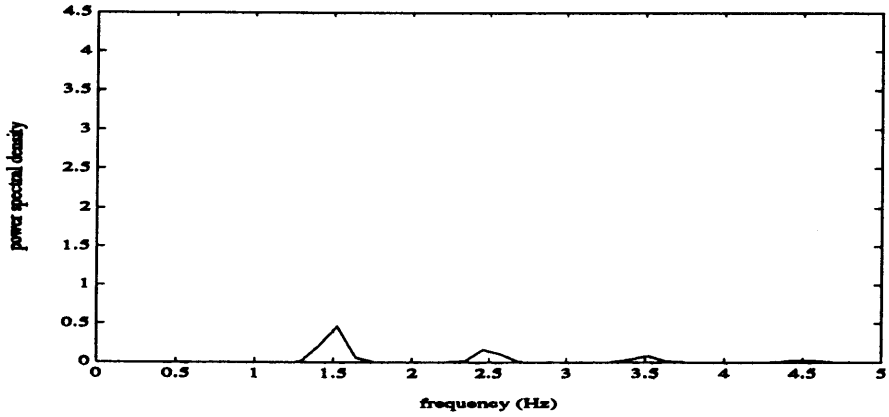

Figure 4-2. Power spectral density plots for (a) a unit amplitude 0.5 Hz sine wave, (b) a unit amplitude 0.5 Hz square wave, and (c) square wave residual obtained by subtracting from the square wave spectrum that portion of the square wave spectrum linearly related to the sine wave spectrum.

effects of linear and non-linear damping, the effects of inertia, and the relationship between tremor and limb position in the workspace.

4.4.2 Tremor and Tracking Performance Scores

Performance scores were also computed from the target and response autospectral densities and from the cross-spectral densities to statistically verify that observed differences in tremor or tracking performance could be attributed, with confidence, to differences in trial conditions. First, "tremor power" was computed by summing the tremor position spectra from the lower frequency f_a to the upper frequency f_b which bounded each participant's tremor band:

$$t_p = \sum_{f=f_a}^{f_b} T_p[f] \tag{4-25}$$

(A summing operation was used, rather than an integration operation, to obtain units of power from MATLAB's definition of power spectrum.) Since data from undamped trials usually exhibited more tremor power than data from damped trials, f_a and f_b were chosen for each participant to bound the tremor band in his or her averaged undamped spectrum. The upper and lower frequency bounds determined from participants' undamped data were then used to analyze participants' damped data as well as data from the age-matched control subjects. The particular bounds used for each subject are shown in Table 4-2. Because it was difficult to distinguish tremor from tracking errors in the low frequency spectra (even though all target frequencies were below 0.25 Hz and target frequencies were continuously varied during the 30 second task), "tremor power" scores probably include power from tracking errors as well as from tremor.

Table 4-2. The upper and lower frequency bounds used to define subjects' "tremor bands".

Subject	*Lower frequency bound*	*Upper frequency bound*
A and N_A	0.6 Hz	6 Hz
B and N_B	0.6 Hz	3 Hz
C and N_C	0.6 Hz	5 Hz
D and N_D	0.6 Hz	5 Hz
E and N_E	0.6 Hz	4 Hz
F and N_F	0.6 Hz	6 Hz

Three other performance scores were computed to assess the effects of trial conditions on subjects' tracking. First, "signal power" was defined from the tremor position cross-power spectra as:

$$s_p = \sum_{f=0}^{f_t} P_{tr}[f] \tag{4-26}$$

where f_t, the target cutoff frequency, was chosen as the frequency below which approximately 95 percent of the power in the target spectra P_{tt} is contained. Next, the ratio of signal power to tremor power was computed to generate a "signal-to-noise" ratio, or measure of tracking fidelity:

$$SNR = \frac{s_p}{t_p} \tag{4-27}$$

This performance score is particularly useful for comparing tremor data from different trial conditions because it reflects changes in both tremor and tracking performance. If the CEDO's damping suppresses tremor and thus allows the user to perform better on pursuit tracking tasks, the SNR for the damped case will be larger than the SNR for the undamped case. If, however, the CEDO's damping suppresses tremor but also interferes with voluntary tracking, the SNR for the highly damped case will perhaps be smaller than the SNR for the lightly damped or undamped case. By maximizing the SNR, then, the optimal level of damping for

performing pursuit tracking tasks can perhaps be found. Lastly, the transfer function, defined as the ratio of the cross-spectral density P_{tr} to the target spectral density P_{tt}:

$$TF = \frac{P_{tr}[f]}{P_{tt}[f]} \tag{4-28}$$

was split into its magnitude and phase components and averaged over the target frequencies to obtain another measure of tracking performance:

$$\text{TF amplitude} = \frac{\sum_{f=0}^{f=f_t} |TF[f]|}{\frac{f_t}{\Delta f}} \tag{4-29}$$

$$\text{TF phase} = \frac{\sum_{f=0}^{f=f_t} \text{angle}(TF[f])}{\frac{f_t}{\Delta f}} \tag{4-30}$$

If an individual's tracking performance is unhindered by the application of damping, then the transfer function magnitude and phase will be approximately constant, independent of damping level, for that individual. If an individual cannot keep up with the target when damping is applied, then a larger phase lag between the target and the response will be seen in the damped trials.

Chapter 5
Presentation and Discussion of Results

The results of the CEDO pursuit tracking experiments are presented and discussed in this chapter. Because the disabled participants' tremors differ in amplitude, frequency, etiology, and consequently in their responses to added damping and inertia, no single individual is considered "typical" in this investigation and plots from *all* disabled participants are included in all sections of the chapter. In contrast, very few differences are perceptible in the tracking results from the able-bodied participants and therefore only plots from subject N_A, the able-bodied subject who made the largest tracking errors; subject N_C, the able-bodied subject who made the smallest tracking errors; and subject N_F, the able-bodied subject who did the 1-dof tracking tasks, are shown to illustrate "normal" tracking ability.

Before proceeding to examine the figures in this chapter in detail, it is important to recognize that multiple peaks in the tremor power spectra do not necessarily imply the existence of multiple tremors caused by different mechanisms nor do they imply the existence of multiple tremors caused by the same mechanism. Tremor amplitudes and frequencies vary with time, and multiple peaks in the spectra may simply be a consequence of fluctuations in the frequency or amplitude of a single tremor. If the amplitude and frequency variation of a subject's tremor are related, e.g. frequency changing inversely proportional to the amplitude, then the resulting tremor spectrum could exhibit asymmetrical sidebands in addition to a band at the central carrier frequency similar to that which might be obtained by modulating the signal from one oscillator with the signal from a second independent oscillator [Gresty & Buckwell 1990]. Alternatively, since tremor is a somewhat irregular periodic phenomenon, peaks may appear in the spectrum at harmonics of the fundamental tremor frequency just as peaks appear at harmonics of the target frequencies when non-linear tracking errors are made.

Finally, as a word of caution, *please check the axes and units of the plots in this chapter carefully when comparing data from different subjects!* Although X and Y components of

each plot are scaled identically, frequency domain plots and plots of performance scores are scaled differently for different individuals depending upon tremor severity so that all data are presented in meaningful form.

5.1 Measurements of Undamped Tremor

Measurements of undamped tremor are presented in Figures 5-1 through 5-9 for disabled subjects A-E, able-bodied subjects N_A and N_C, disabled subject F, and able-bodied subject N_F, respectively (see Section 3.3.2 to review descriptions of participants; subjects F and N_F are presented separately from the other subjects because they did just the 1-dof tasks). These figures each consist of six plots: (a) X and Y target and response time trajectories, (b) X and Y tremor position spectra as defined in Equation 4-23, and (c) X and Y tremor velocity spectra as defined in Equation 4-24 from one typical undamped trial. All data were processed using the analysis methods discussed in Chapter 4.

The plots in Figures 5-1 through 5-9 serve mainly to illustrate the severity range of subjects' tremors measured in this study and the debilitating effects of tremor on purposeful movement as evidenced by comparing the tracking performances of the tremor-disabled subjects to those of the able-bodied subjects. Clearly, involuntary tremor oscillations are present in the tracking trajectories of subjects A-F although the amplitude, frequency, and regularity of the subjects' tremors vary. Whereas time domain plots for subjects C, D, E, and F reveal irregular tremor oscillations superimposed on purposeful tracking, time domain plots for subjects A and B reveal more regular, rhythmical oscillations which, to a large extent, mask all evidence of underlying voluntary activity. In fact, both subject A and subject B found the tracking task nearly impossible to do without damping.

Further insight into the tremor characteristics and tracking abilities of the six disabled subjects is gained by comparing subjects' tremor position spectra, scaled purposely in these figures to illustrate the relative magnitudes of tremor peaks and non-linear tracking errors, to their tremor velocity spectra, in which tracking peaks at lower frequencies are attenuated and

tremor peaks at higher frequencies are accentuated. As discussed in Chapters 3 and as illustrated in these figures, non-linear tracking errors (i.e. components of a subject's tracking response not linearly related to the target) appear at frequencies between 0 and 2 Hz in the position spectra of *all* subjects, while tremor peaks appear at frequencies between 2 and 4 Hz in the spectra of disabled subjects only. When the tremor peaks are comparable in magnitude to the tracking peaks as shown in Figures 5-1 and 5-2 for subjects A and B, the position spectra are similar in appearance to the velocity spectra. When the tremor peaks are much lower in magnitude than the tracking peaks as shown in Figures 5-3 and 5-4 for subjects C and D, some higher-frequency tremor peaks which appear in the velocity spectra are not visible in the position spectra as scaled in these plots. The spectra for the able-bodied subjects shown in Figures 5-6, 5-7, and 5-9 exhibit no power in the frequency range associated with pathological tremor, and the power attributable to tracking errors in these plots is generally less than 10 percent of the power attributable to tracking errors in the plots from the most severely disabled subjects. Subject E, in contrast to the other disabled subjects, does not exhibit a regular oscillatory tremor (he instead exhibits more of an ataxia or lack of coordination) and his tremor spectra (Figure 5-5) resemble those of the able-bodied subjects in both amplitude and frequency content. The approximate peak-to-peak amplitudes and frequencies of subjects' undamped tremors are listed in Table 5-1. Physiological tremor in the 8 to 12 Hz frequency range does not appear in the data from any of the subjects, presumably because the amplitude of physiological tremor is below that which can be detected by the CEDO 1 system.

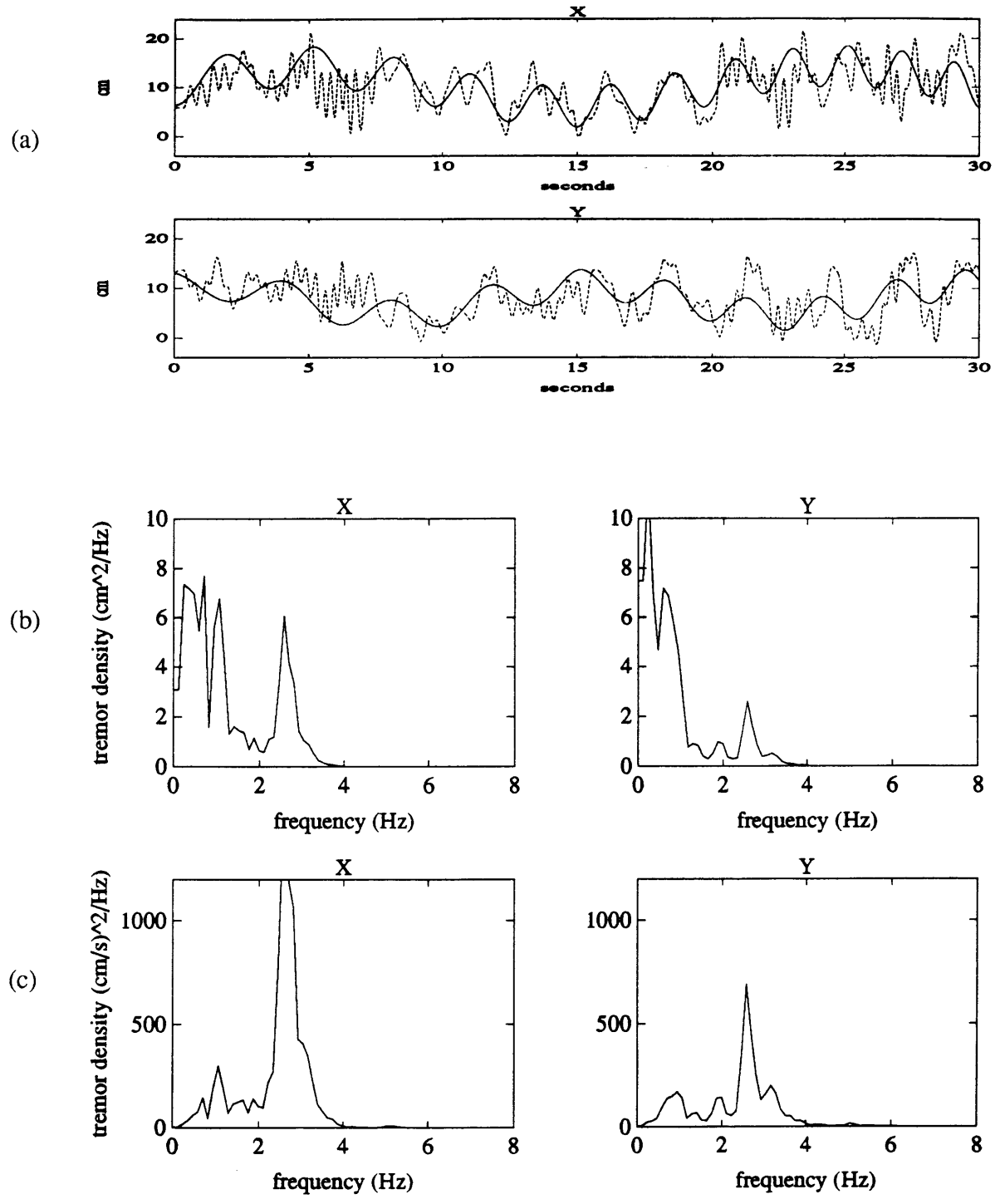

Figure 5-1. *Subject A:* Undamped tremor as measured by (a) time records from tracking tasks, (b) tremor position spectra, and (c) tremor velocity spectra.

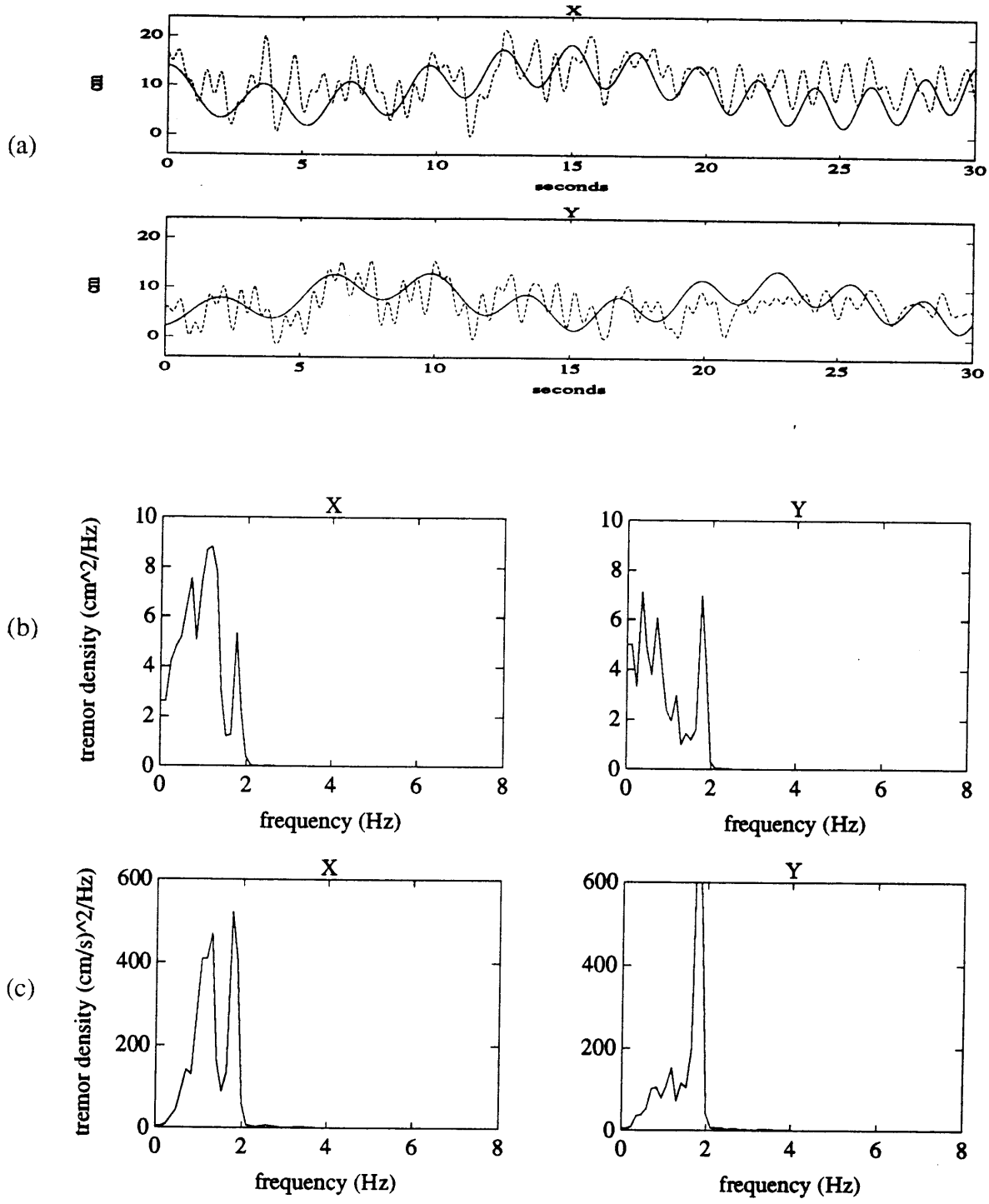

Figure 5-2. *Subject B:* Undamped tremor as measured by (a) time records from tracking tasks, (b) tremor position spectra, and (c) tremor velocity spectra.

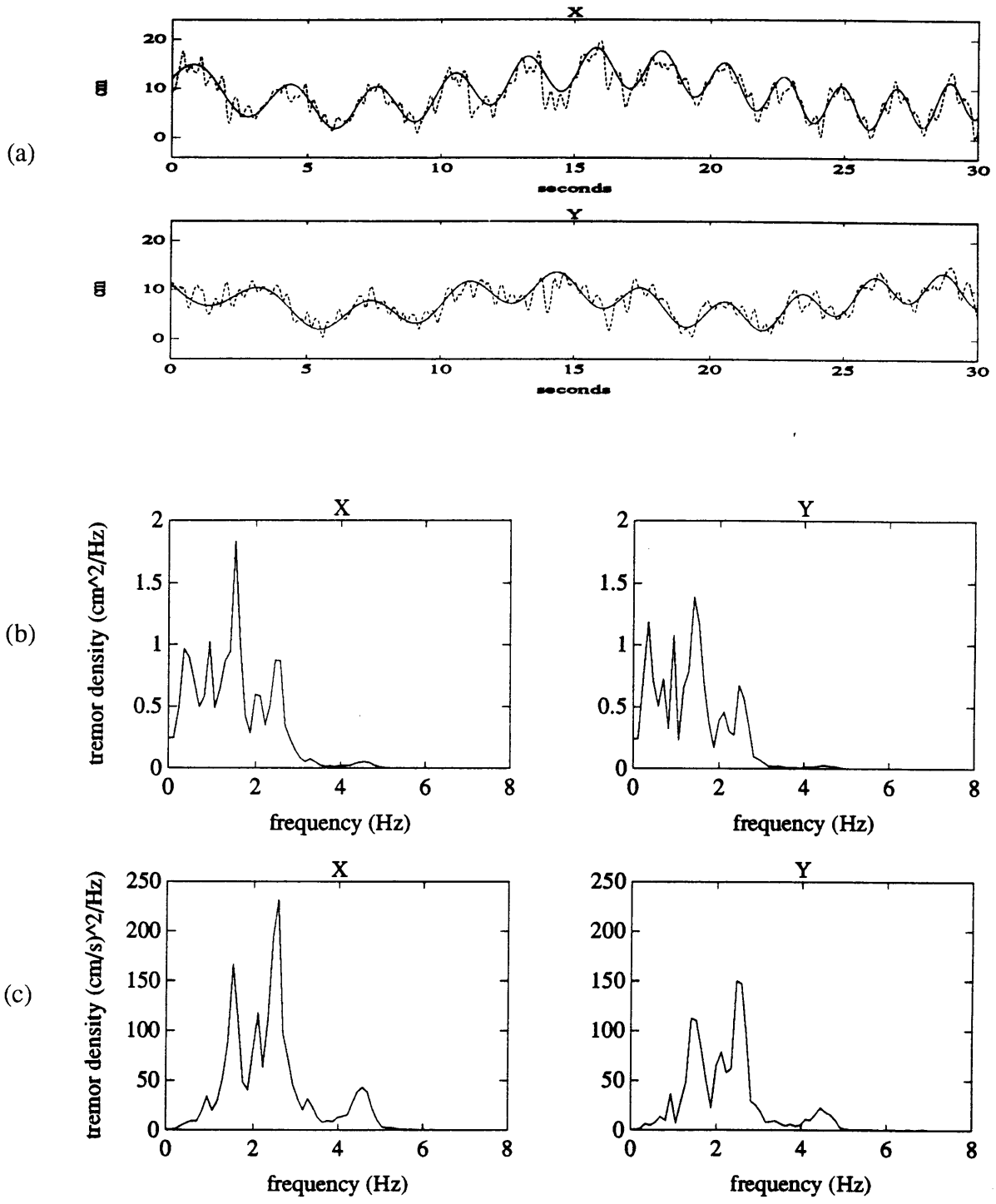

Figure 5-3. *Subject C:* Undamped tremor as measured by (a) time records from tracking tasks, (b) tremor position spectra, and (c) tremor velocity spectra.

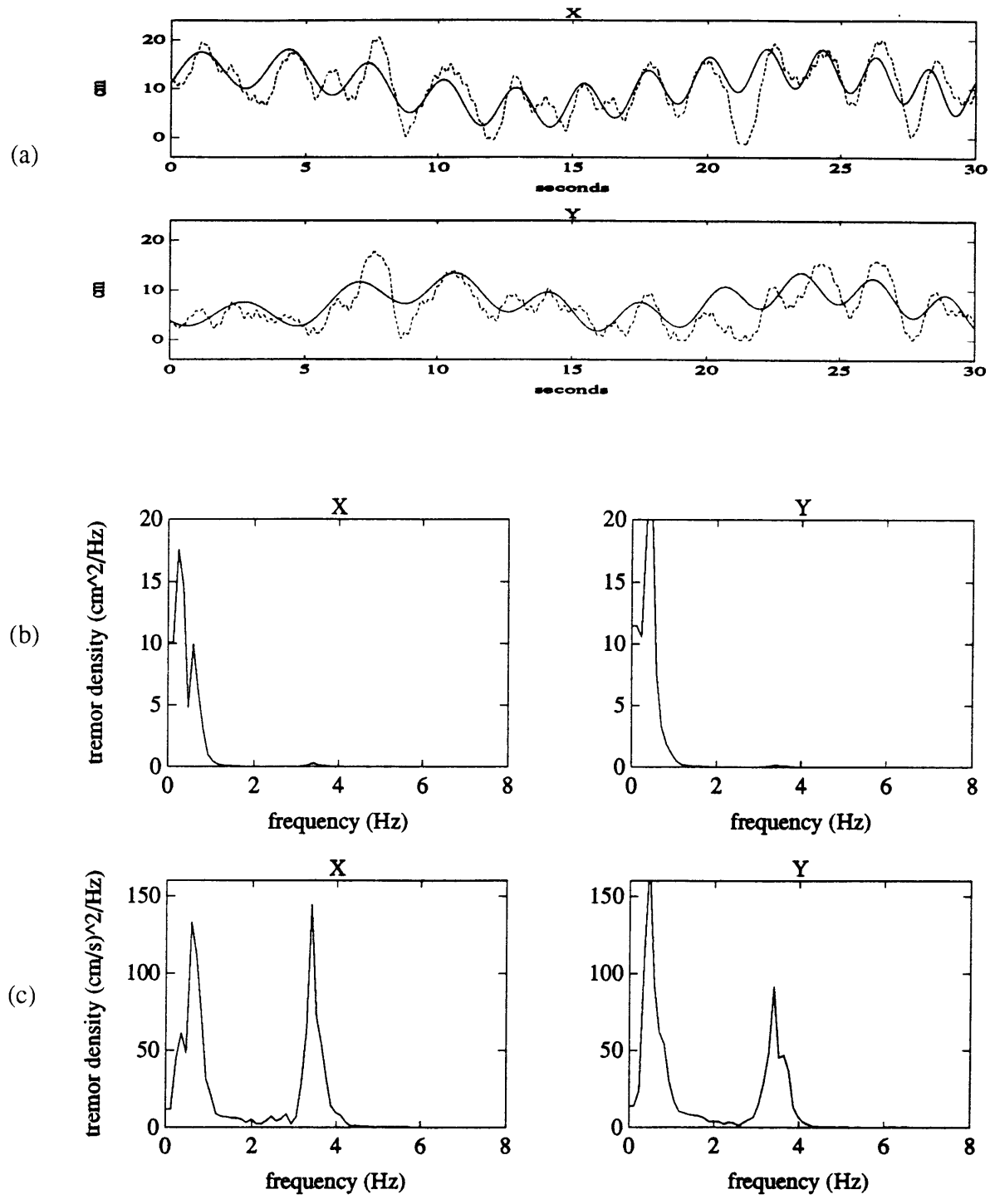

Figure 5-4. *Subject D:* Undamped tremor as measured by (a) time records from tracking tasks, (b) tremor position spectra, and (c) tremor velocity spectra.

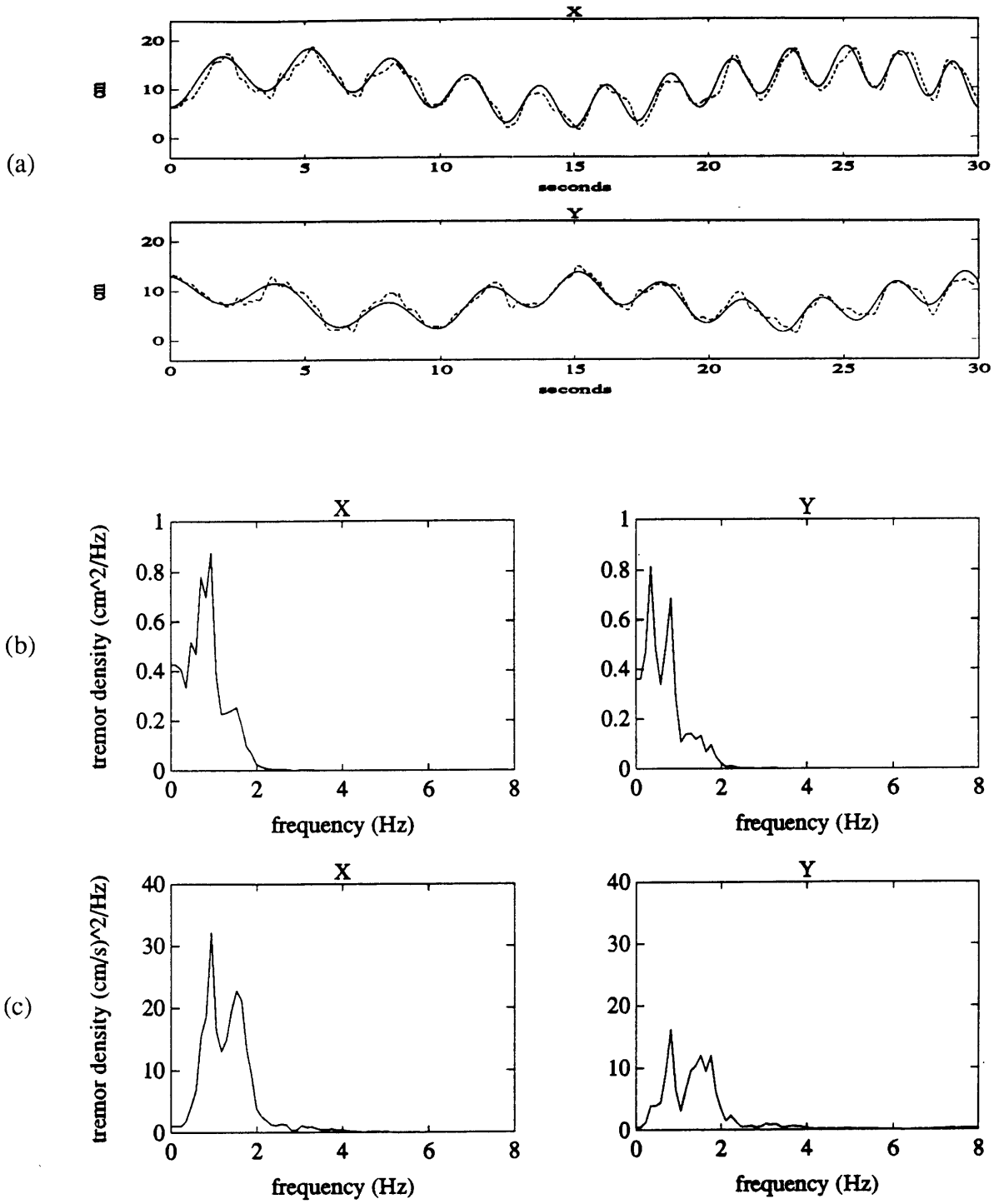

Figure 5-5. *Subject E:* Undamped tremor as measured by (a) time records from tracking tasks, (b) tremor position spectra, and (c) tremor velocity spectra.

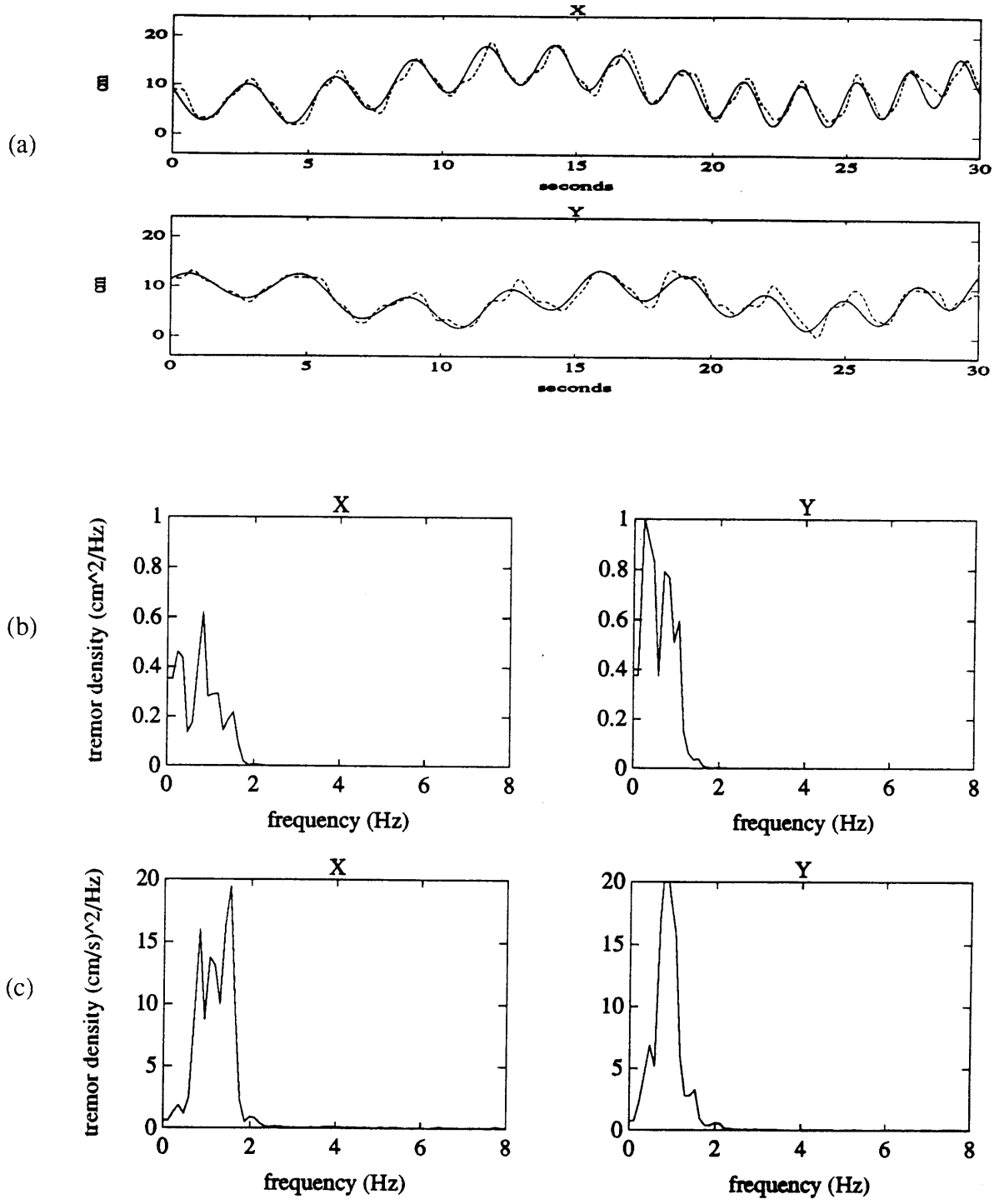

Figure 5-6. *Subject N_A:* Undamped tremor as measured by (a) time records from tracking tasks, (b) tremor position spectra, and (c) tremor velocity spectra.

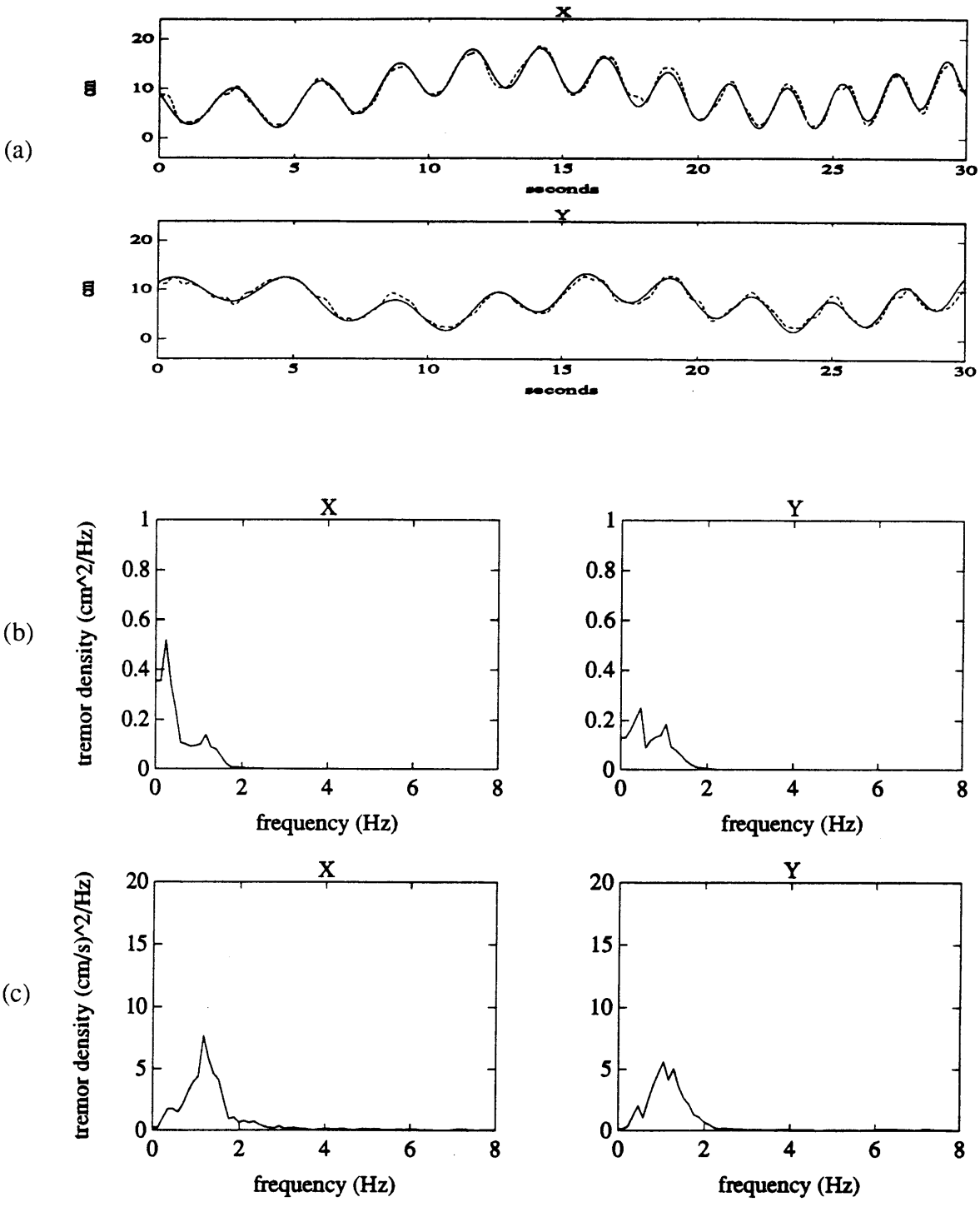

Figure 5-7. *Subject N_C:* Undamped tremor as measured by (a) time records from tracking tasks, (b) tremor position spectra, and (c) tremor velocity spectra.

(a)

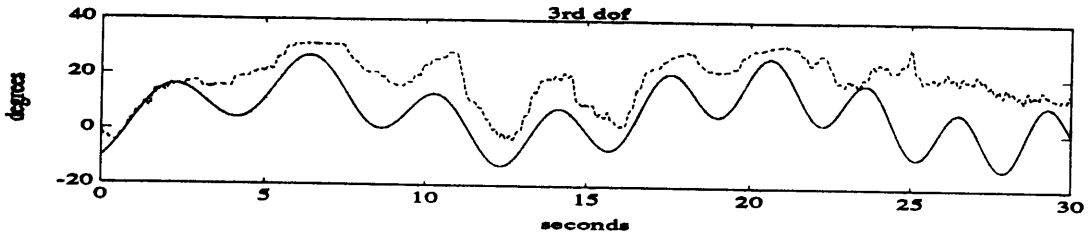

(b)

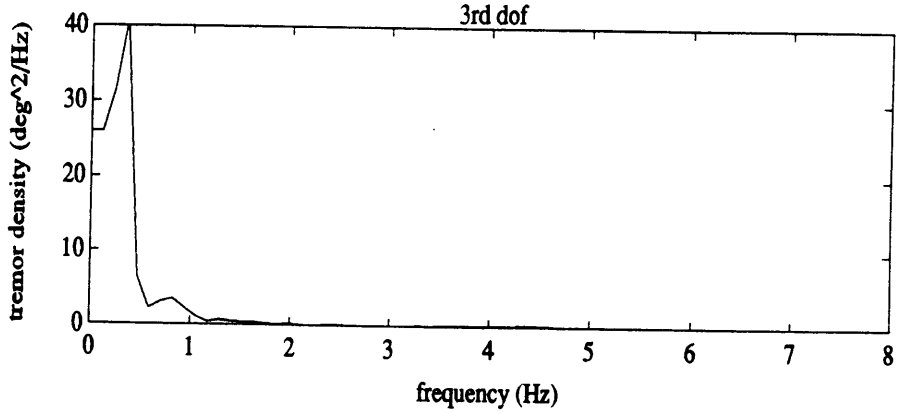

(c)

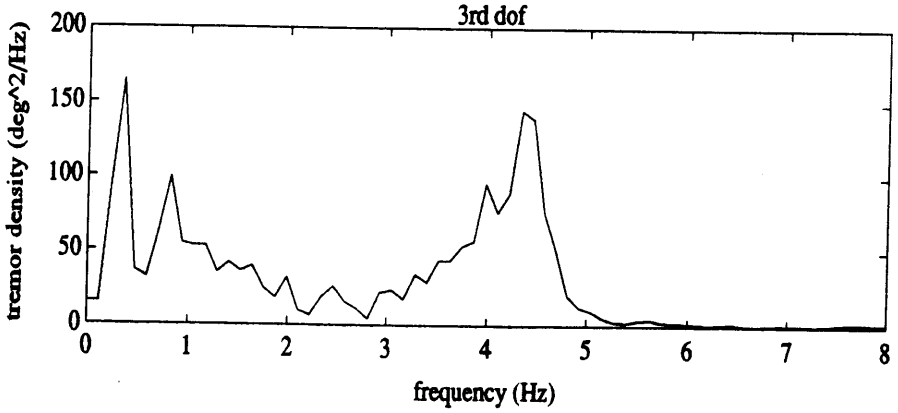

Figure 5-8. *Subject F:* Undamped tremor as measured by (a) time records from tracking tasks, (b) tremor position spectra, and (c) tremor velocity spectra.

(a)

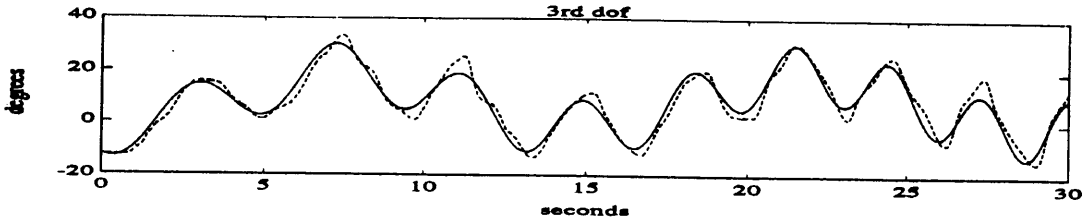

(b)

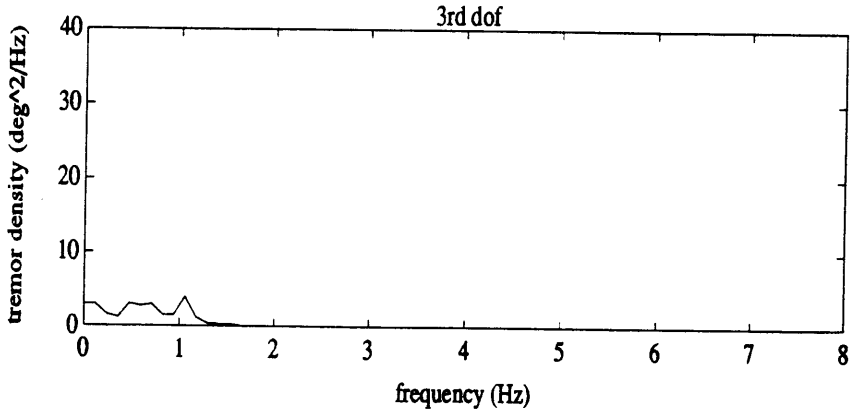

(c)

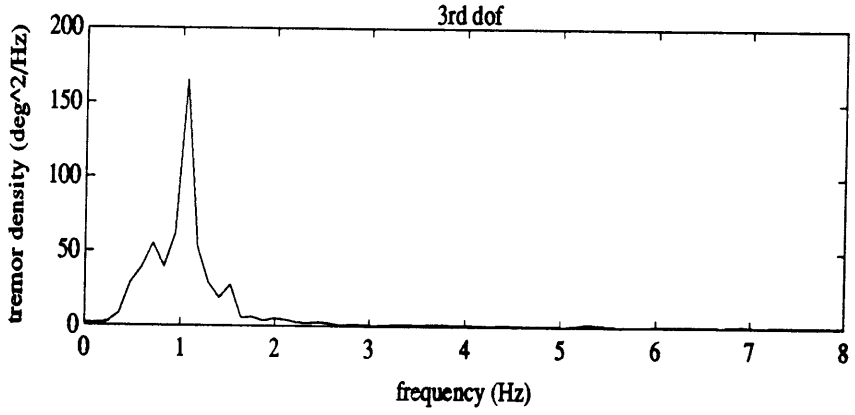

Figure 5-9. *Subject N_F:* Undamped tremor as measured by (a) time records from tracking tasks, (b) tremor position spectra, and (c) tremor velocity spectra.

Table 5-1. Approximate amplitudes and frequencies of subjects' undamped tremors. The "tremor frequency" was determined from each subjects' tremor power spectra as the frequency at which the tremor power is maximum. This peak tremor frequency was, in general, consistent from trial to trial for each subject.

Subject	*Tremor Amplitude*	*Tremor Frequency*
Subject A	12 cm	2.6 Hz
Subject B	10 cm	1.8 Hz
Subject C	7 cm	2.5 Hz
Subject D	2 cm	3.4 Hz
Subject E	2 cm	0.9 Hz
Subject F	3 degrees	4.3 Hz

5.2 Measurements of Damped Tremor

5.2.1 The Effects of Linear Damping

Figures 5-10 through 5-23 illustrate the effects of linear damping on tremor and tracking for disabled subjects A-E, able-bodied subjects N_A and N_C, disabled subject F, and able-bodied subject N_F, respectively. The first figure for subjects A-E shows typical time domain tracking records for comparing tremor and tracking without damping to tremor and tracking with moderate (34 N/m/s) and high levels of viscous damping (68 N/m/s for subject C, 85 N/m/s for subjects A, B, D, and E). The second figure for each subject shows position spectra averaged over all trials at a particular damping level, scaled to highlight the tremor peaks. Six trials per damping level from two test sessions were used for subject A; four trials per damping level from three test sessions were used for subject B; four trials per damping level from two test sessions were used for subjects C and E; three trials per damping level from one test session were used for subjects D, N_A, and N_C; and two trials per damping level from one test session were used for subjects F and N_F. In these plots, the solid line corresponds to the undamped trials, the dashed line corresponds to the 17 N/m/s damped trials, the dash-dot line corresponds to the 34 N/m/s damped trials, the dotted line corresponds to the 51 N/m/s damped trials, the "+" line corresponds to the 68 N/m/s damped trials, and the "*" line corresponds to the 85 N/m/s damped trials. Care was taken to average the same number of trials for each damping level from the different test sessions since subjects' tremors frequently varied from session to session. Time domain plots are not shown for the able-bodied subjects since, for all levels of damping, they resemble the undamped tracking plots presented earlier in Figures 5-6, 5-7, and 5-9.

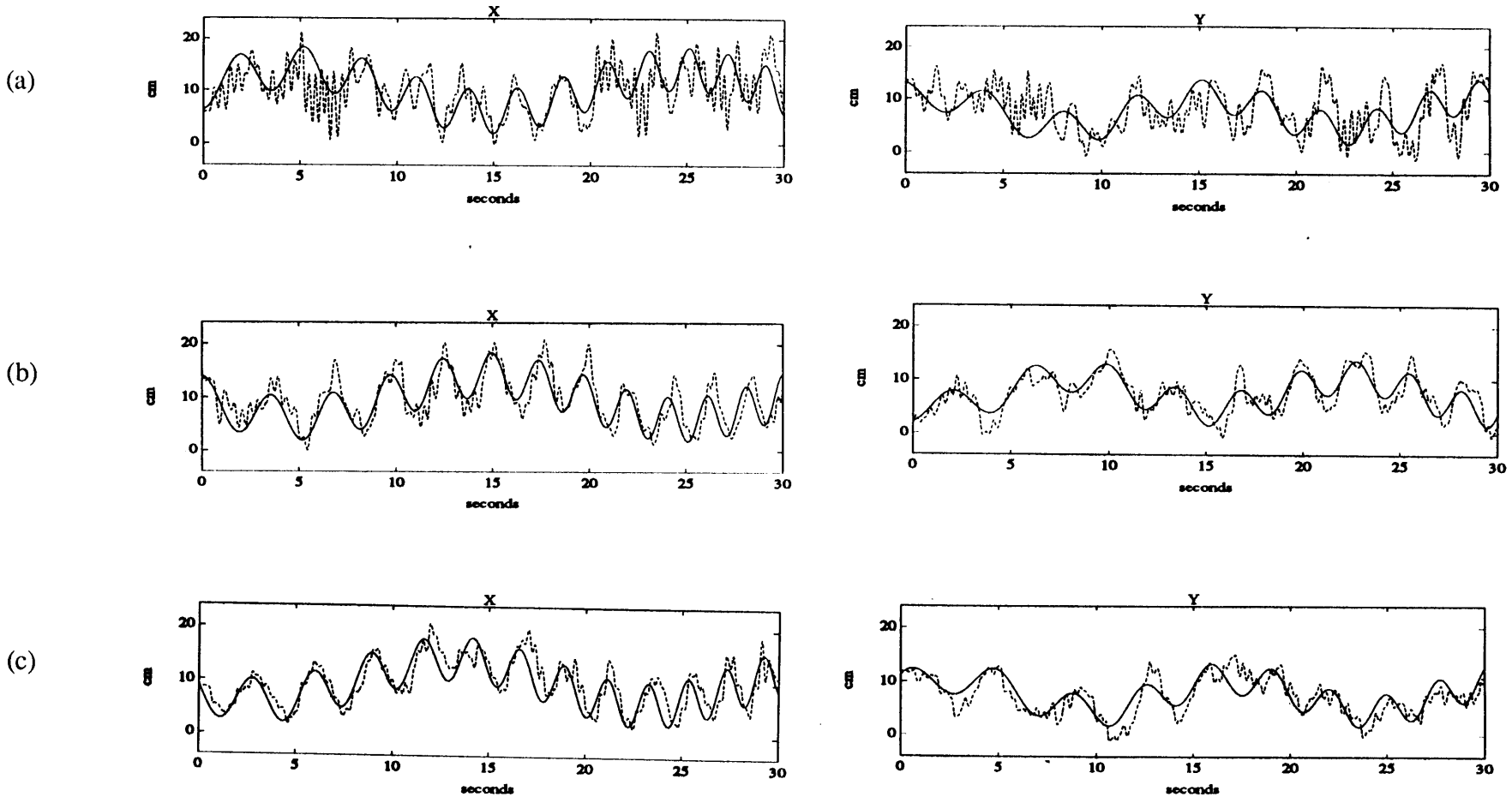

Figure 5-10. *Subject A:* Target and response time trajectories for comparing (a) undamped tremor to (b) tremor damped at 34 N/m/s to (c) tremor damped at 85 N/m/s.

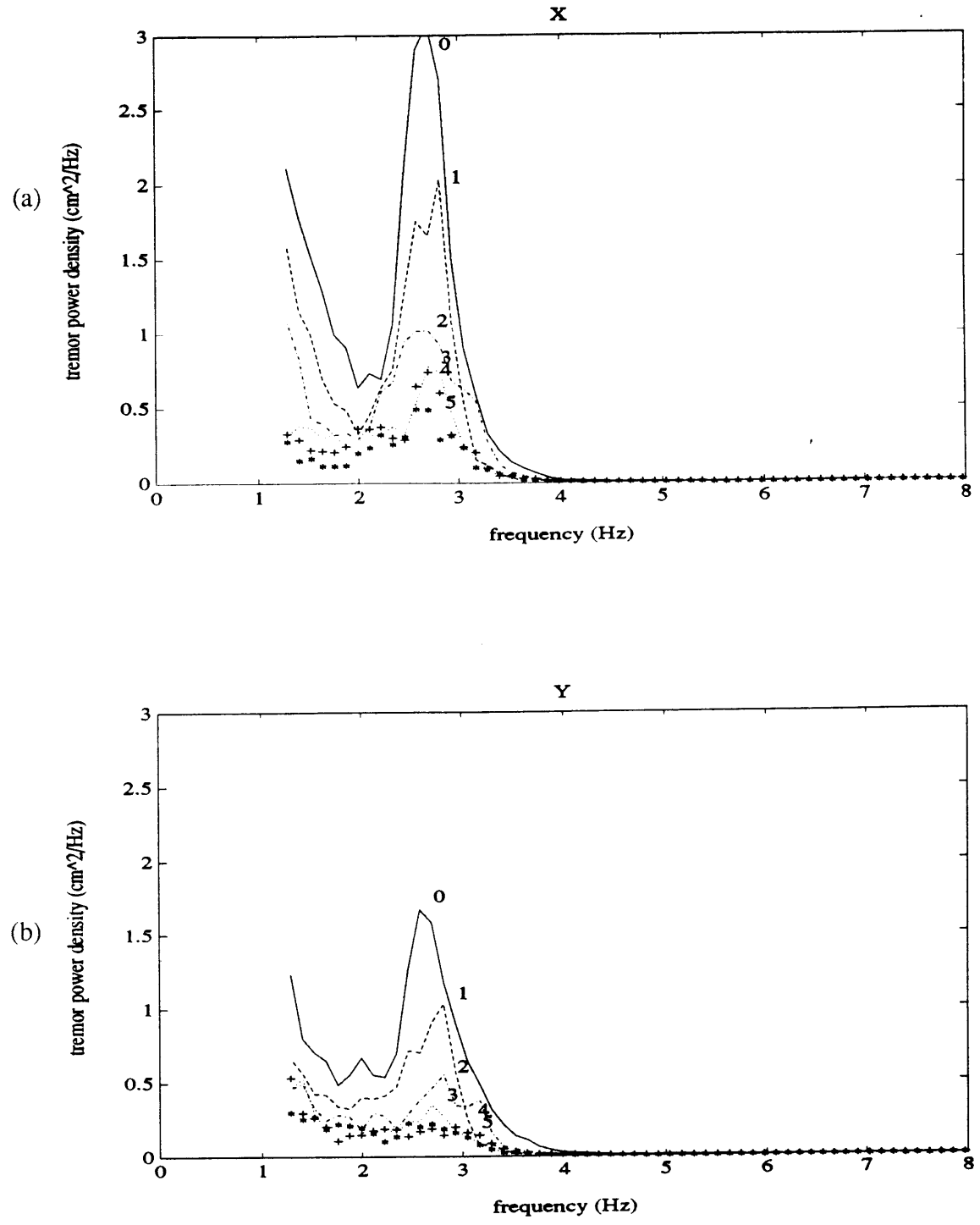

Figure 5-11. *Subject A:* Tremor position spectra illustrating the effects of linear damping. Damping levels 0-5 correspond to actual damping coefficients of 0, 17, 34, 51, 68, and 85 N/m/s, respectively.

(a)

(b)

(c)

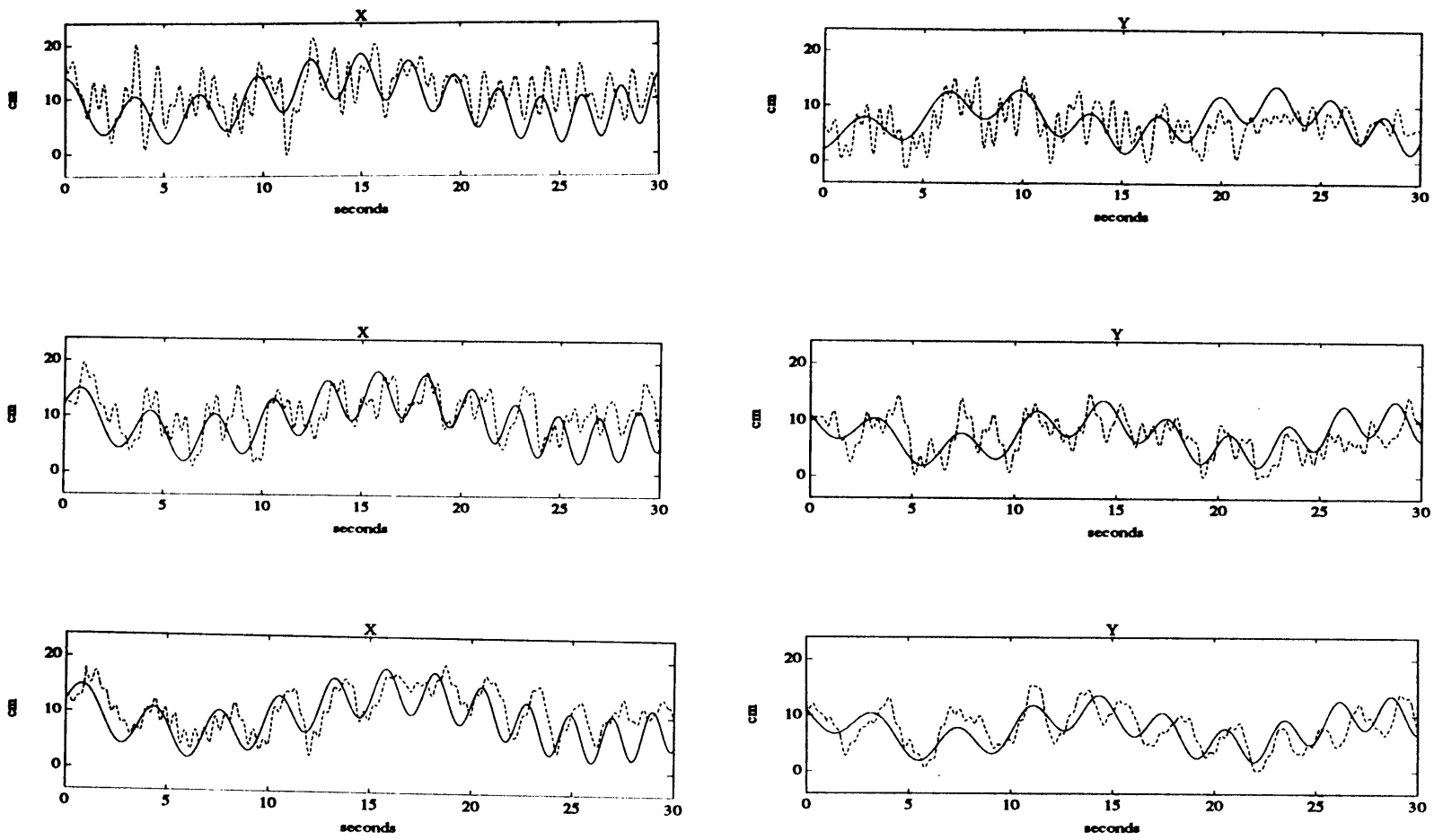

Figure 5-12. *Subject B:* Target and response time trajectories for comparing (a) undamped tremor to (b) tremor damped at 34 N/m/s to (c) tremor damped at 85 N/m/s.

(a)

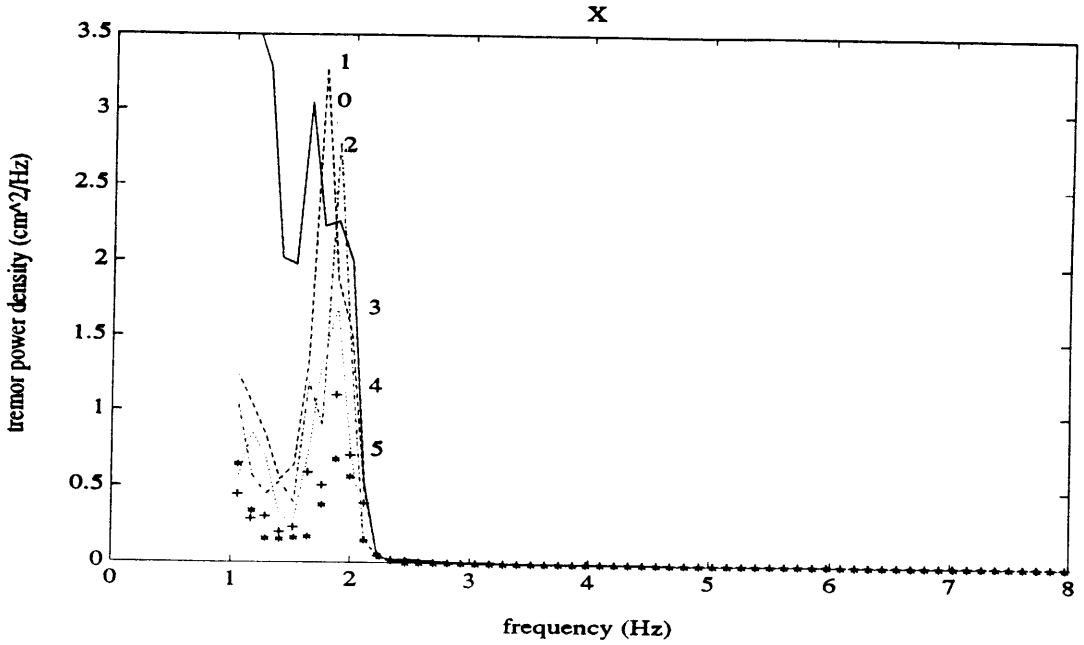

(b)

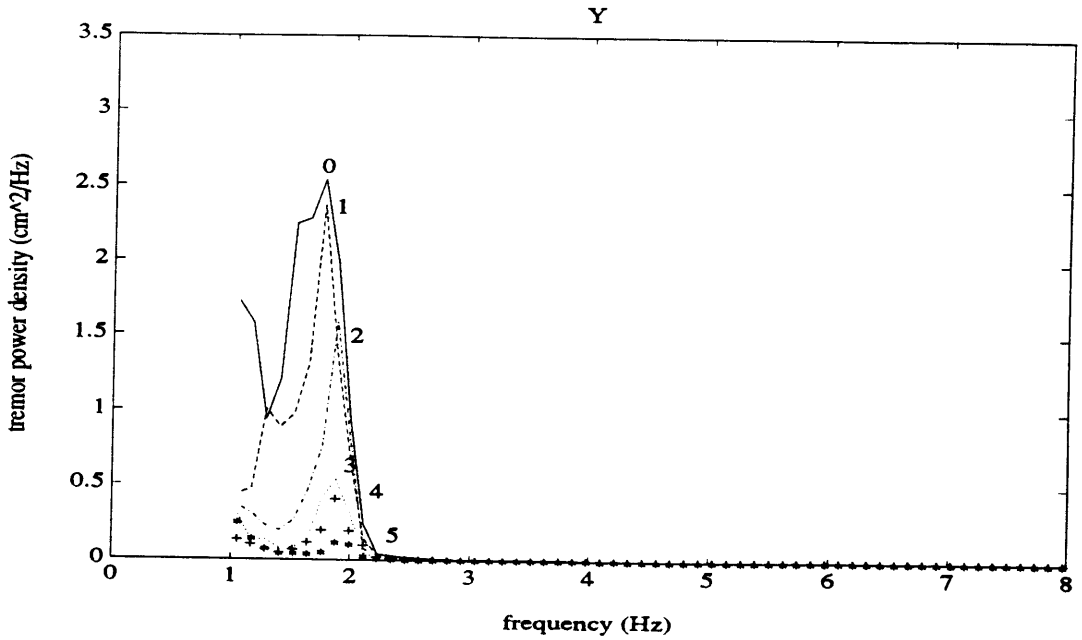

Figure 5-13. *Subject B:* Tremor position spectra illustrating the effects of linear damping. Damping levels 0-5 correspond to actual damping coefficients of 0, 17, 34, 51, 68, and 85 N/m/s, respectively.

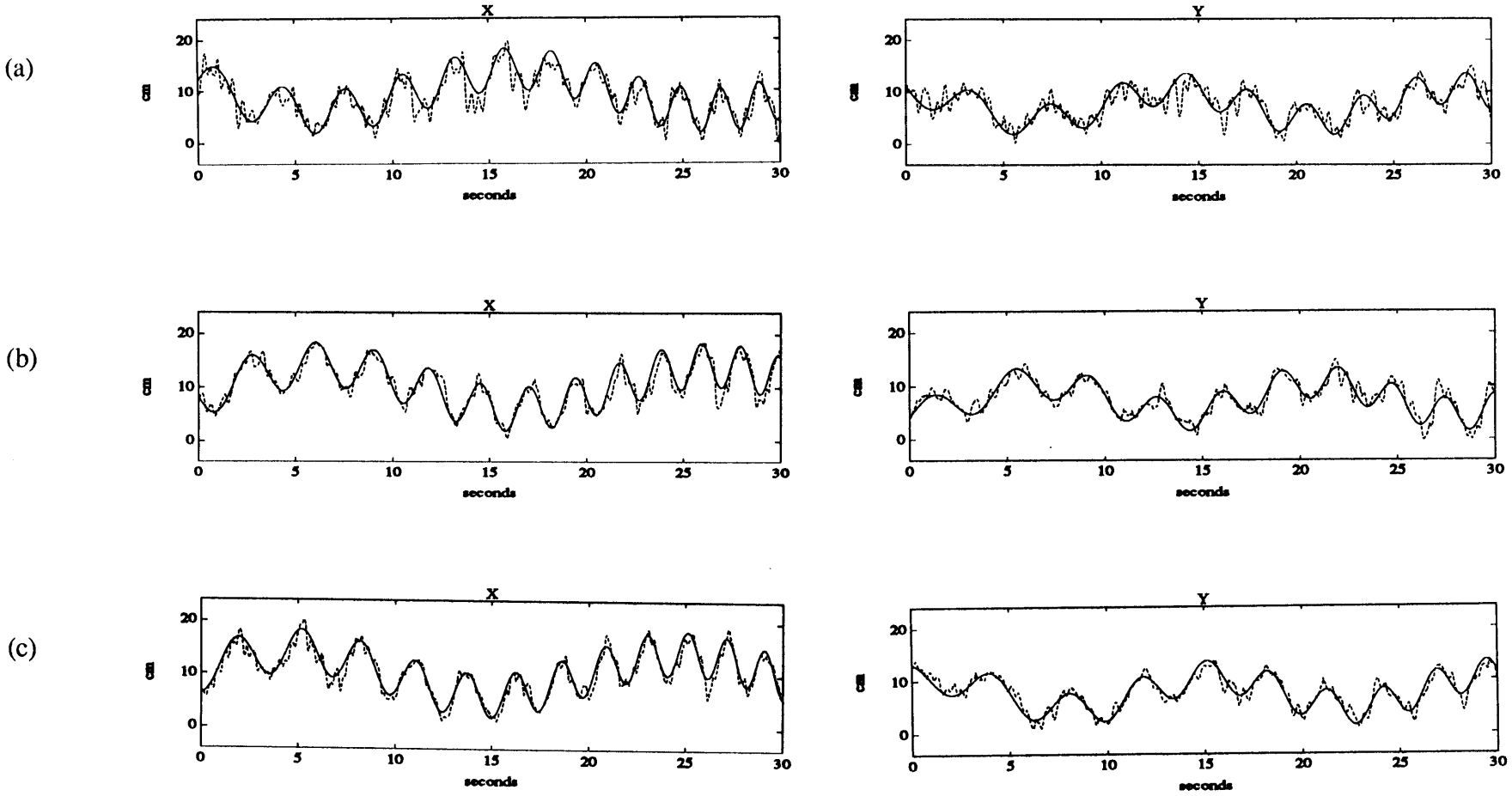

Figure 5-14. *Subject C:* Target and response time trajectories for comparing (a) undamped tremor to (b) tremor damped at 34 N/m/s to (c) tremor damped at 68 N/m/s.

(a)

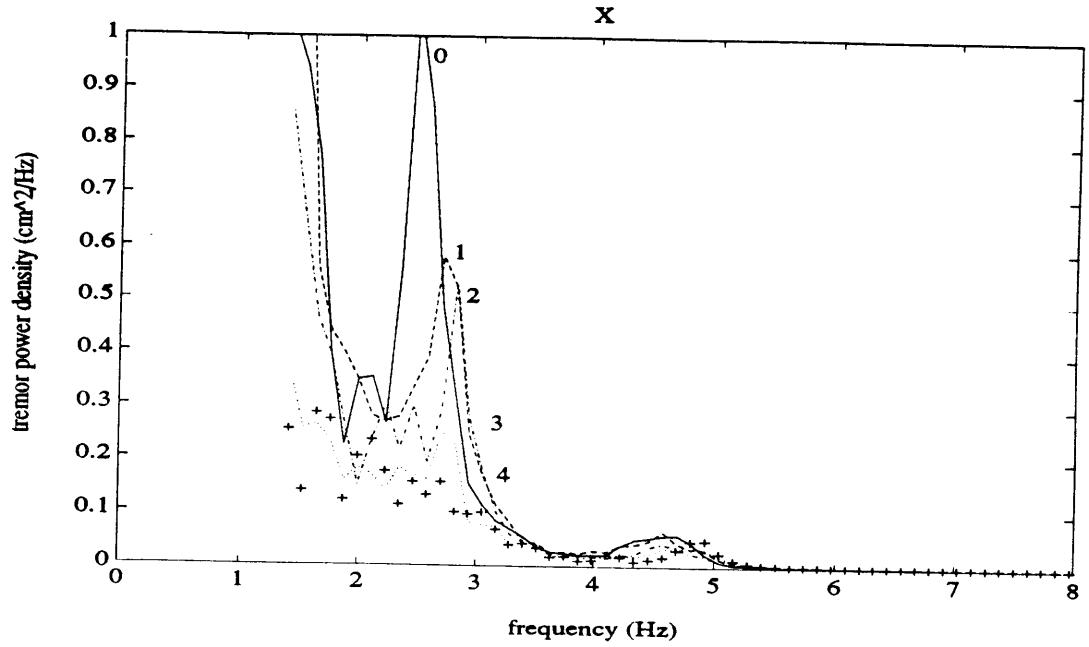

(b)

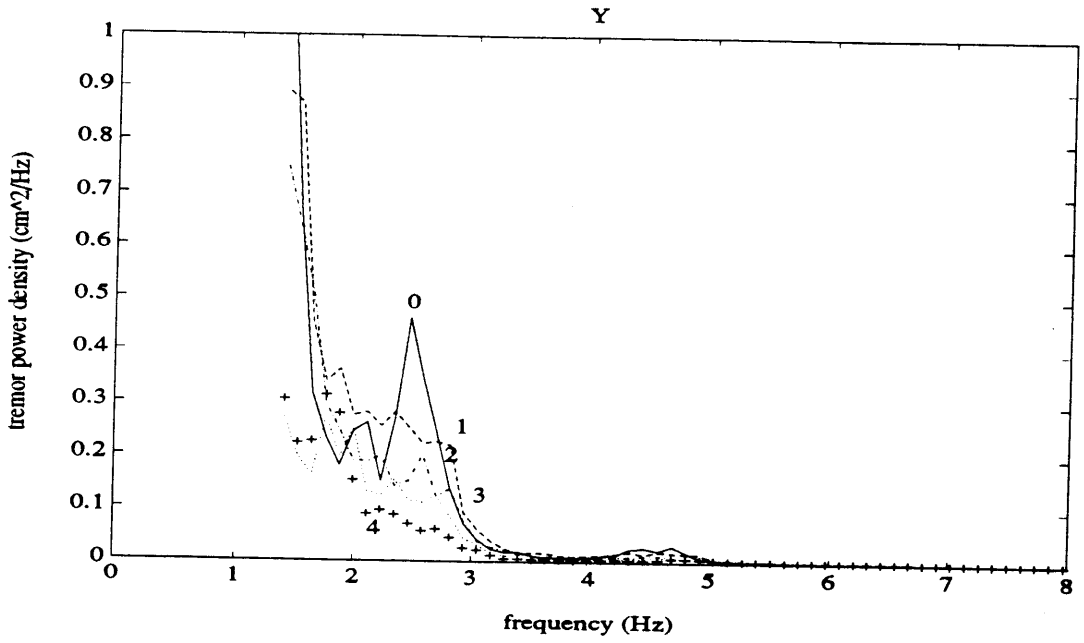

Figure 5-15. *Subject C:* Tremor position spectra illustrating the effects of linear damping. Damping levels 0-4 correspond to actual damping coefficients of 0, 17, 34, 51, and 68 N/m/s, respectively.

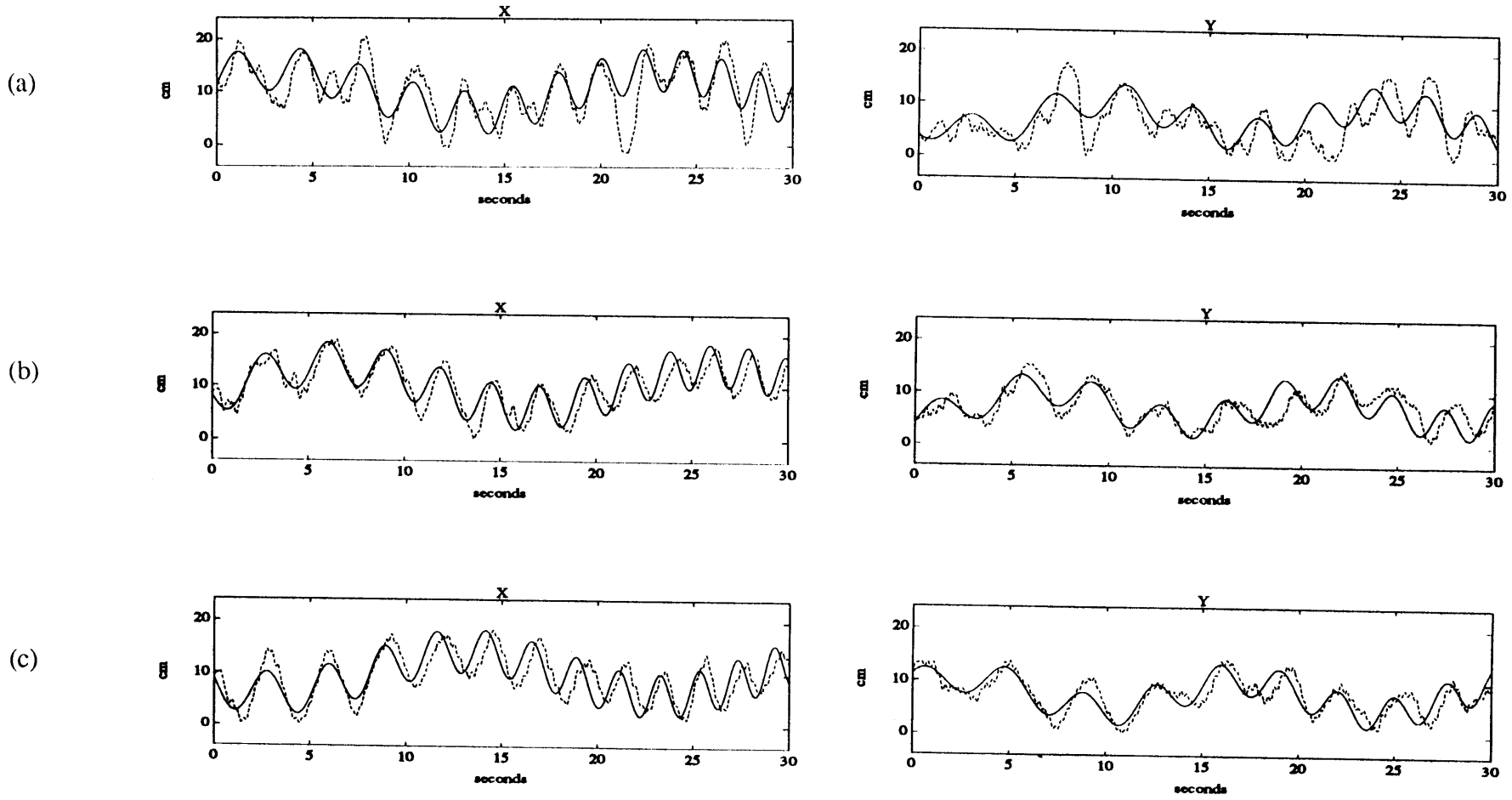

Figure 5-16. *Subject D:* Target and response time trajectories for comparing (a) undamped tremor to (b) tremor damped at 34 N/m/s to (c) tremor damped at 85 N/m/s.

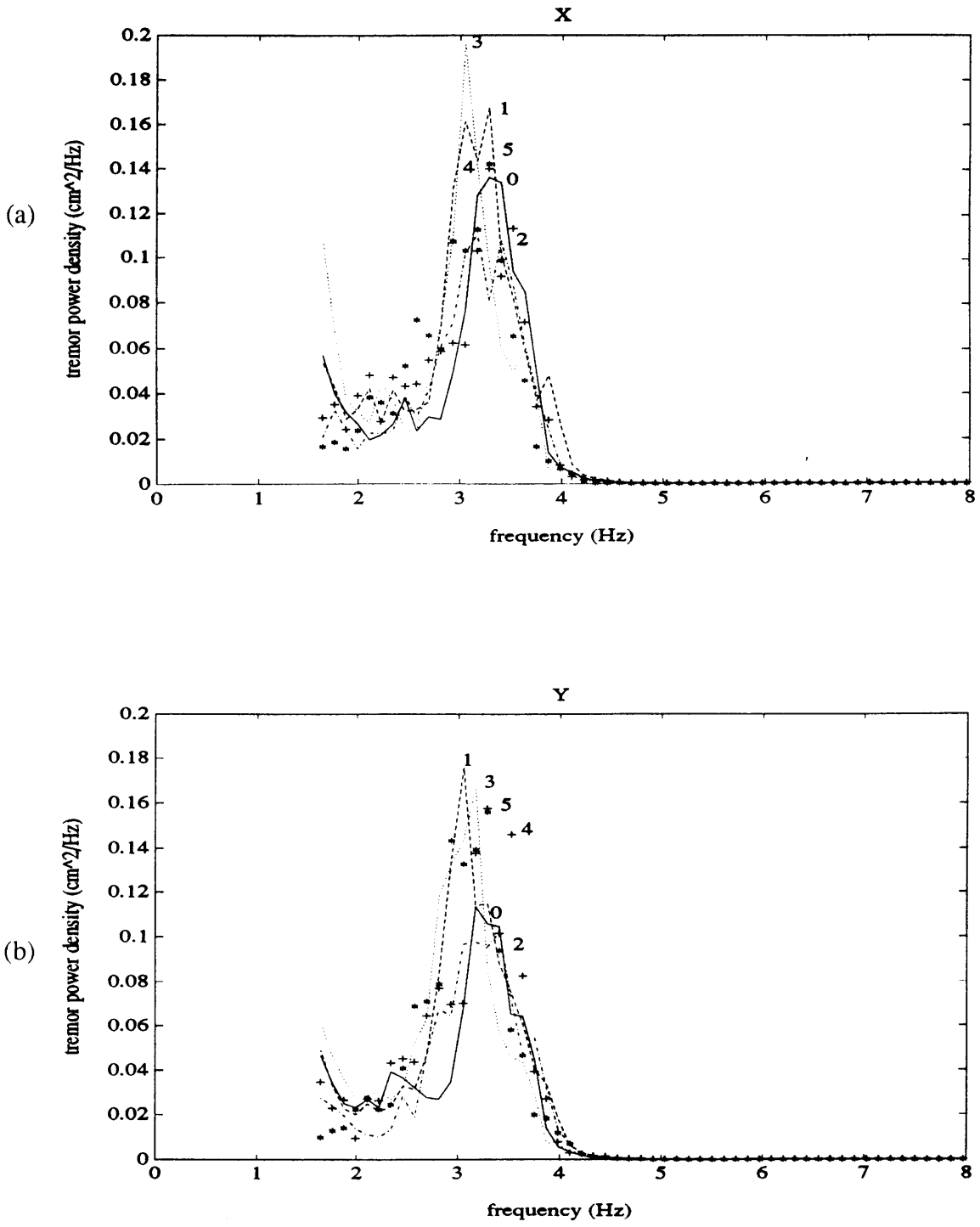

Figure 5-17. *Subject D:* Tremor position spectra illustrating the effects of linear damping. Damping levels 0-5 correspond to actual damping coefficients of 0, 17, 34, 51, 68, and 85 N/m/s, respectively.

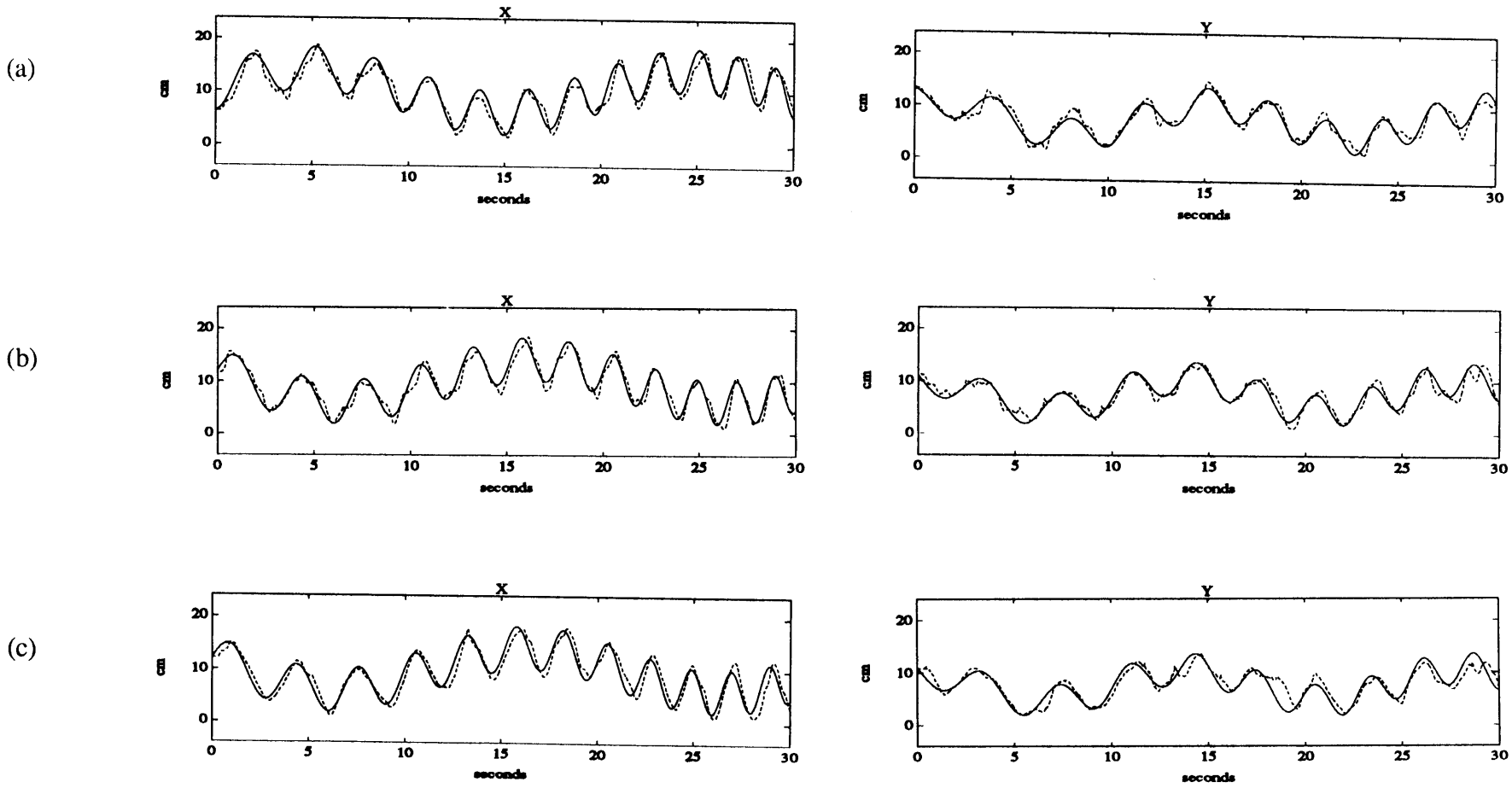

Figure 5-18. *Subject E:* Target and response time trajectories for comparing (a) undamped tremor to (b) tremor damped at 34 N/m/s to (c) tremor damped at 85 N/m/s.

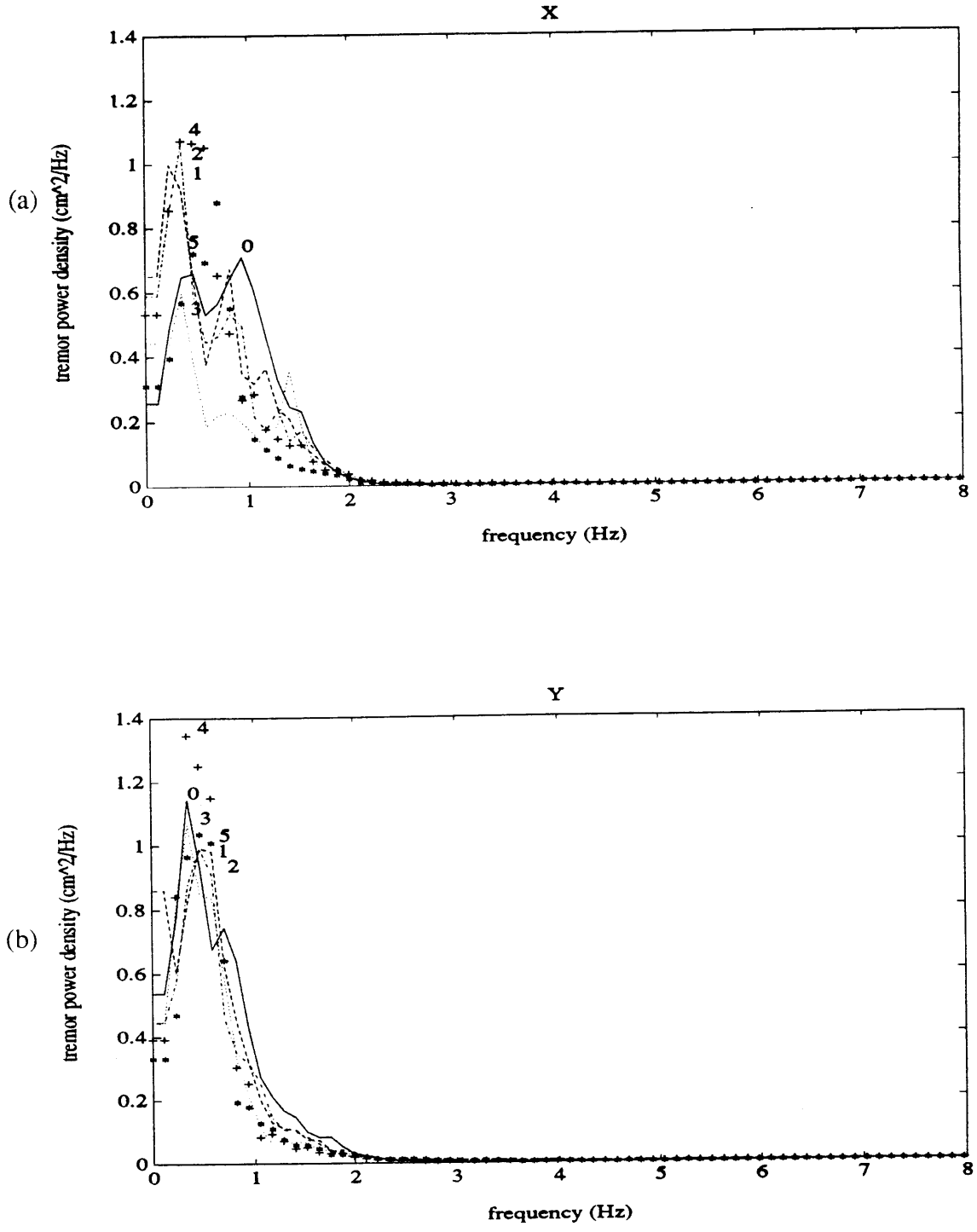

Figure 5-19. *Subject E:* Tremor position spectra illustrating the effects of linear damping. Damping levels 0-5 correspond to actual damping coefficients of 0, 17, 34, 51, 68, and 85 N/m/s, respectively.

(a)

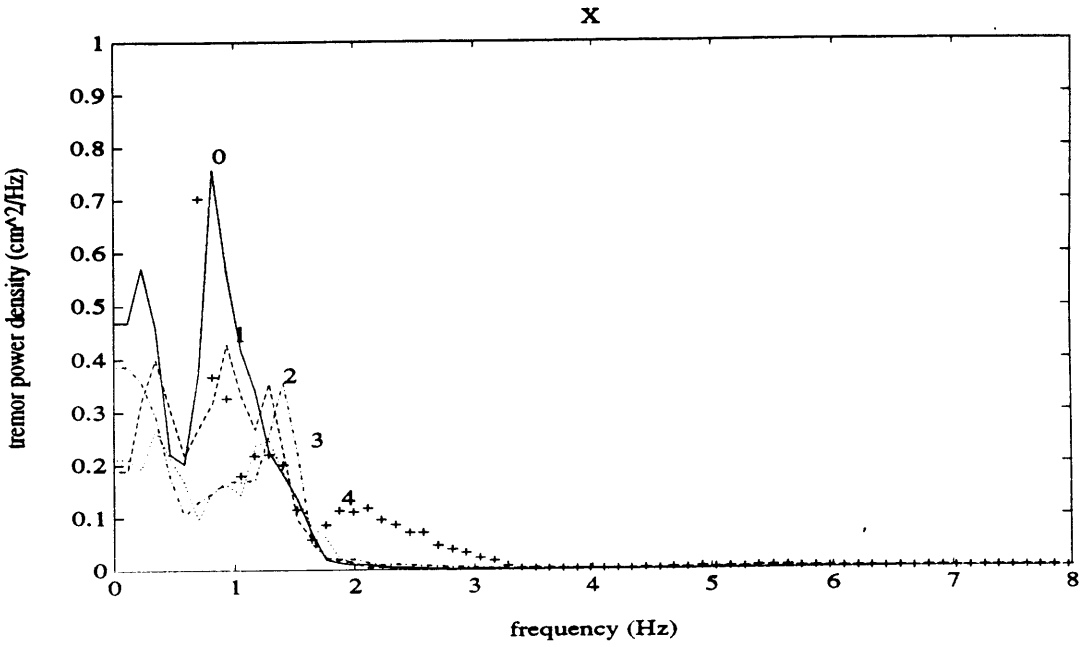

(b)

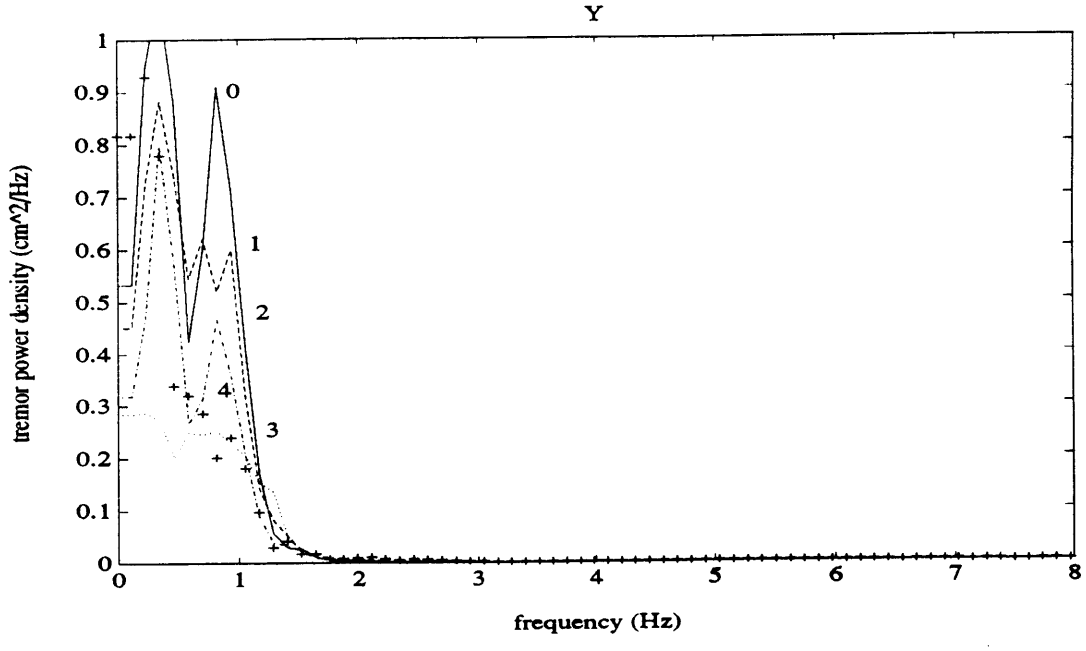

Figure 5-20. *Subject N_A:* Tremor position spectra illustrating the effects of linear damping. Damping levels 0-4 correspond to actual damping coefficients of 0, 17, 34, 51, and 68 N/m/s, respectively.

(a)

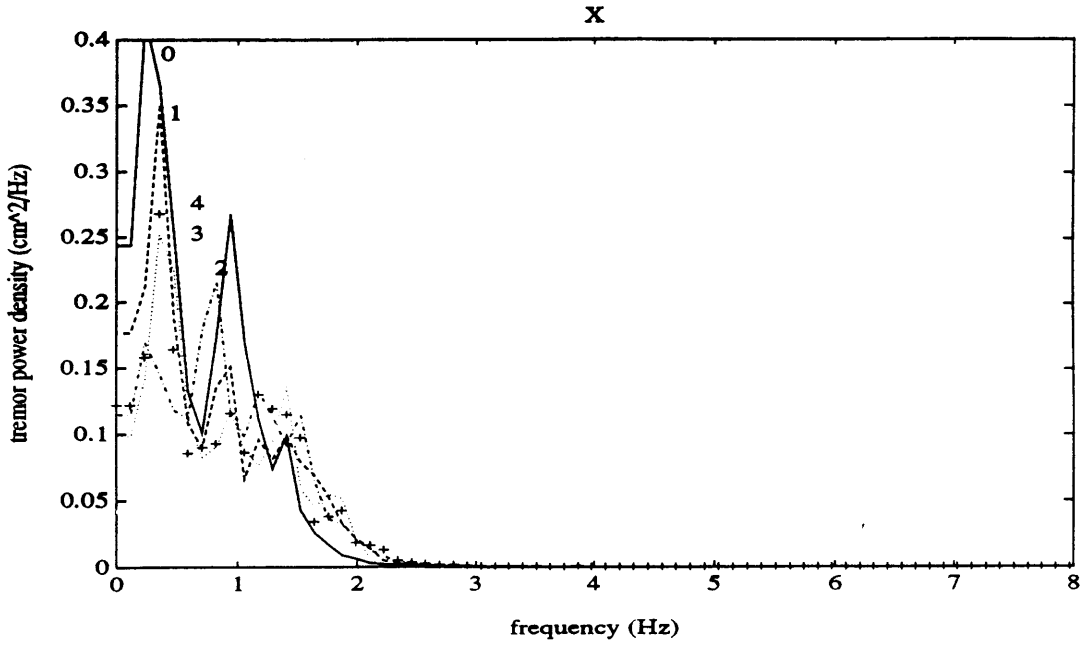

(b)

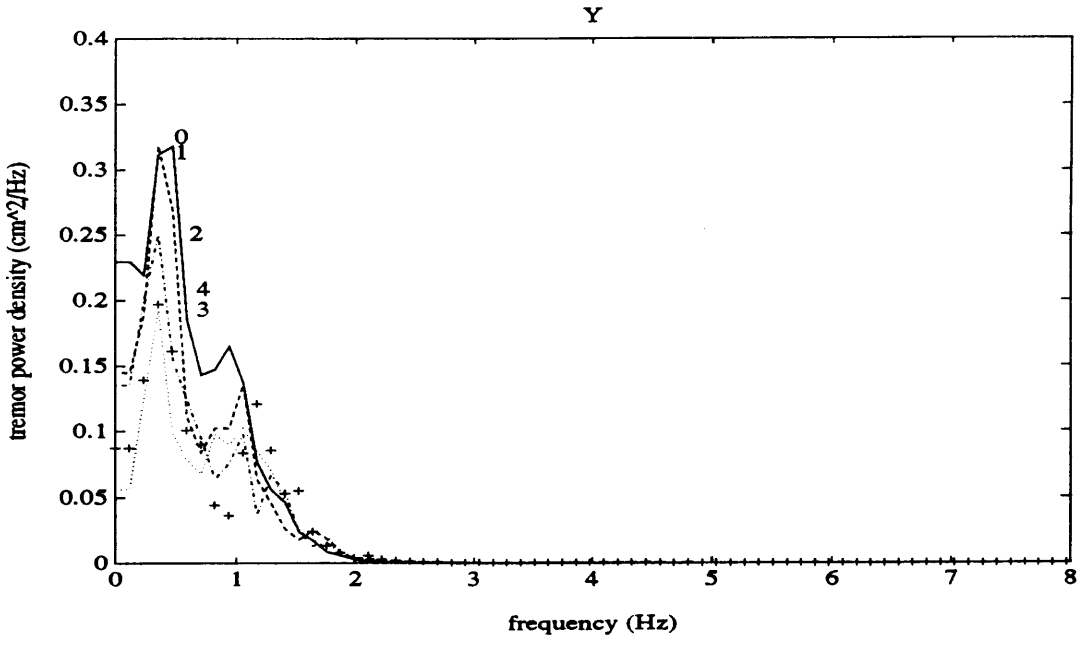

Figure 5-21. *Subject N_C:* Tremor position spectra illustrating the effects of linear damping. Damping levels 0-4 correspond to actual damping coefficients of 0, 17, 34, 51, and 68 N/m/s, respectively.

(a)

(b)

(c)

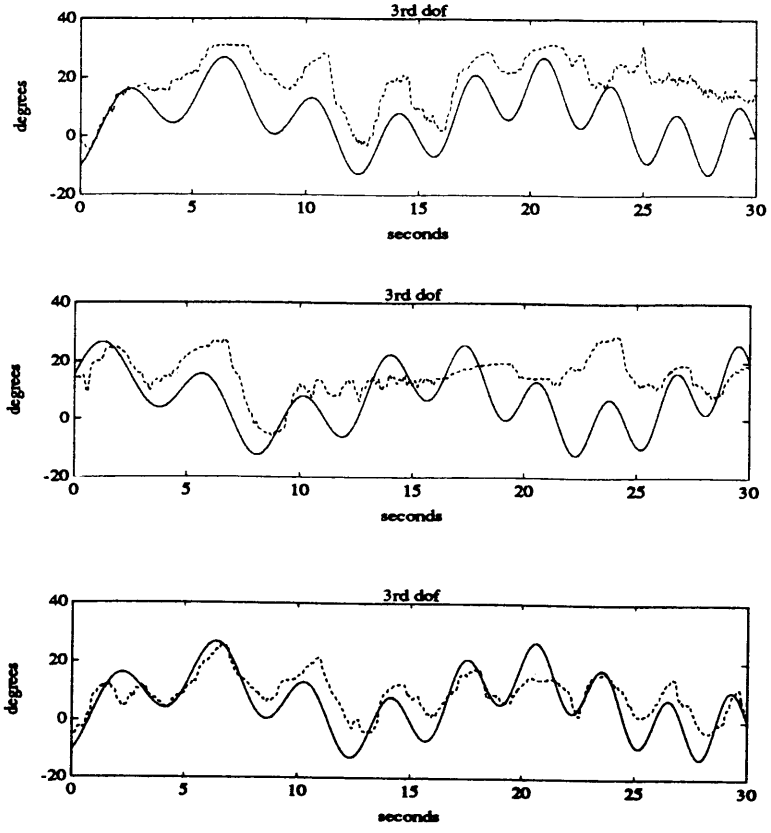

(d)

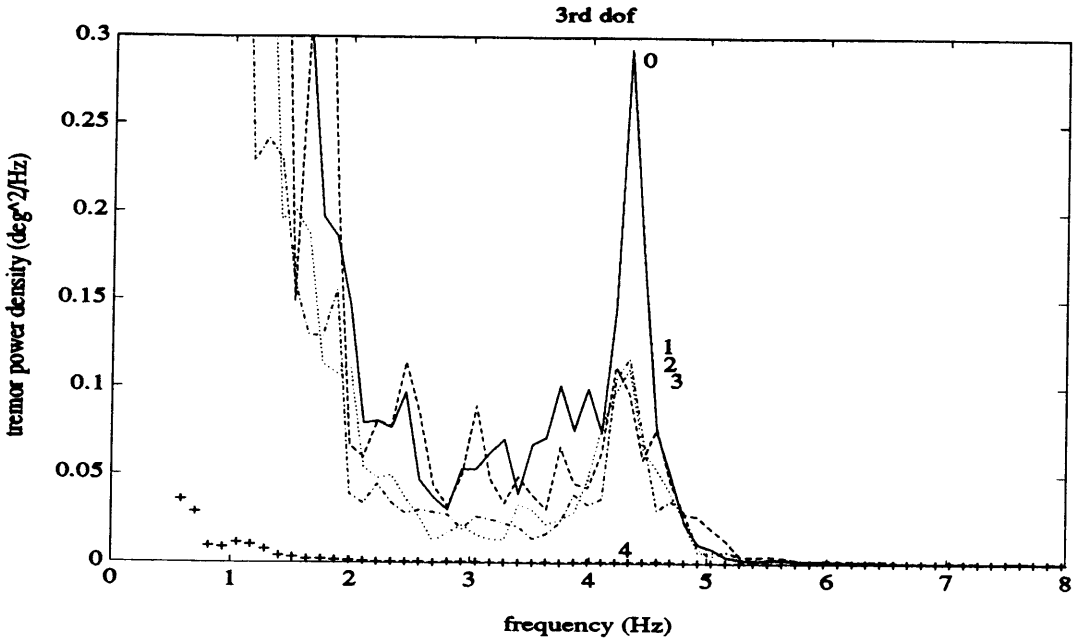

Figure 5-22. *Subject F:* Target and response time trajectories for comparing (a) undamped tremor to (b) tremor damped at 0.34 N/rad/s and (c) tremor damped at 0.68 N/rad/s; (d) tremor position spectra in which damping levels 0-4 correspond to actual damping coefficients of 0, 0.17, 0.34, 0.51, and 0.68 N/rad/s, respectively.

(a)

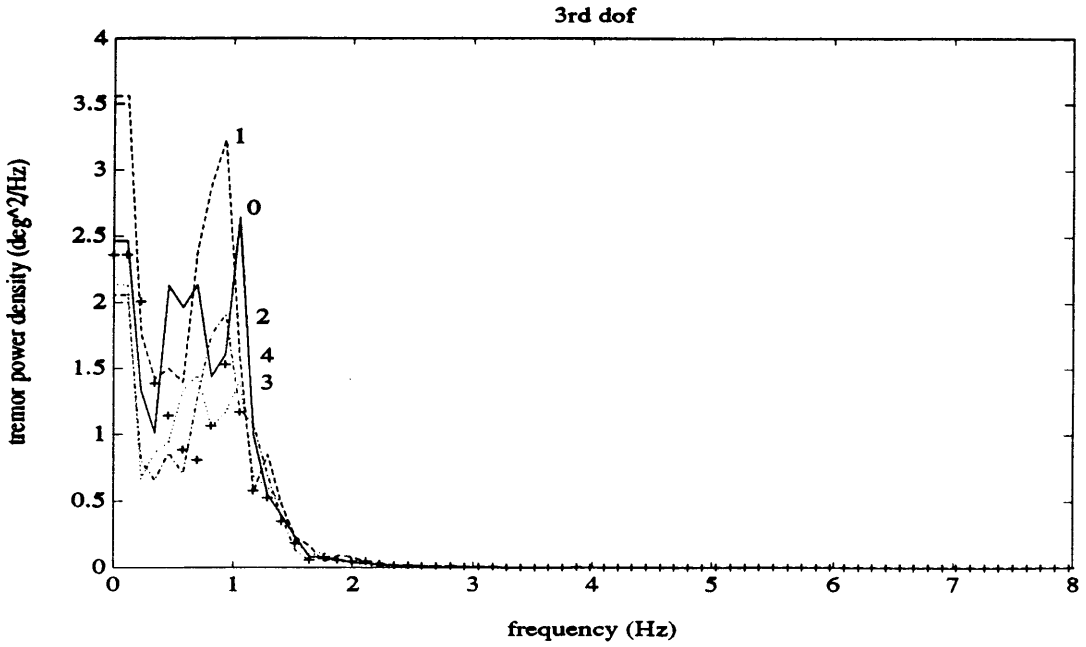

(b)

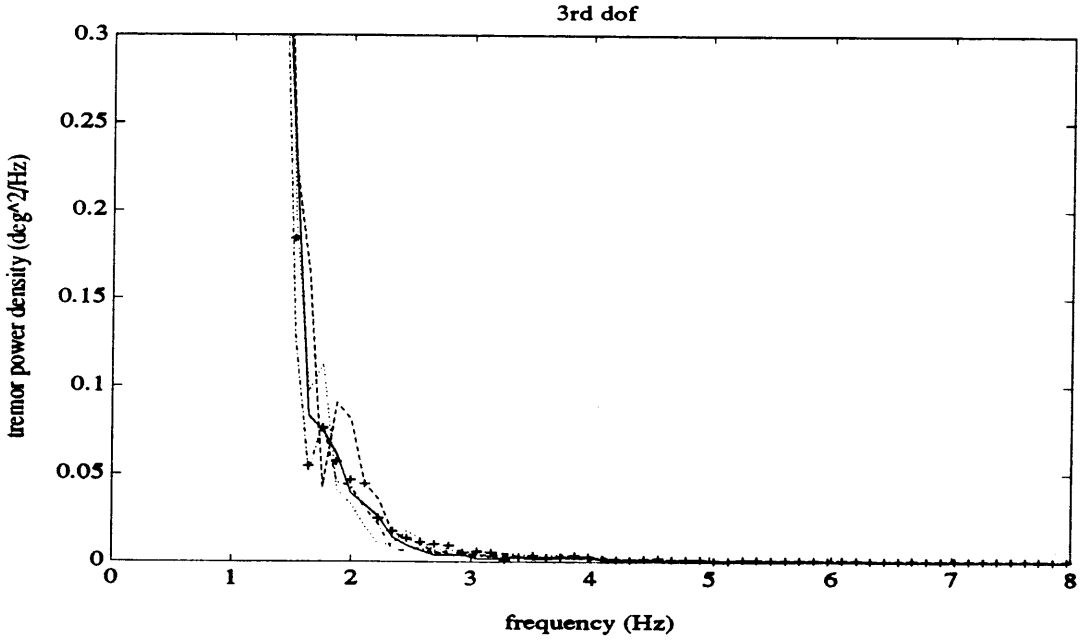

Figure 5-23. *Subject N_F:* Tremor position spectra illustrating the effects of linear damping, scaled to show (a) tracking errors and (b) the absence of tremor at tremor frequencies. Damping levels 0-4 correspond to actual damping coefficients of 0, 0.17, 0.34, 0.51, and 0.68 N/rad/s, respectively.

Responses of Subjects A, B, and C:

The application of viscous damping to the limbs of subjects A, B, and C -- the subjects most debilitated by their movement disorders -- *significantly* reduced their tremors as illustrated in Figures 5-10 through 5-15. In particular, the time domain plots show that the peak-to-peak magnitudes of these subjects' tremors were diminished 70 to 75 percent by the highest viscous loads; i.e. subject A's tremor was reduced from approximately 12 cm in the undamped trial to 3 cm in the highest damped trial; subject B's tremor was reduced from approximately 10 cm in the undamped trial to 3 cm in the highest damped trial; and subject C's tremor was reduced from approximately 7 cm in the undamped trial to 2 cm in the highest damped trial. The time domain plots also show that the viscous loads considerably improved the subjects' performance on pursuit tracking tasks, indicating that energy-dissipating orthoses *can selectively* attenuate tremor while enhancing or leaving unaffected purposeful voluntary movement.

The frequency domain plots in Figures 5-11, 5-13, and 5-15 further verify that viscous damping can attenuate intention tremor. However, these plots also show that when higher and higher levels of damping were used in these experiments, subjects' tremor peaks were reduced by asymptotically smaller and smaller amounts. This trend was previously observed by Sanes et al in 1988 and Baiges in 1989 and may be attributed to any number of physiological and/or experimental causes including:

1. Limited effectiveness of damping -- As detailed in Section 1.2.3, theoretical arguments can be made for any of the three hypothesized tremor mechanisms which predict that the application of damping loads to tremorous limbs will result in selective attenuation of tremor relative to voluntary movement. However, none of the arguments imply that continued increases in damping necessarily result in continued decreases in tremor. If, for example, an individual's tremor is generated by an autonomous reflex oscillation in which damping acts to reduce tremor oscillations by appropriately altering the dynamics of the "physical plant" driven by

the closed-loop neural system, then proportional increases in damping are not necessarily expected to alter the dynamics of the plant in ways which result in proportional decreases in tremor.

2. Effects of increased voluntary force levels -- If tremor amplitude is a function of voluntary muscular force (as it appears to be in some individuals with essential tremor as experimentally observed by Adelstein et al in 1987), then an increase in damping might *enhance* tremor rather than suppress tremor by effectively increasing the voluntary force required to do a task. That is, damping may affect individual's tremor via two (or more) mechanisms such that its net effect depends upon the amount that tremor is attenuated by damping *relative* to the amount that tremor is enhanced by increased voluntary muscular activity.
3. Limitations of the CEDO 1 magnetic particle brakes -- Although careful examination of the torque commands sent to the brake-driver circuitry verifies that the brakes are not saturating (i.e. operating at maximum torque limits) at the highest viscous loads under the experimental conditions of this study, the actual brake torques have not been measured. If the brakes do not respond quickly enough to commands from the computer, then the actual brake torques at high damping levels may not be as large as they are supposed to be and the observation that tremor attenuation "levels off" at high damping loads may simply indicate that the applied resistive loads at these damping levels are in fact less than those specified by the damping coefficient.
4. Effects of soft tissue and limb coupler compliance -- One problem inherent in the application of damping loads to reduce limb tremor is the presence of soft tissue. While the muscle forces which generate tremor are applied to the skeleton, the CEDO applies its resistive loads through the skin and, as a result, the thickness and compliance of the soft tissue layers set a lower limit on the amplitude to which tremor can be reduced. To estimate this lower limit, experiments were done on the static stiffness of coupling cuffs and the soft tissue areas through which coupling

cuffs apply forces by MIT undergraduate Jessie Wong [1990]. Using Wong's estimate of **19750 N/m** for the stiffness of the limb coupler and underlying soft tissue, and assuming the CEDO 1 applies a maximum load of **110 N** as predicted by the dynamic model in Chapter 2, calculations suggest that the CEDO 1 will allow a deviation of approximately **5.5 mm** between its distal joint axis and the user's wrist joint below which tremor movements will not be attenuated.

Responses of Subjects D and E:

As illustrated in Figures 5-16 through 5-19, subjects D and E responded less dramatically to the applied viscous loads than subjects A, B, and C. Figures 5-16 and 5-17, for instance, present data from subject D. Subject D's movement disorder is comprised of a low-amplitude 3.4 Hz intention tremor in addition to a general ataxia in her right limb. Although her tracking accuracy was significantly improved with the application of damping as evidenced by the time domain plots, her low-amplitude 3.4 Hz tremor was *not* reduced with the application of damping as evidenced by both the time domain and frequency domain plots (and was, in fact, aggravated by some damping levels). Thus, the viscous loads improved subject D's overall limb control but did not effectively suppress her tremor, perhaps because the amplitude of her tremor is not very large compared to the compliance of the limb coupler and soft tissue. Similar results were observed for subject E.

Responses of Subjects N_A and N_C:

Interestingly, Figures 5-20 and 5-21 suggest that damping may also reduce, to a certain extent, the non-linear tracking errors of the able-bodied subjects. The limited precision of the spectral estimates, however, prohibits drawing any strong conclusions from the slight differences in power magnitudes observed in these plots.

Responses of Subjects F and N_F:

Figures 5-22 and 5-23 present the 1-dof tracking data for subjects F and N_F and demonstrate that even the small amount of damping contributed by the CEDO's third particle brake (rotational degree of freedom) can reduce the tendency of a tremor-disabled person's limb to oscillate. As shown in Figure 5-22, subject F's tracking was much better, and his tremor was much less pronounced, when his limb was damped. One fact not illustrated in these plots, however, is that in some trials at the highest damping level subject F was unable to lift his elbow and rotate his forearm against the applied resistive loads as much as he was able to in other trials. Data from these trials were not averaged into the spectra because subject F did not complete the task and thus *induced* less tremor in these trials. Frequency domain plots for able-bodied subject N_F, for comparison, are shown in Figure 5-23. The first figure is scaled to illustrate that damping has little effect on subject N_F's tracking. The second figure is scaled to demonstrate that the tremor power spectrum in the range of pathological tremor frequencies for an able-bodied subject is zero.

5.2.2 The Effects of Non-Linear Damping

Figures 5-24 through 5-33 illustrate the effects of non-linear (velocity-squared) damping on tremor and tracking for disabled subjects A-E, respectively. Non-linear damping trials were not done for subject F or for the able-bodied control subjects. As in the previous section, the first figure for each subject shows typical tracking records for comparing tremor and tracking without damping to tremor and tracking with low (69 $N/(m/s)^2$), moderate (138 $N/(m/s)^2$), and high (207 $N/(m/s)^2$) levels of non-linear damping. The second figure for each subject shows tremor position spectra averaged over all trials from a particular damping level. In these plots, the solid line corresponds to the undamped trials, the dashed line corresponds to the 69 $N/(m/s)^2$ damped trials, the dash-dot line corresponds to the 138 $N/(m/s)^2$ damped trials, and the dotted line corresponds to the 207 $N/(m/s)^2$ damped trials.

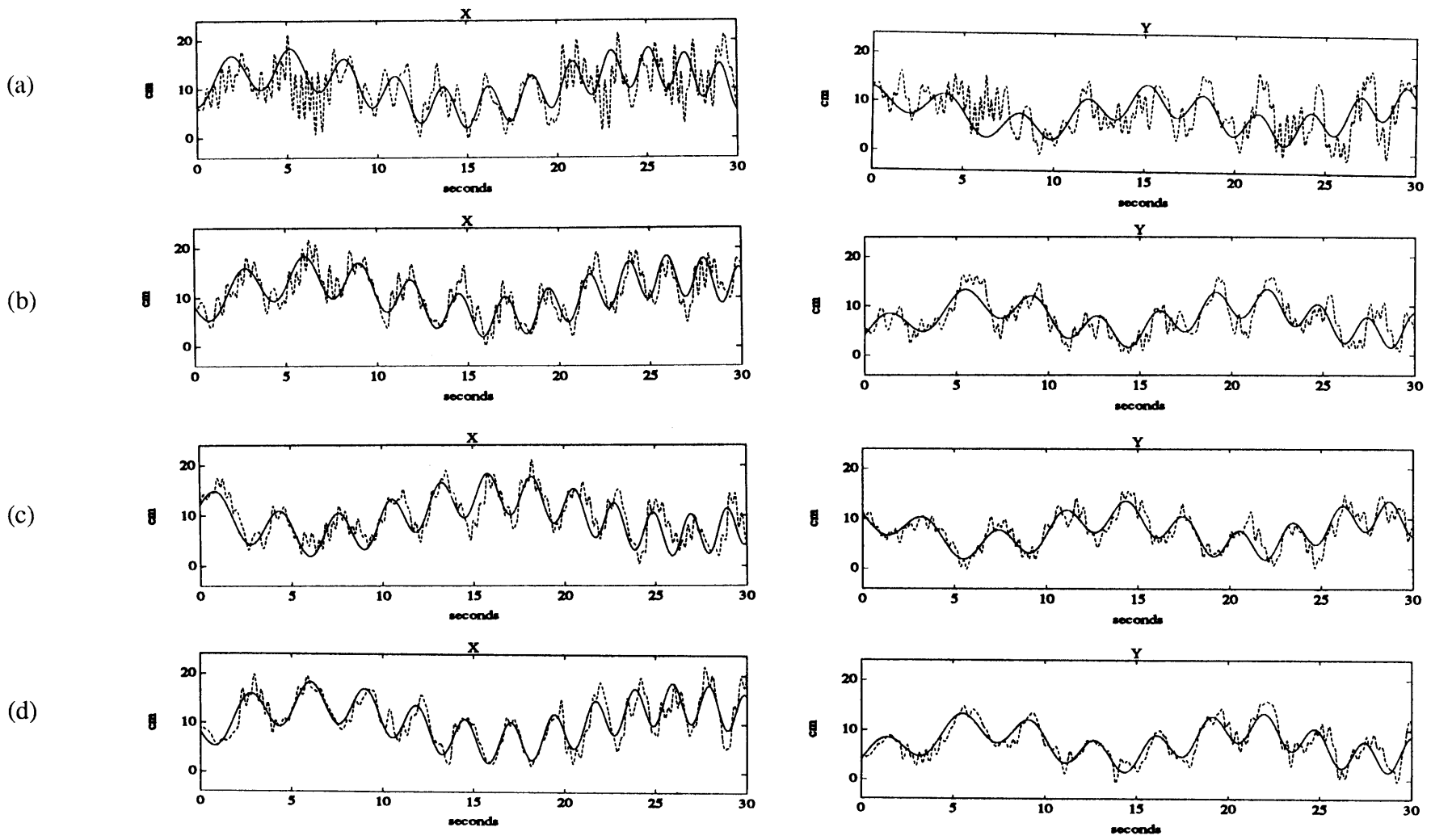

Figure 5-24. *Subject A:* Target and response time trajectories for comparing (a) undamped tremor to (b) tremor damped at 69 N/(m/s)^2 to (c) tremor damped at 138 N/(m/s)^2 to (d) tremor damped at 207 N/(m/s)^2.

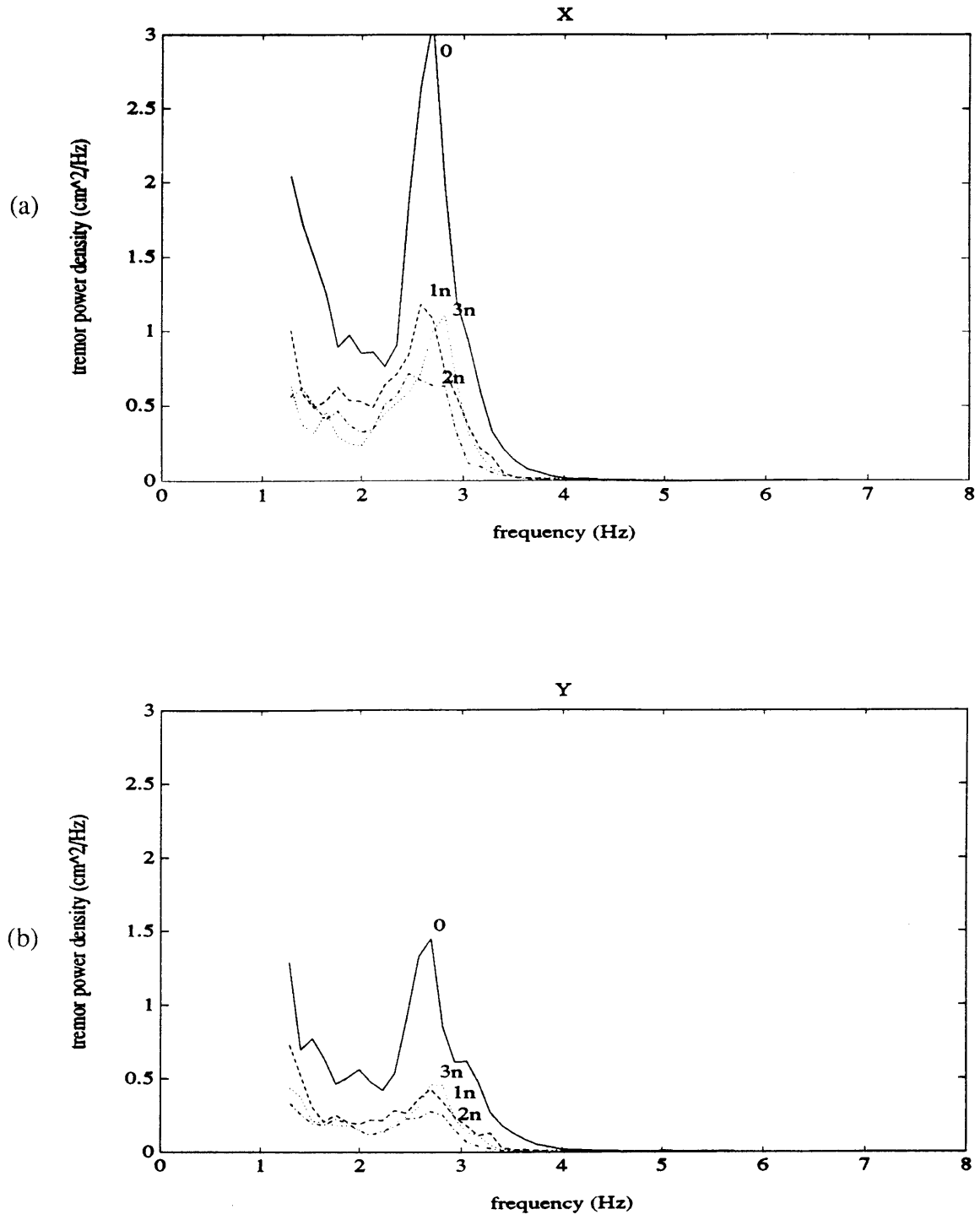

Figure 5-25. *Subject A:* Tremor position spectra illustrating the effects of non-linear damping. Damping levels 0-3n correspond to non-linear damping coefficients of 0, 69, 138, and 207 N/(m/s)^2, respectively.

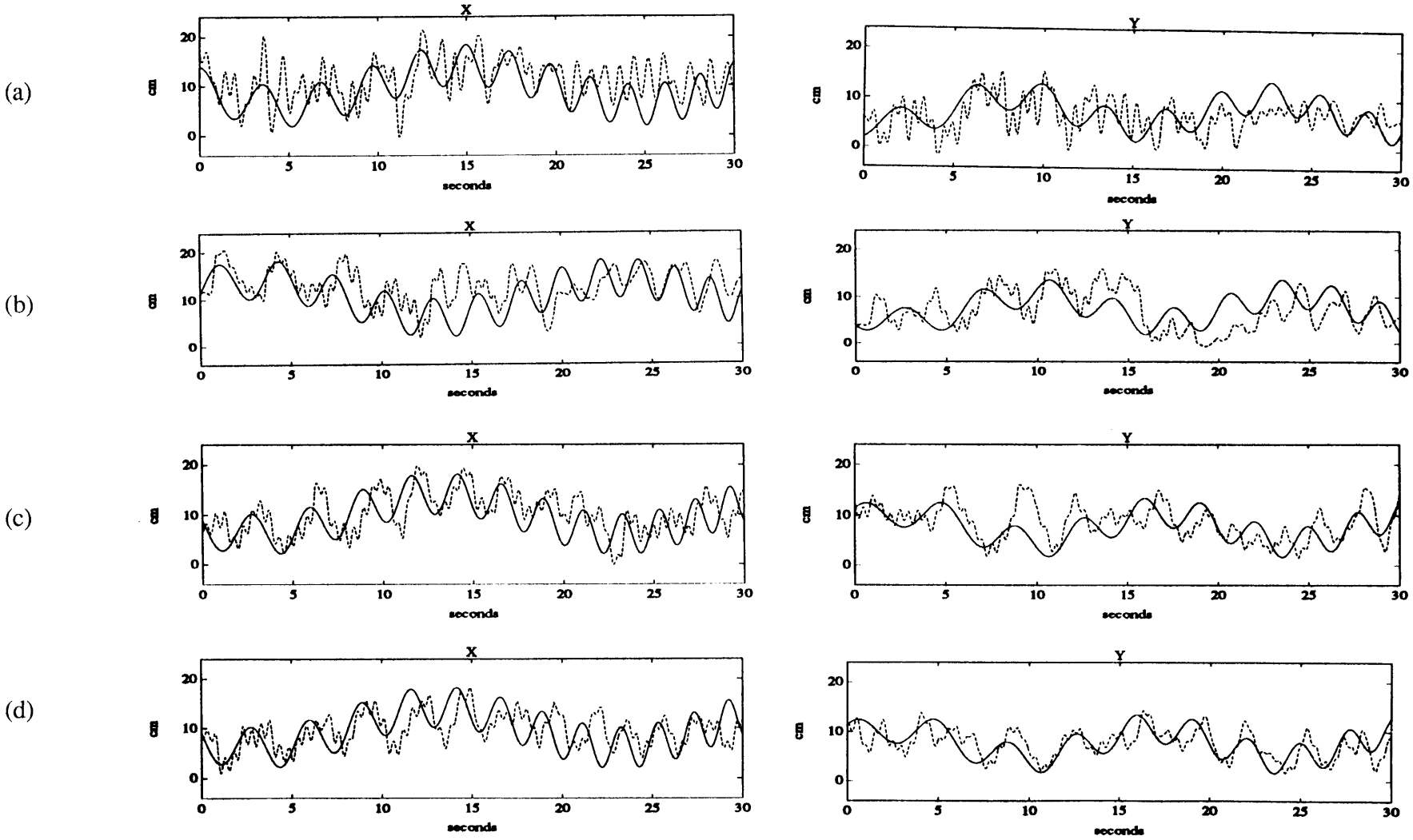

Figure 5-26. *Subject B:* Target and response time trajectories for comparing (a) undamped tremor to (b) tremor damped at 69 N/(m/s)^2 to (c) tremor damped at 138 N/(m/s)^2 to (d) tremor damped at 207 N/(m/s)^2.

(a)

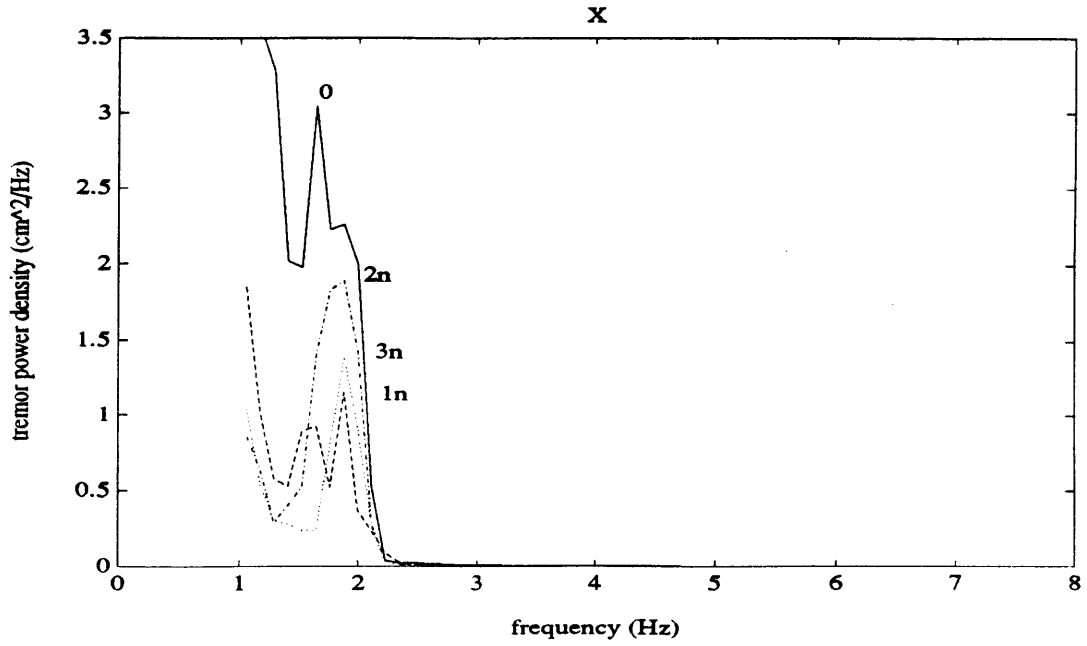

(b)

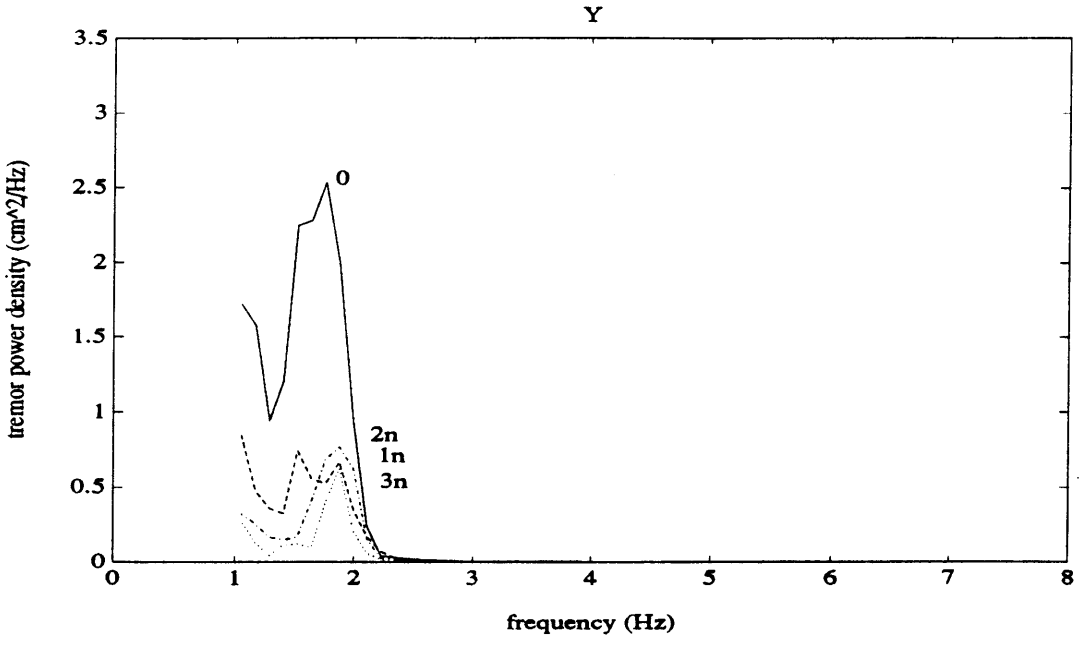

Figure 5-27. *Subject B:* Tremor position spectra illustrating the effects of non-linear damping. Damping levels 0-3n correspond to non-linear damping coefficients of 0, 69, 138, and 207 N/(m/s)^2, respectively.

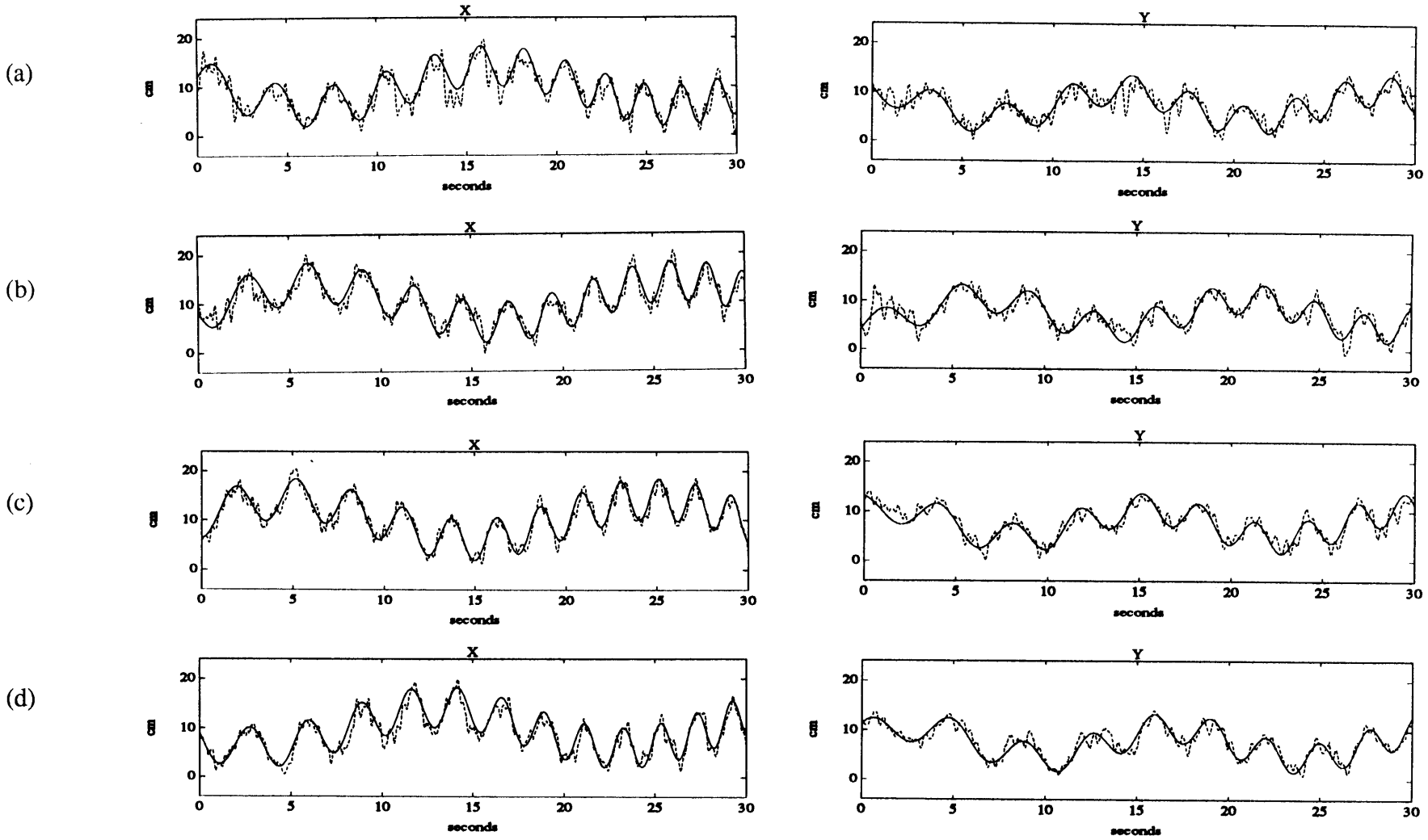

Figure 5-28. *Subject C:* Target and response time trajectories for comparing (a) undamped tremor to (b) tremor damped at 69 N/(m/s)^2 to (c) tremor damped at 138 N/(m/s)^2 to (d) tremor damped at 207 N/(m/s)^2.

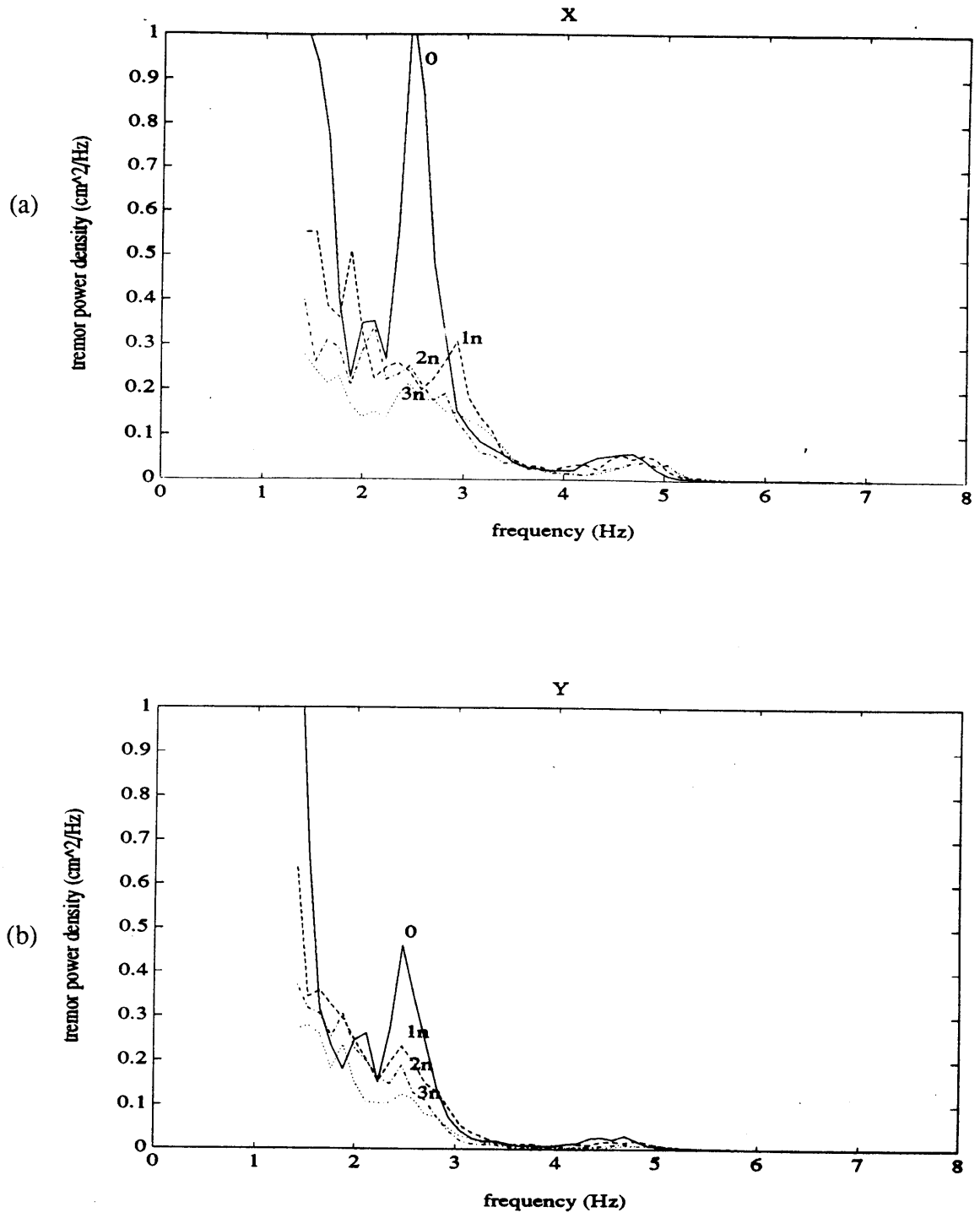

Figure 5-29. *Subject C:* Tremor position spectra illustrating the effects of non-linear damping. Damping levels 0-3n correspond to non-linear damping coefficients of 0, 69, 138, and 207 N/(m/s)^2, respectively.

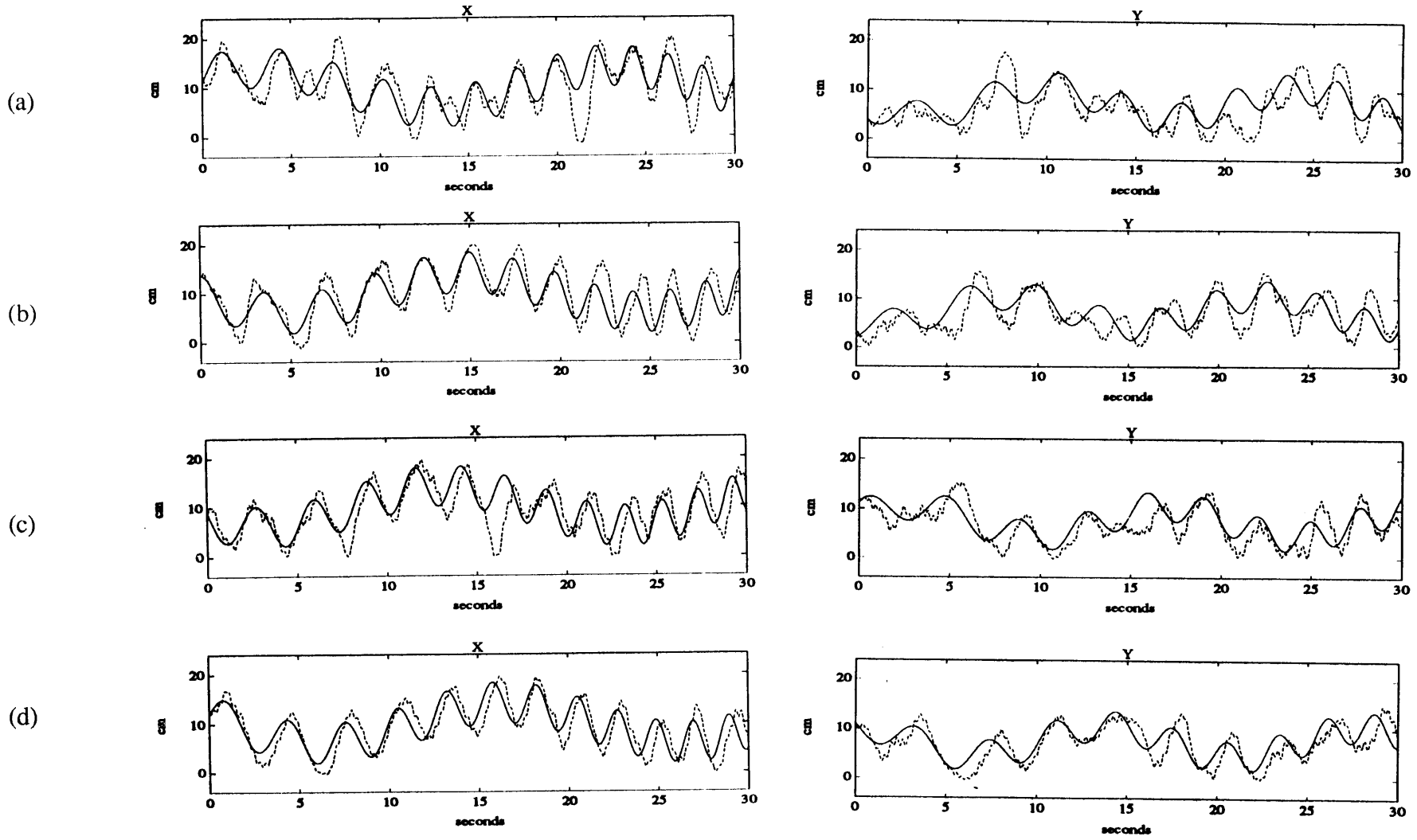

Figure 5-30. *Subject D:* Target and response time trajectories for comparing (a) undamped tremor to (b) tremor damped at 69 N/(m/s)^2 to (c) tremor damped at 138 N/(m/s)^2 to (d) tremor damped at 207 N/(m/s)^2.

(a)

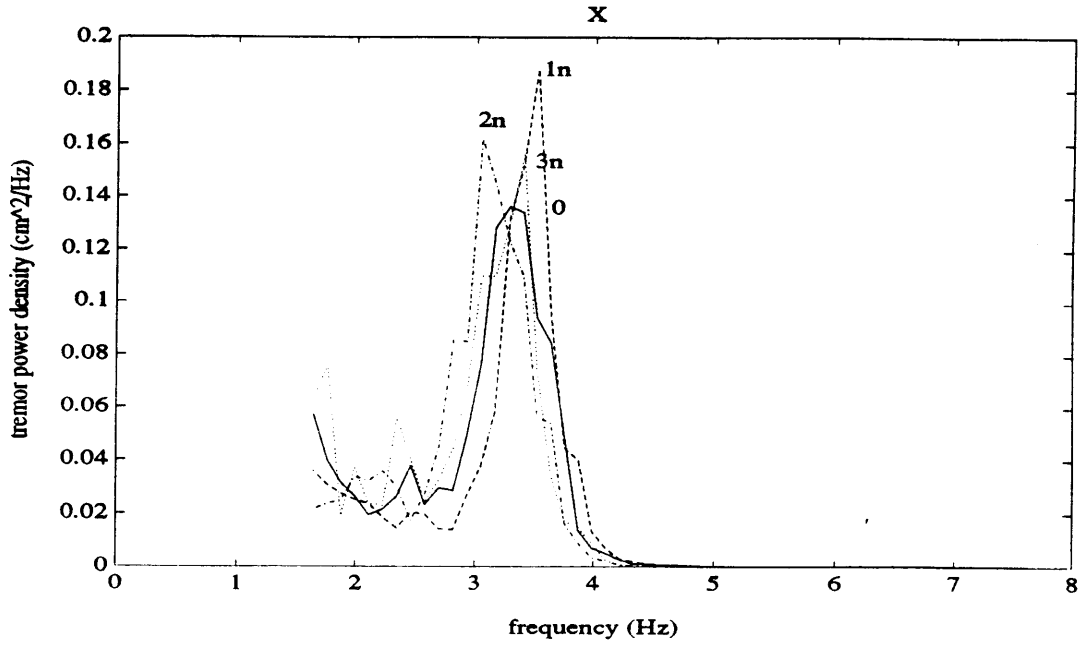

(b)

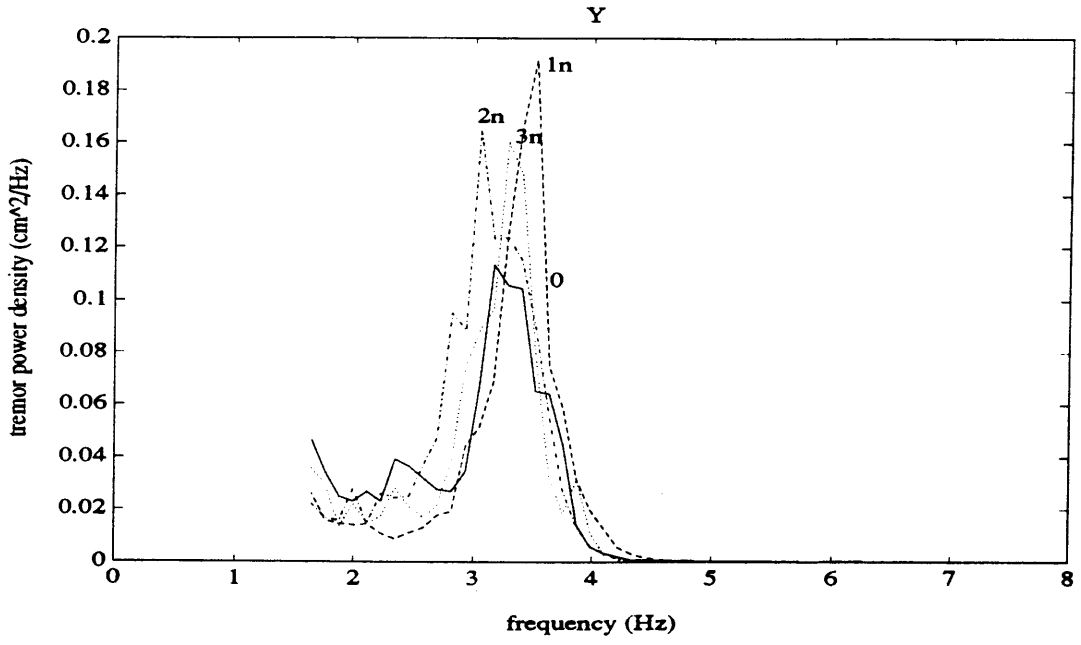

Figure 5-31. *Subject D:* Tremor position spectra illustrating the effects of non-linear damping. Damping levels 0-3n correspond to non-linear damping coefficients of 0, 69, 138, and 207 N/(m/s)^2, respectively.

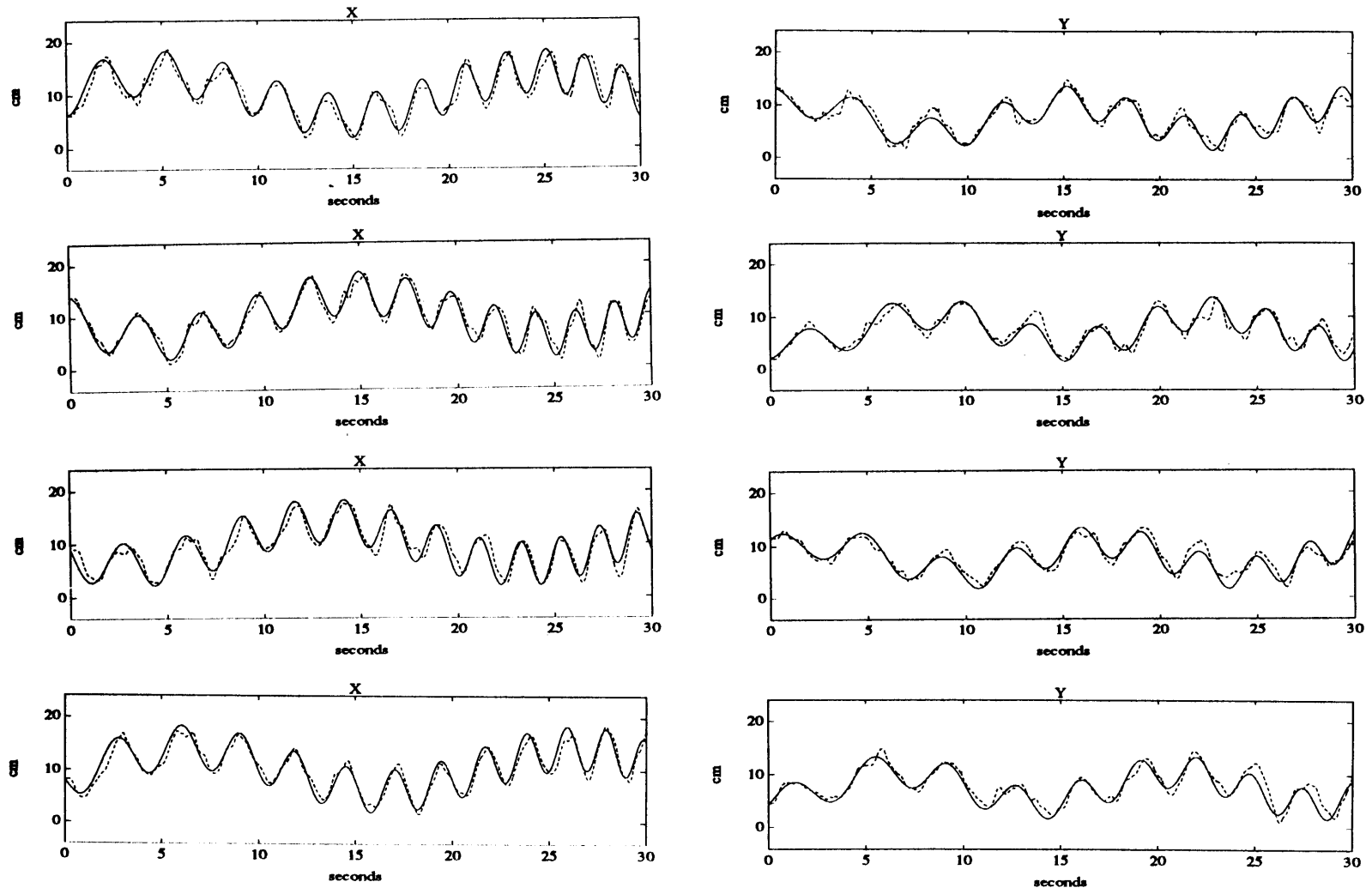

Figure 5-32. *Subject E:* Target and response time trajectories for comparing (a) undamped tremor to (b) tremor damped at 69 N/(m/s)^2 to (c) tremor damped at 138 N/(m/s)^2 to (d) tremor damped at 207 N/(m/s)^2.

(a)

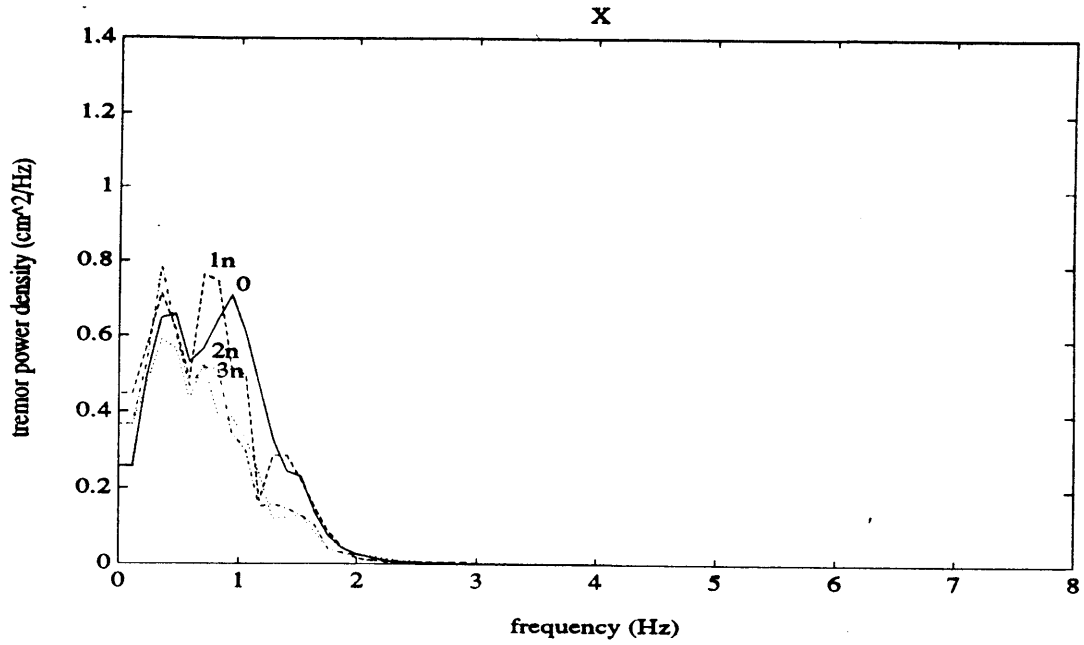

(b)

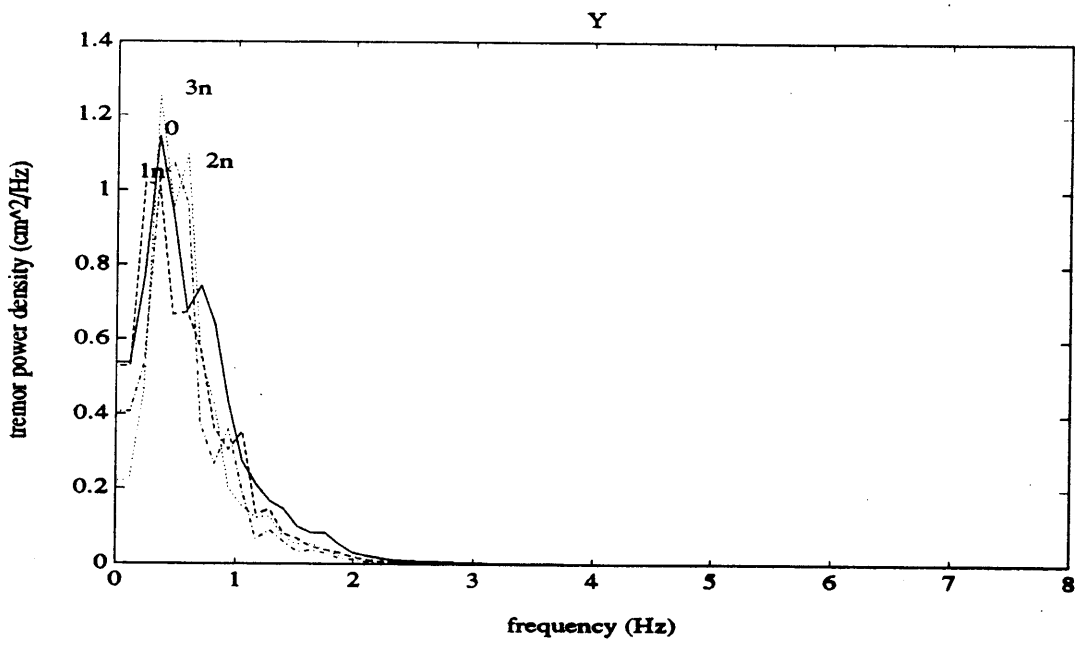

Figure 5-33. *Subject E:* Tremor position spectra illustrating the effects of non-linear damping. Damping levels 0-3n correspond to non-linear damping coefficients of 0, 69, 138, and 207 N/(m/s)^2, respectively.

The results presented in Figures 5-24 through 5-33 for the non-linear damping trials are similar to the results presented in Figures 5-10 through 5-19 for the linear damping trials. As evidenced by the plots, damping reduced tremor and improved tracking accuracy for subjects A, B, and C. Damping did not reduce the low amplitude 3.4 Hz tremor of subject D (and perhaps made it worse), but it did increase her ability to track the targets. Non-linear damping loads had little effect on subject E.

Although large differences in tremor power magnitudes are seen in the non-linearly damped trials compared to the undamped trials, only small differences in tremor power magnitudes are seen in the trials from the different non-linearly damped trials. This finding may indicate that the brakes are not responding fast enough as postulated in Section 5.2.1 above. Because larger rates-of-change of torque output are required to simulate velocity-squared damping than to simulate viscous damping, it is even more critical that the brakes respond quickly for velocity-squared damping simulations than for viscous damping simulations. Linear and non-linear damping schemes are further compared in Sections 5.2.3 and 5.2.4 below.

5.2.3 An Assessment of Tremor Power and Tracking Performance

To confirm that the "damping effects" detected in Figures 5-10 through 5-33 are in fact statistically significant, quantitative tremor power and tracking performance scores were computed for each subject, plotted versus damping level, and analyzed using two-way analysis of variance (ANOVA) techniques. All tremor and tracking performance scores presented in this section were defined previously in Section 4.4.2 of Chapter 4.

Tremor Power:

Tremor power, defined in Section 4.4.2 as the area under the tremor power density spectrum between the lower and upper frequencies which bound a subject's tremor band, is plotted versus damping level in Figures 5-34 through 5-38 for subjects A-E, respectively. In each figure, data from the linear damping trials are shown in the top two plots while data from

the non-linear damping trials are shown in the bottom two plots. Each data point represents the mean tremor power at that damping level, and each error bar denotes one standard deviation about the mean.

Qualitatively, Figures 5-34 through 5-38 show that tremor power decreases with linear and non-linear damping to varying degrees for all subjects. For subjects A, B, and C, the average tremor power from the most linearly damped trials is less than the average tremor power from the most non-linearly damped trials, while for subject D, the average tremor power from the most linearly damped trials is slightly greater than the average tremor power from the most non-linearly damped trials. For subject E, differences in average tremor power scores from both linear and non-linear damping trials are small and consistent trends with damping are not seen. It is important to note that "tremor power" as defined in this investigation includes power from tremor as well as from non-linear tracking errors and that a certain percentage of the observed decreases in tremor power, particularly for subjects D and E, is due to an increase in tracking accuracy rather than a decrease in involuntary rhythmic tremor. Since the primary goal of this investigation is simply to assess whether energy-dissipating orthoses can help individuals disabled by tremor or ataxia function more independently, making further distinctions between tremor and non-linear tracking errors is probably unnecessary. In future investigations, however, particularly those which involve tracking tasks of varying complexity or tasks in which tracking errors comprise a large fraction of the quantitative tremor power scores, further distinguishing tremor and tracking errors may be required.

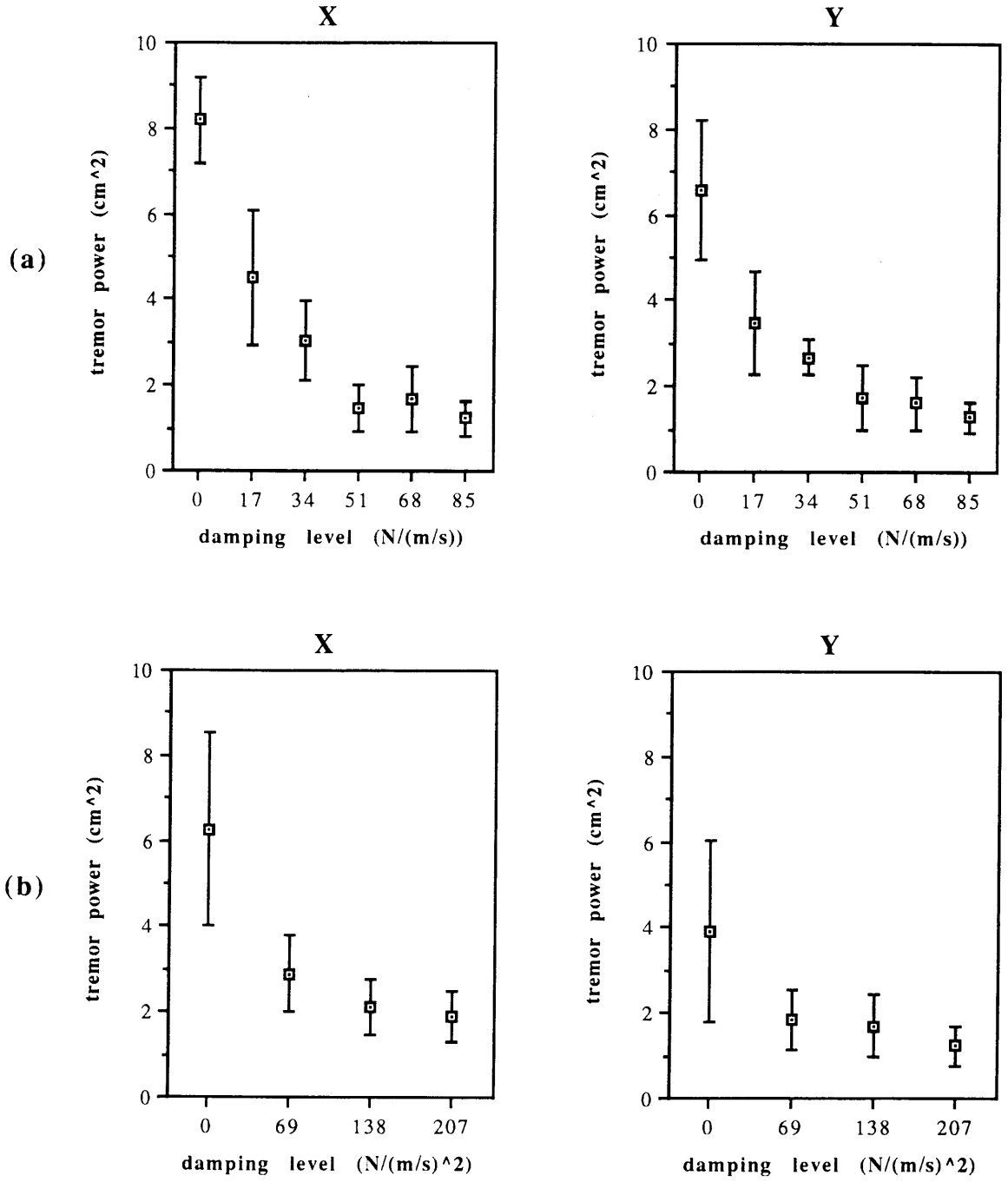

Figure 5-34. *Subject A:* Tremor power as a function of (a) linear and (b) non-linear damping.

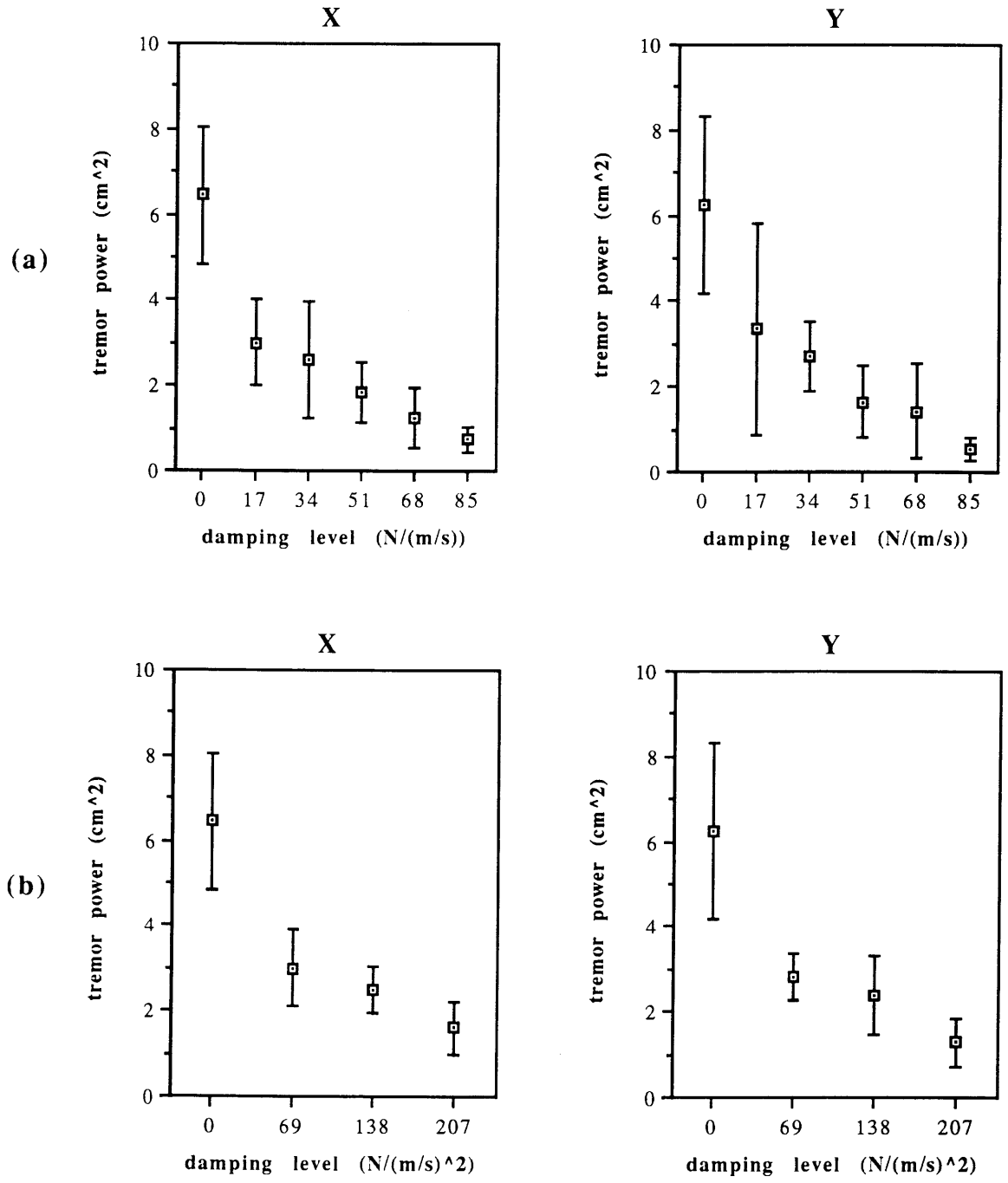

Figure 5-35. *Subject B:* Tremor power as a function of (a) linear and (b) non-linear damping.

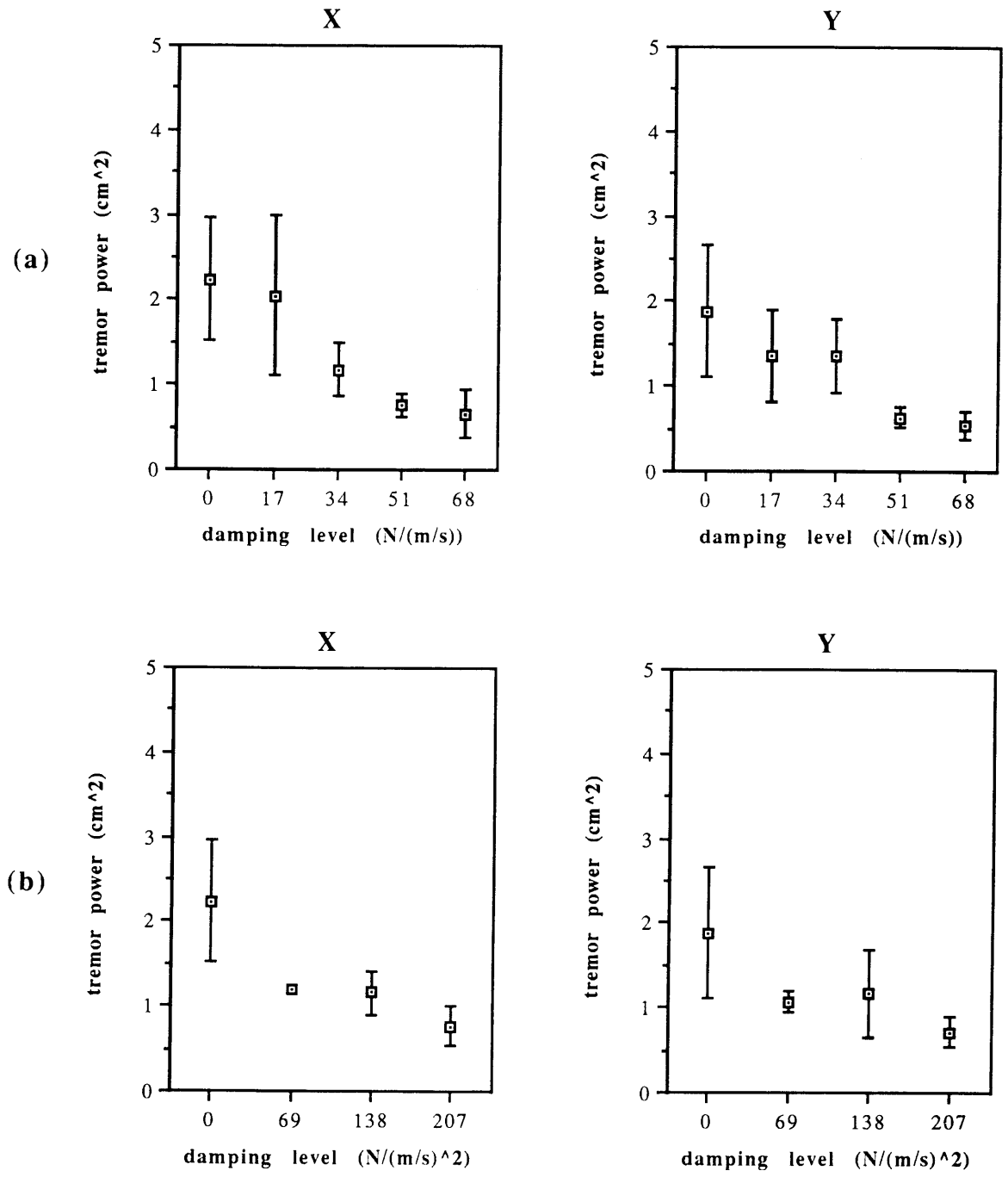

Figure 5-36. *Subject C:* Tremor power as a function of (a) linear and (b) non-linear damping.

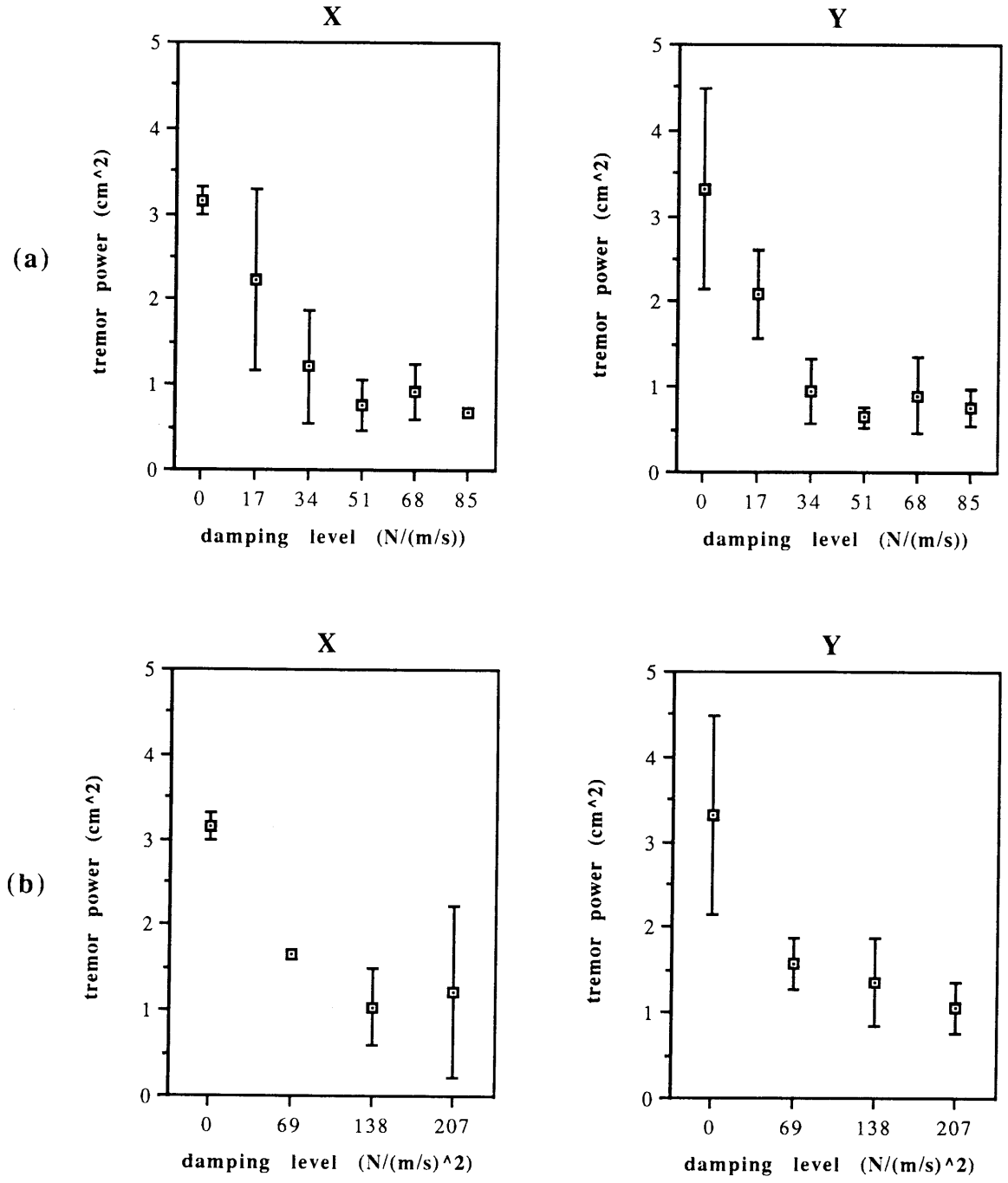

Figure 5-37. *Subject D:* Tremor power as a function of (a) linear and (b) non-linear damping.

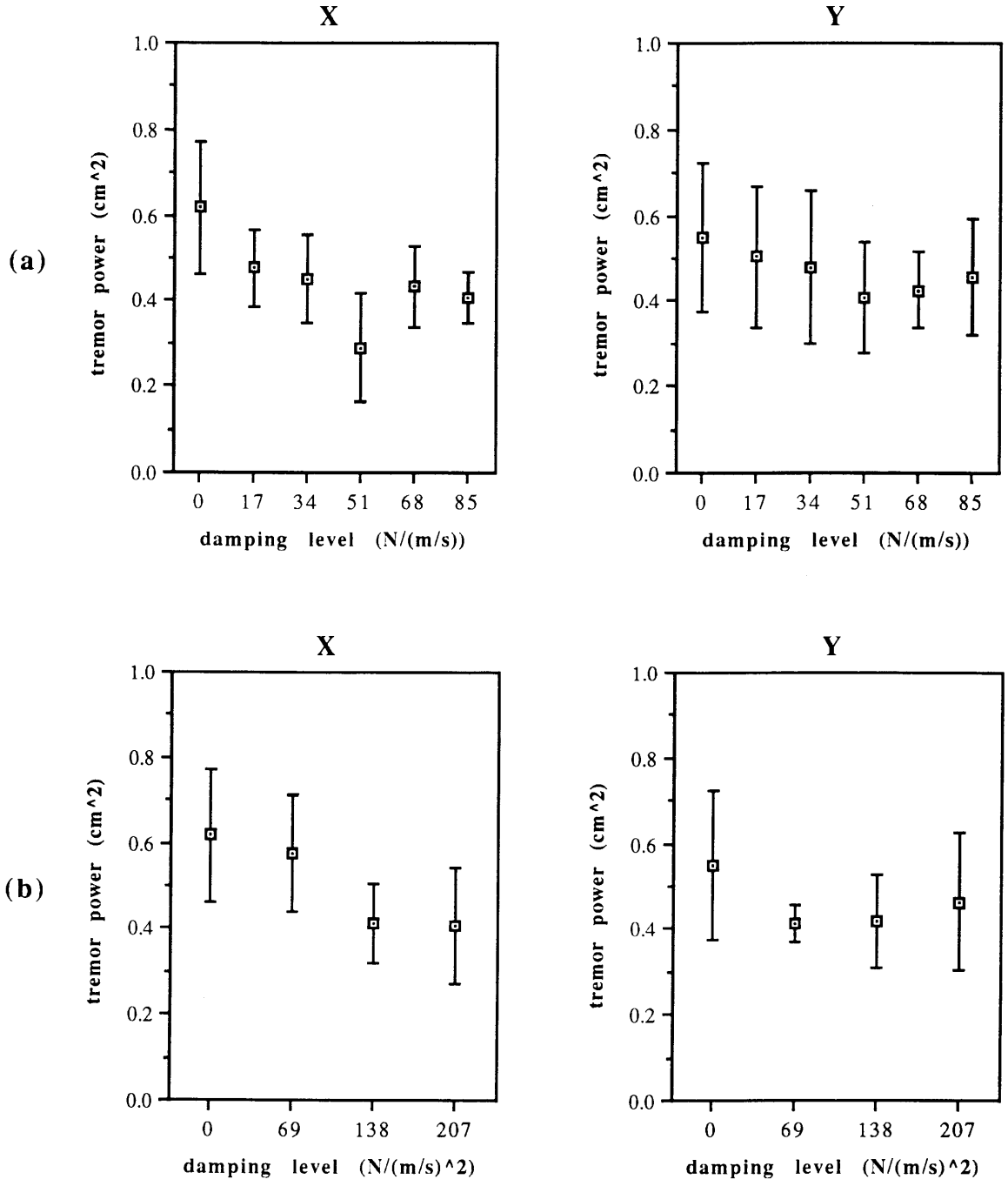

Figure 5-38. *Subject E:* Tremor power as a function of (a) linear and (b) non-linear damping.

The average tremor power scores used to statistically compare the effects of different pairs of damping levels for each subject are listed in Table 5-2. Separate statistical tests were done for each subject, and only data from the main "damping" test session were included (data from more than one session were not used because it was desired, for ease of computation, to use the same number of data points from the same session for each linear and non-linear damping level). In order to utilize both X and Y components of the data, all X data were normalized by the average undamped X tremor power, all Y data were normalized by the average undamped Y tremor, and damping levels and XY directions were considered to be separate factors in two-way analysis of variance (ANOVA) F-tests done for each subject.

F-tests with 8 and 36 degrees of freedom for subjects A and D, 8 and 18 degrees of freedom for subjects B and E, and 7 and 32 degrees of freedom for subject C confirm quantitatively that the decreases in tremor power observed in Figures 5-34 through 5-38 are statistically significant at p-values of less than 0.001 for subjects A, B, C, and D. The decreases in tremor power are not statistically significant for subject E. (The degrees of freedom differed for the subjects depending upon the number of data points available for each.) The results of further tests using Tukey's method of multiple comparisons to compare tremor power means from specific pairs of damping levels at the $\alpha = 0.01$, 0.05, and 0.1 levels of significance are given in Table 5-3 [Rice 1988]. As shown, nearly all of the damped tremor power scores differ significantly from the undamped tremor power scores, but few of the linearly damped tremor power scores differ significantly from each other or from the non-linearly damped tremor power scores for all subjects.

Table 5-2. Mean normalized tremor power combining X and Y data from a single test session for each subject.

Subject	*Damping Level*								
	0 N/m/s	*17 N/m/s*	*34 N/m/s*	*51 N/m/s*	*68 N/m/s*	*85 N/m/s*	*69 N/(m/s)²*	*138 N/(m/s)²*	*207 N/(m/s)²*
A	1.00	0.517	0.420	0.217	0.290	0.196	0.426	0.296	0.261
B	1.00	0.633	0.528	0.311	0.305	0.122	0.456	0.380	0.254
C	1.00	0.981	0.573	0.384	0.355	--	0.622	0.577	0.428
D	1.00	0.670	0.337	0.218	0.284	0.221	0.501	0.370	0.356
E	1.00	0.855	0.790	0.636	0.832	0.931	0.940	0.790	0.719
MEAN A-E	1.00	0.731	0.530	0.353	0.413	0.368	0.589	0.483	0.404
MEAN A-D	1.00	0.700	0.465	0.283	0.309	0.180	0.501	0.406	0.325

Table 5-3. Pairs of damping levels for which statistically significant differences in average tremor power are observed.

Subject	*Level of Significance*		
	$\alpha = 0.01$	$\alpha = 0.05$	$\alpha = 0.1$
A	0 & 17, 34, 51, 68, and 85 N/m/s 0 & 69, 138, and 207 N/(m/s)^2 17 & 51, 68, and 85 N/m/s 17 N/m/s & 138 and 207 N/(m/s)^2 34 & 85 N/m/s 69 N/(m/s)^2 & 85 N/m/s	34 & 51 N/m/s 51 N/m/s & 69 N/(m/s)^2	69 & 207 N/(m/s)^2
B	0 & 34, 51, 68, and 85 N/m/s 0 & 69, 138, and 207 N/(m/s)^2 17 & 85 N/m/s 34 & 85 N/m/s	0 & 17 N/m/s 17 & 68 N/m/s 17 N/m/s & 207 N/(m/s)^2 85 N/m/s & 69 N/(m/s)^2	17 & 51 N/m/s
C	0 & 51 and 68 N/m/s 0 & 207 N/(m/s)^2 17 & 51 and 68 N/m/s	17 N/m/s & 207 N/(m/s)^2	0 & 34 N/m/s 0 & 138 N/(m/s)^2
D	0 & 34, 51, 68, and 85 N/m/s 0 & 69, 138, and 207 N/(m/s)^2 17 & 51 and 85 N/m/s	17 & 68 N/m/s	0 & 17 N/m/s 17 & 34 N/m/s 17 N/m/s & 138 and 207 N/(m/s)^2

Signal-to-Noise Ratio:

The signal-to-noise ratio, or SNR, is defined in Section 4.4.2 as the ratio of signal power, summed over the target frequencies, to tremor power, summed over the frequencies which bound a subject's tremor band. Plots of SNR versus damping level for disabled subjects A-E are shown in Figures 5-39 through 5-43, respectively. Again, the top two plots represent data from the linear damping trials while the bottom two plots represent data from the non-linear damping trials. Each individual plot was obtained by averaging SNR scores from all trials at a given damping level, and error bars in the figures denote one standard deviation above and below the mean SNR scores.

If damping does not attenuate tremor selectively (i.e. if damping hinders purposeful tracking in addition to attenuating tremor), then the SNR is expected to level off or fall for high damping levels. The results of this study show, however, that subjects' SNRs continued to increase as the maximum levels of damping were applied suggesting that either purposeful tracking is not hindered by the application of damping loads, or that the CEDO's damping loads are not large enough to hinder purposeful tracking as measured by the signal power and SNR. In fact, plots of signal power versus damping are relatively flat for all subjects so that the increase in SNR in these figures is due almost entirely to the decrease in tremor power illustrated previously in Figures 5-34 through 5-38.

Transfer Function Magnitude and Phase:

The magnitude and phase components of the transfer function between the target and response are plotted versus damping level for disabled subjects A-E in Figures 5-44 through 5-48, respectively. In these figures, the top two plots represent the magnitude data, the bottom two plots represent the phase data, and only the results from linear damping trials are shown. Each individual plot was obtained by averaging transfer function magnitudes or phases from all trials at a given damping level, and error bars in the figures denote one standard deviation above and below the mean transfer function magnitude or phase.

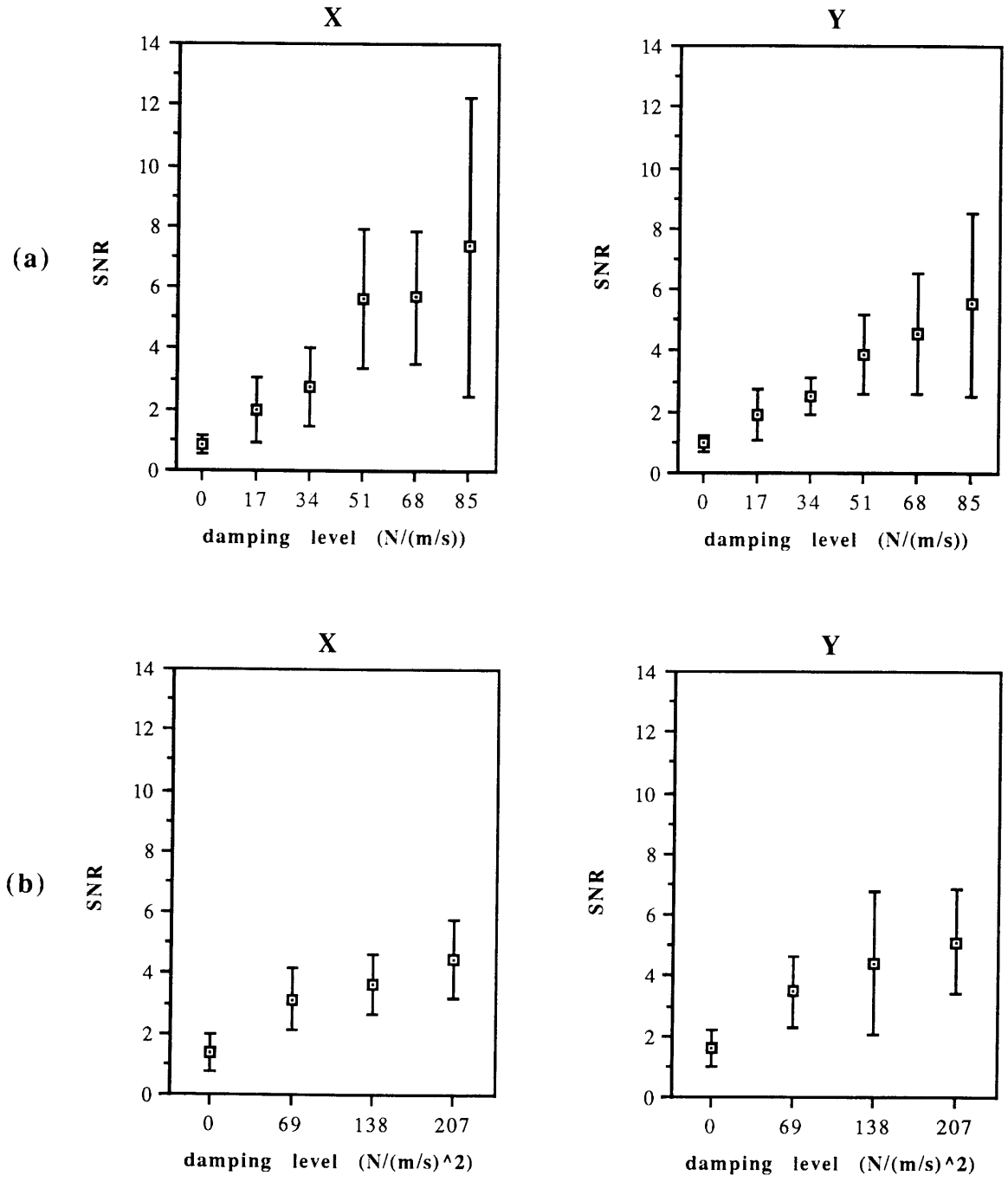

Figure 5-39. *Subject A:* SNR as a function of (a) linear and (b) non-linear damping.

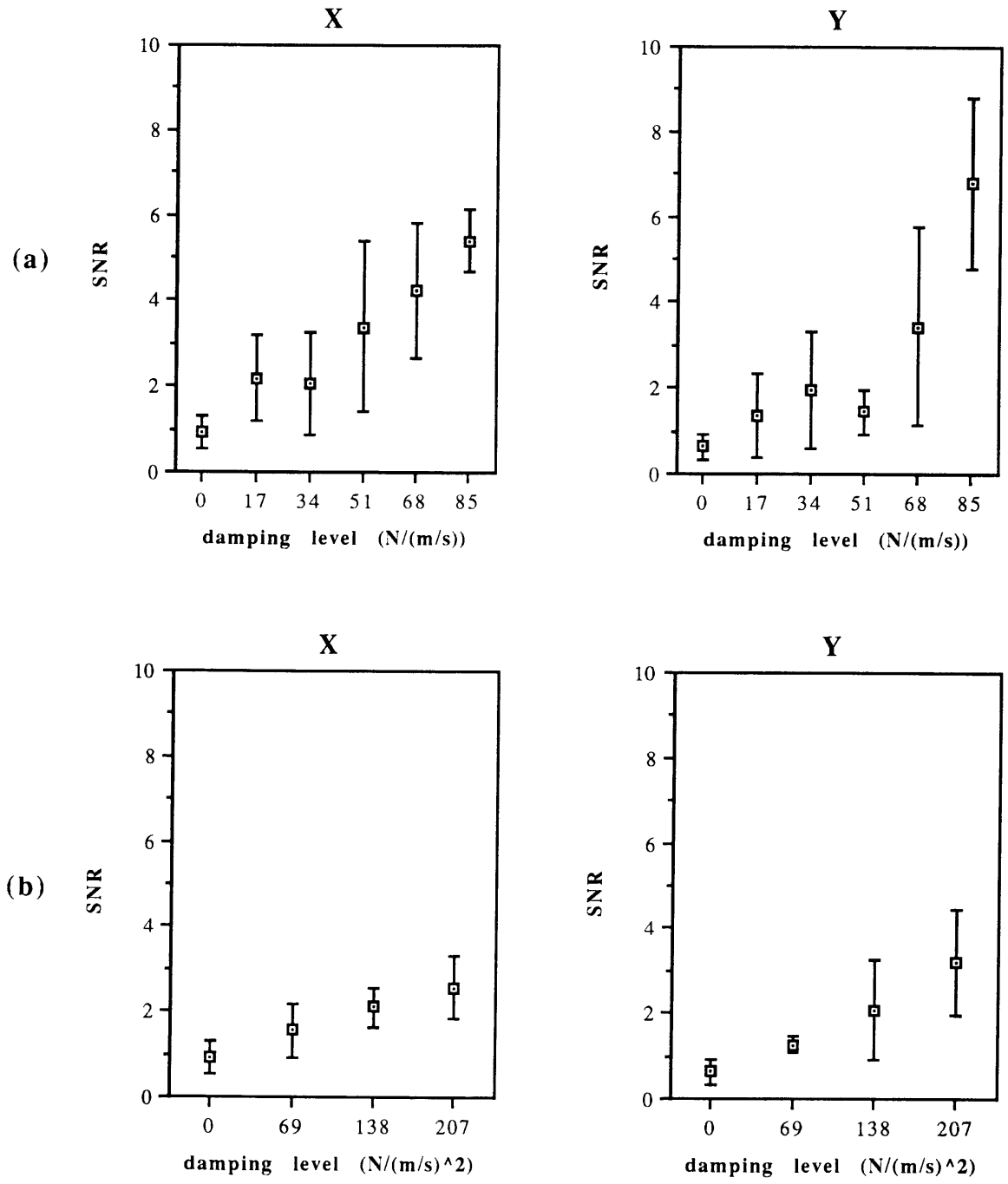

Figure 5-40. *Subject B:* SNR as a function of (a) linear and (b) non-linear damping.

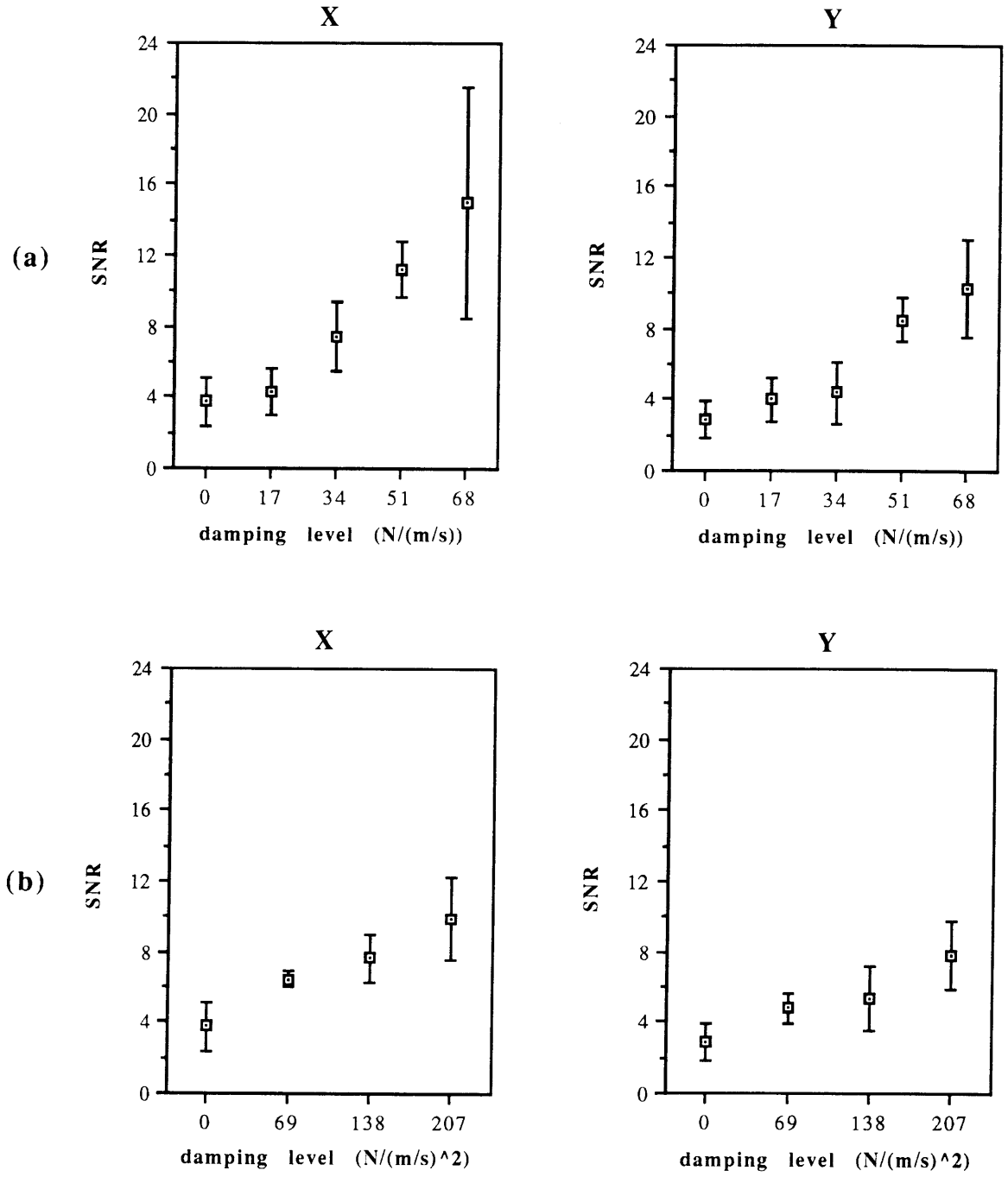

Figure 5-41. *Subject C:* SNR as a function of (a) linear and (b) non-linear damping.

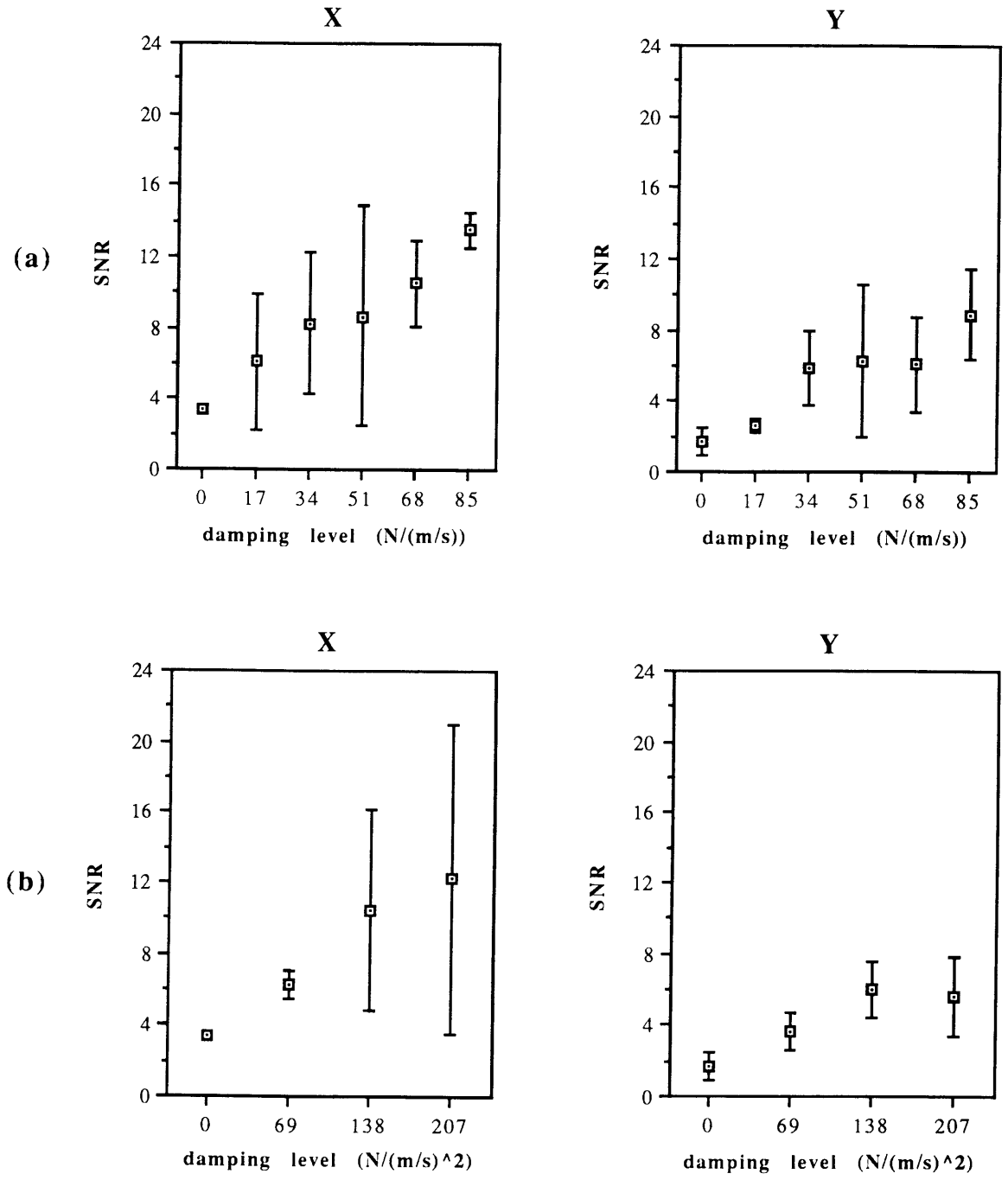

Figure 5-42. *Subject D:* SNR as a function of (a) linear and (b) non-linear damping.

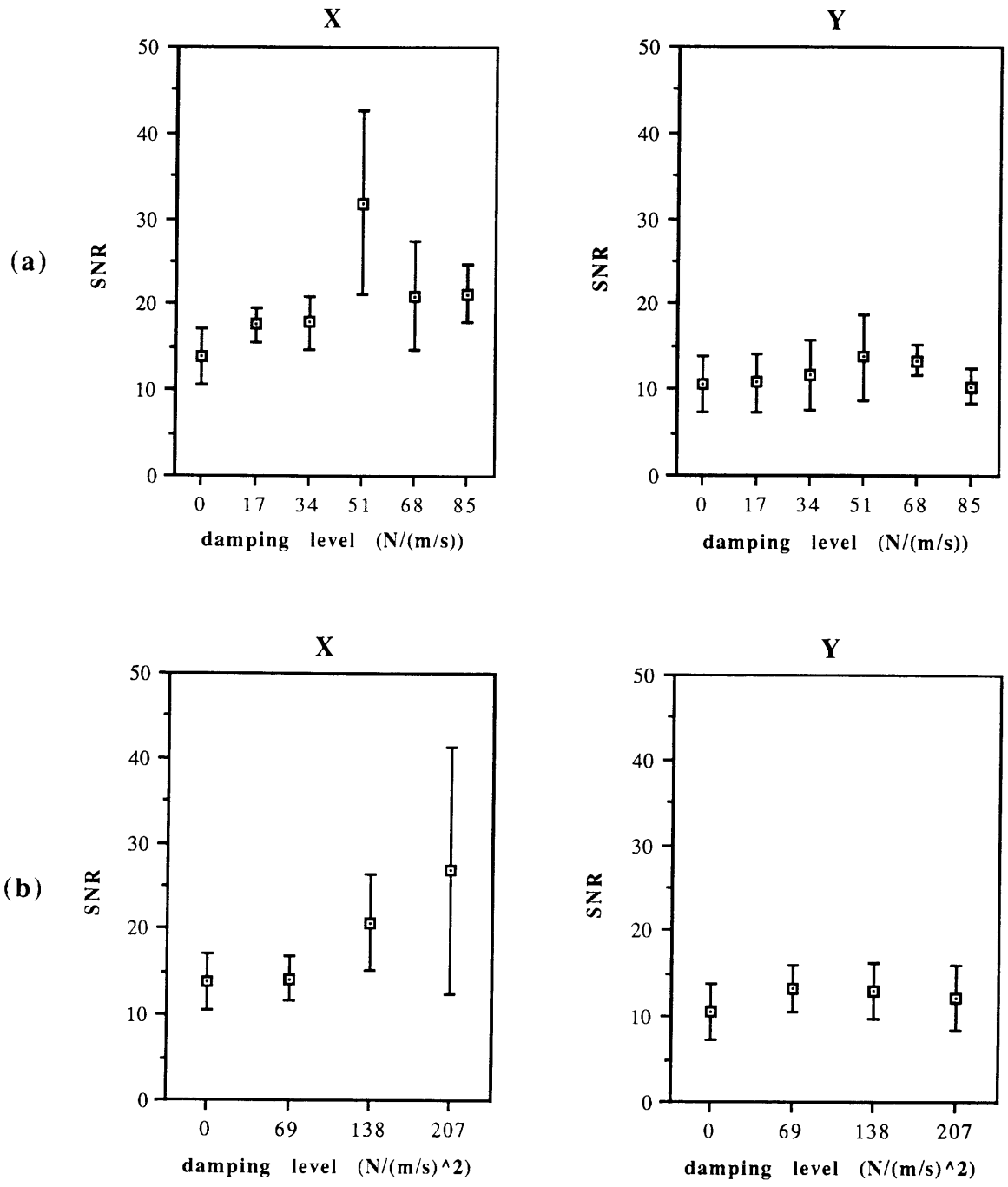

Figure 5-43. *Subject E:* SNR as a function of (a) linear and (b) non-linear damping.

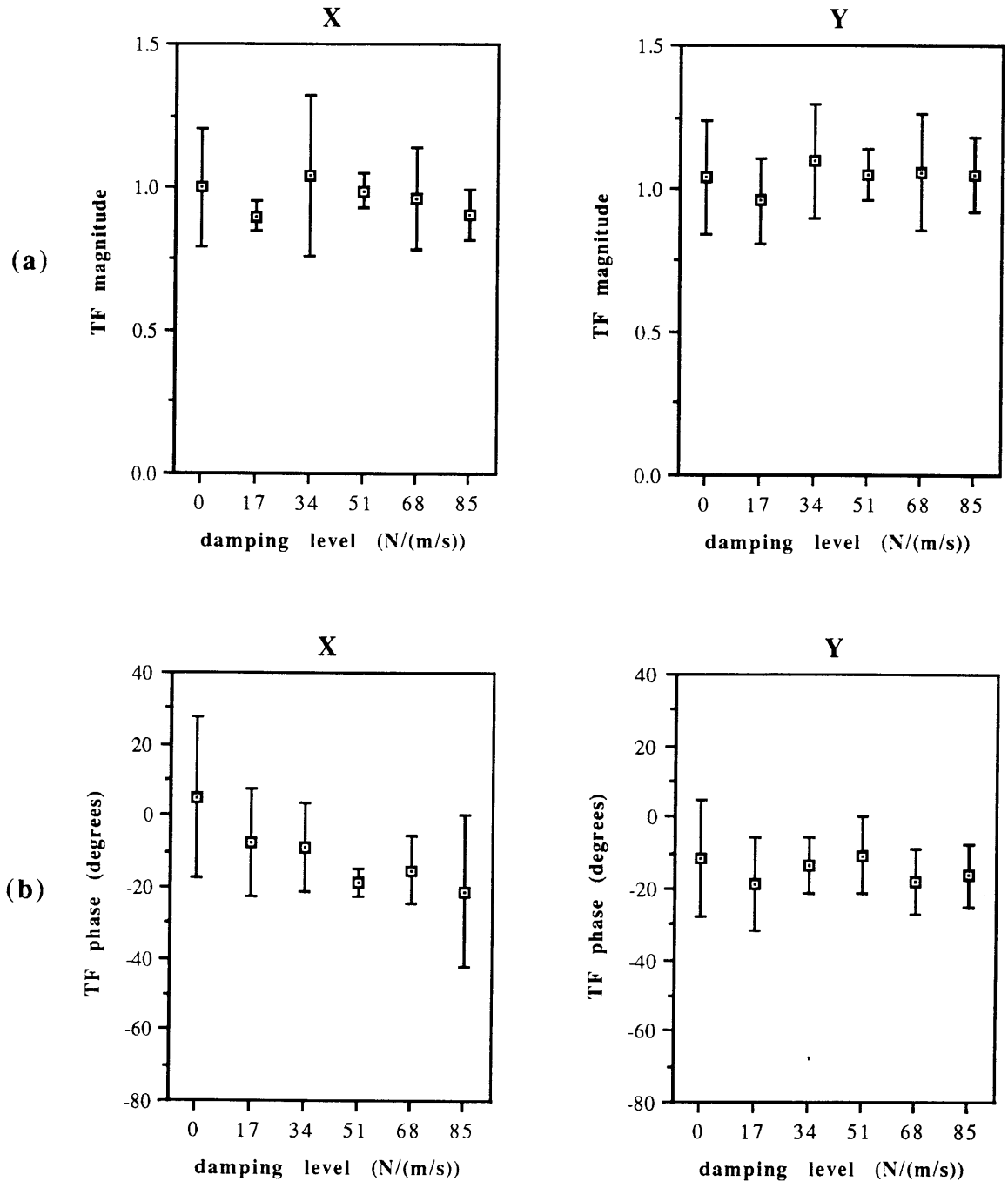

Figure 5-44. *Subject A* : Transfer function (a) magnitude and (b) phase for linear damping.

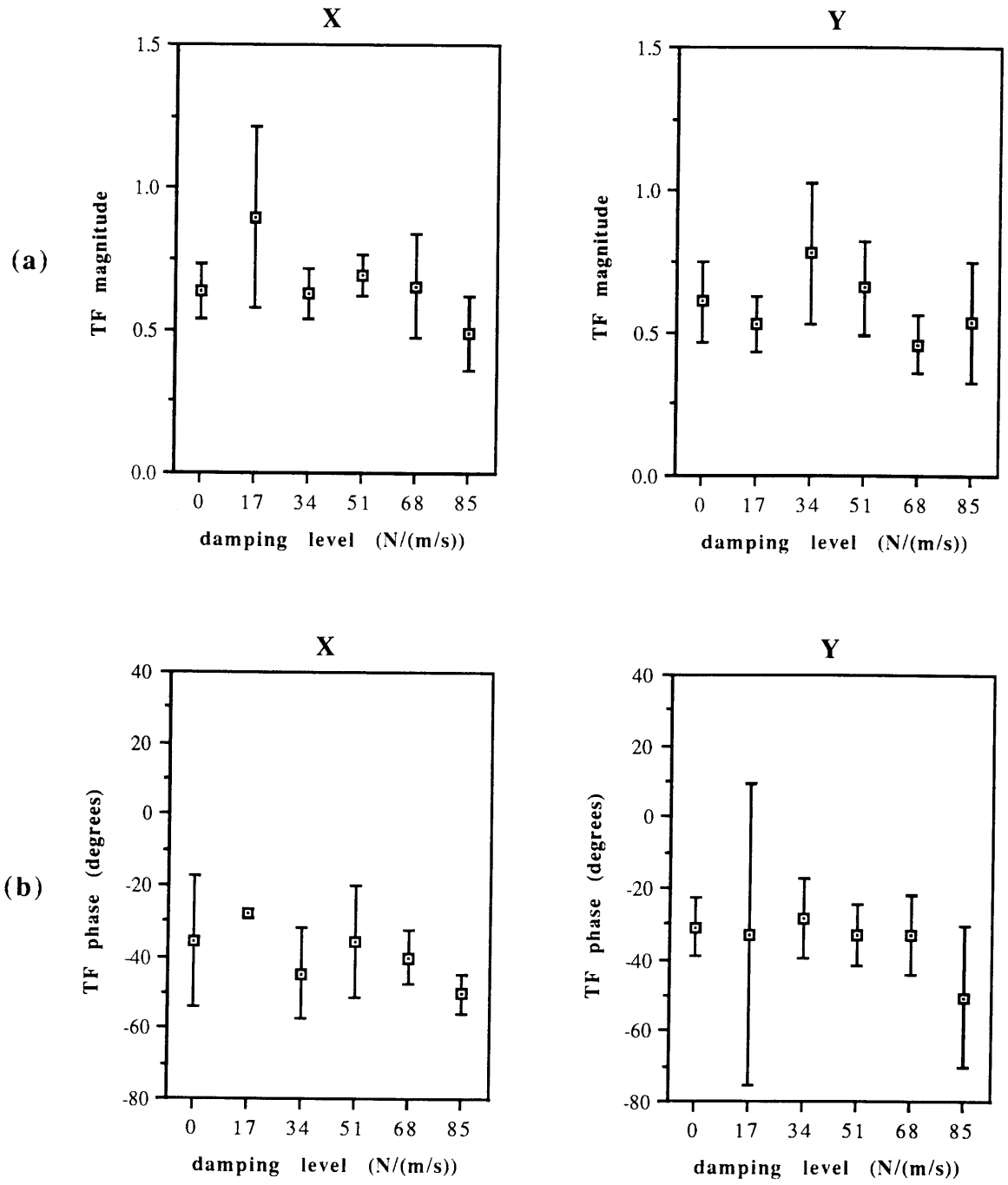

Figure 5-45. *Subject B*: Transfer function (a) magnitude and (b) phase for linear damping.

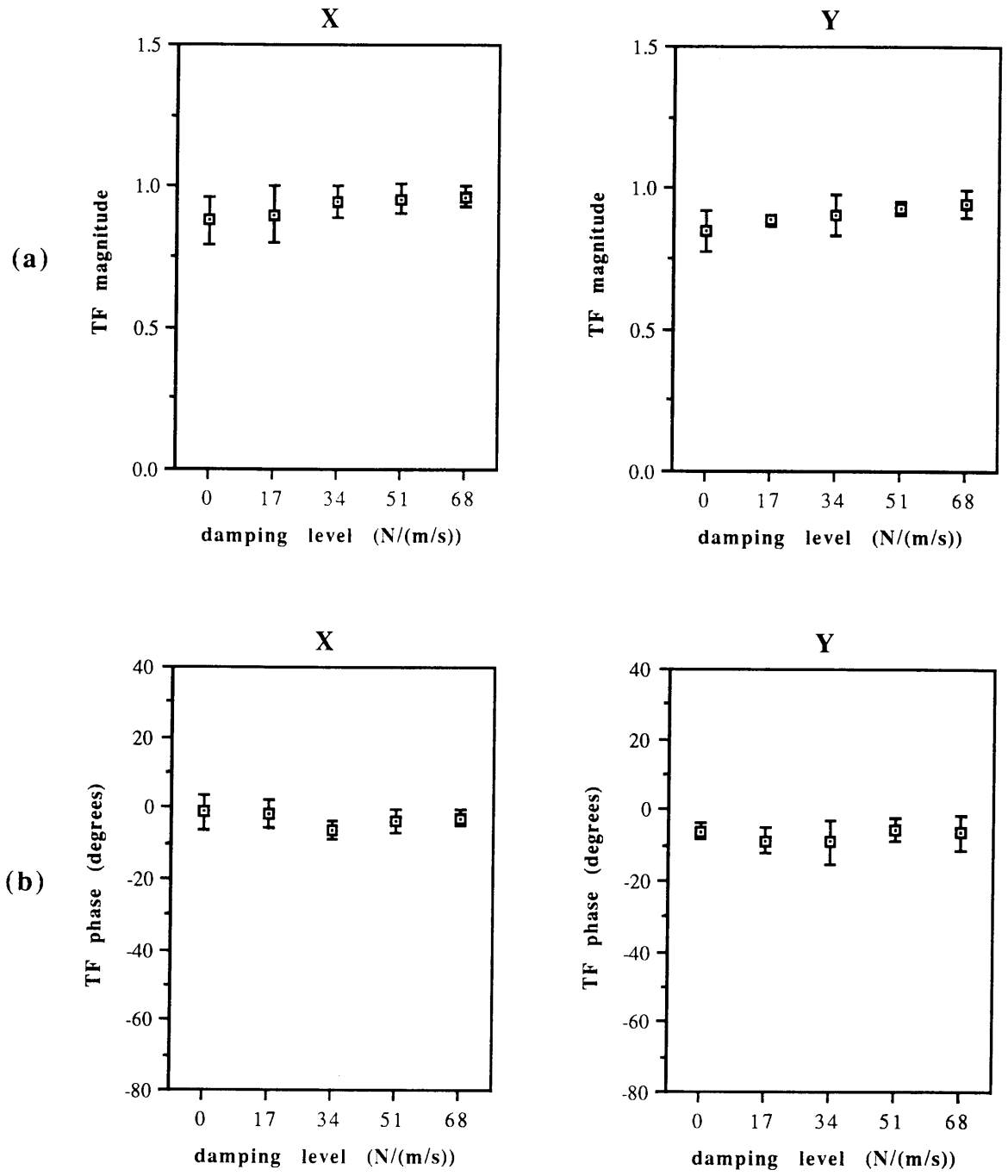

Figure 5-46. *Subject C* : Transfer function (a) magnitude and (b) phase for linear damping.

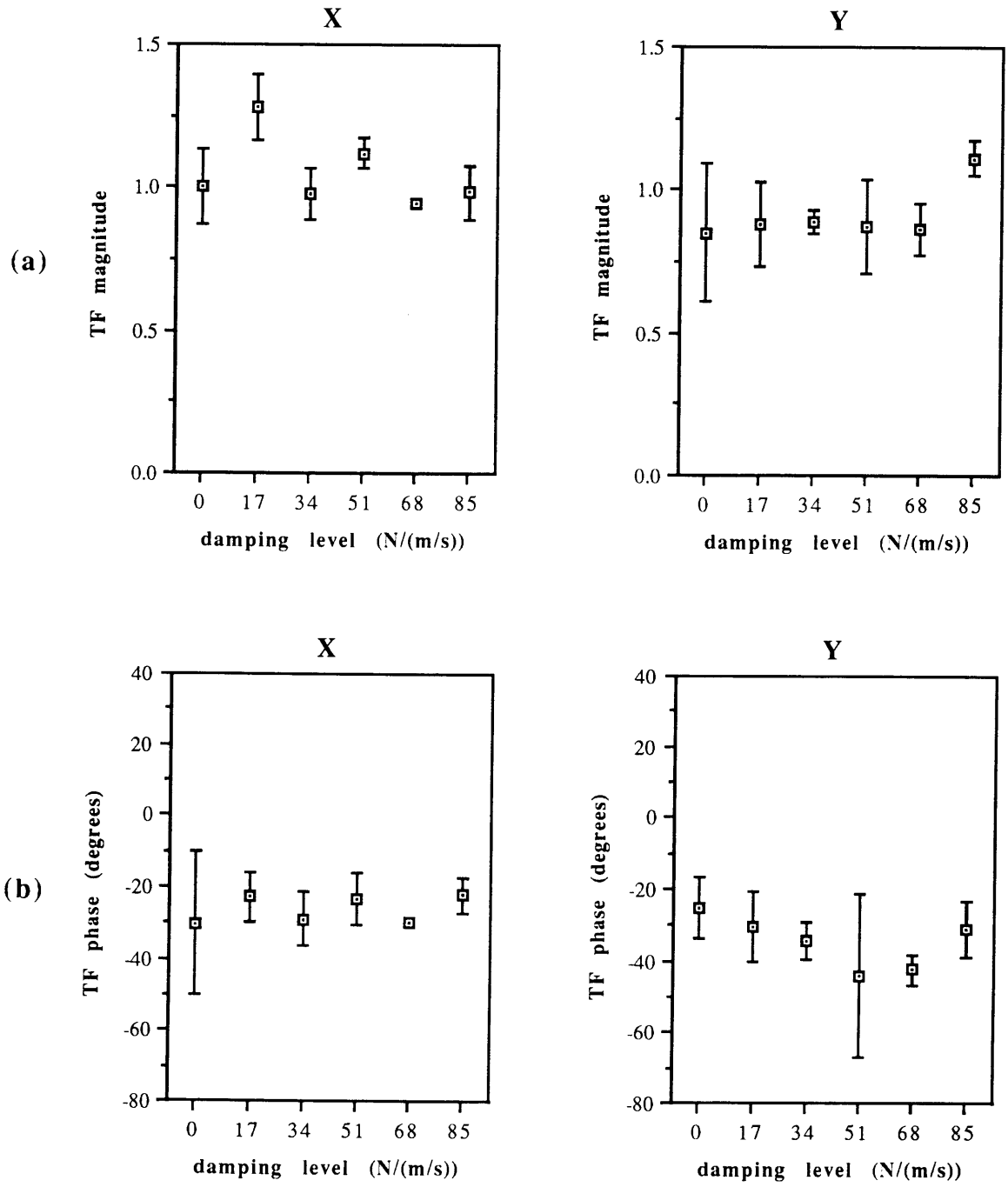

Figure 5-47. *Subject D* : Transfer function (a) magnitude and (b) phase for linear damping.

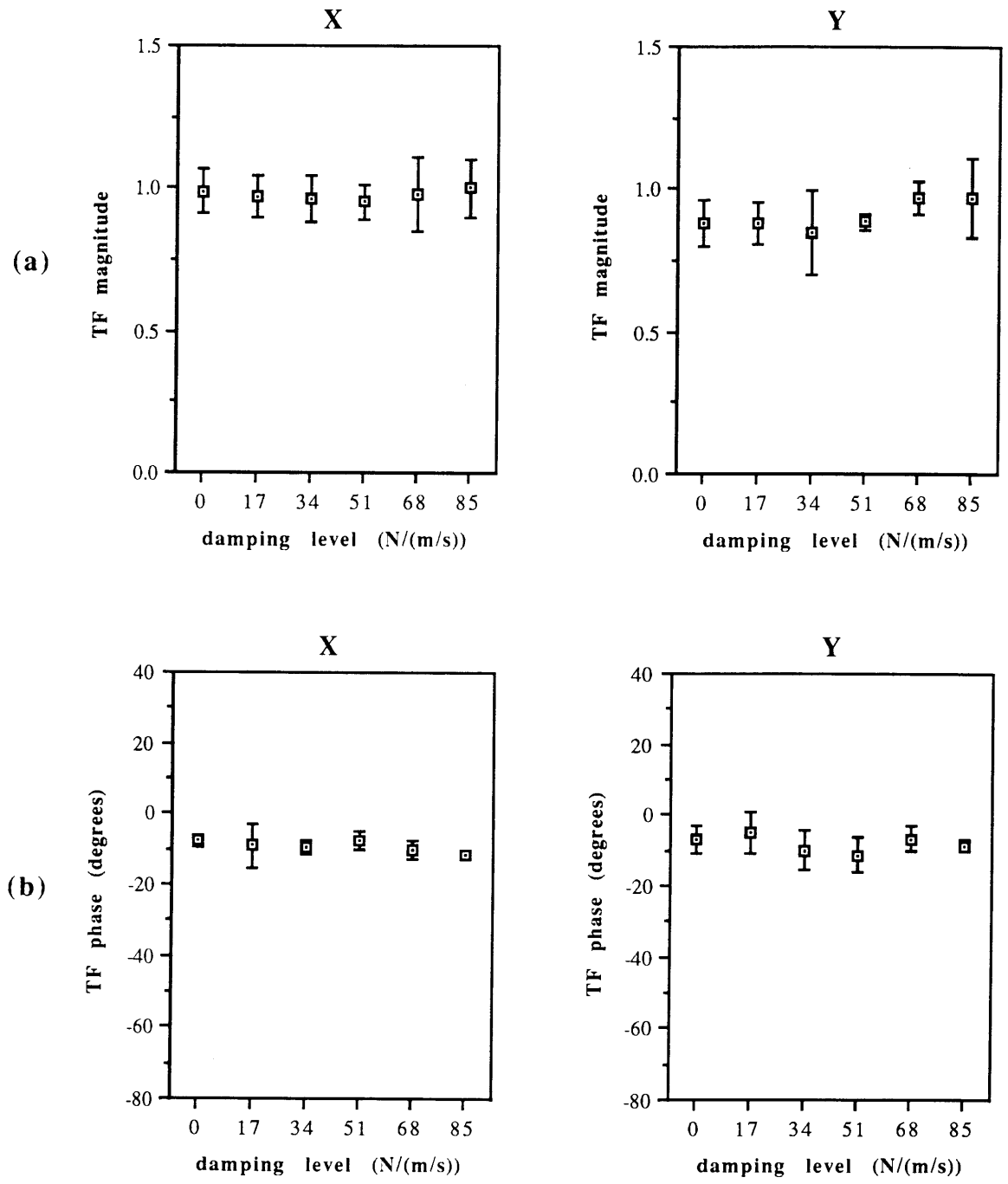

Figure 5-48. *Subject E* : Transfer function (a) magnitude and (b) phase for linear damping.

The plots in Figures 5-44 through 5-48 confirm that the damping loads applied by the CEDO 1 *are* acting in a selective manner. Magnitude plots for subjects A, B, D, and E show no consistent trends with damping, and F-tests with 8 and 36 degrees of freedom for subjects A and D, 8 and 18 degrees of freedom for subjects B and E, and 7 and 32 degrees of freedom for subject C verify that differences in the means are not statistically significant at the $\alpha = 0.1$ level of significance for subjects B, D, and E and at the $\alpha = 0.01$ level of significance for subject A. The slight increase in transfer function magnitude for subject C is significant at the $\alpha = 0.001$ level of significance with a p-value of 0.007. Phase plots for subjects C, D, and E also show no consistent trends with damping, and F-tests for these subjects also verify that differences in the means are not statistically significant at the $\alpha = 0.1$ level of significance. Phase plots for subjects A and B show slightly greater phase lags at the higher damping levels, but F-tests at the $\alpha = 0.01$ level of significance indicate that these differences may not be statistically significant. The mean transfer function magnitudes and phases for all subjects are listed in Tables 5-4 and 5-5, respectively.

5.2.4 A Comparison of Linear and Non-Linear Damping Schemes

A comparison of the tracking records, tremor power spectra, tremor power scores, SNR scores, and transfer function scores from the linearly damped and non-linearly damped trials from each subject suggests that the most severely-disabled subjects responded similarly to the linear and non-linear resistive loads applied by the CEDO. For subjects A, B, and C, both types of loads were shown to attenuate tremor without degrading purposeful tracking. The lowest non-linear damping level used in the experiments (69 $N/(m/s)^2$) suppressed tremor to approximately the same extent as the second lowest linear damping level used (34 N/m/s), and the highest non-linear damping levels used (138 and 207 $N/(m/s)^2$) suppressed tremor to approximately the same extent as the second or third highest linear damping levels used (51 and 68 N/m/s).

Table 5-4. Mean transfer function magnitudes combining X and Y data from a single test session for each subject.

Subject	*Damping Level*								
	0 N/m/s	*17 N/m/s*	*34 N/m/s*	*51 N/m/s*	*68 N/m/s*	*85 N/m/s*	*69 N/(m/s)²*	*138 N/(m/s)²*	*207 N/(m/s)²*
A	1.02	0.952	0.973	0.990	1.11	0.985	1.04	0.860	0.965
B	0.665	0.735	0.680	0.613	0.650	0.598	0.690	0.718	0.703
C	0.874	0.918	0.946	0.937	0.952	--	0.906	0.964	0.947
D	0.925	1.08	0.935	0.997	0.905	1.04	1.02	1.02	1.06
E	0.944	0.966	0.870	0.932	0.905	0.937	0.916	0.905	0.913
MEAN A-E	0.886	0.930	0.881	0.894	0.904	0.890	0.914	0.893	0.918

Table 5-5. Mean transfer function phases combining X and Y data from a single test session for each subject.

Subject	*Damping Level*								
	0 N/m/s	*17 N/m/s*	*34 N/m/s*	*51 N/m/s*	*68 N/m/s*	*85 N/m/s*	*69 N/(m/s)²*	*138 N/(m/s)²*	*207 N/(m/s)²*
A	-0.57	-13.56	-15.03	-12.13	-14.60	-16.69	-18.37	-9.84	-18.82
B	-34.60	-17.78	-36.38	-38.65	-34.33	-54.15	-30.25	-37.90	-42.63
C	-2.02	-5.79	-7.23	-5.19	-5.21	--	-2.51	-3.29	-4.49
D	-27.70	-26.62	-31.76	-33.57	-36.09	-26.64	-21.12	-30.38	-30.68
E	-7.36	-3.27	-7.84	-8.49	-10.56	-9.88	-5.58	-11.32	-8.67
MEAN A-E	*-14.45*	*-13.40*	*-19.65*	*-19.61*	*-20.16*	*-26.84*	*-15.57*	*-18.55*	*-21.06*

A comparison of the endpoint force required by the user to overcome the highest linearly damped loads with the endpoint force required to overcome the highest non-linearly damped load as predicted by the CEDO model using actual tremor data indicates that the mean resistive forces generated by the CEDO during the highest linearly damped trials are larger than those generated by the CEDO during the highest non-linearly damped trials. More specifically, the 10-percent-trimmed-mean endpoint force for the highest linearly damped trials ranged from approximately 12 N for subject A to 5.5 N for subject E, while the 10-percent-trimmed-mean endpoint force for the highest non-linearly damped trials ranged from approximately 8 N for subject A to 1 N for subject E. (The 10-percent-trimmed-mean was used, rather than the mean, to eliminate the effects of outliers in the predicted force records caused by a singularity in the numerical solution when the moment arm of the endpoint force vector about reference point O approaches 0.) The maximum torque commands to individual brakes, however, were generally larger for the non-linearly damped trials than for the linearly damped trials.

Although both types of damping selectively attenuated the tremors of subjects A, B, and C relative to purposeful movement in these experiments, firm conclusions as to which damping scheme is better to use in tremor-suppressing orthoses cannot be drawn. The highest level of linear damping resulted in lower tremor power scores than the highest level of non-linear damping, but it did so by applying a larger resistive force. Improvements to the CEDO must be made to speed up the response times of the brakes and to perhaps provide brake 1 with larger torque capabilities before higher non-linear damping levels can be tried. Making such improvements and continuing non-linear damping experiments, assessing both tremor reduction and long-term fatigue effects, is probably warranted for subjects like A, B, and C with relatively high-amplitude or high-frequency tremors. Continuing non-linear damping experiments on subjects like D and E with ataxia or very low-amplitude or low-frequency tremors, however, is probably unwarranted since these subjects limbs do not move fast enough over sufficient distance to generate much resistance under the velocity-squared damping scheme.

5.2.5 *Subjective Responses from Participants*

All disabled participants tested in this investigation offered positive remarks on the effect of damping. Typical comments include: "I feel more comfortable with damping"; "I can tell the difference immediately when you turn the damping off"; "My tremor is much worse without damping"; "More damping!"; "Damping helps me do the tracking task better"; and "Damping helps me have more control." In contrast, few of the subjects could envision a commercial orthotic device which would be useful in reducing tremor in a functional setting. This perhaps reflects the subjects' unfamiliarity with the notion of mechanical approaches to tremor management and also the non-idealities of the current design discussed further in Chapter 6. When asked to comment on differences between linear and non-linear damping, subjects implied that they did not perceive substantial differences between the two damping schemes over and above general differences in resistance levels dictated by the damping coefficients used in the trials.

5.2.6 *Repeatability of Results*

While the error bars in Figures 5-34 through 5-48 provide some indication of the variability of the data, a more detailed assessment of the variability of tremor data is shown in Figures 5-49 through 5-53 for subjects A-E, respectively. The top two plots in each figure show average tremor power plotted versus damping level for two different test sessions. The bottom two plots in each figure show undamped tremor power plotted versus test session and include data from all undamped trials done. Plot symbols in these figures symbolize the order in which the undamped measurements were taken within each session.

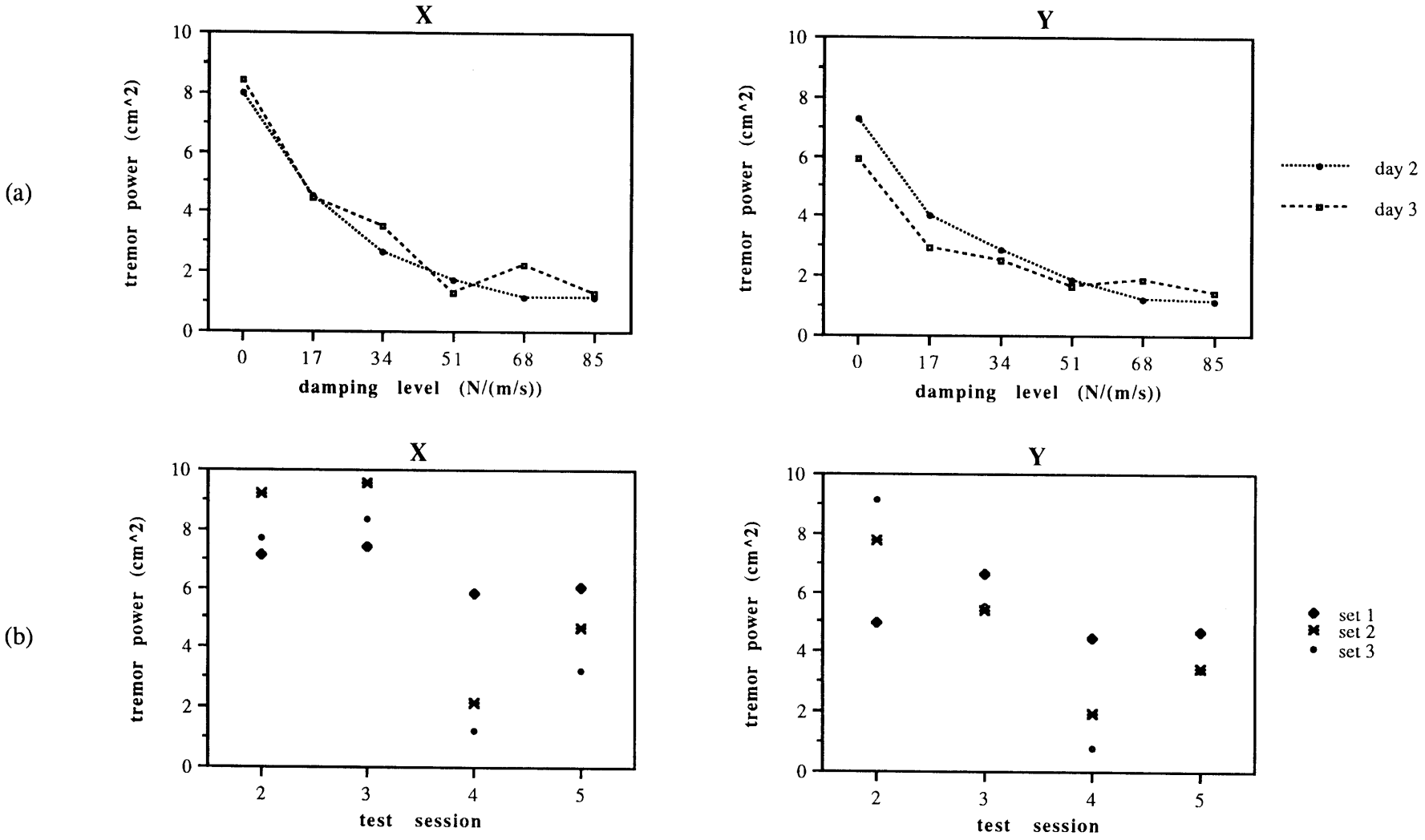

Figure 5-49. *Subject A:* (a) Tremor power as a function of damping for different sessions, and (b) undamped tremor power showing variability within and across sessions.

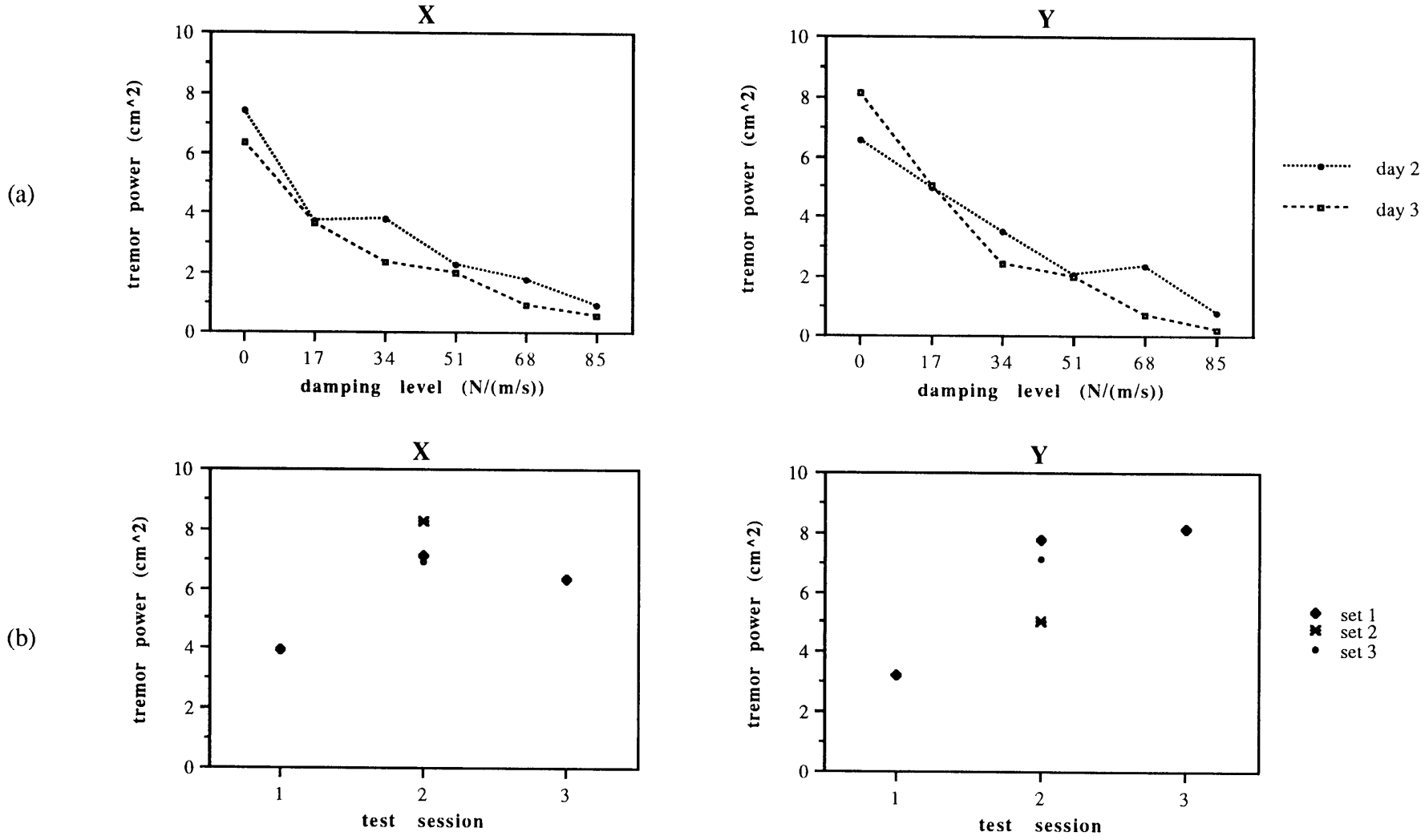

Figure 5-50. *Subject B:* (a) Tremor power as a function of damping for different sessions, and (b) undamped tremor power showing variability within and across sessions.

(a)

(b)

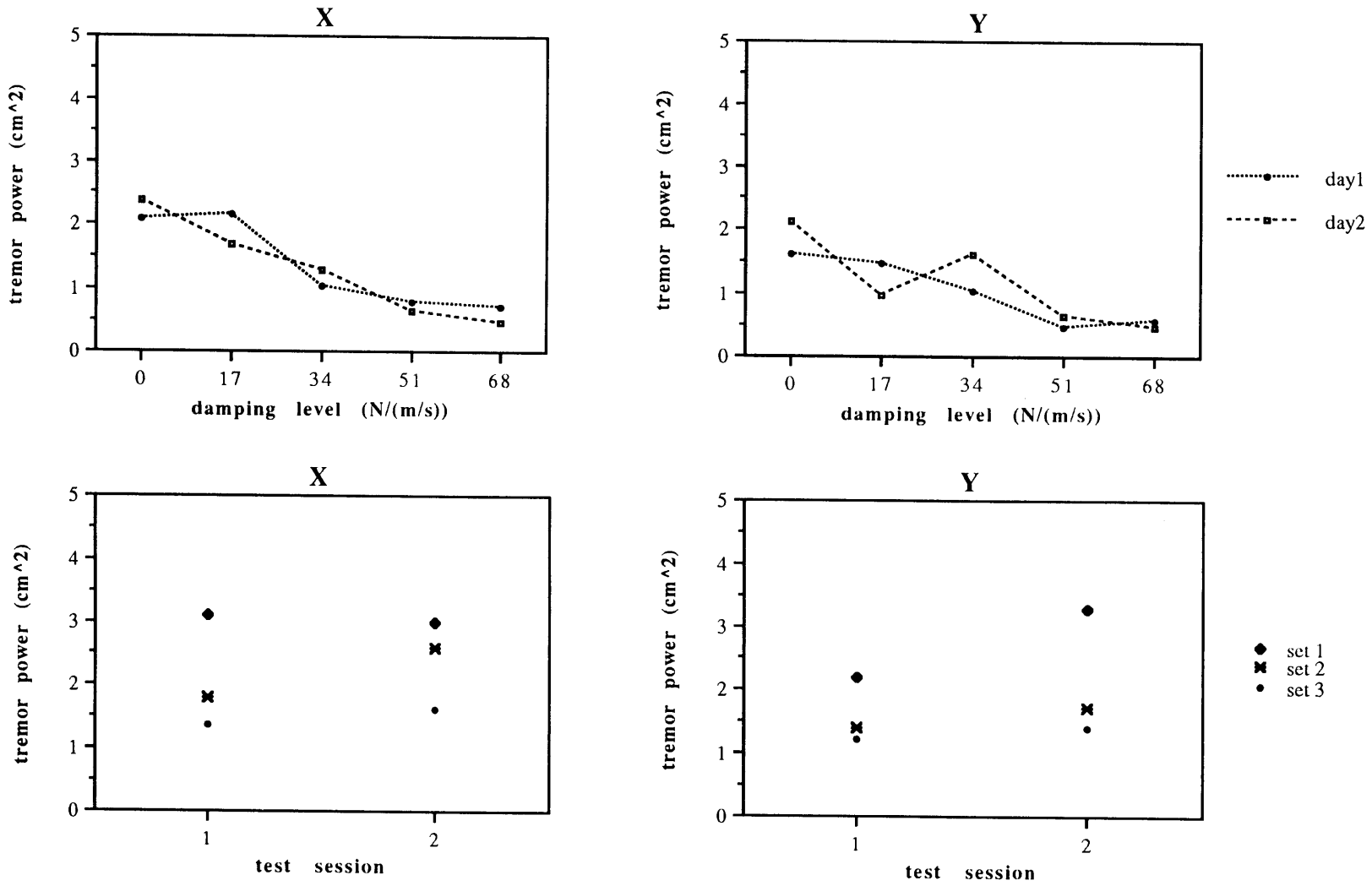

Figure 5-51. *Subject C:* (a) Tremor power as a function of damping for different sessions, and (b) undamped tremor power showing variability within and across sessions.

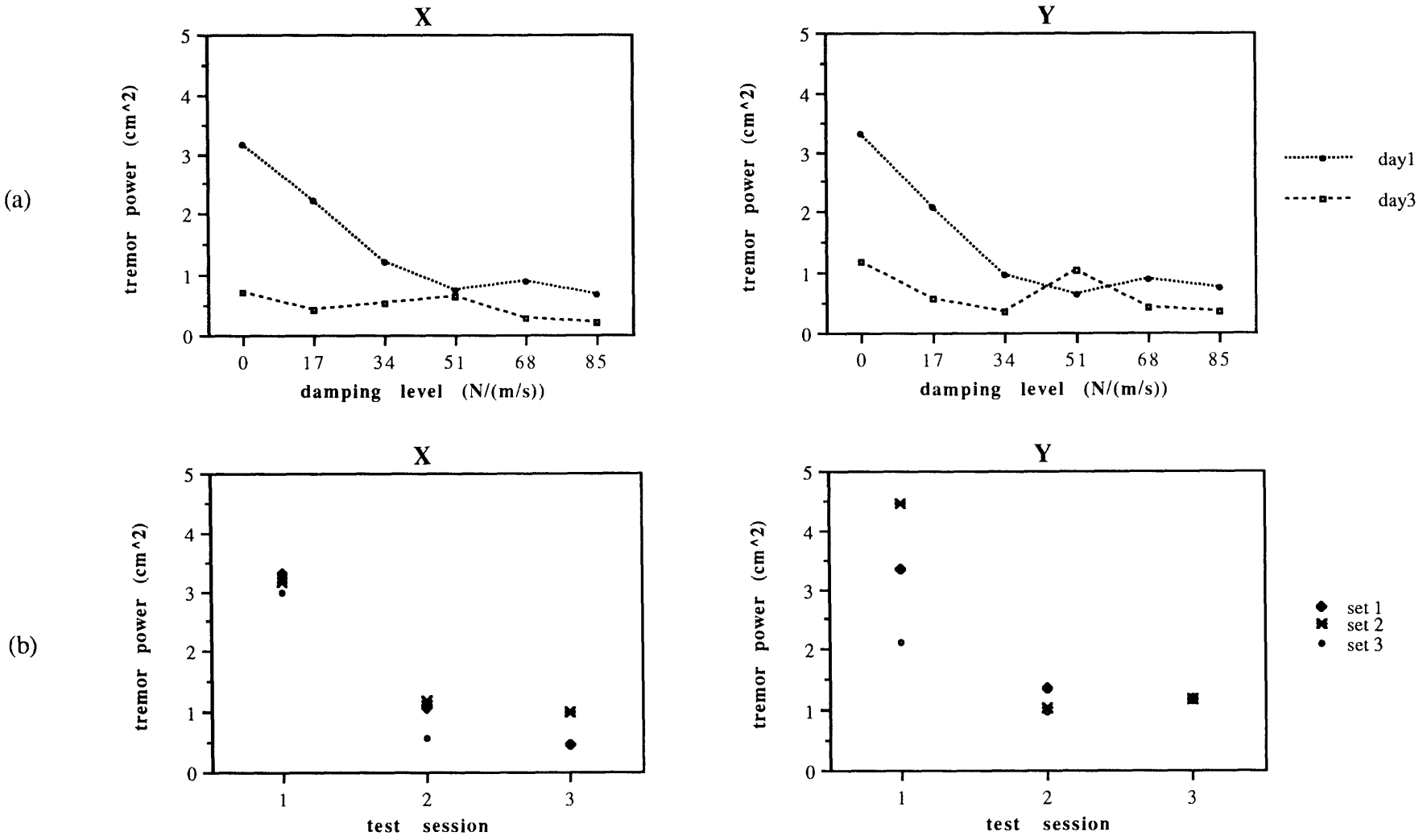

Figure 5-52. *Subject D:* (a) Tremor power as a function of damping for different sessions, and (b) undamped tremor power showing variability within and across sessions.

(a)

(b)

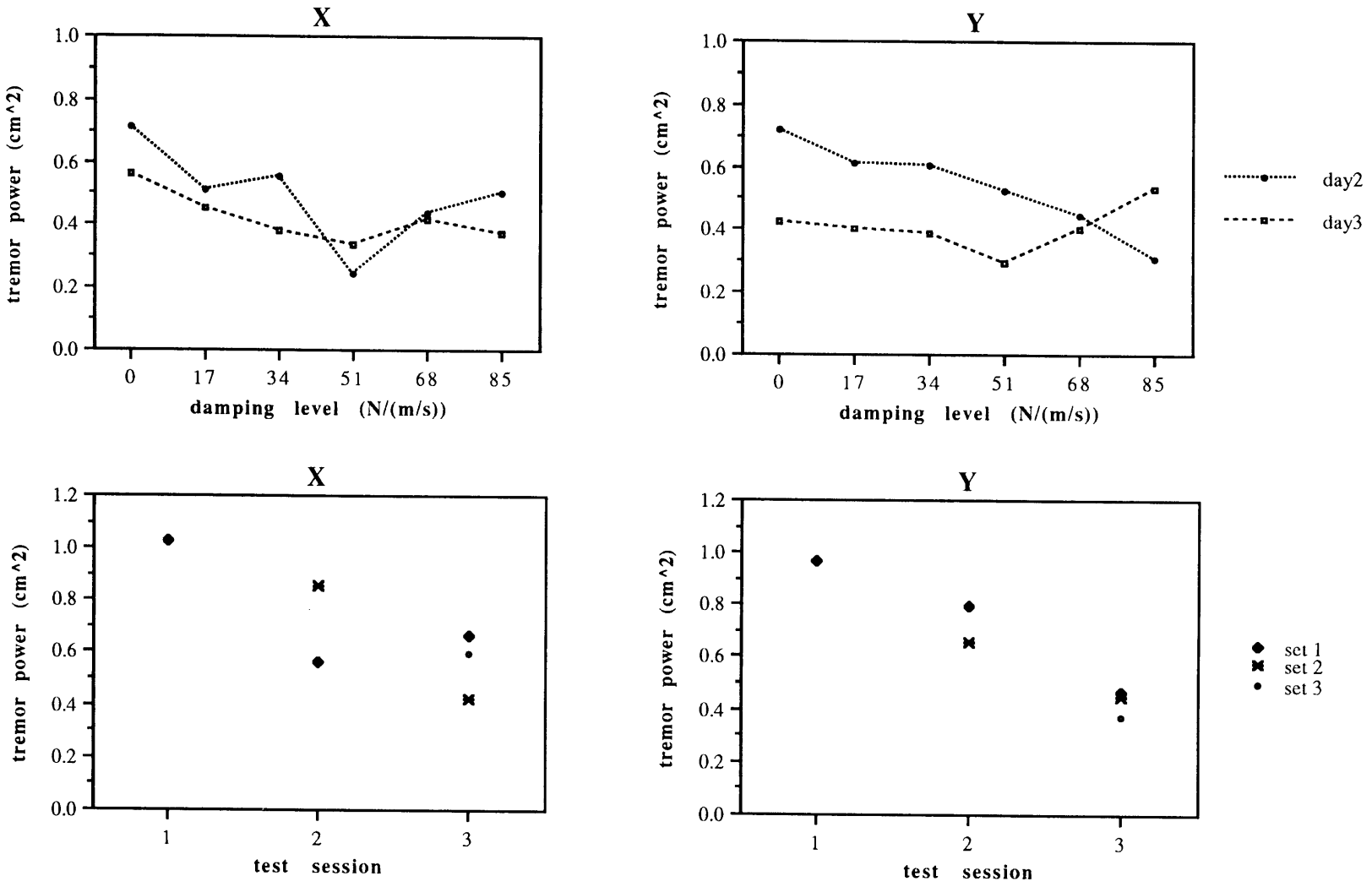

Figure 5-53. *Subject E:* (a) Tremor power as a function of damping for different sessions, and (b) undamped tremor power showing variability within and across sessions.

These data exhibit a number of notable features. First, with regard to the day-to-day repeatability of the effects of damping, very close agreement between the data for two different test sessions is observed in the plots for subjects A, B, and C. These plots show not only the same trends, but also the same approximate magnitudes for the two days on which linear damping was tested. The tremor power versus damping plots for subjects D and E, in contrast, do not show the same trends for the two test sessions. This observation is quite possibly due to a learning effect -- much of the "tremor power" of subjects D and E stems from non-linear tracking errors rather than involuntary tremor. If these subjects learned over time to follow the targets with fewer errors, then their tremor power scores from later test sessions might be less than those from earlier test sessions as demonstrated in Figures 5-52 and 5-53.

With regard to the day-to-day repeatability of undamped tremor, Figures 5-49 through 5-53 reveal that the tremor power scores of subjects A, B, D, and E from different test sessions differ remarkably. For subjects A and B, these differences in tremor power scores probably reflect the normal, expected variations in tremor attributable to factors such as the subject's physiological state, the subject's drug, caffeine, or tobacco intake prior to testing, the subject's general motor activity which proceeded the testing, the time of day of the test session, etc. For subjects D and E, tremor power scores from later test session are less than those from earlier test sessions suggesting, as hypothesized above, that these differences are due in part to learning effects.

Finally, with regard to the within-a-session repeatability of undamped tremor, some variability is seen in the plots for all subjects. For subject C, however, this variability appears to be a function of the trial order -- in both the X and Y components, tremor power is greatest in the first set of each session and lowest in the last set of each session. This observation could be attributed to a number of factors, including:

1. learning or practice within the test session.
2. fatigue or boredom within the test session.
3. psychological factors such as level of anxiety during the test session.

4. equipment factors such as temperature which change during the test session (although if the current signals to the brakes are affected by the temperature of the electronics box or of any of its internal components, trends would be expected to be observed in the data from all subjects).
5. long-term effects of damping.

A similar trend is seen in the data for subject A on test sessions 4 and 5 but not on test sessions 2 and 3.

The observations discussed in this section provide three important guidelines for designing future protocol. First, because undamped tremor varies so much from day to day, one *cannot* plan to directly compare tremor data collected on different days, i.e. linear damping trials done on one day probably cannot be compared to non-linear damping trials done on another day. Second, if possible, subjects should be tested on multiple days in which the first day is devoted to practice and subsequent days are devoted to experiments in order to avoid learning effects. Third, multiple trials under the same test conditions must be done so that scores can be averaged and within-a-session repeatability can be assessed.

5.2.7 A Comparison of the CEDO 1 and a Standard Clinical Assessment

In addition to pursuit tracking tasks, disabled subjects B, C, and D and all able-bodied control subjects were asked to try the whole-arm functional tasks described in Section 3.2.4 of Chapter 3 with and without the CEDO's damping in order to compare the quantitative measures of tremor and tracking performance discussed above to more traditional measures of tremor and functional disability. While all able-bodied subjects could draw between parallel lines and complete the Archimedes spiral test with and without damping without any difficulties, the disabled subjects were much less successful. Subject B, after trying one of the drawing tasks, refused to try any more of the functional tasks because she was frustrated and confident she would fail even with the CEDO's maximum damping. Subjects C and D did do all the tasks,

but only minor improvements were noticed in the results with damping relative to the results without damping.

As explained in Chapter 3, the largest problem in using functional tasks to assess the CEDO's effectiveness is that most functional tasks on clinical tremor assessment forms are difficult if not impossible to do when one's forearm is secured to the CEDO cuff and one's motion is restricted to the three degrees of freedom allowed by the CEDO linkage. These tasks usually require some amount of pronation, supination, wrist flexion, or finger prehension -- movements that are prohibited by the CEDO cuff. Moreover, the configuration of the CEDO 1 linkage prevents its user from resting his or her forearm on a tabletop and thus hinders writing, drawing, and other tabletop activities. The functional tasks devised for this study, which were designed to incorporate mostly whole-arm movements allowed by the CEDO rather than fine wrist movements prohibited by the CEDO cuff, are not really "functional" tasks at all. Very few people use whole-arm movements for writing or drawing, and very few people use an 8-inch long pen to write or draw with their arm unsupported against a desk or table. Clearly, functional issues must be addressed before embarking on the design of the CEDO 2.

5.3 Experimental Factors Which Influence Tremor Measurements

5.3.1 The Effects of Added Inertia and Damped Inertia

Figures 5-54 through 5-63 illustrate the effects of added inertia and damped-inertia on tremor and tracking for disabled subjects A-E, respectively. The first figure for each subject shows typical tracking records for comparing tremor and tracking without damping or inertia to tremor and tracking with inertia (7.5 lbm) and with inertia plus moderate damping (7.5 lbm plus 34 or 51 N/m/s). The second figure for each subject shows tremor position spectra averaged over all trials from a particular test condition. In these plots, the solid line corresponds to the undamped trials, the dashed line corresponds to the damped trials, the dash-dot line corresponds to the inertia trials, and the dotted line corresponds to the damped-inertia

trials. All data were collected during a single test session for each subject. During these trials, the 7.5 lbm (3.375 kg) mass was strapped to the limb coupler at the participant's wrist.

Reports in the tremor literature suggest that different tremors may respond to inertial loads in different ways. As mentioned in Section 1.2.1 of Chapter 1, numerous researchers have detected the presence of a "mechanical reflex" component of physiological tremor which systematically responds to mechanical loads and applied force pulses in a manner predicted by a second order spring-mass-dashpot system with oscillation frequency proportional to $(k/m)^{1/2}$, the square root of the equivalent spring stiffness of the limb divided by the equivalent mass [Robson 1959, Randall and Stiles 1964 & 1967, Fox & Randall 1970, Rietz & Stiles 1974, Joyce & Rack 1974, Elble & Randall 1973, Elble et al 1987]. If pathological tremors also respond to inertial loads in this manner, then Figures 5-54 through 5-63 should depict tremors whose frequencies are lower in the inertia and damped-inertia trials than in the undamped and viscously damped trials. There is some evidence which suggests, however, that not all pathological tremors respond to inertial loads in this manner. In a 1987 study by Homberg et al, for instance, weights ranging from 0.1 to 1.5 kg were strapped to the hands of 6 able-bodied subjects, 15 subjects with essential tremor, and 5 subjects with Parkinson's disease. When the inertial loads were added in this study, the unloaded tremor frequencies of the tremor-disabled subjects remained stable. In another, earlier study by Hewer et al in 1972, wrist cuffs ranging in weight from 240 to 720 grams were strapped to the wrists of 50 subjects with pathological intention tremor. While these researchers also noticed that subjects' tremor frequencies remained relatively stable, they additionally found that the tremor amplitudes of 29 of the subjects were reduced when the inertial loads were added.

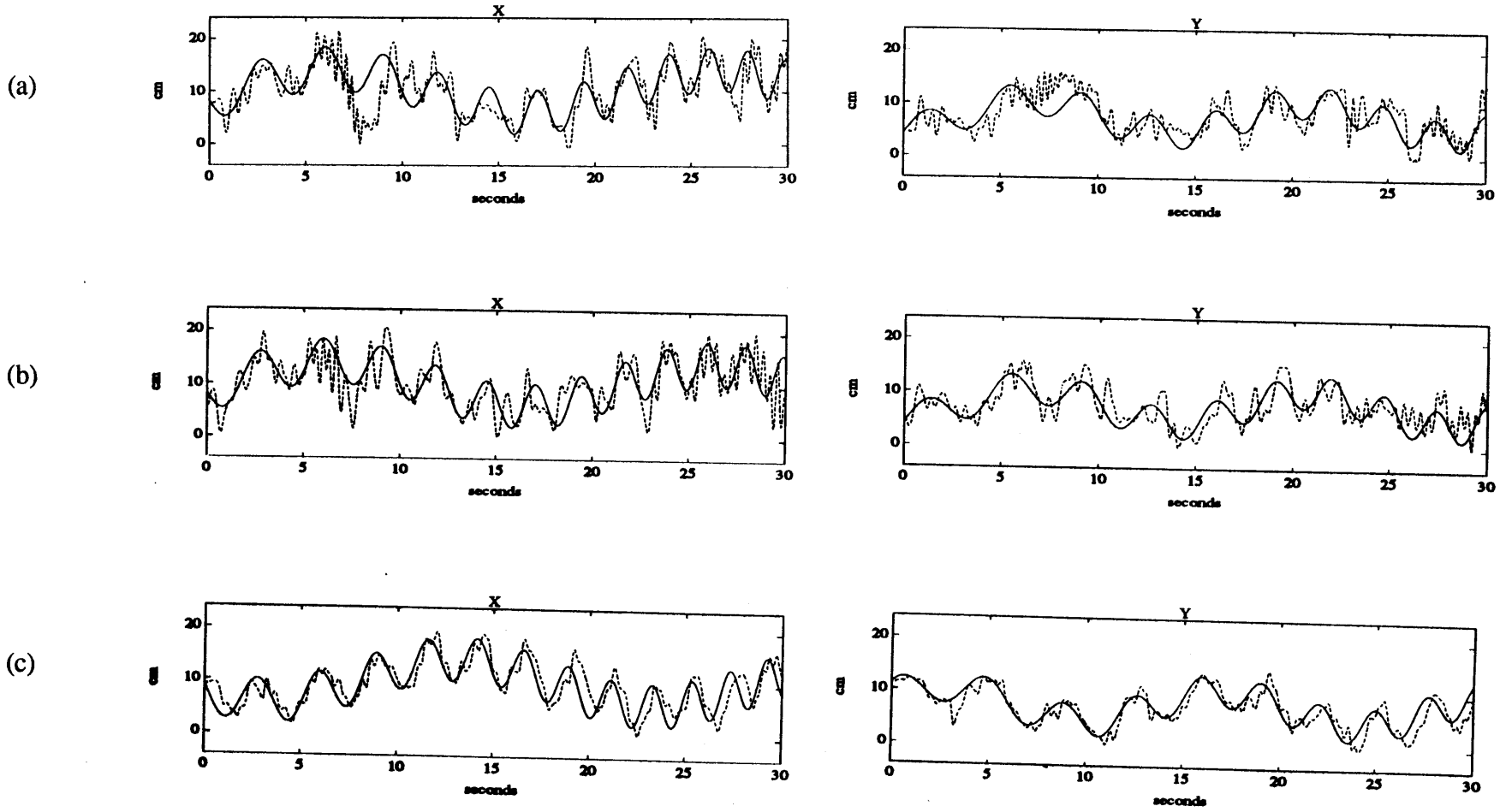

Figure 5-54. *Subject A:* Target and response time trajectories for comparing (a) undamped tremor to (b) tremor with added inertia to (c) tremor with damped inertia.

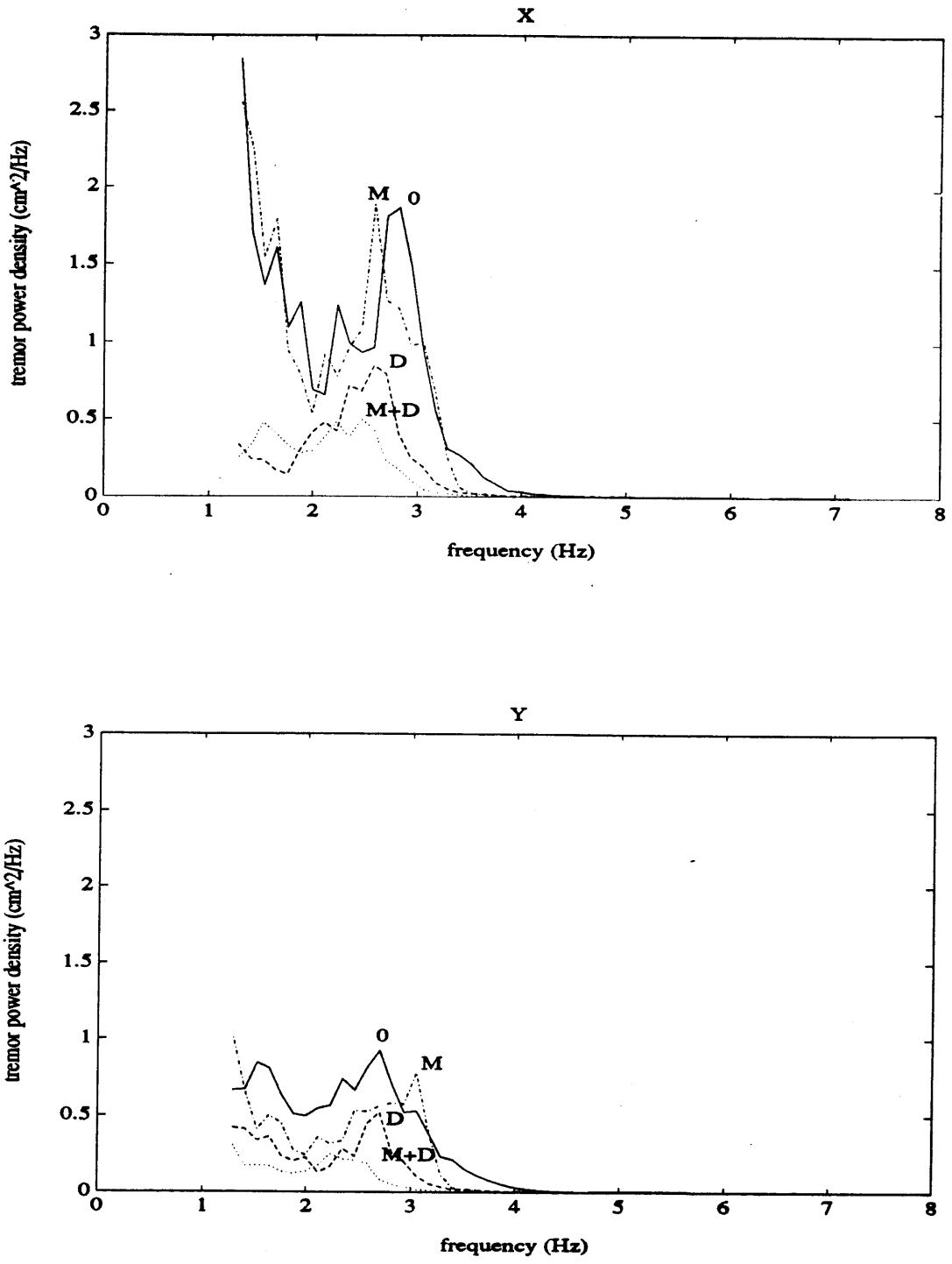

Figure 5-55. *Subject A:* Tremor position spectra illustrating the effects of added inertia. The symbols 0, D, M, and M+D correspond to trials with no damping or mass, 51 N/m/s damping, 7.5 lbm mass, and combined mass and damping, respectively.

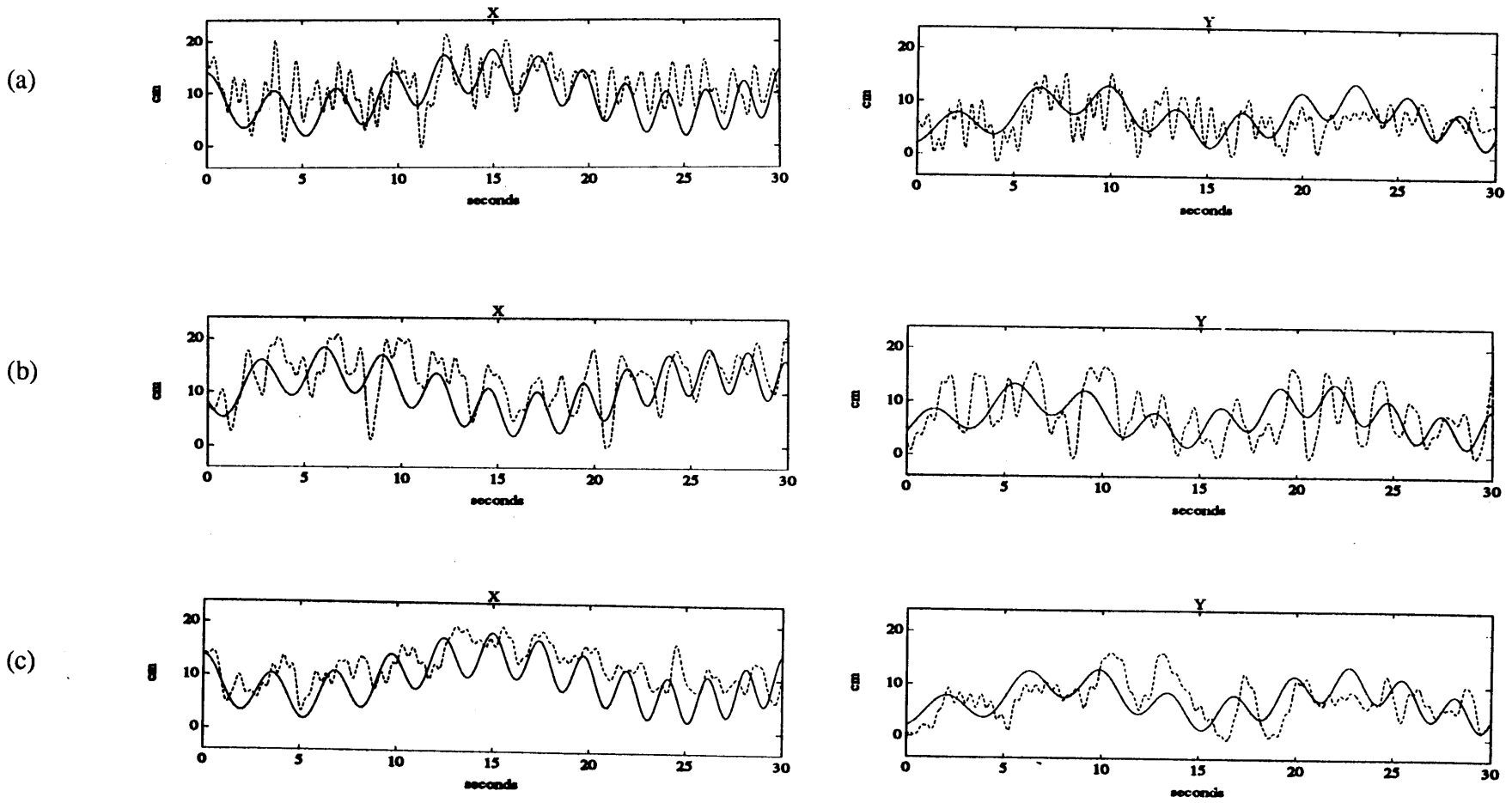

Figure 5-56. *Subject B:* Target and response time trajectories for comparing (a) undamped tremor to (b) tremor with added inertia to (c) tremor with damped inertia.

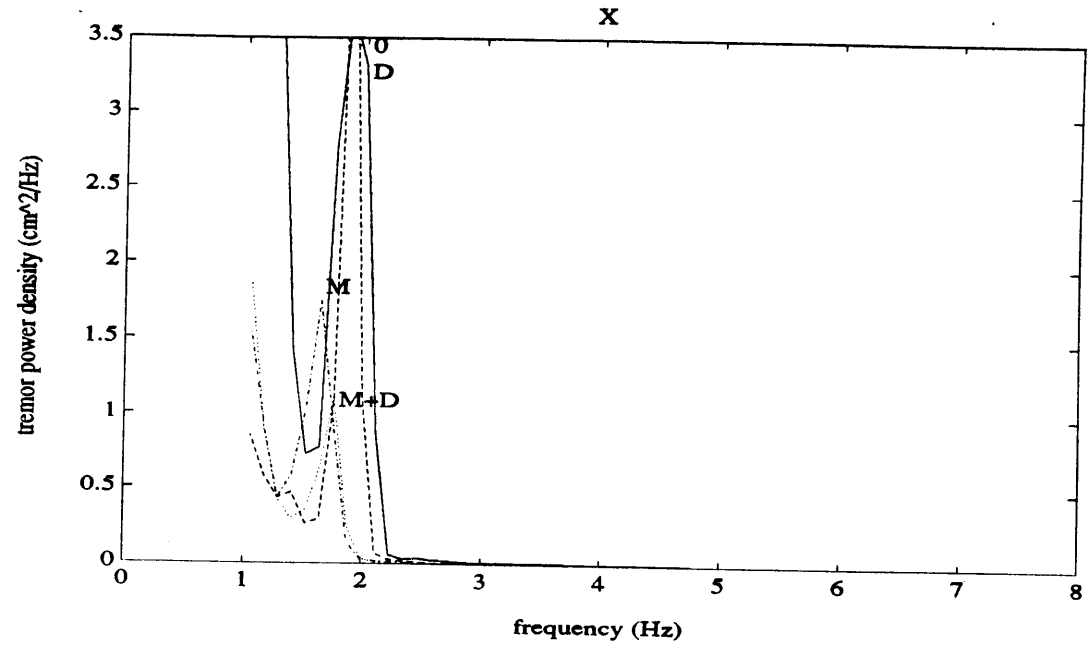

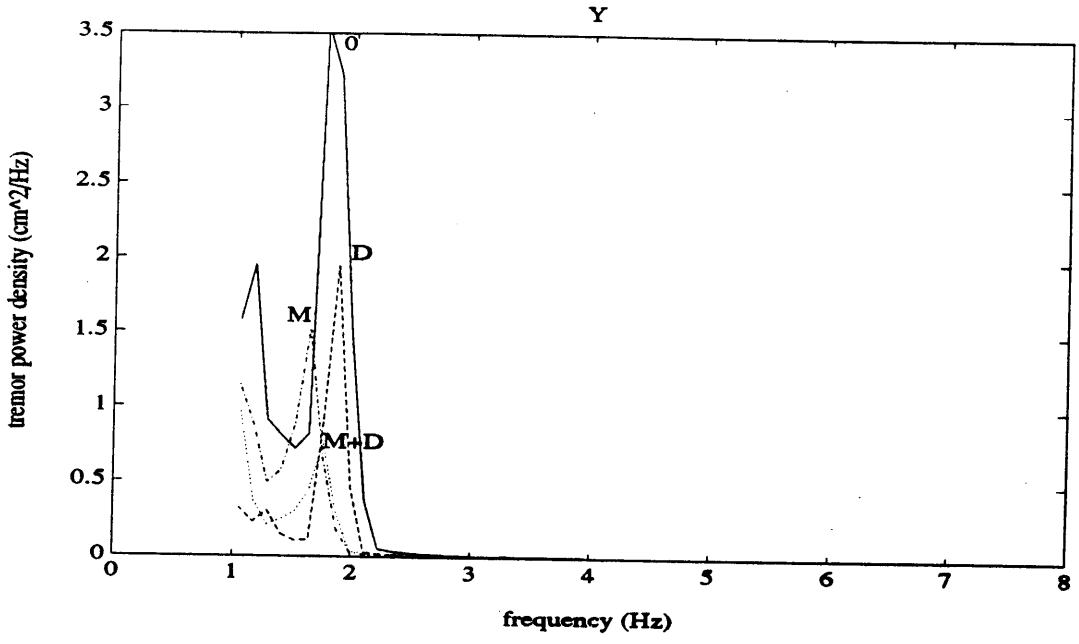

Figure 5-57. *Subject B:* Tremor position spectra illustrating the effects of added inertia. The symbols 0, D, M, and M+D correspond to trials with no damping or mass, 34 N/m/s damping, 7.5 lbm mass, and combined mass and damping, respectively.

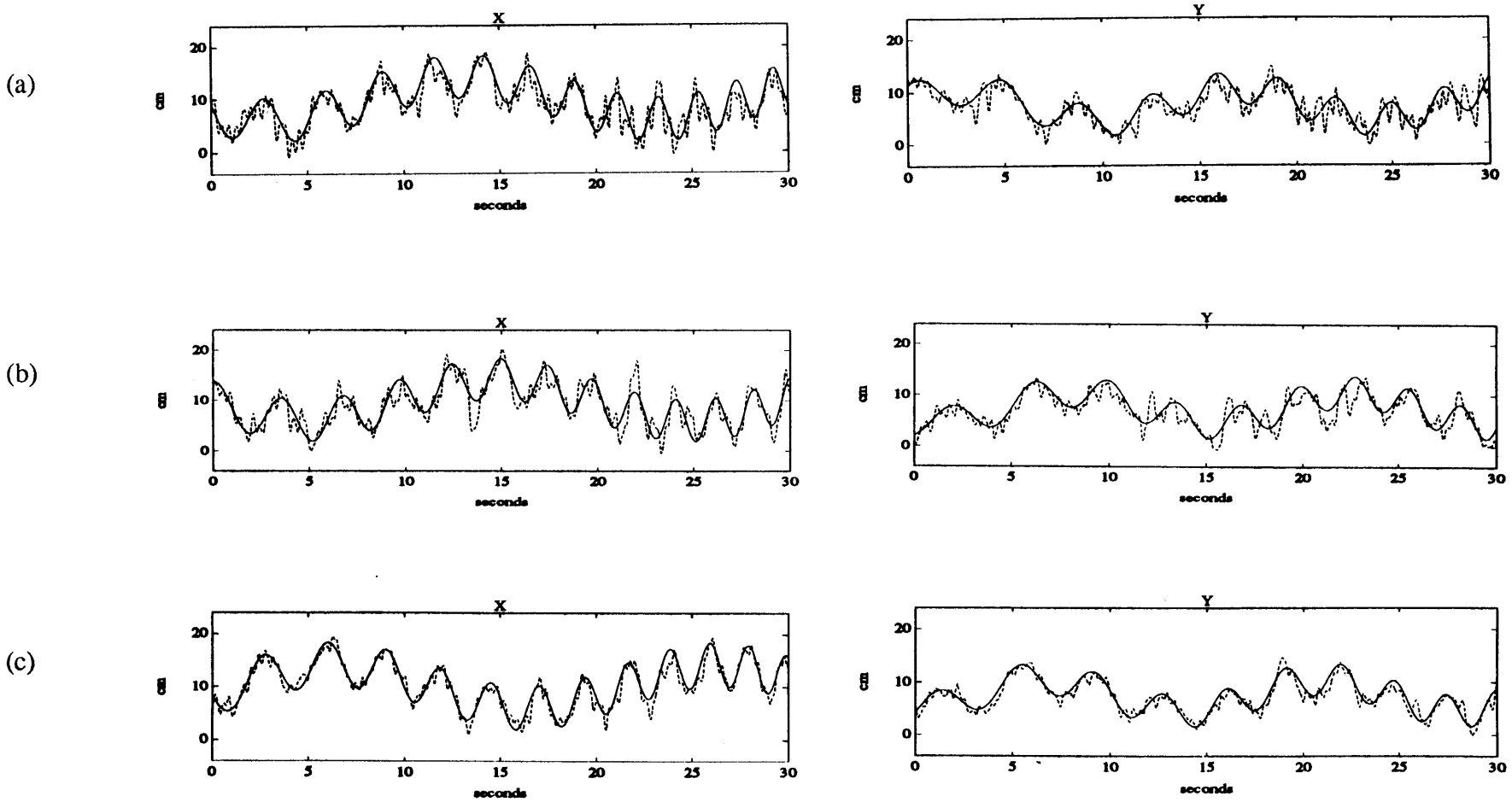

Figure 5-58. *Subject C:* Target and response time trajectories for comparing (a) undamped tremor to (b) tremor with added inertia to (c) tremor with damped inertia.

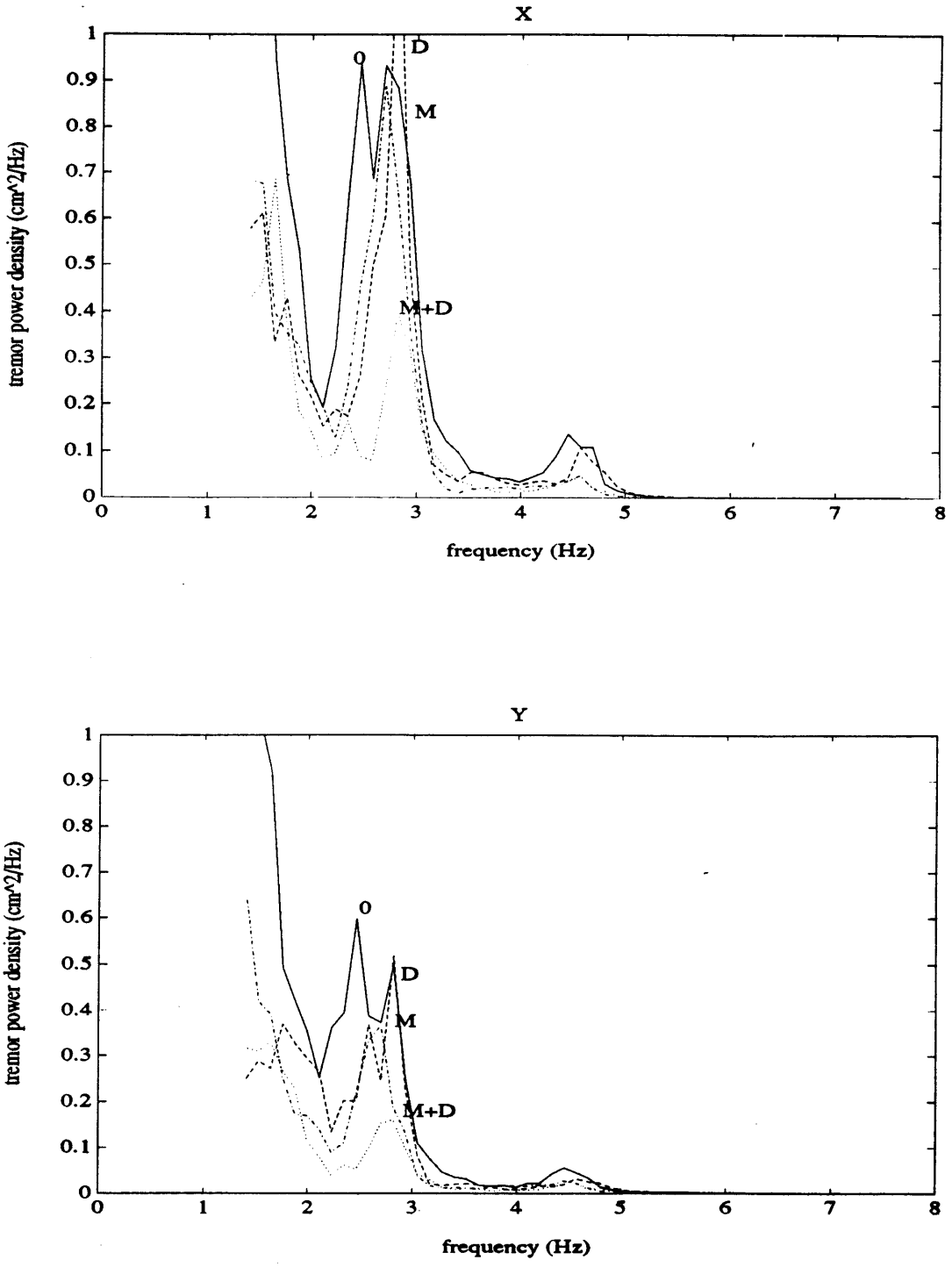

Figure 5-59. *Subject C:* Tremor position spectra illustrating the effects of added inertia. The symbols 0, D, M, and M+D correspond to trials with no damping or mass, 34 N/m/s damping, 7.5 lbm mass, and combined mass and damping, respectively.

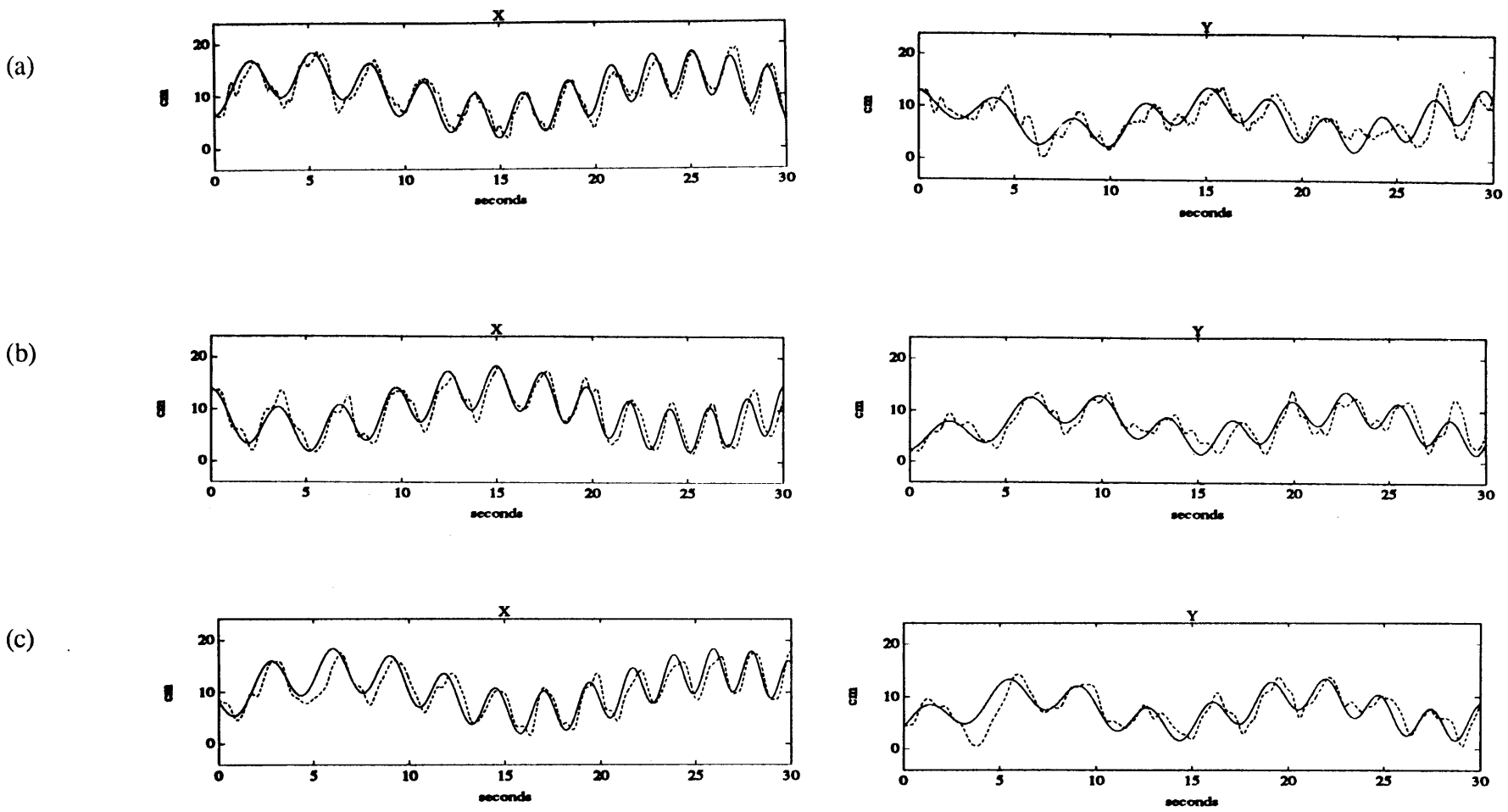

Figure 5-60. *Subject D:* Target and response time trajectories for comparing (a) undamped tremor to (b) tremor with added inertia to (c) tremor with damped inertia.

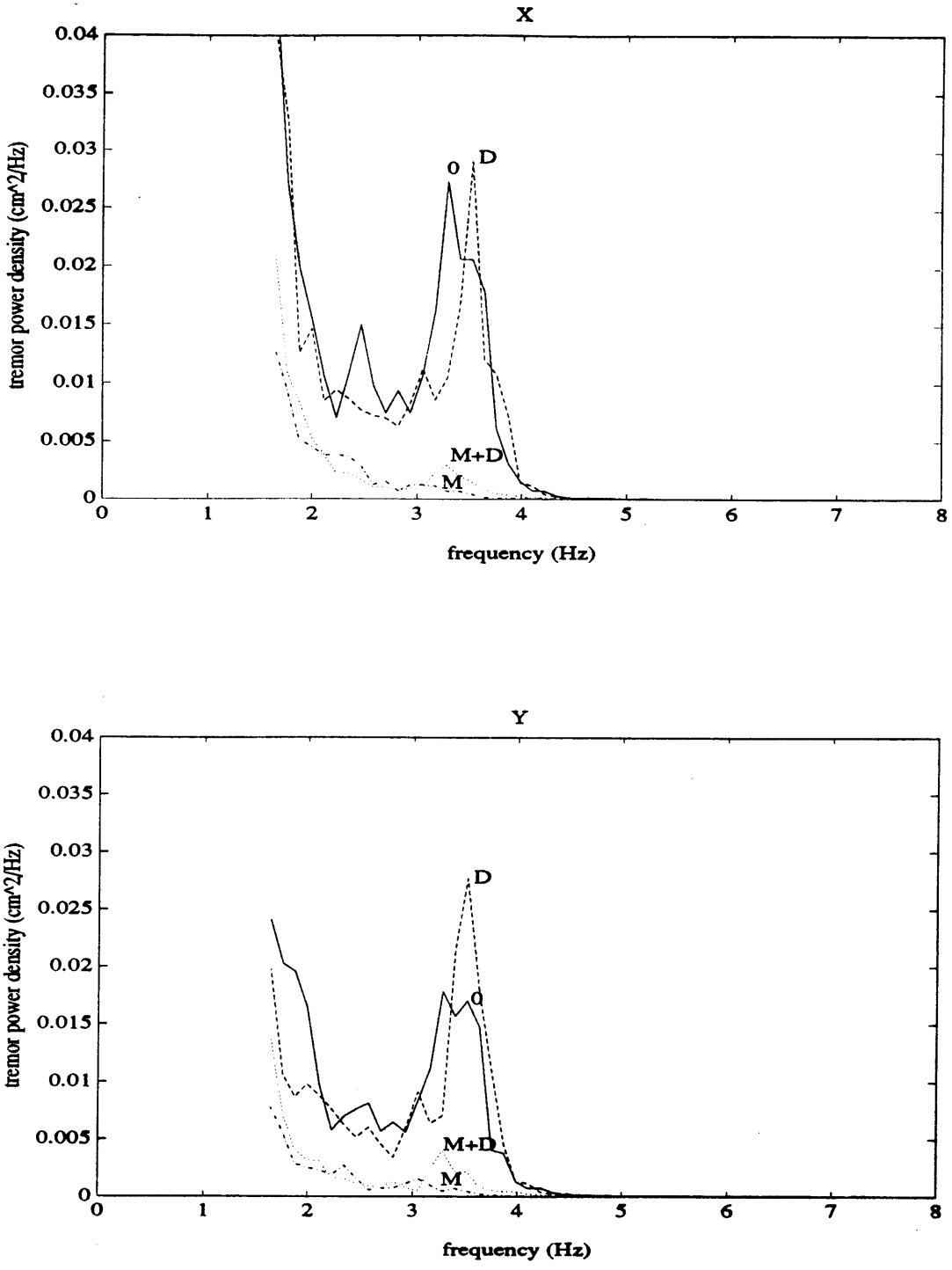

Figure 5-61. *Subject D:* Tremor position spectra illustrating the effects of added inertia. The symbols 0, D, M, and M+D correspond to trials with no damping or mass, 34 N/m/s damping, 7.5 lbm mass, and combined mass and damping, respectively.

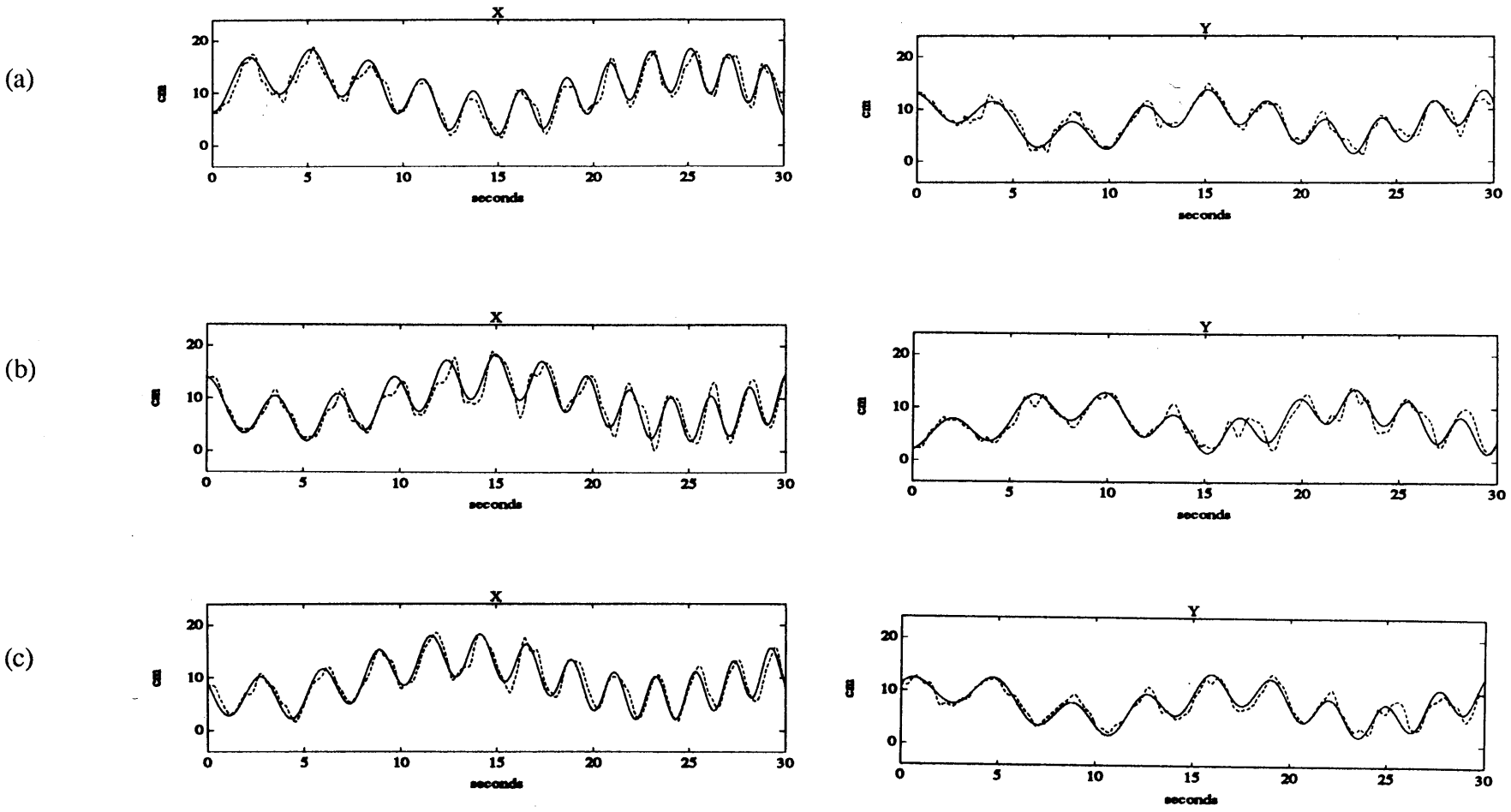

Figure 5-62. *Subject E:* Target and response time trajectories for comparing (a) undamped tremor to (b) tremor with added inertia to (c) tremor with damped inertia.

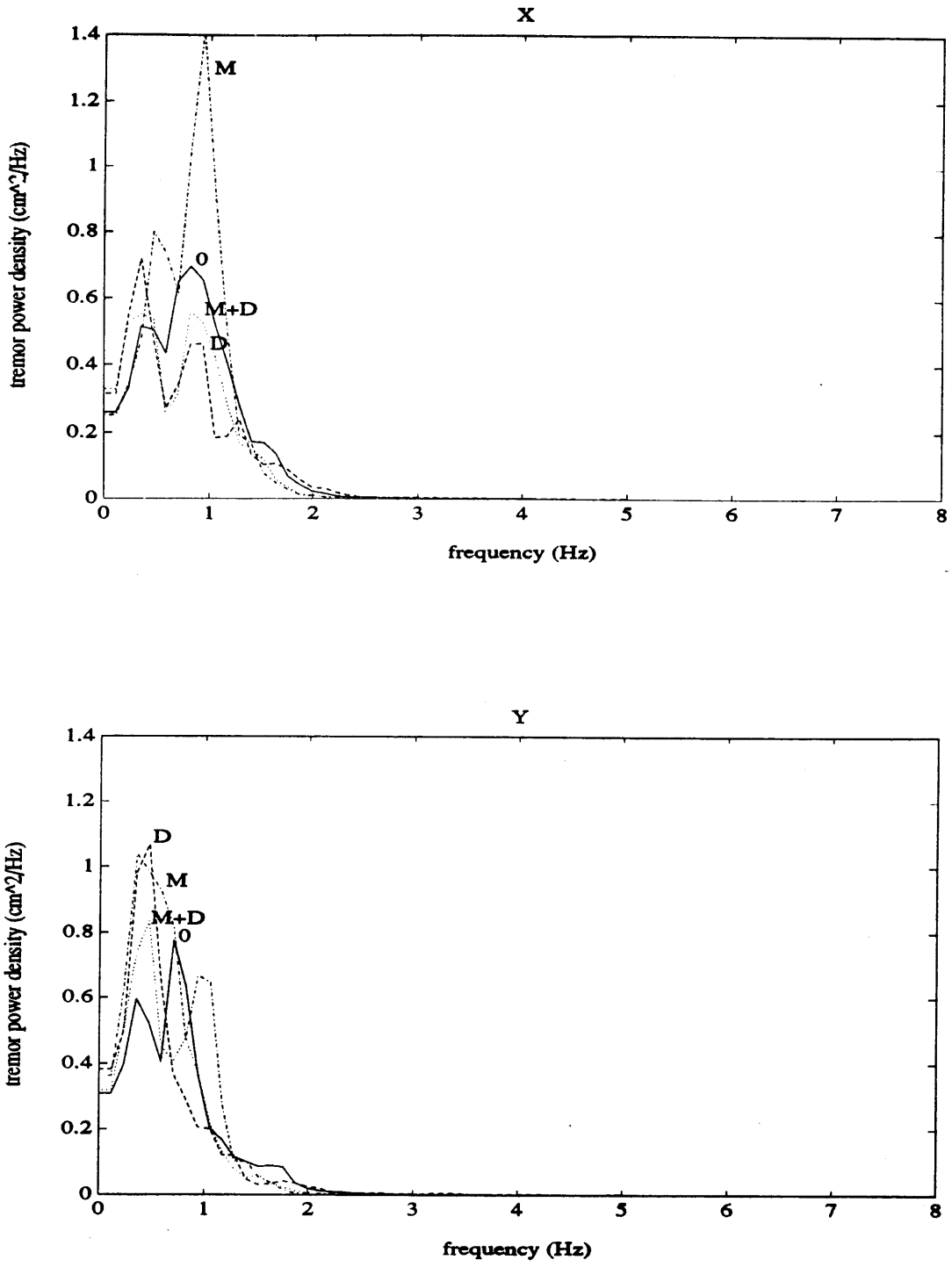

Figure 5-63. *Subject E:* Tremor position spectra illustrating the effects of added inertia. The symbols 0, D, M, and M+D correspond to trials with no damping or mass, 34 N/m/s damping, 7.5 lbm mass, and combined mass and damping, respectively.

In this investigation, different results were indeed observed for different subjects. The tracking records show, for example, that the application of inertial loads did not significantly affect the tremor amplitudes of subjects A, B, C, and E but completely eliminated the small-amplitude 3.4 Hz tremor of subject D. When moderate damping was applied in addition to the inertial load, the tremor amplitudes of subjects A, B, and C were reduced and the tracking accuracy of subject D was improved. Further, the tremor position spectra show that the application of inertial loads did not significantly alter the tremor frequencies of subjects A, C, D, and E but did shift the tremor frequency of subject B from 2 Hz to approximately 1.7 Hz. When moderate damping was applied in addition to the inertial load, the tremor frequency of subject B did not shift as far. The tremor position spectra also show that subjects A, B, and C exhibited the least amount of tremor power when both damping and inertial loads were applied and that subject D, on the other hand, exhibited the least amount of tremor power when just inertial loads were applied.

A examination of the user forces predicted by the CEDO model using actual tremor data provides further information about the CEDO and the degree to which its inertia influences its user. Without any externally-applied inertial loads, inertial forces comprise just 4 to 9 percent of the mean user forces at the highest level of damping. This means that the inertial forces of the CEDO 1 are relatively small compared to the viscous forces at these levels of damping but are quite substantial compared to the viscous forces at low levels of damping. The CEDO model also predicts that when a 7.5 lbm inertial load is applied in combination with a moderate amount of viscous damping, inertia forces comprise 20 to 40 percent of the mean user forces. Interestingly, the mean user forces during the damped-inertia trials were estimated by the CEDO model for subjects A and B to be 60 to 75 percent of the mean user forces during the inertia trials. For these subjects, the applied viscous loads must have suppressed tremorous limb motion to the extent that an increase in the applied viscous force was compensated for by a decrease in the inertial force.

In summary, the inertia of a tremor-suppressing orthosis *may affect* the characteristics of its user's tremor. However, the most appropriate or "optimum" inertia probably varies for different individuals and, even if inertial loads alone or in combination with damping significantly attenuate tremor during an experimental trial, they may be too fatiguing for long-term use in a tremor-suppressing orthosis.

5.3.2 The Effects of Workspace Size and Location

Figures 5-64 through 5-73 illustrate the effects of workspace size and location on tremor and tracking for disabled subjects A-E, respectively. The first figure for each subject shows typical time domain tracking records for comparing tremor and tracking in the left workspace to tremor and tracking in the middle and right workspaces. The second figure for each subject shows tremor position spectra averaged over the three trials from a particular workspace. In these plots, the solid line corresponds to the left workspace, the dashed line corresponds to the right workspace, and the dash-dot line corresponds to the middle workspace. All data were collected during a single test session with some damping applied (85 N/m/s for subject A, 34 N/m/s for subjects B-E). The coordinates of the 5 by 4 inch left, middle, and right workspaces as well as the standard 8 by 6 inch workspace used in this study are listed in Table 3-2 of Chapter 3.

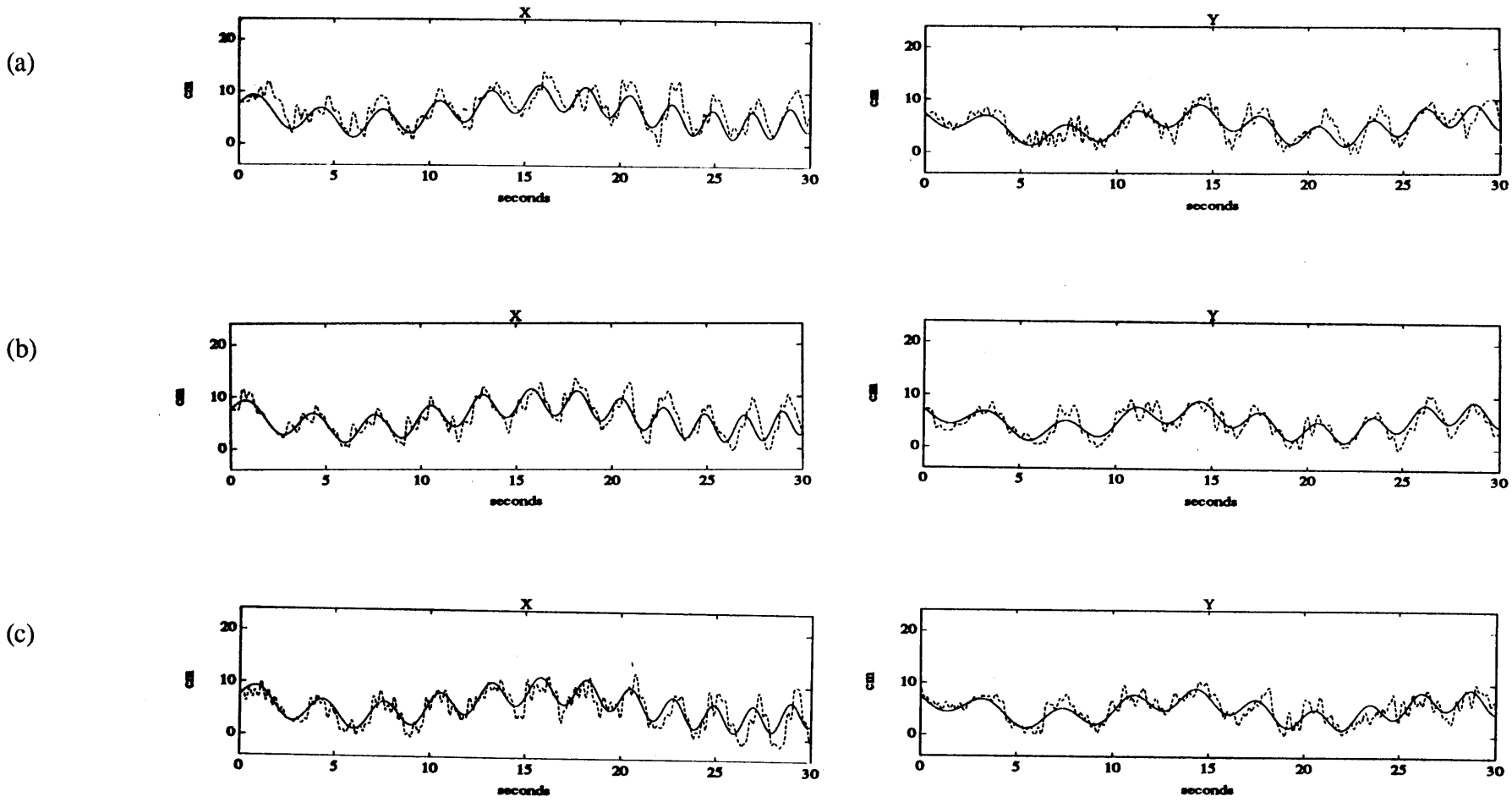

Figure 5-64. *Subject A:* Target and response time trajectories for comparing tremor and tracking in (a) the left workspace, (b) the middle workspace, and (c) the right workspace.

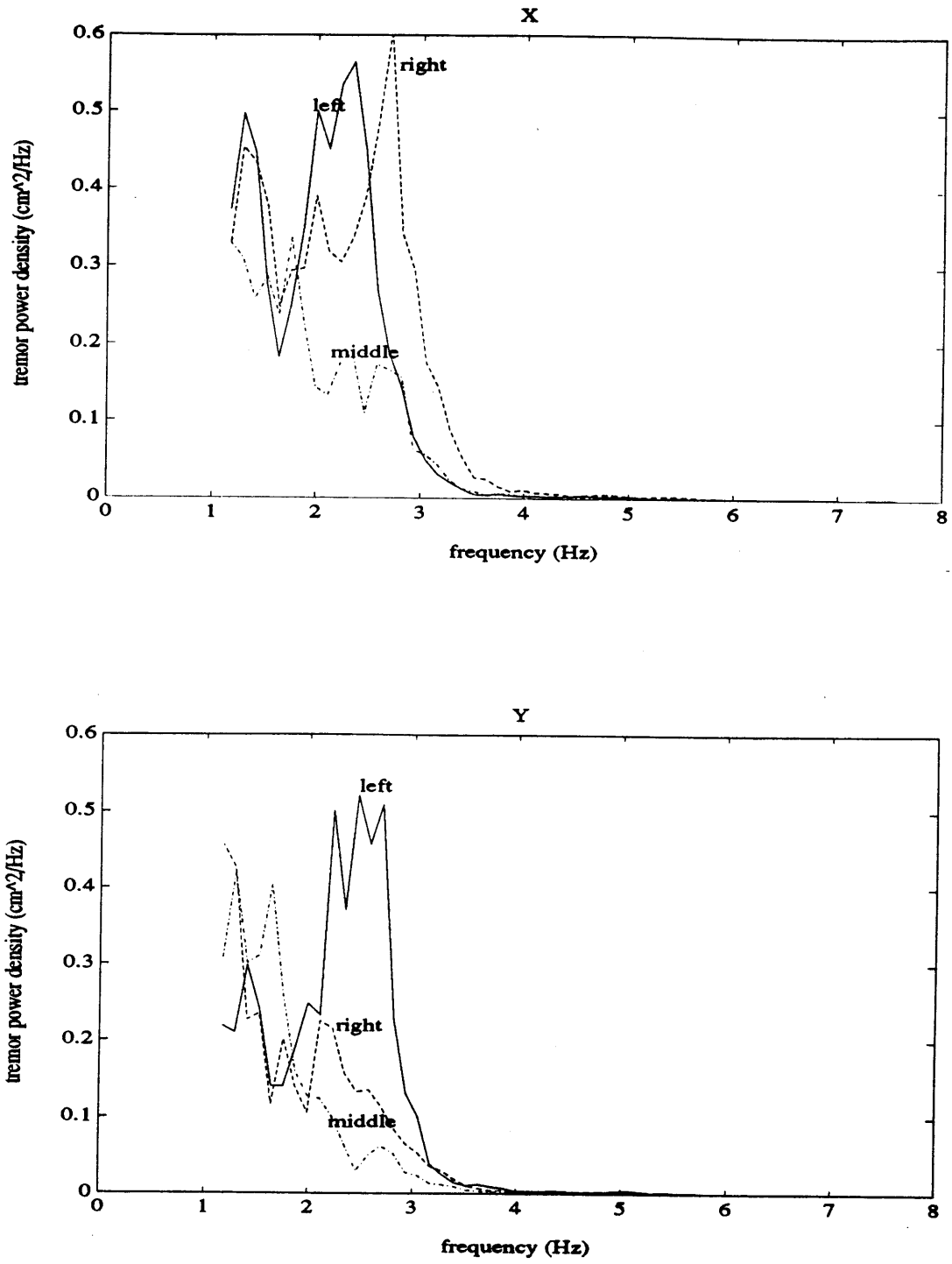

Figure 5-65. *Subject A:* Tremor position spectra illustrating the effects of limb position in the workspace (damping of 85 N/m/s).

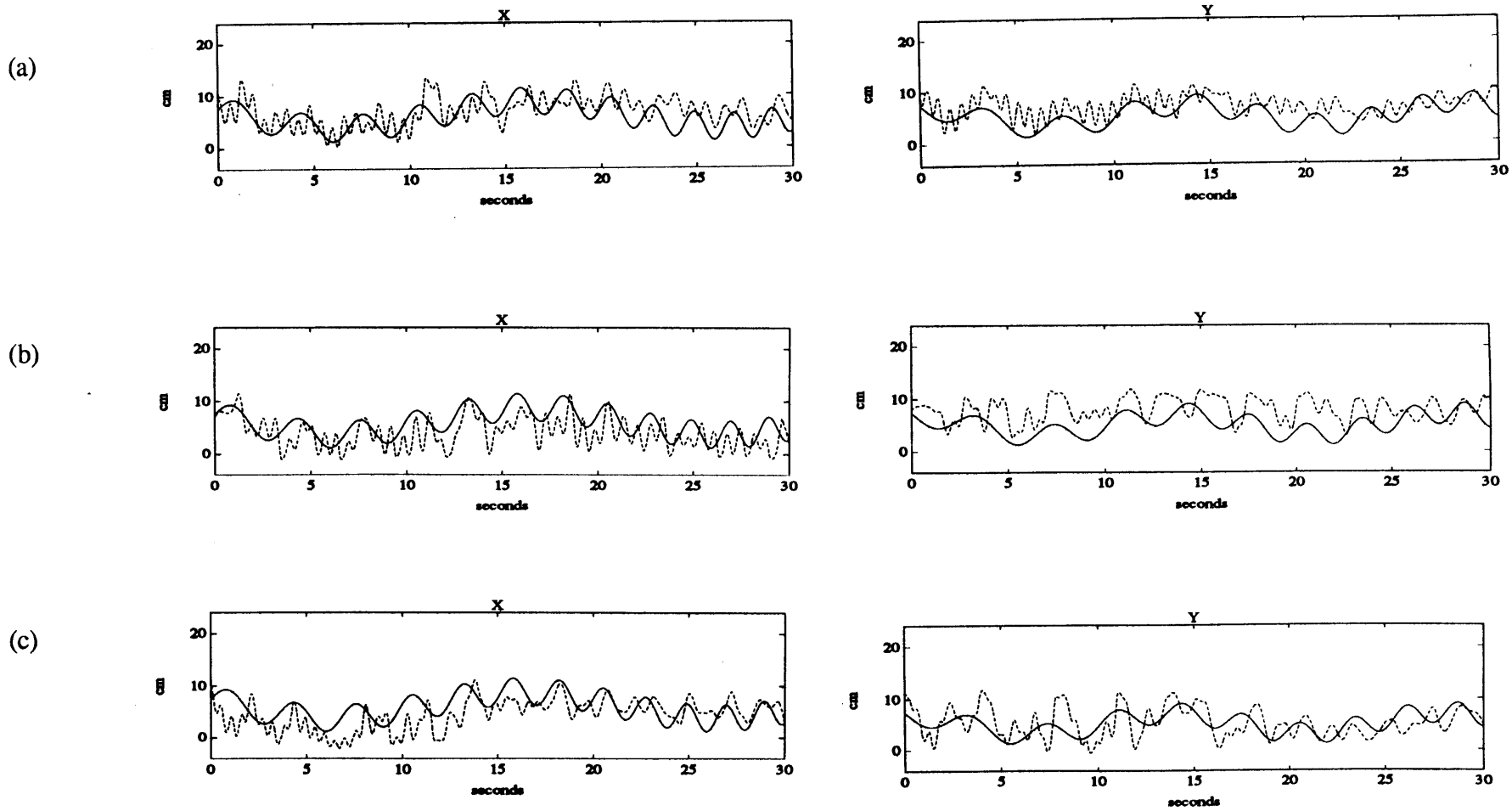

Figure 5-66. *Subject B:* Target and response time trajectories for comparing tremor and tracking in (a) the left workspace, (b) the middle workspace, and (c) the right workspace.

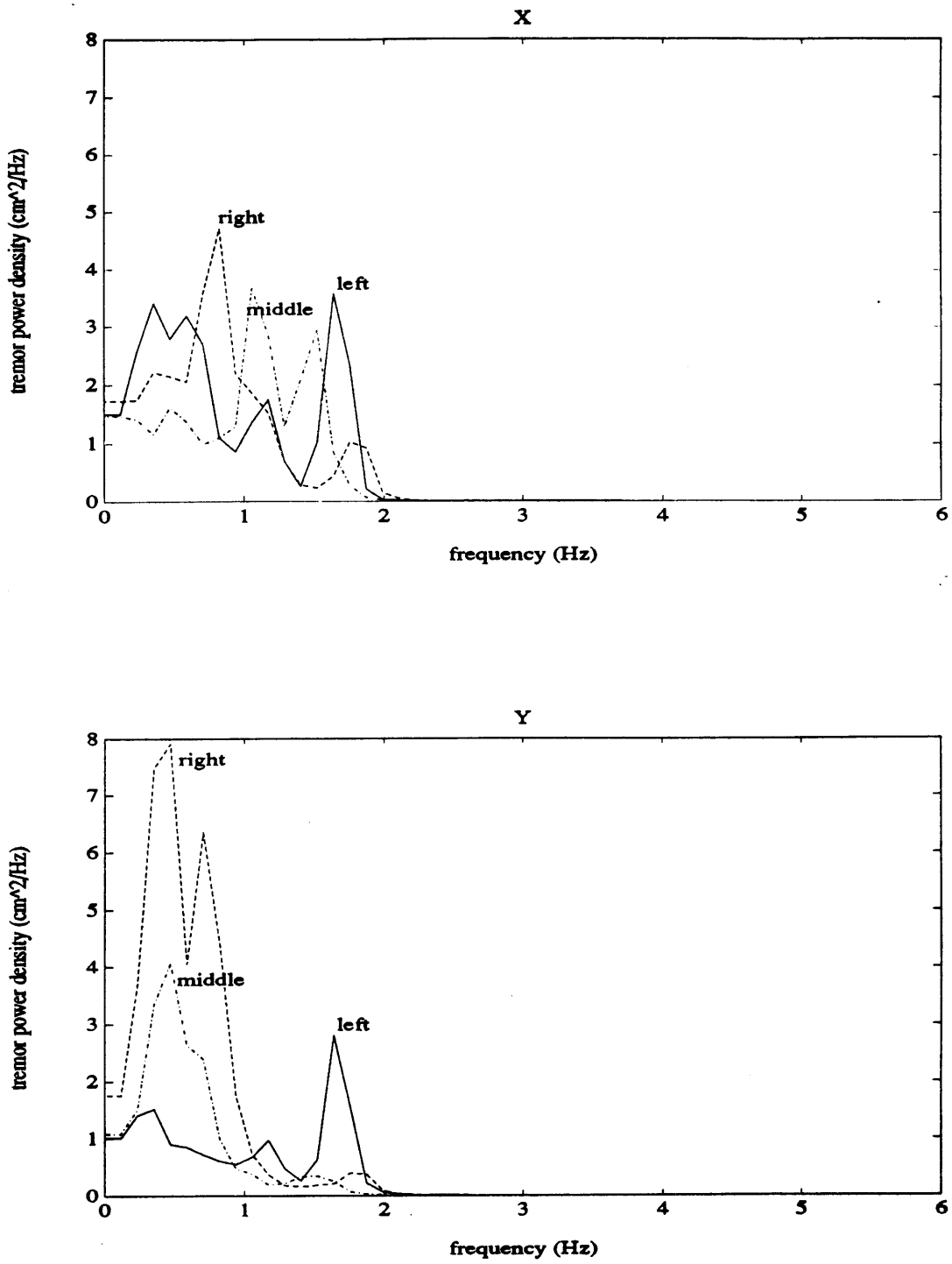

Figure 5-67. *Subject B:* Tremor position spectra illustrating the effects of limb position in the workspace (damping of 34 N/m/s).

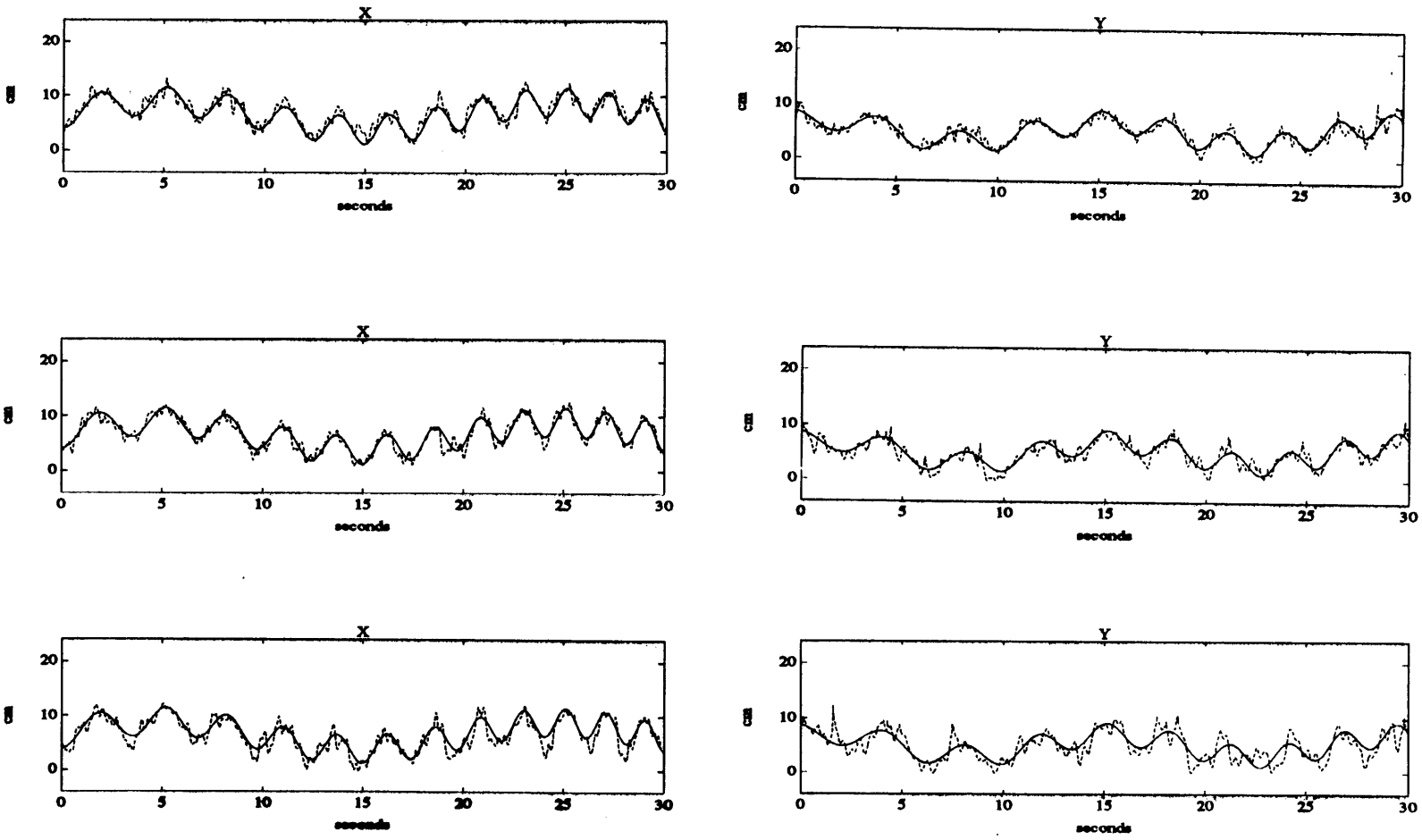

Figure 5-68. *Subject C:* Target and response time trajectories for comparing tremor and tracking in (a) the left workspace, (b) the middle workspace, and (c) the right workspace.

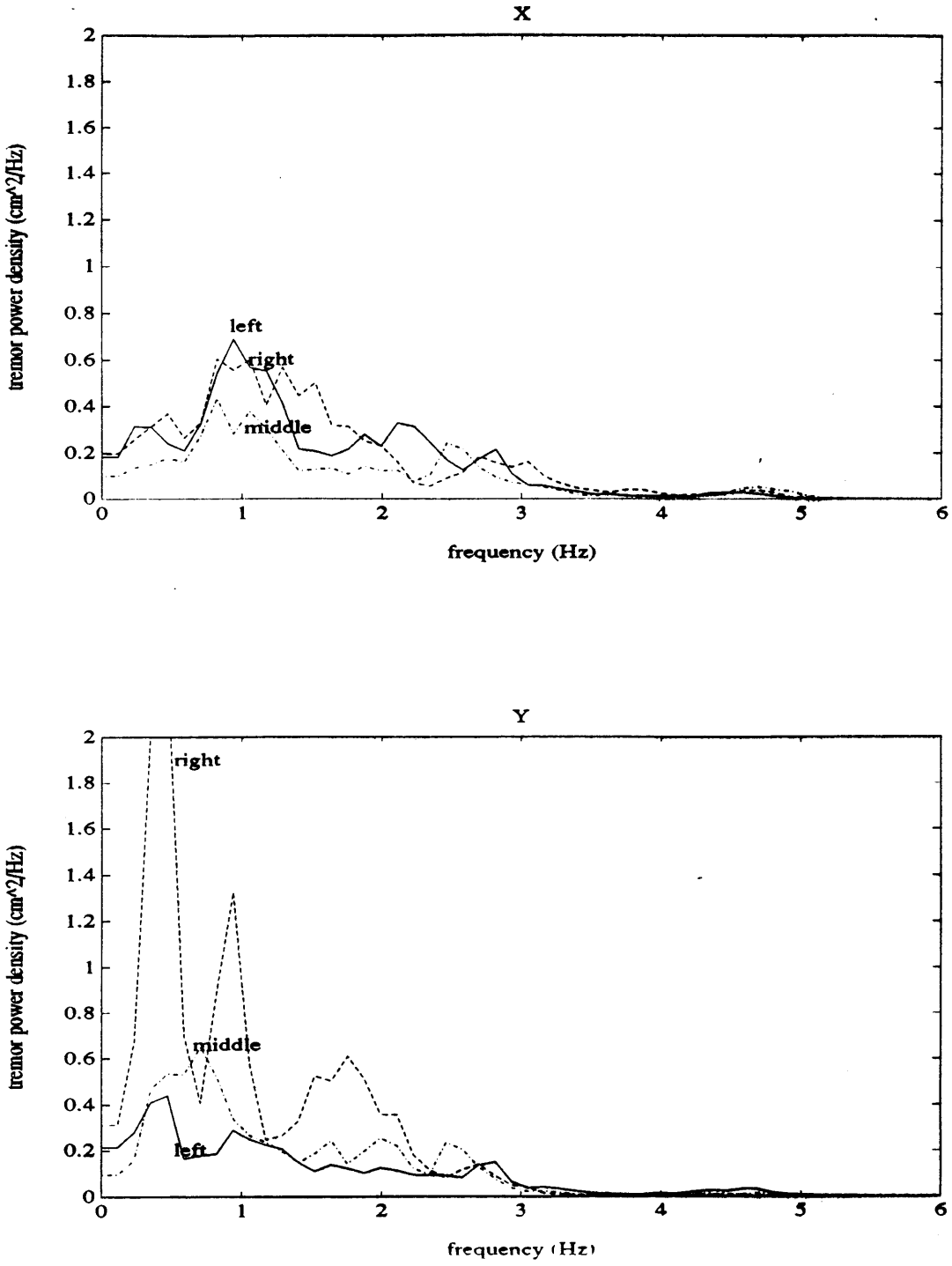

Figure 5-69. *Subject C:* Tremor position spectra illustrating the effects of limb position in the workspace (damping of 34 N/m/s).

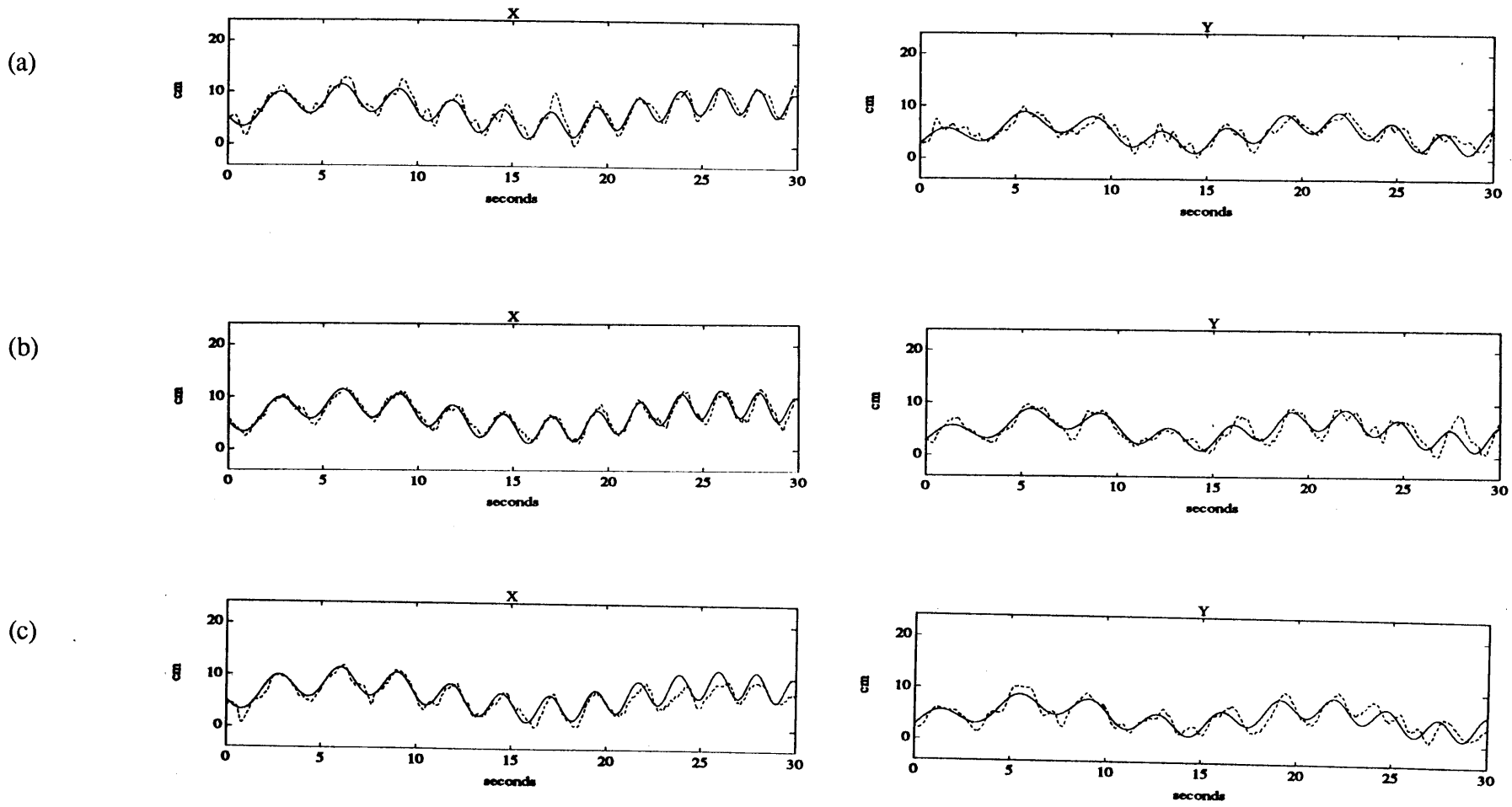

Figure 5-70. *Subject D:* Target and response time trajectories for comparing tremor and tracking in (a) the left workspace, (b) the middle workspace, and (c) the right workspace.

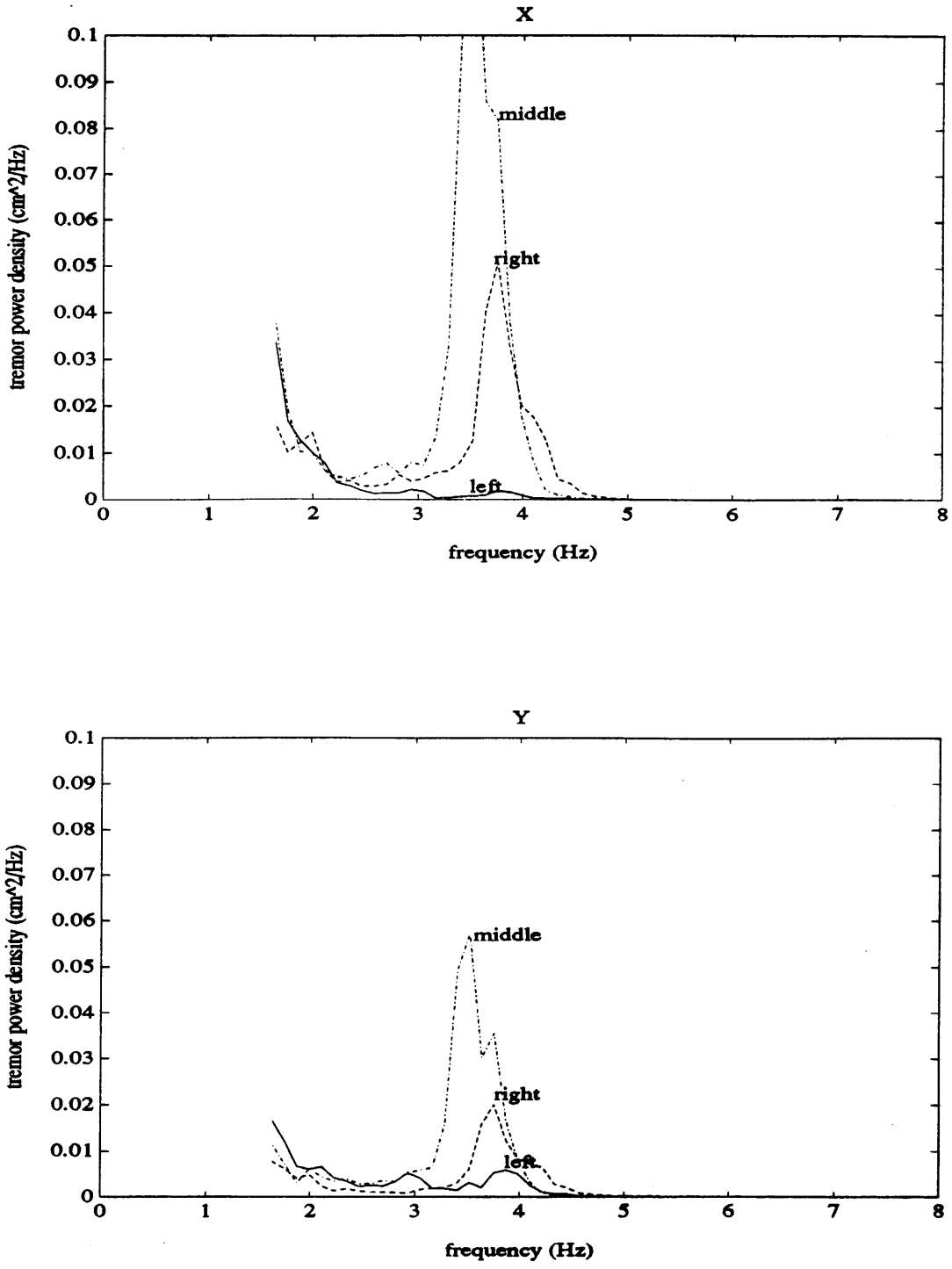

Figure 5-71. *Subject D:* Tremor position spectra illustrating the effects of limb position in the workspace (damping of 34 N/m/s).

(a)

(b)

(c)

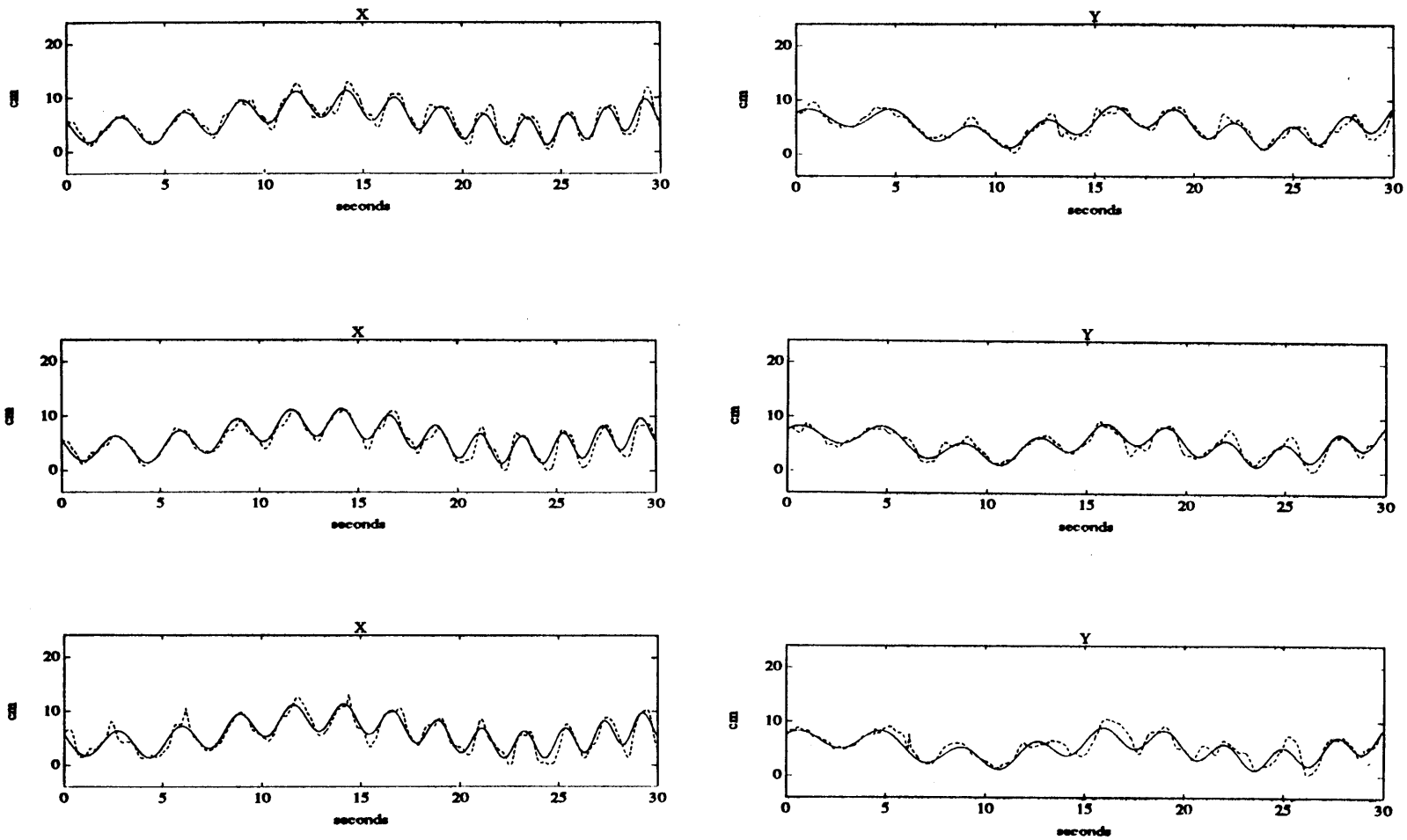

Figure 5-72. *Subject E:* Target and response time trajectories for comparing tremor and tracking in (a) the left workspace, (b) the middle workspace, and (c) the right workspace.

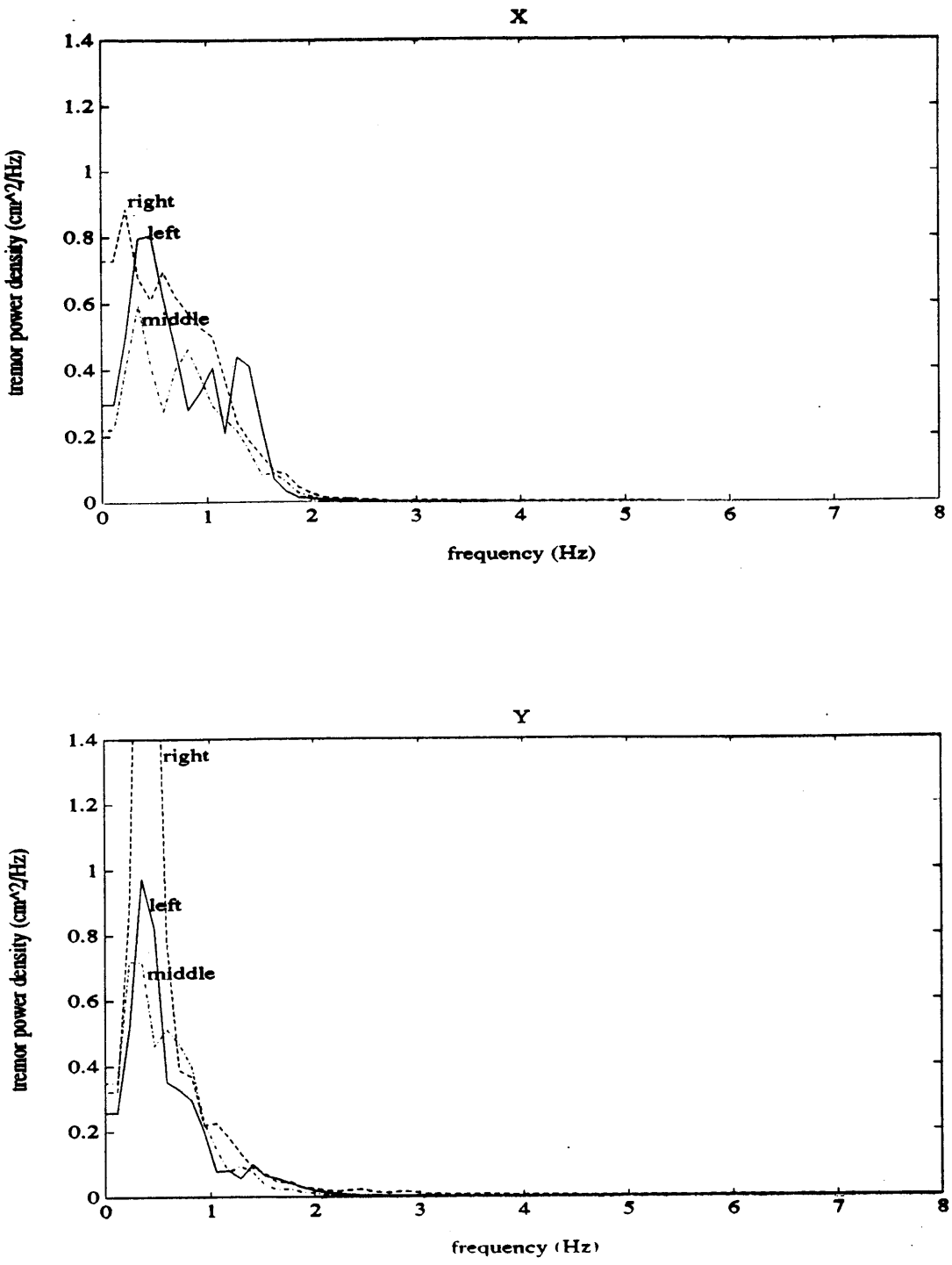

Figure 5-73. *Subject E:* Tremor position spectra illustrating the effects of limb position in the workspace (damping of 34 N/m/s).

The results of these experiments indicate that care must be taken when designing and analyzing data from mulit-dof whole-arm tremor studies. While workspace size does not seem to significantly affect subjects' tremors, workspace location can affect subjects' tremors or at least can affect measurements of subjects' tremors made in multiple degrees of freedom. The tremor spectra for subject A, for example, reveal that the magnitudes of her tremor peaks in the Y direction are greater when her arm is in the left workspace than when her arm is in the right workspace. This observation makes sense when one recognizes that subject A's tremor occurs largely about the elbow joint and that the measured component of tremor in the Y direction is larger when the arm is in the left workspace with the elbow flexed than when the arm is in the right workspace with the elbow somewhat extended. The opposite effect is seen when a subject's tremor occurs largely about the shoulder joint. The tremor spectra for subject C, for instance, reveal that the magnitudes of his tremor peaks in the Y direction are greater when his arm is in the right workspace than when his arm is in the left workspace; i.e. the measured component of tremor in the Y direction due to tremor at the shoulder is greater when the elbow is extended in the right workspace than when the arm is in front of the body in the left workspace. These observations indicate that the position of a subject's arm in space can affect the way tremor is measured in two degrees of freedom, and they suggest that in future investigations, target tracking trajectories should be designed to cover all portions of the workspace so that comparisons between trials with different targets can be made and measurement artifacts can be avoided.

Three other observations from Figures 5-64 through 5-73 should be noted. First, considerable differences are noticed in subject B's Y tremor records from trials in each of the different workspaces in both the time domain plots and the frequency domain plots. In particular, the frequency of subject B's tremor in the Y direction shifts dramatically from near 2 Hz in the left workspace to below 1 Hz in the middle and right workspaces, indicating perhaps that biomechanical factors are influencing subject B's tremor. Hogan et al have reported that the shape and orientation of upper-extremity multi-joint postural stiffness patterns and limb

inertial properties vary systematically with the location of the hand in the workspace [1987]. Assuming tremor oscillation frequencies are proportional to $(k/m)^{1/2}$, and using schematic diagrams of limb stiffness and inertial properties in different postural positions provided by Hogan et al, one might predict tremor frequencies in the Y direction to be greater when the limb is in the left workspace than when the limb is in the right workspace as observed for subject B. The shift of subject B's tremor frequency could also be explained by a shift in her tremor from tremor about the shoulder to tremor about the elbow if tremors about these joints exhibit different characteristics. Second, with regard to tracking, all subjects found the tracking task to be most difficult in the right workspace, and the amplitudes of low-frequency non-linear tracking peaks in the tremor spectra reflect their subjective observations. Third, why subject D exhibits more tremor power at lower frequencies in the middle workspace and less tremor power at higher frequencies in the left workspace is unknown. This pattern was observed in all three sets of trials done.

5.3.3 The Effects of the Tracking Task Target

To determine the effect of target type (i.e. time course) and speed on tremor and tracking measurements, some subjects were asked to track a variety of targets as described in Section 3.2.3 of Chapter 3. Simple targets in which position varied linearly with time (illustrated in the figures to follow), in particular, were used to verify that the low frequency peaks in the spectral plots presumed to be tracking harmonics are smaller in amplitude when fewer tracking errors are made. These targets were also used to determine whether simple, predictable targets induce intention tremor to the same extent as more unpredictable targets comprised of sums of sine waves.

A sample of the results from these experiments are illustrated in Figures 5-74 through 5-79 for disabled subjects A , D, and E, respectively. The first figure for each subject shows typical time domain tracking records for comparing tremor and tracking of a linear target to tremor and tracking of a slow sinusoidal target (frequency components < 0.23 Hz) and a faster sinusoidal

target (frequency components < 0.46 Hz). The second figure for each subject shows tremor position spectra averaged over two trials for each target. In these plots, the solid line corresponds to the linear target trials, the dashed line corresponds to the slow sinusoidal target trials, and the dash-dot line corresponds to the faster sinusoidal target trials. All data were collected during a single test session with some damping applied (85 N/m/s for subject A, 34 N/m/s for subjects D and E).

All three subjects found the fast sinusoidal target to be the most difficult to track and their time domain and frequency domain plots reflect this in that the amplitudes of the low frequency peaks in the spectra are generally greater for the fast sinusoidal target than for the slower sinusoidal or linear targets. In fact, all subjects in this study reported that the faster and more demanding a task, in general, the worse their tremor becomes. The slow, predictable linear target still induced intention tremor in subjects A and D, but subject A's tremor power at pathological tremor frequencies was lower when she tracked this target than when she tracked the sinusoidal targets. The observations from these experiments imply simply that the type and speed of targets used in pursuit tracking tasks should be considered when designing protocol to test tremor-suppressing orthoses.

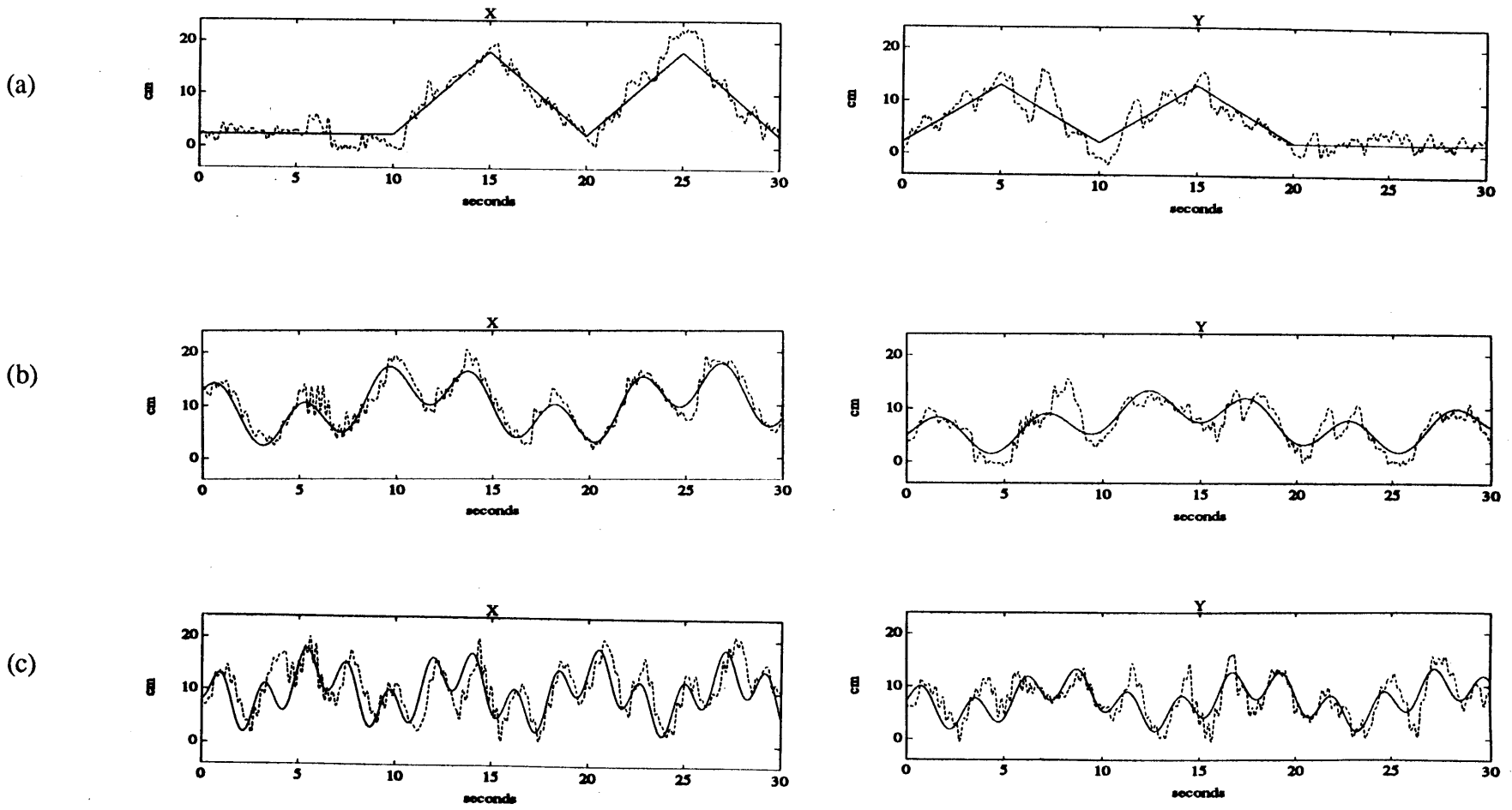

Figure 5-74. *Subject A:* Target and response time trajectories for comparing tremor and tracking using (a) a linear target, (b) a sinusoidal target with frequency content below 0.23 Hz, and (c) a sinusoidal target with frequency content below 0.46 Hz.

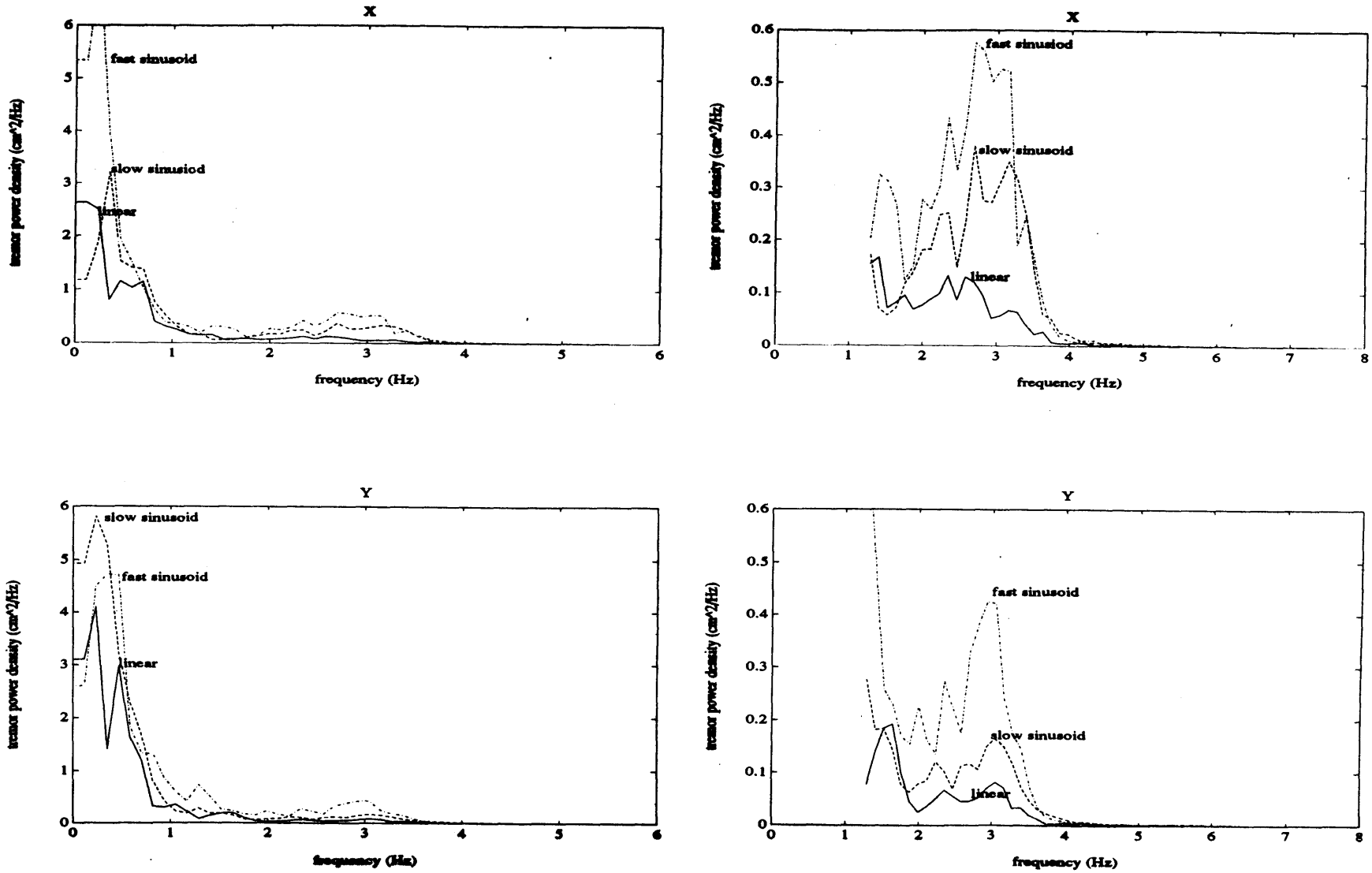

Figure 5-75. *Subject A:* Tremor position spectra illustrating the influence that the tracking task target has on tremor power (damping of 85 N/m/s).

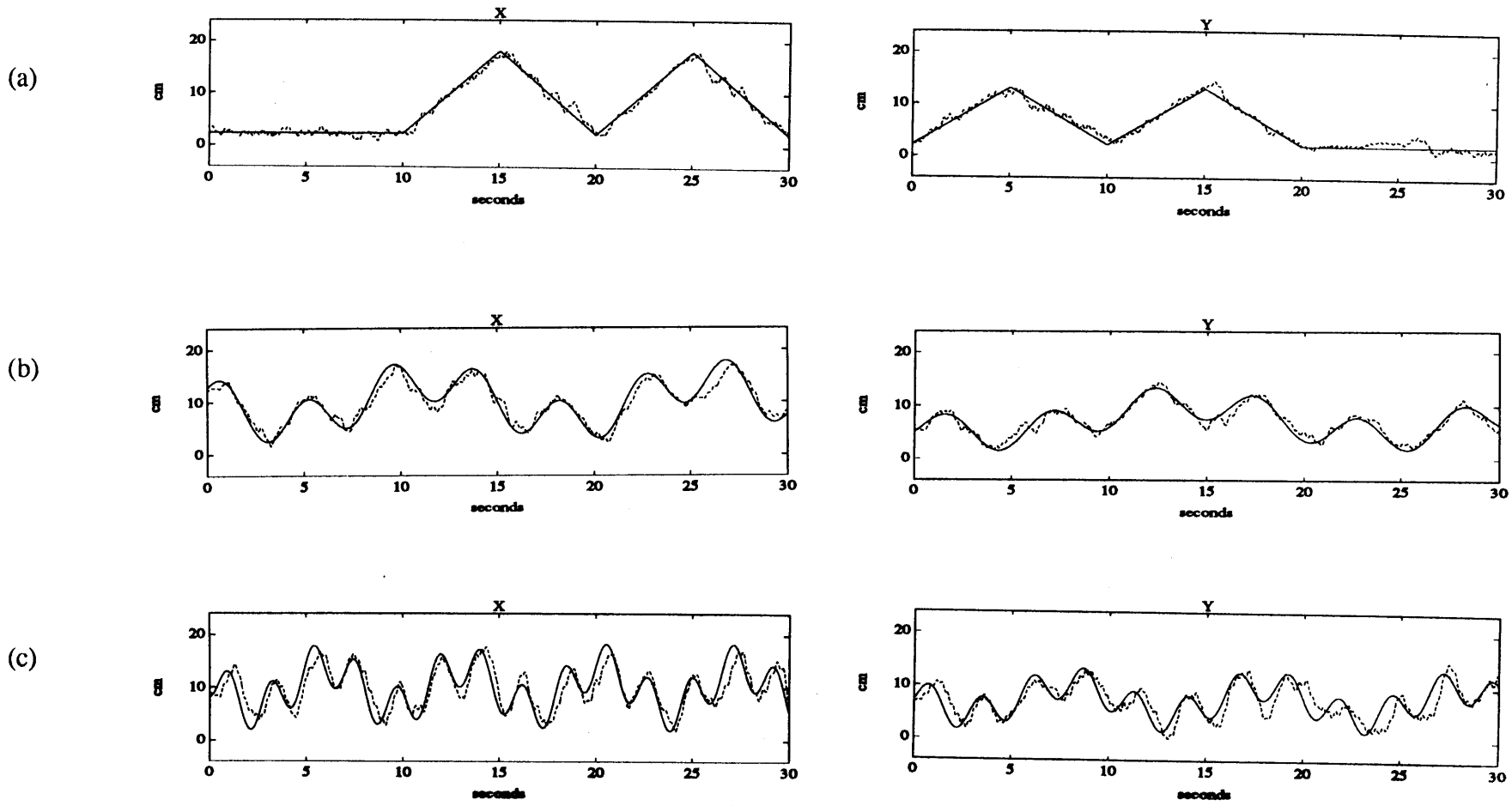

Figure 5-76. *Subject D:* Target and response time trajectories for comparing tremor and tracking using (a) a linear target, (b) a sinusoidal target with frequency content below 0.23 Hz, and (c) a sinusoidal target with frequency content below 0.46 Hz.

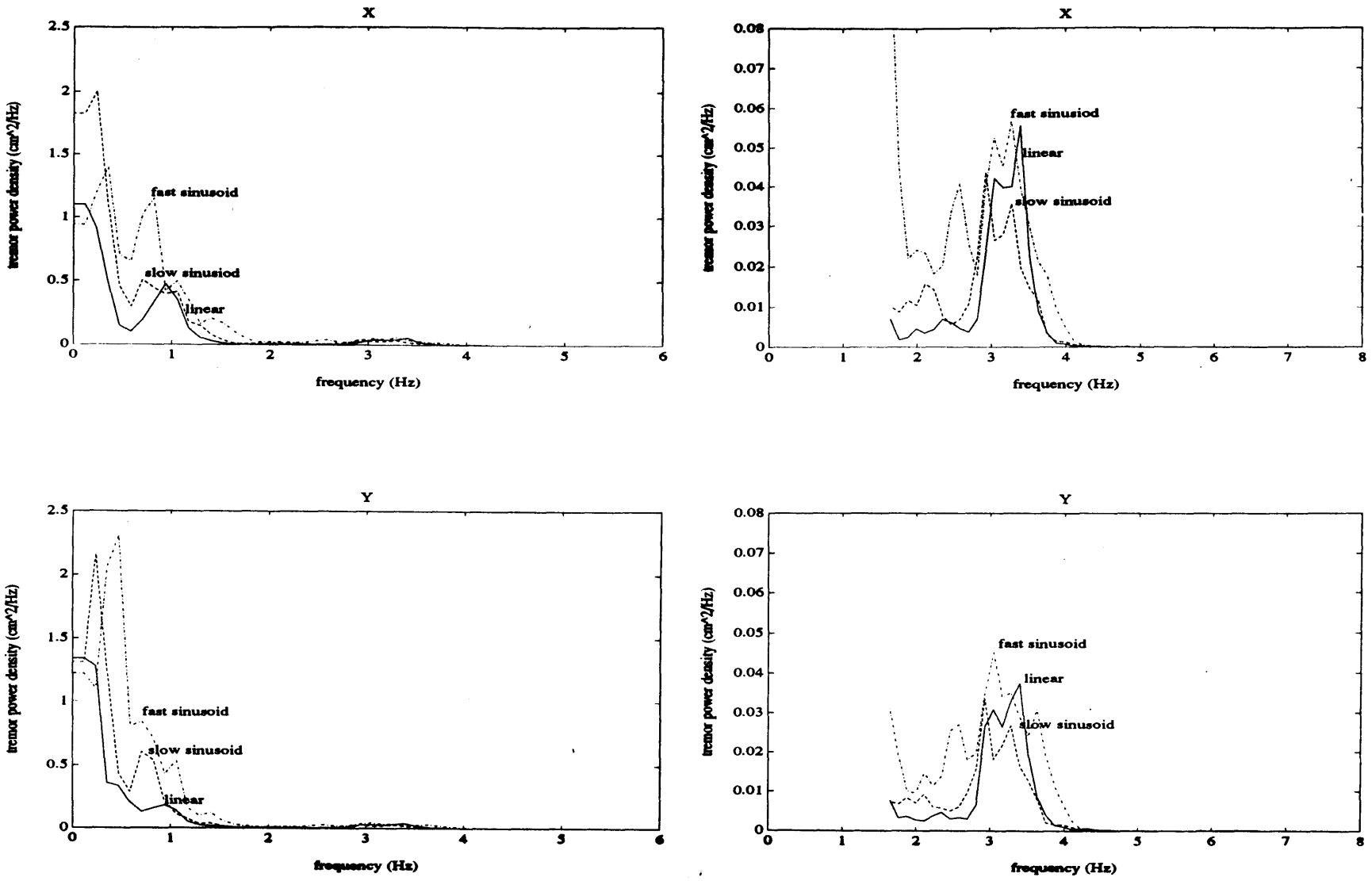

Figure 5-77. *Subject D:* Tremor position spectra illustrating the influence that the tracking task target has on tremor power (damping of 34 N/m/s).

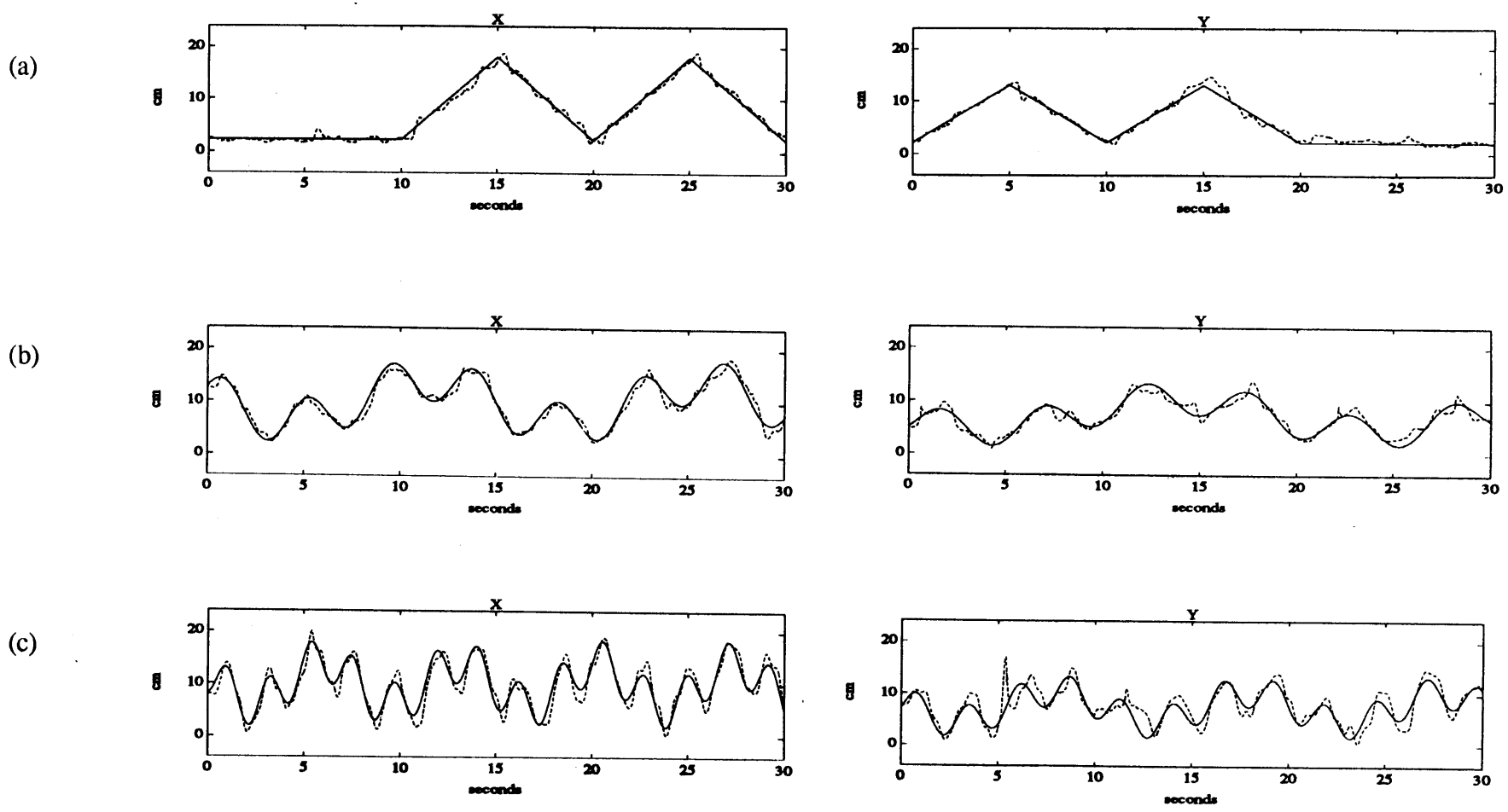

Figure 5-78. *Subject E:* Target and response time trajectories for comparing tremor and tracking using (a) a linear target, (b) a sinusoidal target with frequency content below 0.23 Hz, and (c) a sinusoidal target with frequency content below 0.46 Hz.

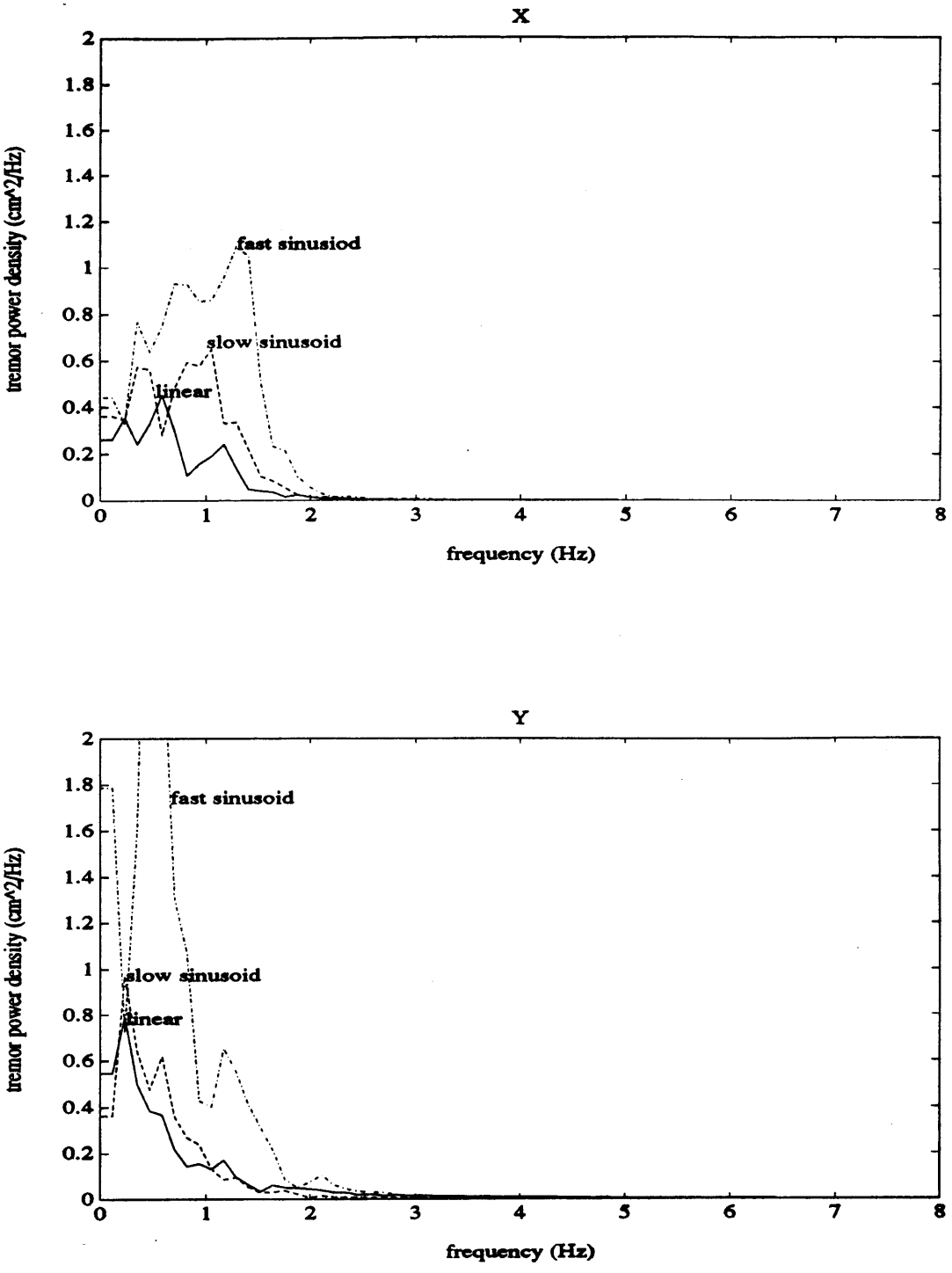

Figure 5-79. *Subject E:* Tremor position spectra illustrating the influence that the tracking task target has on tremor power (damping of 34 N/m/s).

5.3.4 The Effects of Force-Velocity Non-Colinearity

As demonstrated in Section 2.2.1 of Chapter 2, the CEDO 1 cannot provide endpoint force-velocity colinearity for all endpoint locations and all directions of movement. Thus, important questions to consider before designing the CEDO 2 include whether participants notice the non-colinearity of the CEDO 1 and if so, whether it hinders their tracking. The answers to these questions were explored in two ways. First, in preliminary experiments, the CEDO 1 was purposely made to be non-colinear by using different damping coefficients in the X and Y directions. Second, in the experiments for this investigation, participants were asked to remark on the "feel" of the CEDO 1 and any changes with damping level they noticed while doing the tracking tasks.

In both the preliminary and the final experiments, participants' awareness of the non-colinearity property varied in an apparently systematic way with the severity of their tremors and the level of damping. When asked to remark on the "feel" of the CEDO 1 and any changes with damping level, the subjects with the most severe tremors made no comments that indicated they had noticed the non-colinearity or had been bothered by it, even when different damping levels in different directions were used. Subjects with less severe tremors and able-bodied control subjects, however, noticed a definite "jerkiness" in the damping simulation when different damping levels in different directions were used. When these subjects did normal tracking tasks, they noticed nothing remarkable at damping levels up to 34 N/(m/sec) but commented on sensations of "lumpiness" or "jerkiness" at higher damping levels whose endpoint position-dependence suggested that they were aware of locations where non-colinearity was worst. None of the subjects, however, seemed to be bothered by the absence of force-velocity colinearity to the extent that it hindered their performances on the tracking tasks.

Chapter 6
Conclusions and Recommendations for Future Work

6.1 Conclusions from this Investigation

6.1.1 Experimental Findings

Five main conclusions can be drawn from this investigation regarding the CEDO's potential use as a tremor-suppressing orthosis and its effectiveness as a multi-dof tremor measurement device:

1. Linear and non-linear damping loads *can* selectively attenuate upper-extremity intention tremor in more than one degree of freedom without degrading purposeful movement. In this investigation, the application of linear and non-linear damping loads to subjects' right limbs during 2-dof pursuit tracking tasks produced statistically significant reductions in tremor as measured by a "tremor power" score with p-values of less than 0.001 for four of the five tremor-disabled subjects tested. The application of linear damping loads about the CEDO's third axis (rotational degree of freedom) also reduced tremor significantly in a sixth disabled subject who did just 1-dof tracking tasks about that axis. Differences in the transfer function magnitudes and phases from trials with and without damping were not statistically significant for five of the six tremor-disabled subjects tested, verifying that subjects' tracking performances were, in general, not hindered by the resistive loads applied.

2. Tremor-disabled individuals do not all respond to damping loads applied by the CEDO 1 in the same manner. In this study, damping loads substantially attenuated the severe tremors of subjects A, B, and C. However, damping loads had little effect on subject D's low-amplitude 3.4 Hz tremor even though they improved her tracking ability and thus reduced her "tremor power" score.

3. Inertial loads, damped inertial loads, workspace location, and target characteristics *can* affect subjects' tremors and 2-dof tremor measurements. However, subjects' responses to these experimental factors vary. As shown in this study, the frequency of subject B's tremor

changed with the location of her arm in space, but the frequencies and amplitudes of other subjects' tremors were largely invariant to such "biomechanical factors".

4. The differences in subjects' responses to damping loads and other factors in this study do not appear to be related to etiology; rather, subjects' responses seem to depend upon the amplitudes, frequencies, and severities of their tremors. (In this investigation, subjects A, B, and E had MS; subjects C and D suffered from head injuries; and subject F had a cerebellar degenerative disease).

5. Subjects' awareness of the force-velocity non-colinearity of the CEDO varies in an apparently systematic way with the severity of their tremors and the level of damping used. In this investigation, the most severely disabled subjects made no comments that indicated they had noticed the CEDO's non-colinearity characteristics. The less severely disabled subjects and able-bodied subjects, on the other hand, described sensations of "lumpiness" or "jerkiness" at damping levels above 34 N/m/s apparently at locations where non-colinearity was the worst. Regardless of whether subjects noticed the non-colinearity of the CEDO or not, none were seemingly bothered by it to the extent that it hindered their performance on the pursuit tracking tasks.

6.1.2 Guidelines for Planning Future Protocols

One purpose of this investigation was to establish guidelines for pursuit tracking experiments and methods for interpreting tremor power spectra that are applicable to future tremor studies. Based on the experimental results of this study, the following recommendations and "rules of thumb" are proposed:

1. Because undamped tremor varies considerably from day to day, one cannot expect to directly compare the results of trials done one day to the results of trials done another day. For example, one probably cannot determine whether linear or non-linear damping is more appropriate for use in a tremor-suppressing orthosis by directly comparing the results of linear damping trials done during session 1 to the results of non-linear damping trials done during

session 2. For future investigations, it may be worthwhile to explore whether some method of normalizing tremor across days (perhaps relative to some average undamped tremor) would allow such comparisons to be made in spite of the day-to-day variations in tremor observed.

2. To minimize learning effects, subjects participating in pursuit tracking experiments should be tested on multiple days, if possible, so that the first day's protocol can be devoted to practice and subsequent days' protocol can be devoted to data collection. Even though reasonably slow simple targets were used in this investigation, and even though subjects were allowed to practice before data were collected, learning effects were quite possibly detected in three of the twelve subjects tested over a period of two to three days.

3. If possible, multiple trials for each test condition should be done so that results can be averaged, within-a-session variability can be assessed, and "sampling" errors can be minimized. A minimum of three trials per test condition is recommended.

4. If the protocol involves pursuit tracking tasks, the frequencies of the targets should be chosen with care. As observed in this investigation, target frequencies may influence the observed characteristics of subjects' tremors. The tremor-disabled subjects tested in this study generally agreed that the faster and more demanding the task, the more debilitating their tremors seem to become. The target frequencies must also be chosen carefully for the purposes of data analysis. As explained in Chapter 3, target frequencies may influence the positions of low frequency peaks visible in tremor power spectra. Although the data collected in this investigation were not uniform enough across subjects to assert that all humans track sine waves like "square waves" or "triangle waves", and the limited resolution of the spectra combined with leakage effects make it difficult to determine whether subjects' tracking peaks occurred at specific harmonics of the target frequencies, the data do suggest that the low frequency peaks in the tremor spectra depend upon target frequencies and can be attributed with reasonable certainty to tracking errors not linearly related to the target. This finding implies that if tremor peaks are to be distinguished from tracking peaks in frequency domain analyses, target frequencies must be low enough to prevent peaks at approximately the third or fourth

target harmonics from interfering with peaks at the tremor frequencies. The strategy tried in this investigation, in which target frequencies were incremented continuously during a trial in attempt to "spread out" subjects' tracking peaks at low frequencies, did not allow tremor peaks to be more clearly distinguished from tracking peaks as had been originally hoped.

5. Because the position of a subject's arm in space may affect 2-dof tremor measurements, tracking task targets should be designed to cover similar portions of the workspace if comparisons are to be made among trials in which different targets are utilized.

6.2 Recommendations for Future Work

6.2.1 Remaining Experimental Questions

Several questions remain to be answered before the CEDO can be marketed commercially as a tremor-suppressing orthosis. In particular:

1. This investigation failed to determine specifically the amount of damping a whole-arm tremor-suppressing orthosis must provide. Before this question can be addressed, however, standards for evaluating tremor-suppressing orthoses must be defined. The ultimate objective standard for success is, of course, the reduction of pathological tremor to the amplitude of physiological tremor. For improvements short of this ideal, "How good is good enough?" depends on the user -- more specifically, on the activities the user wishes to be able to undertake independently (with orthotic support) and on the tradeoffs between functional benefits gained and various "costs" incurred. An individual whose financial independence and personal satisfaction depends on electronic assembly, for example, would impose tighter specifications for tremor reduction on the CEDO than someone whose primary need is to turn pages. For some tremor-disabled individuals, the range of damping loads applied in this investigation will probably be adequate. For others, however, more damping is almost certain to be required. Higher damping levels were not able to be used in this investigation, not because they interfered with subjects' purposeful tracking, but because damping simulations at

these levels felt "lumpy" perhaps due to the slow response times of the brakes and the insufficient torque output of brake 1.

2. This investigation also failed to determine whether non-linear damping is preferable to linear damping in a tremor-suppressing orthosis and whether the answer depends, like so many other factors, on the specific user and his or her tremor. Both types of damping appear to suppress tremor. What if loading comprised of a combination of viscous and velocity-squared damping is tried? Is one type of loading more fatiguing than the other over long periods of use?

3. While experiments in this investigation demonstrated that inertial loads (and therefore the inertia of a tremor-suppressing orthosis) can affect subjects' tremors, they provided no indication of what the most appropriate or "optimum" amount of inertia might be. A light-weight orthosis seems advantageous in that it minimizes fatigue and prevents the possibility of the CEDO linkage resonating as discussed in Chapter 2, but appropriate inertial loads may, in fact, help suppress the tremor of someone like subject D.

4. To provide a basis for design optimization, detailed experimental data must be gathered on the mechanisms of tremor; the effects of loading; and the relationships between tremor, loading, and the physiology of fatigue and strengthening. More specifically, a physiological understanding of why damping loads attenuate tremor and how they might cause undesirable (*or* desirable) fatigue effects, "carryover" effects, or strengthening effects in everyday use is essential for designing better, more effective tremor-suppressing orthoses. Future testing of the CEDO should provide not only the additional data needed to test the orthosis's effectiveness as a product in activities of daily living, but should also allow the following hypotheses about fatigue, "carryover", and strengthening effects to be tested experimentally. (Relevant background information on muscle fatigue and exercise physiology is provided in Appendix I.)

Potential Fatigue Effects -- When using the CEDO, the user's musculature is required to produce three classes of forces: those normally required for intended movement to overcome the impedances and external forces imposed by the limb and the environment; those necessary

to move the *orthosis* at the frequencies of the voluntary activity; and those associated with tremor. The onset and development of fatigue depends on the populations (not necessarily distinct) of muscle fibers meeting each of these force requirements, the levels of force required of each population, their fatigue properties, *and* on how all these characteristics vary among tremor types. While there is considerable literature on the metabolic mechanisms of muscle fatigue [for example, Edwards 1981] and on the fatigue characteristics of fiber types I, IIa and IIb [for example, Binder 1989 and Williams 1990], there are very few publications on the specificity of involvement of distinct fiber types in pathological tremors or on how normal fiber recruitment patterns are altered by tremorogenic pathologies. Edstrom [1970] and Shahani and Wierzbicka [1990] have reported some observations of motor unit recruitment and fiber type involvement in Parkinson's Disease, essential tremor, spasticity, and cerebellar ataxia, but detailed facts are unavailable. Fatigue effects may also be influenced by the mechanism by which tremor is attenuated. If tremor is centrally driven and tremorogenic muscle torques are undiminished by the presence of damping, for example, fatigue may occur at a different rate than if the applied damping effectively compensates oscillatory reflex dynamics such that the tremor torques themselves are reduced.

The CEDO 1 has not been used in experimental sessions which approximate a full work day. Rather, experimental sessions to date have run 1.5 hours at most during which the ratio of tracking time to rest time was 1 to 3 and the duration of each experimental trial was 30 to seconds to 1 minute. A consistent observation from such sessions is that subjects' often describe themselves as being "tired" when the session is over. In fact, only 30-minute experimental sessions were done for two of the six tremor-disabled subjects in this study *because* they complained of getting tired. One should recognize, however, that virtually all of these subjects were unaccustomed to being physically active due to their disability and that they probably would have found the tracking tasks to be as tiring (or *more* tiring) without damping; i.e. it seemed to be limb use in general that the subjects found tiring. Only two of the subjects exhibited any signs of muscle fatigue in the arm muscles associated with the tracking motions

during a session, and none reported subsequent muscle soreness. While these observations provide a basis for pondering the potential fatigue effects of a tremor-suppressing orthosis, they are not adequate. In future investigations, the CEDO must be used in activities of daily living during which muscular fatigue is monitored more carefully, perhaps by recording surface myoelectric activity [Furr et al 1989, Merletti & DeLuca 1989].

Potential "Carryover" Effects -- A question often raised by clinicians with regard to tremor-suppressing orthoses is whether undesirable "carryover" effects might occur immediately after decoupling the user's limb from the orthosis. To date, no experimental evidence for either a sudden aggravation of tremor or a prolonged attenuation of tremor immediately following the withdrawal of an energy-dissipating load has been reported, nor have data been published which suggest that tremor is generated by a physiological regulator which is adaptive, i.e. one which makes parametric adjustments to maintain a reference level of tremor in spite of external changes which tend to diminish it.

In experiments with the CEDO 1 thus far, evaluation protocols have not yet focused on detecting and quantifying beneficial or detrimental after-effects of its use. However, certain related observations have been made. First, objective performance data for three of five tremor-disabled subjects in this study exhibited no statistically discernable trend toward either an increase or an attenuation of tremor over the course of a multiple-day series of trials; in other words, use of the CEDO on Session i was not consistently followed by lower tremor in Session i+1. The tremor power scores of subjects D and E from later test sessions *were* consistently less than those from earlier test sessions, but as postulated in Chapter 5, these trends were quite possibly due to learning effects rather than physiological effects. Other observations to note include the discovery that subject A's tremor was often dramatically reduced following the first five or six trials of each session, and the finding that subject C's tremor power scores were greatest from the first set of each session and smallest from the last set of each session. Unfortunately, it is not known whether these observations should be attributed to a physiologically-mediated after-effect of damping or whether they are simply

artifacts of other possible effects such as fatigue, (re)familiarization with the tracking task, or "warm-up" effects of the CEDO 1 itself. Future CEDO studies must address these issues.

Potential Strengthening Effects -- A possible longer-term result of using the CEDO on a daily basis is related to its incidental function as an exercise device. If the CEDO 1 increases the strength of the loaded muscles, then it's tremor reduction effectiveness *may be diminished* over time by increasing the forces generated by a given level of tremorogenic motoneuron activity. The potential for such a strengthening effect may depend upon the mechanism by which loading affects tremor -- loading which only diminishes movement resulting from unaltered rhythmic muscle force might alter muscular strength differently than loading which reduces muscle force oscillations themselves.

The author has found no literature to date which explains the long term effects of pathological tremor on muscle strength or the interaction between exercise physiology and tremor physiology. The literature on muscle response to exercise, however, does make it possible to state explicitly the conditions which must be met for prolonged use of the CEDO to yield muscle changes which decrease its effectiveness. First, to attain the increase in fiber diameter necessary for increased strength, the fast-twitch glycolytic IIb muscle fibers must be recruited during short duration high-intensity exercise (like weight lifting). Lower intensity sustained exercise (like long-distance running) does *not* increase strength, but rather improves endurance by increasing the number of mitochondria in the I and IIa muscle fibers and by improving the microcirculation around these fibers [see Vander et al 1985 for example]. Diminished effectiveness of the CEDO from extended use would thus require:

- movement with the CEDO requiring force levels sufficient to exercise the IIb fibers, thereby increasing their strength; and
- larger amplitude tremor resulting from strengthened IIb fibers, i.e. IIb fibers playing a role in tremor movement and, when strengthened, producing higher forces *from the same level of tremorogenic efferent neural activity* (as opposed to just increasing the maximum IIb force level).

If these conditions are not met, prolonged use of the CEDO might actually prove favorable if endurance is increased by exercising type I fibers or if strength is increased (countering disuse atrophy or degeneration) by exercising type II fibers in a manner which does not increase tremor amplitude.

Another issue related to strengthening is the phenomenon of fiber type conversion, i.e. the documented change in the contractile properties of fast-twitch fibers to slow-twitch characteristics in response to sustained electrical stimulation [Edstrom & Grimby 1986] and the apparent change in the proportion of more fatigue-resistant IIa fibers relative to IIb fibers in endurance-training athletes. If there is an advantageous relationship between the latter effect, any specificity of fiber type involvement in tremor, and any specificity of fiber type strengthening by viscous loading, then the possibility exists that the strengthening effects of a tremor-suppressing orthosis would be *favorable* by means of another mechanism. This too must be the focus of extended-use experiments with the CEDO.

5. All stages of experimentation outlined in this section should ideally be accompanied by increasingly detailed tremor modeling. Modeling can help guide not only the planning of future experimental protocol, but also the design of more nearly optimal tremor-suppressing orthoses.

6.2.2 Design Goals for the CEDO 2

As explained in Chapter 2, the CEDO 1 is an experimental prototype, not a commercial product. It was designed to be evaluated by potential users in abstract and functional tasks, and it was intended to be modified in time as design specifications are refined and improved designs are generated. A final outcome of this investigation, then, is the following set of design goals for the CEDO 2:

1. Functional Compatibility -- From observing the CEDO 1 in use, it is evident that a mechanical design change is needed at the point of limb attachment to clear the space between the user's arm and a tabletop. The mounting of brake 3 and the limb coupler in the current design elevate the user's arm about six inches above the linkage and thus prohibit users from

resting their forearms against a desk or table for writing or eating. The most obvious alternative is to suspend the limb coupler and the user's arm *below* the orthosis so that little or no mechanism intrudes between the cuff and the table. Another design change which would perhaps make the CEDO more functionally compatible involves mounting the CEDO base to the front or side of the user rather than from behind, allowing the orthosis to be in a more flexed state at the most frequent endpoint positions and thus mitigating the effects of force-velocity non-colinearity. Before re-mounting the CEDO 1 in another position, however, the designer should make sure that the new position of the linkage will not interfere with objects the user is likely to interact with on a desk or tabletop such as a computer monitor or a glass full of water (!).

2. Damping Capability -- The engineer designing the CEDO 2 must determine how to provide the orthosis with greater damping capability. Options include modifying the current brake driver circuitry, investing in a power supply with a higher output voltage, exploring the use of other brakes, and/or considering the use of transmission elements.

As explained in detail in Chapter 2, the response time of a magnetic particle brake depends upon the magnitude of the voltage which develops across its coil. Although lead compensation techniques were used in the CEDO 1 brake-driver circuitry to compensate for the response times of the CEDO brakes, experience gained in this investigation suggests that the current circuitry is not adequate, particularly if higher non-linear damping simulations are to be achieved. To estimate what the response times of the brakes *need* to be, records of commanded brake torque during maximum linear and non-linear damping trials for subject A (the subject with the most severe tremor) were examined. This data suggest that brake 1 must be capable of providing a 150 lbf-in change in torque (0 to maximum or maximum to 0) in less than 30 ms for greater linear damping or less than 10 ms for greater non-linear damping; brake 2 must be capable of providing a 150 lbf-in change in torque in less than 55 ms for greater linear damping and less than 30 ms for greater non-linear damping; and brake 3 must be capable of providing a 15 lbf-in change in torque in less than 50 ms for greater linear or non-

linear damping capability. Since these response times are *not* orders of magnitude smaller than what the compensated circuitry currently provides, one solution might simply involve purchasing a power supply with a higher supply voltage and re-designing the circuitry accordingly.

A further concern is whether the brakes' torque capabilites are adequate to achieve the damping loads necessary for tremor suppression. The actual torques the brakes must produce depend upon the damping constant and the velocity of the user's tremor. To determine just how close the brakes came to their rated loads during the tracking experiments in this investigation, the commanded brake torques were examined. For subject A, brake 1 reached (or should have surpassed) its rated 150 lbf-in output 2-3 percent of the time during the highest linearly-damped trials and 6-10 percent of the time during the highest non-linearly-damped trials. Brake 2 only reached its rated 150 lbf-in output 1 percent of the time during the highest non-linearly damped trials, and brake 3 did not reach its rated 15 lbf-in output at any time during the trials. The commanded brake torques for the other subjects were generally less than those for subject A. If higher damping simulations are to be achieved, then, it appears that more torque at brake 1 may be needed for at least some individuals.

The best way to generate more torque at brake 1, should it be necessary, remains to be decided. The "direct-drive" configuration of the current CEDO orthosis is advantageous in that it avoids many of the problems associated with more conventional transmissions involving belts (or cables or metal bands) and pulleys, or a gear train. All of these would have introduced backlash, i.e. a dead zone around any operating point, within which undamped movement of the orthosis endpoint when unloaded would have been possible. All of these would also have introduced substantial friction in excess of that contributed by the bearings, adding a finite breakaway force to the load function applied to the user's limb. Belt systems, in particular, would have introduced series compliance considerably greater than that introduced by the linkage transmission and the possibility of slippage or cogging. Furthermore, the tensioning required to minimized these effects would have increased the loads on the joints and

the friction in the bearings, and thus larger bearings would have been required to provide the necessary bearing life.

The disadvantage of having used a direct-drive configuration, however, is that no step up of the brake torques is obtained. Brakes with higher torque ratings could possibly be used in the CEDO 2, but they would have to meet other design criteria which specify acceptable size, weight, reponse time, and cost. Cable transmissions, alternatively, were used successfully by Maxwell to obtain greater output torques in the MED Arm device [Maxwell 1990] and would perhaps be feasible for use in the CEDO 2.

3. Comfort and Ease of Use -- The designer of the CEDO 2 will also need to more carefully consider issues of comfort and ease of use. The location of the coupling between the user and the orthosis, for instance, should not force the user to accept an uncomfortable position when using the orthosis, nor should it require the user to sustain muscular contractions to support his/her arm. From observing participants in this investigation, it is apparent that the CEDO 1 cuff supports the arm at a point sufficiently distal that it requires some users to maintain shoulder activity, particulary the deltoids, to keep their elbow from dropping. Participants in this investigation for whom the coupling posed a problem typically complained that they got tired of maintaining the required force. A future CEDO 2 limb coupler should also take into account the tasks the user wishes to do. While future cuffs must be large and stiff enough to transmit resistive loads to the user comfortably, they must also maximize functionality. Any cuff which covers part of the hand may prohibit its user from gripping certain objects or from writing.

Other ease-of-use issues which warrant attention involve the ways in which the user must interact with the orthosis. While it is unreasonable to expect a tremor-disabled individual who needs an orthosis to place his or her limb in the limb coupler of the device without the assistance of another person, the CEDO 2 *can be designed* to make the transition from unaided to orthosis-aided more or less simple. If the limb cuff does not need to be held open manually to receive the user's limb, for example, an assisting attendent could devote all of his/her efforts

to stabilizing the user's arm. Finally, because a commercial version of the CEDO will probably make available to the user a control for adjusting the damping constant, the nature and placement of such an interface, taking into account the disabilites of the users, should be considered.

5. Marketing -- Although not a "design goal", a professional approach to market research should be pursued in parallel with the technical design and evaluation of the CEDO 2 to firmly establish the demand for tremor-suppressing orthoses, to test the likelihood of third-party reimbursement, to decide how best to make tradeoffs between competing product features, and to determine how the answers to these questions vary among identifiable market segments. This will need to be an ongoing process as new approaches to financing assistive technology are put in place, as new entitlement and civil rights legislation is written, and as consumers with disabilities continue to make themselves heard in the marketplace.

References

Adelstein, B. *Peripheral Mechanical Loading and the Mechanism of Abnormal Intention Tremor*. M.S. Thesis, Department of Mechanical Engineering, MIT, July 1981.

Adelstein, B., Rosen, M., and Aisen, M. Differential diagnosis of pathological tremors according to mechanical load response. *Proceedings from the RESNA 10th Annual Conference*, San Jose, CA, 1987, pp. 829-831.

Adelstein, B. *A Virtual Environment System for the Study of Human Arm Tremor*. Ph.D. Thesis, Department of Mechanical Engineering, MIT, June 1989.

Aisen M., et al. Glutethimide treatment of disabling action tremor in patients with multiple sclerosis and traumatic brain injury. *Archives of Neurology* 49:513-515, 1991.

Baiges, I. *The Development of a Whole Arm Orthosis for Abnormal Intention Tremor Suppression*. M.S. Thesis, Department of Mechanical Engineering, MIT, August 1989.

Baiges, I. and Rosen, M. Development of a whole-arm orthosis for tremor suppression. *Proceedings from the RESNA 12th Annual Conference*, New Orleans, LA, 1989, pp. 290-291.

Basmajian and DeLuca. *Muscles Alive*. Baltimore: Williams and Wilkins, 1979.

Beckwith, Buck, and Marangoni. *Mechanical Measurements*, 3rd edition. Reading, MA: Addison-Wesley, 1982.

Bendat, J. and Piersol, A. *Engineering Applications of Correlation and Spectral Analysis*. New York: John Wiley & Sons, 1980.

Bendat, J. and Piersol, A. *Random Data: Analysis and Measurement Procedures*, 2nd edition. New York: John Wiley & Sons, 1987.

Beringhause, S. *Viscously Damped Joystick for Proportional Control by Tremor Patients*. M.S. Thesis, Department of Mechanical Engineering, MIT, June 1988.

Beringhause, S., Rosen, M., and Huang, S. Evaluation of a damped joystick for people disabled by intention tremor. *Proceedings from the RESNA 12th Annual Conference*, New Orleans, LA, 1989, pp. 41-42.

Biological Signal and Image Processing. Class notes from MIT course number 6.555J/HST582/16.356J--Biological Signal and Image Processing, Department of Electrical Engineering & Computer Science and the Harvard-MIT Heath Sciences and Technology Program, Spring 1991.

Binder, M. Properties of Motor Units, in *Textbook of Physiology: Excitable Cells and Neurophysiology*, 21st edition. Patton, H. et al, eds. Philadelphia: W.B. Saunders Company, 1989, pp. 1-18.

Bishop, G., Clare, M., and Price, J. Patterns of tremor in normal and pathological conditions. *Journal of Applied Physiology*, 1:123-147, 1948.

Brongo, D. *Design of Patient Interface and Assessment Manager for Computer-Based Tremor Characterization System.* M.S. Thesis, Department of Mechanical Engineering, MIT, August 1990.

Brongo, D. and Rosen, M. Design of the patient interface for a computer-based tremor characterization system. *Proceedings from the RESNA 14th Annual Conference*, Kansas City, MO, 1991.

Brumlik, J. and Yap, C. *Normal Tremor: A Comparative Study.* Springfield, IL: Charles C. Thomas, 1970, pp. 3-15.

Burne, J. Reflex origin of Parkinsonian tremor. *Experimental Neurology*, 97:327-339, 1987.

Calzetti, S., et al. Frequency/amplitude characteristics of postural tremor of the hands in a population of patients with bilateral essential tremor: Implications for the classification and mechanism of essential tremor. *Journal of Neurology, Neurosurgery, and Psychiatry*, 50:561-567, 1987.

Chen, A. *Analysis of the Rehabilitation of Tremor Patients.* M.S. Thesis, Sloan School of Management, MIT, May 1991.

Cook, N. *Mechanics and Materials for Design.* New York: McGraw-Hill, 1984.

Corcoran, P. Neuromuscular Disease, in *Handbook of Severe Disability*, Stolov and Clowers, eds. U.S. Dept. of Education, Rehabilitation Services Administration, 1981, pp. 83-100.

Corell, R. and Wijnschenk, M. *Design and Development of the Case Research Arm Aid*, Report number EDC 4-64-4. Case Institute of Technology and Highland View Hospital, 1964.

Dunfee, D. *Suppression of Intention Tremor by Mechanical Loading.* M.S. Thesis, Mechanical Engineering Department, MIT, February 1979.

Easton, J., and Halpern, D. Cerebral Palsy, in *Handbook of Severe Disability*, Stolov and Clowers, eds. U.S. Dept. of Education, Rehabilitation Services Administration, 1981, pp. 137-154.

Edstrom, L. Selective changes in the sizes of red and white muscle fibers in upper motor lesions and Parkinsonism. *Journal of the Neurological Sciences*, 11:537-550, 1970.

Edstrom, L., and Grimby, L. Effect of exercise on the motor unit. *Muscle and Nerve*, 9:104-126, 1986.

Edwards, R. Human muscle function and fatigue, in *Human Muscle Fatigue: Physiological Mechanisms*, Ciba Foundation Symposium '82. London: Pitman Medical, 1981.

Elble, R. and Randall, J. Motor unit activitiy responsible for the 8 to 12 Hz component of human physiological finger tremor. *Journal of Neurophysiology*, 39:370-383, 1976.

Elble, R. Physiology and essential tremor. *Neurology*, 36:225-231, 1986.

Elble, R., Higgins, C., and Moody, C. Stretch reflex oscillations and essential tremor. *Journal of Neurology, Neurosurgery, and Psychiatry*, 50:691-698, 1987.

Elble, R. and Koller, W. *Tremor.* Baltimore: The Johns Hopkins University Press, 1990.

Elble, R., Sinha, R., and Higgins, C. Quantification of tremor with a digitizing tablet. *Journal of Neuroscience Methods*, 32:193-198, 1990.

Elek, J. and Prochazka, A. Attenuation of human wrist tremor with closed-loop electrical stimulation of muscles. *Journal of Physiology*, 414:17P, 1989.

Fahn, S. Pharmacological differentiation of tremor; in *Movement Disorders: Tremor.* L.J. Findley and R. Capildeo, eds. New York: Oxford University Press, 1984.

Fahn, S. Cerebellar tremor: Clinical aspects; in *Movement Disorders: Tremor.* L.J. Findley and R. Capildeo, eds. New York: Oxford University Press, 1984.

Fahn, S., et. al. Clinical rating scale for tremor; in *Parkinson's Disease and Movement Disorders.* J. Jankovic and E. Tolosa, eds. Baltimore: Urban and Schwarzenberg, 1988.

Findley, L. The pharmacology of essential tremor; in *Movement Disorders 2*, C.D. Marsden and S. Fahn, eds. London: Butterworth & Co., 1987.

Findley, L. Tremors: differential diagnosis and pharmacology; in *Parkinson's Disease and Movement Disorders*, J. Jankovic and E. Tolosa, eds. Baltimore: Urban & Schwarzenberg, 1988.

Findley, L. and Capildeo, R. Classification of tremor; in *Movement Disorders: Tremor*, L.J. Findley and R. Capildeo, eds. New York: Oxford University Press, 1984.

Flament, D. and Hore, J. Comparison of cerebellar intention tremor under isotonic and isometric conditions. *Brain Research*, 439:179-186, 1988.

Fornoff, H. and Thornton, W. Experimental evaluation of remote manipulator systems. *Remotely Manned Systems: Exploration and Operation in Space; Proceedings of the First National Conference*, California Institute of Technology, Pasadena, CA, 1973.

Fox, J. and Randall, J. Relationship between forearm tremor and the biceps electromyogram. *Journal of Applied Physiology*, 29(1):103-108, 1970.

Frost, J. Triaxial vector accelerometry: A method for quantifying tremor and ataxia. *IEEE Transactions on Biomedical Engineering*, BME-25:17-27, 1978.

Fukumoto, I. Computer simulation of Parkinsonian tremor. *Journal of Biomedical Engineering*, 8(1):49-55, 1986.

Furr P, et al. Use of quantitative electromyography (EMG) in the evaluation of fatigue associated with pressure glove work. In: SAE Technical Paper Series 891473, *19th Intersociety Conference on Environmental Systems*, 1989.

Gottlieb, S. and Lippold, O. The 4-6 Hz tremor during sustained contraction in normal human subjects. *Journal of Physiology*, 336:499-509, 1983.

Gresty, M. and Buckwell, D. Spectral analysis of tremor: understanding the results. *Journal of Neurology, Neurosurgery, and Psychiatry*, 53:976-981, 1990.

Gunderson, C. *Quick Reference to Clinical Neurology*. Philadelphia: J. B. Lippincott Company, 1982.

Hainaut, K., et al. Differential effects on slow and fast motor units of different programs of brief daily muscle training in man, in *Motor Unit Types, Recruitment and Plasticity in Health and Disease, Progress in Clinical Neurophysiology,* Volume 9. Desmedt, ed. Basel: Karger, 1981, pp. 241-249.

Hendriks, J., Rosen, M., Berube, N., and Aisen, M. A second-generation joystick for people disabled by tremor. *Proceedings from the RESNA 14th Annual Conference*, Kansas City, MO, June 1991.

Hewer, R., Cooper, R., and Morgan, M. An investigation into the value of treating intention tremor by weighting the affected limb. *Brain*, 95:579-590, 1972.

Hogan, et al. Controlling multijoint behavior. In: *Exercise & Sport Science Reviews*, American College of Sports Medicine Series Volume 15, K.B Pandolf, ed. MacMillan Publishing Co., 1987.

Homberg, V., et al. Differential effects of changes in mechanical limb properties on physiological and pathological tremor. *Journal of Neurology, Neurosurgery, and Psychiatry*, 50:568-579, 1987.

Jaeco, Orthopedic Specialities, Hot springs, AR. Jaeco Arm Positioner. Product literature.

Jankovic, J. and Fahn, S. Physiologic and pathologic tremors. *Annals of Internal Medicine*, 93:460-465, 1980.

Joffroy, A. and Lammare, Y. Rhythmic unit firing in the precentral cortex in relation with postural tremor in a deafferented limb. *Brain Research*, 27:386-389, 1971.

Joyce, G. and Rack, P. The effects of load and force on tremor at the normal human elbow joint. *Journal of Physiology*, 240:375-396, 1974.

Karchak, A., Jr. and Allen, J. *Investigation of Externally Powered Orthotic Devices*, Final Project Report V.R.A. Grant Rd-1461-m-67. Attending Staff Association of the Rancho Los Amigos Hospital, Inc., Downey, CA, 1968.

Kazerooni, H. Human/robot interaction via the transfer of power and information signals, part I: dynamics and control analysis. *Proceedings from the IEEE International Conference on Robotics and Automation*, Scottsdale, AZ, May 1989.

Klausen, K. Strength and weight-training, in *Physiology of Sports*, Reilly et al, eds. London: E. & F.N. Spon, 1990, pp. 41-67.

Lee, R. The pathophysiology of essential tremor; in *Movement Disorders 2*, C.D. Marsden and S. Fahn, eds. London: Butterworths, 1987.

Legg, N. Treatment of cerebellar tremor; in *Movement Disorders: Tremor*, L.J. Findley and R. Capildeo, eds. New York: Oxford University Press, 1984.

Lenman, A., et al. Muscle fatigue in some neurological disorders. *Muscle and Nerve*, 12:938-942, 1989.

Lippold, O. Oscillation in the stretch reflex arc and the origin of the rhythmical 8-12 Hz component of physiological tremor. *Journal of Physiology*, 206:359-382, 1970.

Lippold, O. Physiological tremor. *Scientific American*, 224(3):65-73, 1971.

Lohnberg, P. Linear modeling of possible mechanisms for Parkinson tremor generation. *Annels of Biomedical Engneering,* 6(4):531-543, 1978.

Marsden, C., et al. The role of the ballistocardiac impulse in the genesis of physiological tremor. *Brain*, 92:647-662, 1969.

Maxwell, S. *A Modulated-Energy-Dissipation Manipulator and Application to Suppressing Human Arm Tremor.* Ph.D. Thesis, Department of Mechanical Engineering, MIT, June 1990.

Merletti, R. and DeLuca, C. New techniques in surface electromyography. In: *Computer-Aided Electromyography and Expert Systems*, Desmedt, J. ed. Elsevier Science Publishers B.V., 1989:115-124.

Michaelis, J. Introducting the Neater-Eater, Graham Jones, reporter. *Action Research: The Magazine of the National Fund for Research into Crippling Diseases,* 6(1):Spring 1988.

Morrice, B., et al. Viscous loading improves manual tracking accuracy in humans with cerebellar incoordination. *Abstracts--Society for Neuroscience 17th Annual Meeting* 13(3):1700, 1987.

Nickel, V. *Investigation of Externally Powered Orthotic Devices*, Final Project Report V.R.A. Grant RD-518. Attending Staff Association of the Rancho Los Amigos Hospital, Inc., Downey, CA, 1964.

Ogata, K. *Modern Control Engineering*. Englewood Cliffs, NJ: Prentice-Hall, 1970.

Oppenheim, A., and Schafer, R. *Discrete-Time Signal Processing*. Englewood Cliffs, NJ: Prentice-Hall, 1989.

Potvin, et al. Validity of quantitative tests measuring tremor. *American Journal of Physical Medicine* , 54(5):243-252, 1975.

Press, W. et al. *Numerical Recipes in C: The Art of Scientific Computing*. Cambridge: Cambridge University Press, 1988.

Randall, J. and Stiles, R. Power spectral analysis of finger acceleration tremor. *Journal of Applied Physiology*, 19:357-360, 1964.

Reswick J. A rigid lightweight structure for a damped orthosis. Technical support package, Southwest Researach Institute Biomedical Applications Program problem RNV-40; 1976.

Rietz, R. and Stiles, R. A viscoelastic-mass mechanism as a basis for normal postural tremor. *Journal of Applied Physiology*, 37:852-860, 1974.

Rice, J. *Mathematical Statistics and Data Analysis*. Belmont, CA: Wadsworth, Inc., 1988.

Robson, J. The effect of loading upon the frequency of muscle tremor. *Journal of Physiology*, 149:29P-30P, 1959.

Rondot, P., Jedynack, C., and Ferrey, G. Pathological tremors: nosological correlates; in *Physiological Tremor, Pathological Tremor and Clonus,* J.E. Desmedt, ed. *Prog. Clin. Neurophysiol.*, 5:95-113, Karger, Basel 1978.

Rosen, M., Gesink, J., and Rowell, D. Suppression of intention tremor by application of viscous damping. *Proceedings from the 4th Annual New England Bioengineering Conference*, pp. 391-394, 1976.

Rosen, M., Sloan, M., and Biber, C. A damped joystick: adaptive control for the tremor-disabled. *Proceedings from the 2nd Interagency Conference on Rehabilitation Engineering*, Atlanta, GA, August 1979.

Rosen, M. and Biber, C. Attenuation of abnormal intention tremor following viscous exercise: work in progress. *Proceedings from the International Conference on Rehabilitation Engineering*, pp. 202-203, 1980.

Rosen, M. and Adelstein, B. The effect of mechanical impedance on abnormal intention tremor. *Proceedings from the 9th Annual Northeast Bioengineering Conference.* Elmsford, NY: Pergamon Press, Inc., March 1981.

Rosen, M. et al. A controlled-energy-dissipation orthosis for functional suppression of intention tremors. Submitted to the *Journal of Rehabilitation Research and Development*, April 1992.

Sabra, A. and Hallett, M. Action tremor with alternating activity in antagonist muscles. *Neurology,* 34:151-156, 1984.

Salisachs, P. and Findley, L. Problems in the differential diagnosis of essential tremor; in *Movement Disorders: Tremor*, L.J. Findley and R. Capildeo, eds. New York: Oxford University Press, 1984.

Saltin, B. Muscle fiber recruitment and metabolism in prolonged exhaustive dynamic exercise, in *Human Muscle Fatigue: Physiological Mechanisms*, Ciba Foundation Symposium '82. London: Pitman Medical, 1981, pp. 41-58.

Sanes, J., LeWitt, P., and Mauritz, K. Visual and mechanical control of postural and kinetic tremor in cerebellar system disorders. *Journal of Neurology, Neurosurgery, and Psychiatry*, 51:934-943, 1988.

Scheinberg, L., and Holland, N. eds. *Multiple Sclerosis: A Guide for Patients and Their Families*, 2nd edition. New York: Raven Press, 1987.

Shahani, B. and Young, R. Action tremors: a clinical neurophysiological review; in *Physiological Tremor, Pathological Tremor and Clonus,* J.E. Desmedt, ed. *Prog. Clin. Neurophysiol.*, 5:95-113, Karger, Basel 1978.

Shahani, B., and Wierzbicka, M. Assessment of motor control in normal subjects and patients with movement disorders, in *Movement Disorders*, Chokroverty, ed. PMA Publishing Corp., 1990, pp. 87-111.

Sheridan, T. and Ferrel, W. *Man-Machine Systems*. Cambridge: The MIT Press, 1974.

Stein, R. and Oguztoreli, M. Tremor and other oscillations in neuromuscular systems. *Biological Cybernetics*, 22:147-157, 1976.

Stein, R. and Oguztoreli, M. Reflex involvement in the generation and control of tremor and clonus; in *Physiological Tremor, Pathological Tremor and Clonus,* J.E. Desmedt, ed. *Prog. Clin. Neurophysiology*, 5: Kargel, Basel, 1978.

Stiles, R. and Randall, J. Mechanical factors in human tremor frequency. *Journal of Applied Physiology*, 23:324-330, 1967.

Stiles, R. Mechanical and neural feedback factors in postural hand tremor of normal subjects. *Journal of Neurophysiology*, 44:40-59, 1980.

U.S. Department of Health, Education, and Welfare. *Multiple Sclerosis: Hope Through Research.* Pamphlet printed by the Public Health Service, National Institutes of Health.

Vander, A., et al. *Human Physiology: The Mechanisms of Body Function*, 4th edition. New York: McGraw Hill Company, 1985.

Van Cott, H. and Kinkade, R, eds. *Human Engineering Guide to Equipment Design.* Washington DC: Superintendent of Documents, U.S. Government Printing Office, 1972.

Vilis, T. and Hore, J. Effects of changes in mechanical state of limb on cerebellar intention tremor. *Journal of Neurophysiology*, 40(5):1214-1224, 1977.

Vykukal, H., King, R., and Vallotton, W. An anthropomorphic master-slave manipulator system. *Remotely Manned Systems: Exploration and Operation in Space; Proceedings of the First National Conference*, California Institute of Technology, Pasadena, CA, 1973.

Westerblad, H., et al. Cellular mechanisms of fatigue in skeletal muscle. *American Journal of Physiology*, 261(2):195-209, 1991.

Will, A. et al. Quantitative analysis of tremor and chorea using the VPL Data Glove. Program and Abstracts, Fourth Annual Symposium, PSG/MDS. *Annals of Neurology,* 28(2):299, 1990

Williams, C. Metabolic aspects of exercise, in *Physiology of Sports*, Reilly et al, eds. London: E. & F.N. Spon, 1990, pp. 1-40.

Wong, J. *Development of Equipment for the Study and Management of Pathological Tremor.* S.B. Thesis, Department of Mechanical Engineering, MIT, June 1990.

Young, R. and Hagbarth, K. Physiological tremor enhanced by manoeuvres affecting the segmental stretch reflex. *Journal of Neurology, Neurosurgery, and Psychiatry*, 43:248-256, 1980.

Zahalak, G. and Cannon, S. Predictions of the existence, frequency, and amplitude of physiological tremor in normal man based on measured frequency-response characteristics. *Journal of Biomechanical Engineering,* 105:249-257, 1983.

Appendix A

Neurological Disorders Which Cause Tremor

Pathological tremor is a symptom of neurological disorders or trauma affecting the cerebellum, basal ganglia, spinal cord, or other parts of the central (CNS) and peripheral (PNS) nervous systems. Definitions of clinical terms related to tremor and a summary of the most common disorders associated with tremor are provided below.

Definitions

akinesia:	immobility
ataxia:	involuntary oscillation of the limbs, head, trunk, or other part of the body characterized by irregularity in both speed and amplitude; usually the result of cerebellar lesions, but may occur with proprioceptive loss or mild weakness
athetosis:	constant writhing movements in which the distal extremities alternate between supination and pronation
chorea:	small, jerky, involuntary movements which are usually present at rest and which are amplified when holding a tonic posture
clonus:	simple rhythmic oscillation of a joint in response to stretch; characteristic of upper motor neuron lesions
dystonia:	large amplitude writhing movements similar to athetosis but involving proximal joints and axial musculature
hyperkinesia:	constant movement
myotonia:	an abnormality of muscle in which muscle fibers contract but fail to relax as promptly as they should when carrying out a forceful voluntary act
rigidity:	steady resistance which cannot be inhibited; characteristic of basal ganglia lesions
spasticity:	a centrally-mediated abnormality of the lengthening response elicited by a passive stretch; consists of the reflex shortening of a stretched muscle and usually diminishes with continued pressure
tremor:	an involuntary rhythmic oscillation of the limbs, head, trunk, or other part of the body superimposed on purposeful movement

Demyelinating Disorders

Multiple Sclerosis (MS):

MS is a disease of unknown cause in which myelin, the fatty sheath that insulates nerves, is destructed in an erratic and seemingly random fashion. At "multiple" sites throughout the CNS, "sclerosed" or scar tissue forms in place of the myelin and weakens, slows, or blocks the electrical signals from the brain. MS does not attack the PNS. Depending upon which sites in the brain and spinal cord are affected, sensory and/or motor functions of the body may be impaired and different symptoms may last for different amounts of time. Symptom type and severity are determined by the extent of myelin damage and by the function ordinarily performed by the affected nerves. Common symptoms of MS include optic neuritis, a disorder of the optic nerve which produces "blind spots" in the center of vision and which causes blurriness or transient blindness; impaired coordination; weakness; intention tremor, caused by widespread lesions of the cerebellum and brainstem; spasticity; bladder and bowel problems; and sexual impotence. Individuals are typically between the ages of 20 and 40 years old when diagnosed with MS and can expect to live their normal life span. They are usually spared any mental disability. To date, no treatment has proven effective in stopping MS and patients are given drugs which combat the symptoms rather than the cause [US Dept. of Health, Education, and Welfare].

Guillain-Barre Syndrome:

Guillain-Barre syndrome is a disease in which segments of the myelin sheath of PNS axons are progressively destroyed, slowing the conduction of nerve impulses to the limbs. Common symptoms of Guillain-Barre syndrome include facial and respiratory muscle paralysis and intention tremor. Motor deficits are usually uniform and symmetrical. There is rarely any sensory loss or cerebral damage. Although the exact cause of the disease is unknown, about two-thirds of those inflicted with the disease report a history of a preceding infection of the upper respiratory or gastrointestinal tracts. Other experimental evidence exists supporting a

link between the disease and allergic or autoimmune factors. Approximately 85 percent of those with Guillain-Barre syndrome recover from the disease with no neurological residuals in which the myelin sheaths slowly regenerate and full muscle strength returns after many months. In the remaining 15 percent inflicted with the disease, however, the affected axons degenerate and muscle function is permanently lost [Gunderson 1982].

Basal Ganglion Disorders

Parkinson's Disease:

Parkinson's disease is a progressive disorder which typically affects older adults between the ages of 50 and 70 years. Pathological findings in advanced cases include extensive degenerative changes in the basal ganglia (nuclear masses buried within the cerebral hemispheres), cerebral cortex, and brain stem. Physical symptoms of the disease include muscle rigidity, difficulty initiating movements, and a characteristic 3 to 4 Hz tremor in the hands and fingers which occurs during rest, intensifies with emotion or anxiety, and can be suppressed for several seconds with voluntary effort. Individuals with Parkinson's disease have difficulty performing more than one physical task at a time. Muscle stiffness causes fatigue after minor exertion, and the acts of communicating, chewing, and swallowing are slow and tedious. Individuals with Parkinson's disease may also suffer from mental deterioration, confusion, decreased drive, or impaired judgement. Although the precise cause of the disease is unknown, experimental evidence of a deficiency in the neurotransmitter dopamine in affected areas of the brain has led to the successful use of the drugs levodopa and carbidopa in treating the disease. Regulating the dosage of these drugs to achieve the optimum therapeutic effect sometimes takes months, however, and side effects such as nausea, loss of appetite, and postural hypotension are common. Although Parkinson's disease is not considered fatal in the direct sense, it is associated with a shortened life expectancy if not treated [Corcoran 1981, Gunderson 1982].

Huntington's Chorea:

Huntington's chorea is an inherited progressive disease with an onset age of 30 to 50 years characterized by choreoathetotic movements and mental deterioration. The main symptoms of the disease include jerky involuntary movements of the trunk, limbs, head, and/or face which are increased in intensity by emotional stress or physical tasks, progressive loss of memory, loss of intellectual functioning, and impulsive behavior. Pathologically, individuals with Huntington's chorea exhibit a diffuse loss of neurons in the basal ganglion and cortex. Death seldom results from the disease directly, but is more commonly caused by injuries, infections, suicide, or other results of mental deterioration. There is no known treatment to date that halts or slows the steady progression of the disease [Corcoran 1981, Gunderson 1982].

Cerebral Palsy (CP):

The term cerebral palsy refers not to a specific disease but rather to a collection of movement disorders resulting from damage to the brain during its growth or development. Most cases of CP are acquired, either congenitally or postnatally, although a few show evidence of being hereditary. Since areas within the brain in addition to the motor areas may be involved, the diagnosis of CP does not have the precision or accuracy of most other medical diseases. The manifestations of CP depend upon the location and severity of the brain damage, and the motor problem is typically lack of control of the muscles rather than muscle weakness. Children with CP may exhibit athetosis, ataxia, chorea, dystonia, tremor, rigidity or some combination of these movement disorders. Motor and sensory defects of children with cerebral palsy are generally stable but may be complicated by mental defects, visual or auditory impairment, or epilepsy [Easton & Halpern 1981, Gunderson 1982].

Spinocerebellar Degenerative Disorders

The spinocerebellar degenerative disorders are a family of hereditary diseases which affect, to varying degrees, the cerebellum, the brain stem, and the long tracts of the spinal cord. The cause(s) of these disorders is unknown. Symptoms usually include unsteady gait, clumsiness of the hands, thick slurred speech, weakness and easy fatigability of the limbs, and occasionally an intention tremor of the head or limbs. Vision and hearing are unaffected. The disorders progress at variable rates, and, to date, no known medical or surgical treatment has proven effective in slowing the degenerative processes.

Friedreich's Ataxia:

Friedreich's ataxia is a hereditary disease of unknown cause which manifests during childhood or adolescence. Pathologically, the dorsal roots of the spinal cord (where sensory afferent signals travel to the brain from the periphery) and the spinocerebellar track steadily degenerate, leaving many patients severely incapacitated by the time they reach their middle twenties. The first signs of the disease are clumsiness and incoordination. As muscles atrophy and fatigue more rapidly, ambulation becomes progressively unsafe and laborious, speech becomes thick and slurred, swallowing becomes difficult, and respiration becomes irregular. Medical or surgical treatments which effectively alter the course of the disease have not yet been found [Corcoran 1981, Gunderson 1982].

Olivopontocerebellar Atrophy (OPC):

OPC, including Shy-Drager syndrome, is a group of slowly progressive disorders characterized by atrophy and cell loss in the pons, inferior olives, and cerebellar hemispheres of the brain. Lesser degrees of degeneration are widespread in the basal ganglia and other parts of the CNS. The symptoms of OPC, which appear in middle age, include ataxia and a gross intention tremor which is regular in rhythm and amplitude [Gunderson 1982].

Other Disorders Which Cause Tremor

Essential Tremor (ET):

ET is a diagnostic label applied to a ubiquitous group of movement disorders which share the common feature of postural tremor. Diagnosis is supported by the absence of other neurological signs. Typically ET presents as a distal postural tremor of the upper limbs with a frequency which is slower than physiological tremor and faster than Parkinsonian tremor, usually between 5 and 8 Hz. It is absent at rest but may reappear at the end of goal-directed movements. Though more common among older age groups, ET can commence at any age and can affect any body part. The disorder is exacerbated by such factors as stress, anxiety, and fatigue, and in some patients, is suppressed by alcohol. Approximately 30 percent of patients with ET report a family history of ET symptoms. To date, the cause and pathogenesis of the disorder remains unknown [Lee 1987, Findley 1988].

Drug-Induced Tremors:

Most modern drugs that act centrally on the nervous system such as phenothiazines, reserpine, tetrabenazine, tricyclic antidepressants, indole derivatives, and anticonvulsants can produce tremor as a side effect. Drug-induced tremors are typically postural in nature and cause varying degrees of disability [Findley 1988].

Central Nervous System Trauma:

Trauma to the head and neck caused by automobile accidents, falls, fights, and falling objects is one of the most common sources of CNS lesions and is thus one of the most common causes of movement disorders including intention tremor. Symptoms and treatment vary widely depending upon the nature and extent of the lesion [Gunderson 1982].

Appendix B
CEDO 1 Circuitry Schematics

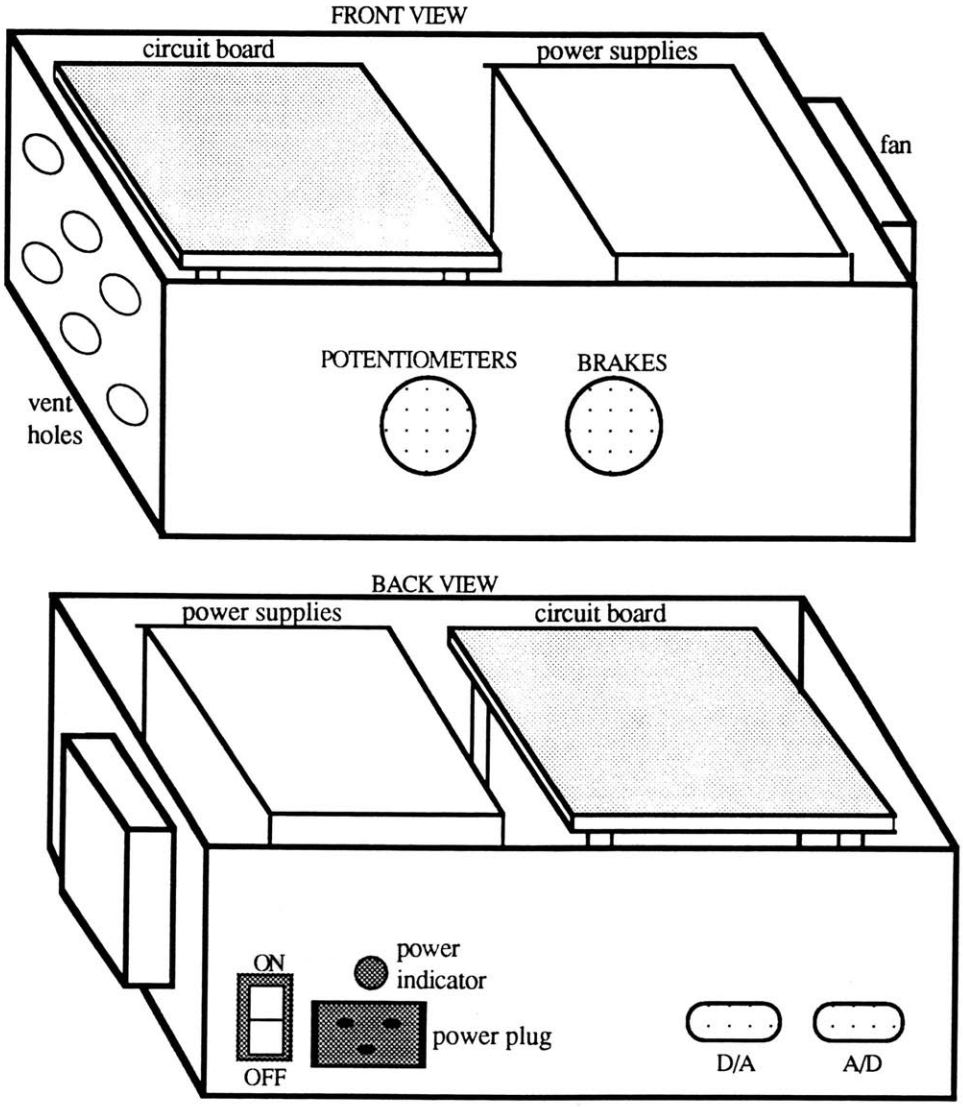

Figure B-1. Layout of the CEDO 1 electronics box.

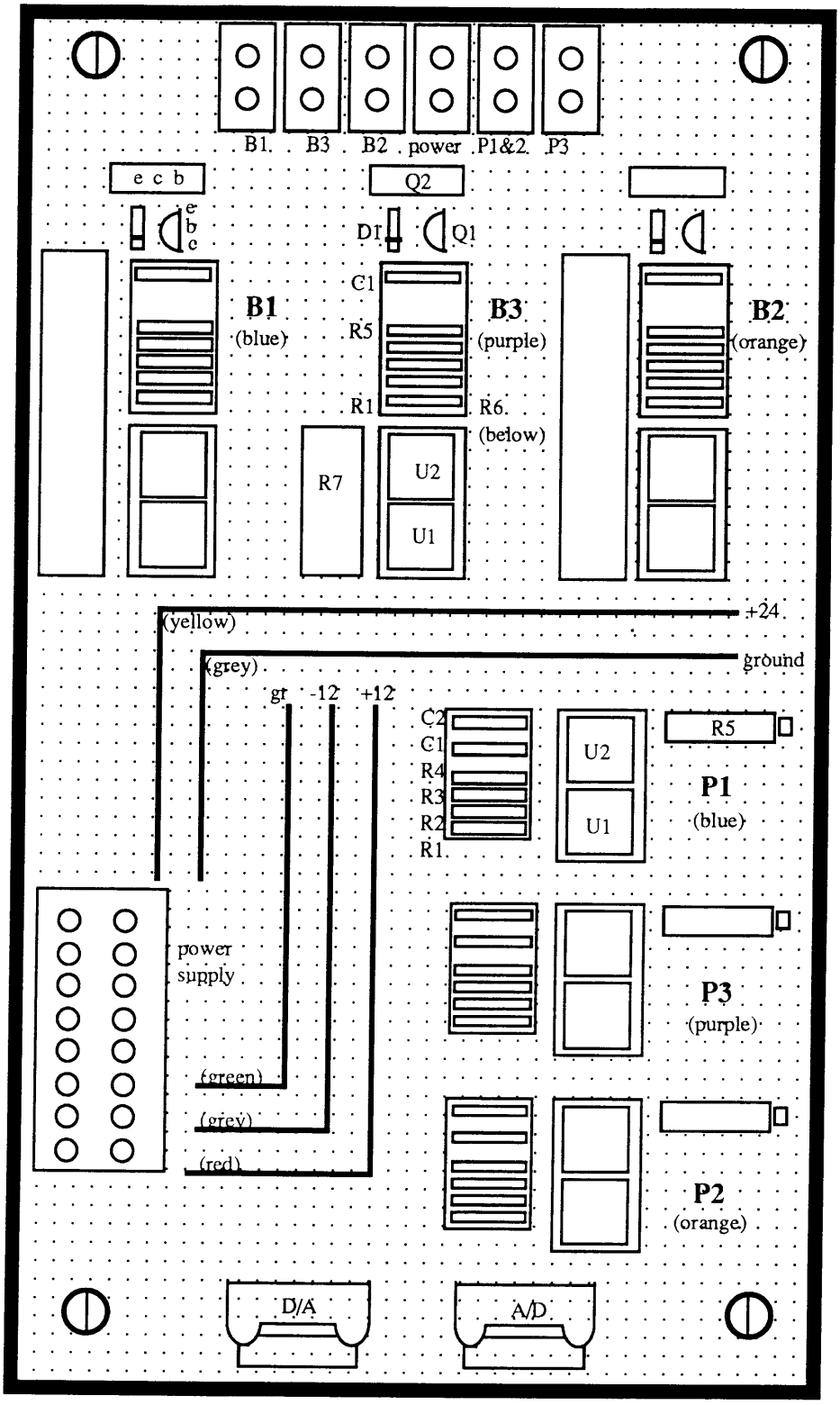

Figure B-2. Layout of the CEDO 1 circuitry.

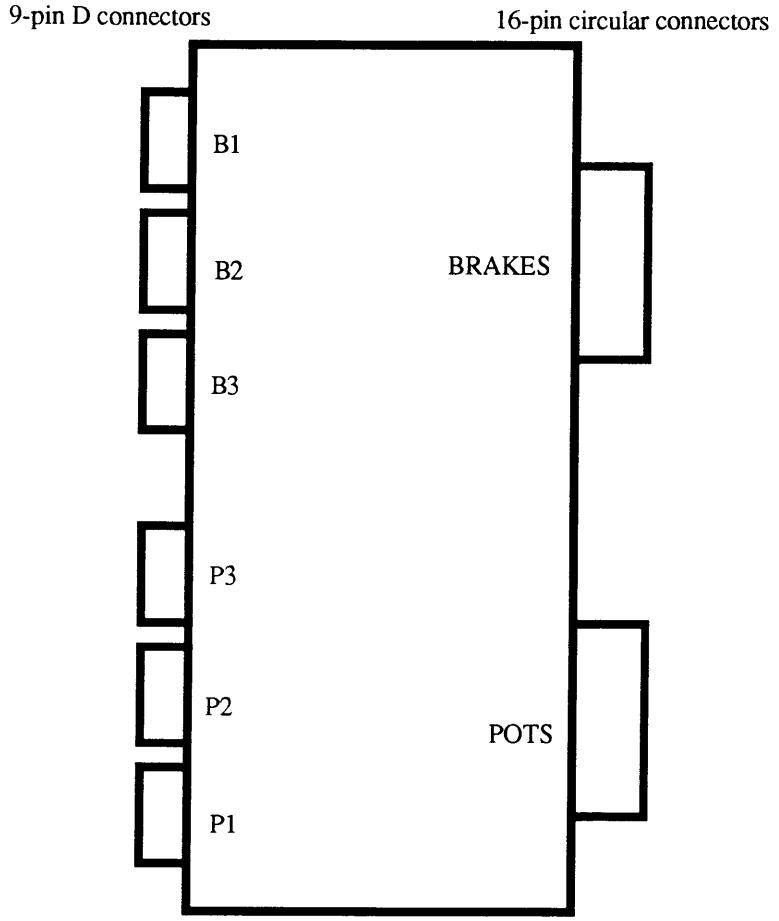

Figure B-3. Schematic of connectors to brakes and potentiometers.

Table B-1. Pinouts for connectors to brakes and potentiometers.

D connector	*Circular connector*	*Function*
B2--pin 8 (black)	brakes--pin 10 (black)	to brake 2 circuit (orange)
B2--pin 9 (red)	brakes--pin 9 (purple)	to +24 V (yellow)
B1--pin 8 (black)	brakes--pin 12 (blue)	to brake 1 circuit (blue)
B1-pin 9 (red)	brakes--pin 11 (yellow)	to +24 V (yellow)
B3--pin 8 (black)	brakes--pin 8 (white)	to brake 3 circuit (purple)
B3--pin 9 (red)	brakes--pin 7 (green)	to +24 V (yellow)
P1--pin1 (black)	pots--pin 6 (green)	pot 1output signal (blue)
P2--pin 1 (black)	pots--pin 5 (yellow)	pot 2 output signal (orange)
P3--pin 1 (black)	pots--pin 4 (blue)	pot 3 output signal (purple)
P1--pin 2 (red)	pots--pin 7 (red)	to +12 V (green)
P1--pin 3 (white)	pots--pin 8 (brown)	to -12 V (red)
P 2, 3--pin 2 (red)	pots--pin 7 (red)	to +12 V (red)
P 2, 3--pin 3 (white)	pots--pin 8 (brown)	to -12 V (green)

DT2814 A/D Converter to Position/Velocity Circuits:

- Base Address: 220 Hex
- Input to A/D converter: ±5 volts
- Output from A/D converter: 0-4095 LSBs
- 20 pin A/D connector is numbered all odds on arrow side, all evens on other (so that the ribbon cable is numbered sequentially)
- All unused input channels are connected to analog ground at the 25-pin male connector

Table B-2. Pinouts for the DT2814 A/D converter to position/velocity circuits.

20 pin (A/D)	*25 pin D-type*	*9 pin D-type*	*10 pin socket*	*FUNCTION*
pin 1 (brown)	pin 1	pin 1 (red)	pin 5	pos 1 (channel 0)
pin 2 (red)	pin 2			unused
pin 3 (orange)	pin 3	pin 2 (yellow)	pin 4	vel 1 (channel 1)
pin 4 (yellow)	pin 4			unused
pin 5 (green)	pin 5	pin 3 (blue)	pin 3	pos 2 (channel 2)
pin 6 (blue)	pin 6			unused
pin 7 (purple)	pin 7	pin 4 (grey-white)	pin 2	vel 2 (channel 3)
pin 8 (grey)	pin 8			unused
pin 9 (white)	pin 9	pin 5 (black)	pin 1	pos 3 (channel 4)
pin 10 (black)	pin 10			unused
pin 11 (brown)	pin 11	pin 6 (orange)	pin 7	vel 3 (channel 5)
pin 12 (red)	pin 12			unused
pin 13 (orange)	pin 13			unused
pin 14 (yellow)	pin 14			unused
pin 15 (green)	pin 15			unused
pin 16 (blue)	pin 16			unused
pin 18 (grey)	pin 18	pin 7 (green)	pin 8	Analog Ground

MetraByte DDA-06 D/A Converter to Brake Driver Circuits:

- Base Address: 300 Hex
- Input to D/A converter: 0-4095 LSBs
- Output from D/A converter: 0-5 volts

Table B-3. Pinouts for the DDA-06 D/A converter to brake driver circuits.

37 pin (D/A)	*9 pin D-type*	*10 pin socket*	*FUNCTION*
pin 18	pin 1 (red)	pin 5	brake 1 (channel 0)
pin 16	pin 2 (yellow)	pin 4	brake 2 (channel 1)
pin 14	pin 3 (blue)	pin 3	brake 3 (channel 2)
pin 15	pin 9 (white)	pin 10	Signal Ground

MetraByte DAS-08 A/D Converter and Timer Board:

- Base Address: 330 Hex
- Used only for timing--The clock 2 output (pin 6) is cascaded to the clock 1 input (pin 4) and the clock 1 output (pin 5) is connected to the interrupt pin (pin 24) on the 37 pin connector.

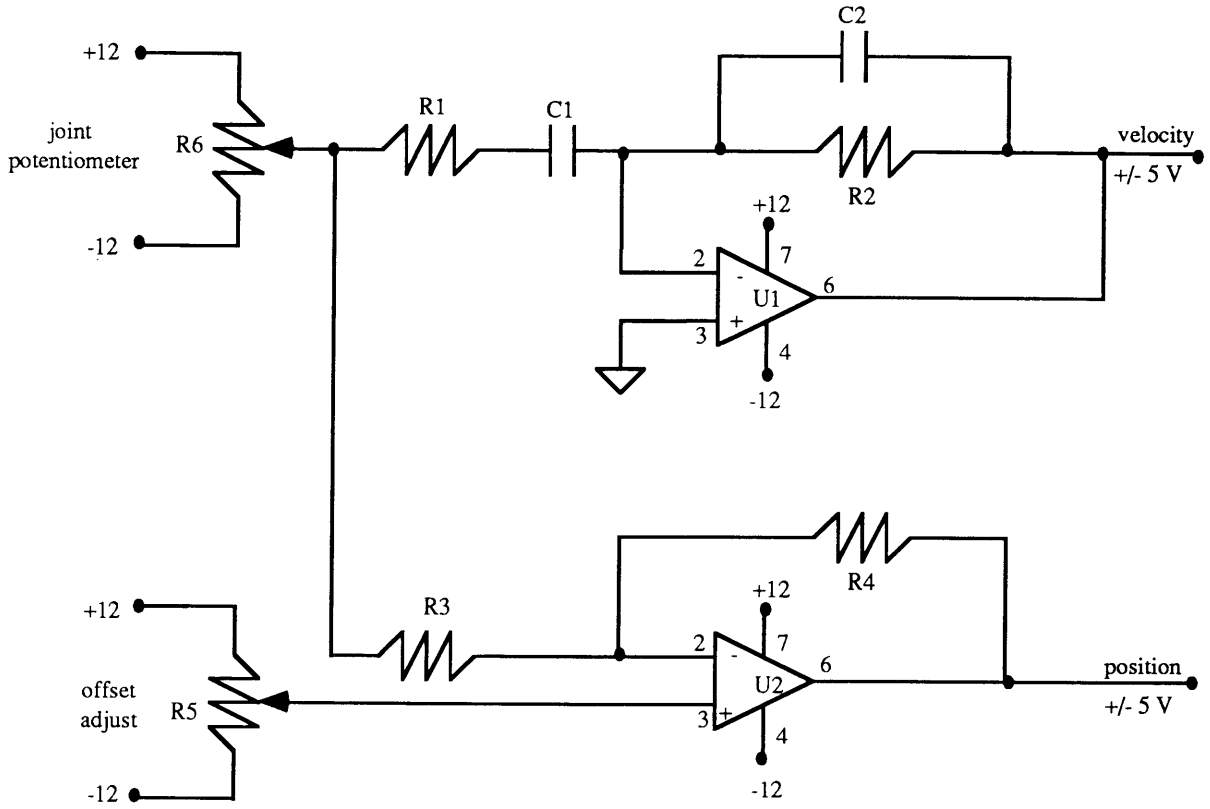

Figure B-4. Schematic of the CEDO 1 position/velocity circuitry.

Table B-4. Components of the CEDO 1 position/velocity circuits.

Component	*Axis 1*	*Axis 2*	*Axis 3*
R_1	12 kΩ	12 kΩ	180 kΩ
R_2	330 kΩ	330 kΩ	1.5 MΩ
R_3	180 kΩ	180 kΩ	200 kΩ
R_4	200 kΩ	200 kΩ	180 kΩ
R_5	5 kΩ	5 kΩ	5 kΩ
R_6	5 kΩ	5 kΩ	5 kΩ
C_1	1 μF	1 μF	0.1 μF
C_2	0.027 μF	0.027 μF	0.015 μF
U_1	LM741	LM741	LM741
U_2	LM741	LM741	LM741

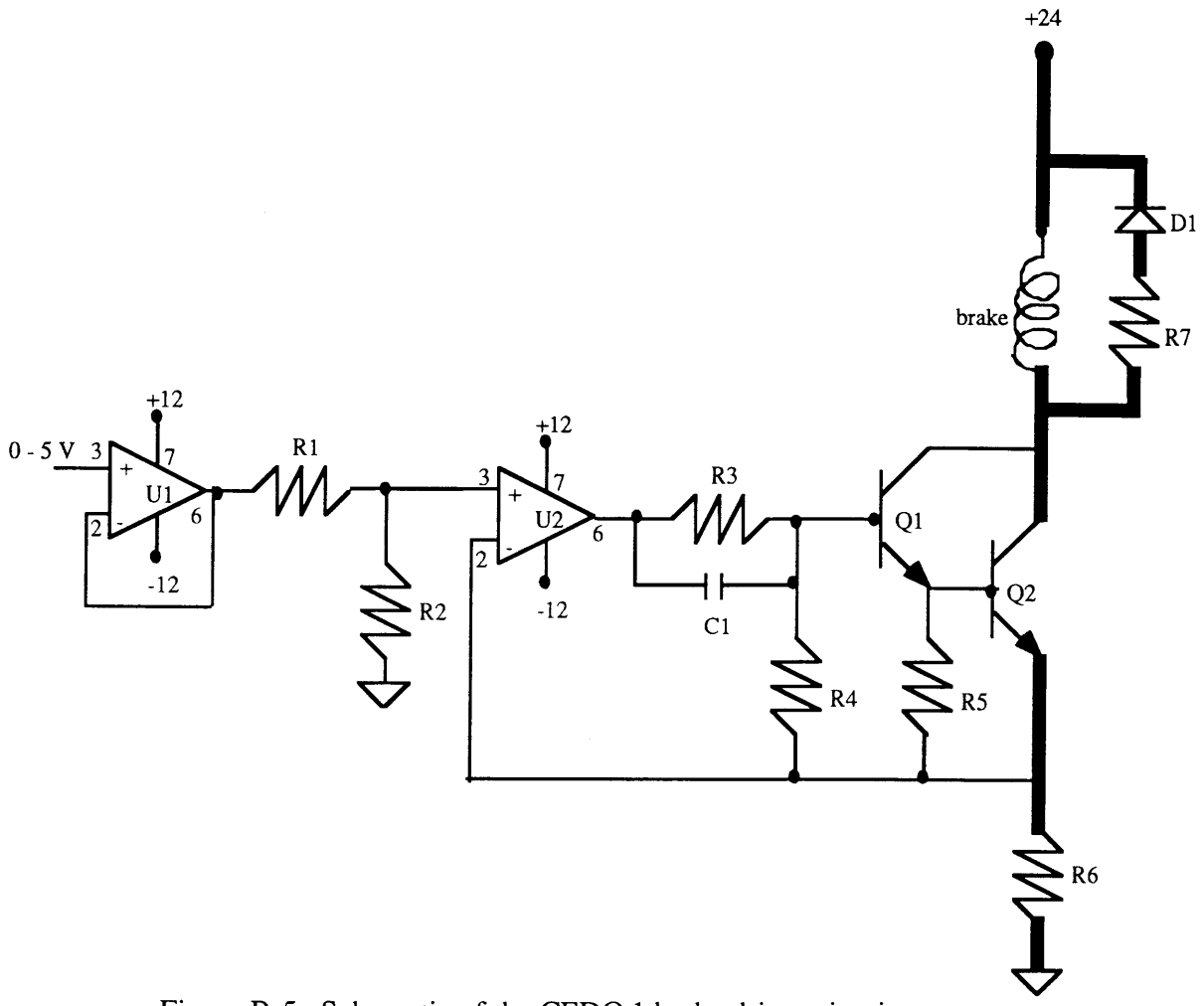

Figure B-5. Schematic of the CEDO 1 brake driver circuitry.

Table B-5. Components of the CEDO 1 brake driver circuits.

Component	*Axis 1*	*Axis 2*	*Axis 3*
R_1	3.3 kΩ	3.3 kΩ	5.1 kΩ
R_2	5.1 kΩ	5.1 kΩ	3.3 kΩ
R_3	3.9 kΩ	3.9 kΩ	3.9 kΩ
R_4	1 kΩ	1 kΩ	1 kΩ
R_5	10 kΩ	10 kΩ	10 kΩ
R_6	2 Ω	2 Ω	10 Ω
R_7	2 Ω	2 Ω	10 Ω
C_1	100 pF	100 pF	-
D_1	1N4001	1N4001	1N4001
U_1	LM741	LM741	LM741
U_2	LM741	LM741	LM741
Q_1	2N3904	2N3904	2N3904
Q_2	TIP 41B	TIP 41B	TIP 31B

Appendix C

CEDO 1 Electronics Parts List

Position/Velocity Circuits:

Component	*Description*	*Vendor/Part Number*
R1	33 kΩ resistor (axes 1&2) 330 kΩ resistor (axis 3)	MIT Physics Stockroom
R2	470 kΩ resistor (axes 1&2) 1.5 MΩ resistor (axis 3)	MIT Physics Stockroom
R3	180 resistor (axes 1&2) 200 kΩ resistor (axis 3)	MIT Physics Stockroom
R4	200 resistor (axes 1&2) 180 kΩ resistor (axis 3)	MIT Physics Stockroom
R5	5 kΩ trimpot	Digi-Key #01B53
R6	Bourns 5 kΩ precision potentiometer	Gerber #6637S-1-502
C1	1 μF capacitor (axes 1&2) 0.1 μF capacitor (axis 3)	Digi-Key #EF1105 Digi-Key #EF1104
C2	0.027 μF capacitor (axes 1&2) 0.015 μF capacitor (axis 3)	Digi-Key #EF1273 Digi-Key #EF1153
U1	LM741 op amp	Digi-Key #LM741CN
U2	LM741 op amp	Digi-Key #LM741CN

Brake Driver Circuits:

Component	*Description*	*Vendor/Part Number*
R1	3.3 kΩ resistor (axes 1&2) 5.1 kΩ resistor (axis 3)	MIT Physics Stockroom
R2	5.1 kΩ resistor (axes 1&2) 3.3 kΩ resistor (axis 3)	MIT Physics Stockroom
R3	3.9 kΩ resistor	MIT Physics Stockroom
R4	1 kΩ resistor	MIT Physics Stockroom
R5	10 kΩ resistor	MIT Physics Stockroom
R6	2 Ω, 10 W resistor (axes 1&2) 10 Ω, 5 W resistor (axis 3)	Digi-Key #2W-10-ND Digi-Key #10W-5-ND
R7	2 Ω, 10 W resistor (axes 1&2) 10 Ω, 5 W resistor (axis 3)	Digi-Key #2W-10-ND Digi-Key #10W-5-ND
C1	100 pF capacitor (axes 1&2)	MIT Biomechanics Lab Supply
D1	1N914 diode	Gerber #1N914
D2	1N4001 diode	Digi-Key #1N4001
U1	LM741 op amp	Digi-Key #LM741CN
U2	LM741 op amp	Digi-Key #LM741CN
Q1	2N3094 transistor	Gerber #2N3094
Q2	TIP41B transistor (axes 1&2) TIP31B transistor (axis 3)	Gerber #TIP41B Gerber #TIP31B

Connectors:

Description	*Vendor/Part Number*	*Quantity*
9-pin D connectors (solder)	Digi-Key #109-M-ND (male) Digi-Key #109-F-ND (female)	8 8
37-pin D connectors (solder)	Digi-Key #137-F-ND (female)	2
9-pin and 37-pin D connector backshells	Digi-Key #909P-ND Digi-Key #937P-ND	8 2
10-pin right-angle wire-wrap socket connectors and headers	Digi-Key #CKR10G-ND Digi-Key #CHA10G-ND	2
20-pin ribbon cable socket connector	MIT Biomechanics Lab Supply	1
16-pin CPC connectors, plugs, cable clamps, and shells	Digi-Key #A1305, A1304, A1689	4 each
Waldom terminal housings and crimp terminals	Newark #31F1027, 31F1026	1
Waldom terminal housings and crimp terminals	Digi-Key WM2103, WM2300	1
Waldom 2-pin quick connector plug and receptacle	Digi-Key #WM1220, WM1230	8 each

Miscellaneous:

Description	*Vendor/Part Number*
Computer Products, Inc. NFS110-7602 110W Universal Input Switching Power Supply	Bell Industries, Distributor. Andover, MA
Bud Enclosure	Gerber #DB1682
Panasonic Fan	Digi-Key #P9984-ND
Beldon 17250 Power Cord	MIT Physics Stockroom
IDI indicator light	Gerber #1030QD1
SPST 6 amp 125VAC switch	Radio Shack #275-690

Appendix D

CEDO 1 Programs

Calibration Programs:

PCALC	Potentiometer calibration program which produces the datafile of the best-fit slopes and intercepts to convert measured angular positions in LSBs to radians. The output file *PCALC.DAT* has the format: int 1, slope 1, int 2, slope 2, int 3, slope 3
VCALC	Velocity calibration program which, along with the velocity offsets in *OFFSETC.DAT*, convert angular velocity from LSBs to radians/sec. The velocity conversion factors are computed from the electronic circuitry gains G_p and G_d and from the position calibration slopes in *PCALC.DAT*. Note that G_p and G_d are written into the program as constants and must be changed if any of the resistors or capacitors in the CEDO electronics box are changed. The output file *VCALC.DAT* has the format: vcal 1, vcal 2, vcal 3
OFFSETC	Velocity offset program used to measure any small voltage drifts which occur in the system and which are subtracted from angular velocity readings in the control programs to improve accuracy. It is crucial that the CEDO be stationary while this program is running. The voltages corresponding to each velocity output are written to the file *OFFSETC.DAT* in the form: offset 1, offset 2, offset 3 (LSBs)

Basic Test Programs:

STIFFC	Makes the MIT CEDO stiff by setting the current to all three particle brakes to half of of maximum.
FLABBYC	Makes the MIT CEDO flabby by setting the current to all three particle brakes to zero.
CHECKC	Allows the user to view raw input data (in units of LSBs, volts, or physical units) or to output data to any of the three D/A channels to check the brakes.
CONTROLC	Controls the MIT CEDO and allows the values of the viscous or turbulent damping coefficients to be incremented or decremented. Input files include *PCALC.DAT, VCALC.DAT, OFFSETC.DAT,* and *DVALC.DAT*.

Test Session Setup Programs:

DVALC	Allows the user to update the values of the viscous and velocity-squared (turbulent) damping coefficients for each of the three axes. Possible viscous damping coefficients range from 0 to 0.5 lbf/(in/s) and 0 to 8.0 in-lbf/(rad/s) for the large and small brakes, respectively. Possible velocity-squared damping coefficients range from 0 to 0.05 $lb/(in/s)^2$ and 0 to 1.6 $in\text{-}lb/(in/s)^2$ for the large and small brakes, respectively. The damping values are written to the file *DVALC.DAT* in the format: bv1, bv2, bv3, bt1, bt2, bt3

SCALEC	Scales the CEDO workspace to the screen and/or allows scaling parameters to be checked for a two degree-of freedom test--the left-right x axis of the CEDO workspace corresponds to the horizontal axis of the screen while the front-back y axis of the CEDO workspace corresponds to the vertical axis of the screen. The program outputs the endpoint positions (in units of inches relative to the CEDO origin in the workspace) which correspond to the corners of the computer screen to the file *SCALEC.DAT* in the form: left scale, right scale, top scale, bottom scale

SSCALE	Scales the CEDO workspace to the screen and/or allows scaling parameters to be checked for a one-degree-of-freedom test--the rotational position of the third axis corresponds to the vertical axis of the screen. The program outputs the endpoint positions (in units of radians relative to the CEDO origin in the workspace) which correspond to the extremes of the computer screen to the file *SCALES.DAT* in the form: top scale, bottom scale, center point for axes 1-2

Tracking Task Target Generation Programs:

TAR1DOF	Produces a target datafile for a vertical one-degree-of-freedom pursuit tracking task. The user can select the target type (linear, single sinusoid, or sum of 2 sinusoids), the target speed (slow, fast, or variable), and the output file number. The target data, in units of pixels, are written to the output file *STAR#.DAT* in the form: horizontal data , vertical data

TAR2DOF	Produces a target datafile for the pursuit tracking task using the summation of multiple sine waves in two degrees of freedom. The user can select the number of sine waves to be summed (between 1 and 7) and the output file number. The target data, in units of pixels, are written to the output file *TAR#.DAT* in the form: horizontal data, vertical data

TAR2SIN	Produces a target datafile for the pursuit tracking task using the summation of 2 sine waves in two degrees of freedom. The user can select the output file number. The target data, in units of pixels, are written to the output file *TAR#.DAT* in the form: horizontal data, vertical data

TARGETC	Produces a target datafile for the pursuit tracking task in two degrees of freedom. The user can select the target type (linear, single sinusoid, or sum of 2 sinusoids), the target speed (slow, fast, or variable), and the output file number. The target data, in units of pixels, are written to the output file *TAR#.DAT* in the form: horizontal data, vertical data

Data Collection and Control Programs:

VSTORE TSTORE	Controls the MIT CEDO with viscous (V) or turbulent (T) damping assuming a 2nd order torque-current relationship and writes 30 seconds of data sampled at 60 Hz to the file *aadate#.pos* in the format: damping coefficients 1 2 3 pos 1, pos 2, pos 3 (degrees) and to the file *aadate#.vel* in the format: damping coefficients 1 2 3 vel 1, vel 2, vel 3 (deg/sec) The program also allows the user to view plots of axis position, endpoint position, and/or axis velocity vs time. Input files include *PCALC.DAT, VCALC.DAT, OFFSETC.DAT,* and *DVALC.DAT.*

LVSTORE LTSTORE	Controls the MIT CEDO with viscous (V) or turbulent (T) damping assuming a linear torque-current relationship and writes 30 seconds of data sampled at 60 Hz to the file *aadate#.lp* in the format: damping coefficients 1 2 3 pos 1, pos 2, pos 3 (degrees) and to the file *aadate#.lv* in the format: damping coefficients 1 2 3 vel 1, vel 2, vel 3 (deg/sec) The program also allows the user to view plots of axis position, endpoint position, and/or axis velocity vs time. Input files include *PCALC.DAT, VCALC.DAT, OFFSETC.DAT,* and *DVALC.DAT.*

VCEDO VCEDO3 (for 386) TCEDO TCEDO3 (for 386)	Controls the MIT CEDO with viscous (V) or turbulent (T) damping assuming a 2nd order torque-current relationship, presents a 30 second pursuit tracking task to the subject, and writes the data, sampled at 60 Hz, to the file *aadate#.dat* in the format: damping coefficients 1 2 3 xtarget, xresponse, ytarget, yresponse (pixels) and to the file *aadate#.p3* in the format: damping coefficients 1 2 3 time, pos 3 (degrees) and to the file *aadate#.tor* in the format: damping coefficients 1 2 3 torque 1, torque 2, torque 3 (in-lbs) Input files include *PCALC.DAT, VCALC.DAT, OFFSETC.DAT, DVALC.DAT, SCALEC.DAT,* and *TAR#.DAT* (where # is between 0 and 9).

CCEDO CCEDO3 (for 386)	Controls the MIT CEDO with viscous (V) or turbulent (T) damping assuming a 2nd order torque-current relationship, presents a 30 second pursuit tracking task to the subject, and writes the data, sampled at 60 Hz, to the file *aadate#.dat* in the format: damping coefficients 1 2 3 xtarget, xresponse, ytarget, yresponse (pixels) and to the file *aadate#.ang* in the format: damping coefficients 1 2 3 angle 1, angle 2, angle 3 (radians) and to the file *aadate#.w* in the format: damping coefficients 1 2 3 vel 1, vel 2, vel 3 (radians/sec) and to the file *aadate#.tor* in the format: damping coefficients 1 2 3 torque 1, torque 2, torque 3 (in-lbs) Input files include *PCALC.DAT, VCALC.DAT, OFFSETC.DAT, DVALC.DAT, SCALEC.DAT,* and *TAR#.DAT* (where # is between 0 and 9). Damping values and damping types can be updated within the program.

SCEDO SCEDO3 (for 386)	Controls the MIT CEDO with viscous (V) or turbulent (T) damping assuming a 2nd order torque-current relationship, presents a 30 second one-degree-of-freedom pursuit tracking task to the subject, and writes the data, sampled at 60 Hz, to the file *aadate#.dat* in the format: damping coefficients 1 2 3 xtarget, xresponse, ytarget, yresponse (pixels) and to the file *aadate#.ang* in the format: damping coefficients 1 2 3 angle 1, angle 2, angle 3 (radians) and to the file *aadate#.w* in the format: damping coefficients 1 2 3 vel 1, vel 2, vel 3 (radians/sec) and to the file *aadate#.tor* in the format: damping coefficients 1 2 3 torque 1, torque 2, torque 3 (in-lbs) Input files include *PCALC.DAT, VCALC.DAT, OFFSETC.DAT, DVALC.DAT, SCALEC.DAT,* and *STAR#.DAT* (where # is between 0 and 9). Damping values and damping types can be updated within the program.

VLOCK VLOCK3 (for 386) TLOCK TLOCK3 (for 386)	Controls the MIT CEDO with viscous (V) or turbulent (T) damping in 2 degrees of freedom while setting the third degree of freedom to half of maximum torque. The program presents a 30 second pursuit tracking task to the subject, and writes the data, sampled at 60 Hz, to the file *aadate#.dat* in the format: damping coefficients 1 2 3 xtarget, xresponse, ytarget, yresponse (pixels) and to the file *aadate#.p3* in the format: damping coefficients 1 2 3 time, pos 3 (degrees) and to the file *aadate#.tor* in the format: damping coefficients 1 2 3 torque 1, torque 2, torque 3 (in-lbs) Input files include *PCALC.DAT, VCALC.DAT, OFFSETC.DAT, DVALC.DAT, SCALEC.DAT,* and *TAR#.DAT* (where # is between 0 and 9).

Data Analysis Programs:

RUNS.m	MATLAB programs which perform a runs test for stationarity of the data record in x and y for one or two data files.

DYNAMICS.m	MATLAB program which determines the mean endpoint force required by the user in a particular trial given the position and velocity data, the damping coefficients, and the amount of any added mass.

INSPECTOR.m	MATLAB program which performs spectral analysis on the target and response data records, computes tremor performance scores, and saves the spectra for further processing. The user may revise the program to change the number of segments that the data records are divided into, the number of points that the segments overlap, and the bands of summation for tremor power and signal power.

TIMEPLOTS.m	MATLAB program which plots target and response time records.

FPLOTS.m	MATLAB program which plots tremor power spectral densities.

Appendix E

CEDO 1 Instructions

Step 1.
Make sure the following are connected properly:

- MetraByte A/D Timer Board 37 pin connector on computer (male) to separate 37 pin connector (female).
- DT2814 A/D Board 20 pin socket connector on computer to 20 pin header connector with ribbon cable to 25 pin connector with grey cable to 9 pin A/D connector on electronics box.
- MetraByte D/A Board 37 pin connector on computer (male) to 37 pin connector (female) to 9 pin D/A connector on electronics box.
- Power cord from electronics box to wall outlet.
- Circular CPC connector for potentiometer signals from wheelchair to front of electronics box.
- Circular CPC connector for brake signals from wheelchair to front of electronics box.
- 9 pin connectors from potentiometers and brakes to housing on back of the CEDO.

Step 2.
Turn on the computer. Type ***cd cedo*** at the computer's C> prompt to enter the CEDO directory. This directory contains all of the programs to setup and control the MIT CEDO.

Step 3.
Turn on the electronics box power switch (red rocker switch) located on the back of the electronics box. The red power light and the fan should both be on whenever the power is on.

Step 4.
To make sure the CEDO is working properly, run the program **FLABBYC** by typing ***flabbyc*** at the computer's prompt. This program sets the brake currents to 0. Then run the program **STIFFC** by typing ***stiffc*** at the computer's prompt. This program sets brake currents to approximately half of their maximum.

Step 5.
Before beginning a data collection session, run the program **OFFSETC** by typing ***offsetc*** at the computer's C:> prompt. Do not touch the CEDO while this program is running.

Step 6.
After the program **OFFSETC** is run, the CEDO is ready to be used in experiments. Make sure the patient is seated comfortably in the chair, adjust and tighten the lap belt, place the subject's right forearm in the proper size cuff (sizes small, medium, and large are available), and secure the cuff to the CEDO 1 in the desired position.

Step 7.
To experiment with different damping levels and different damping functions, run the program **CONTROLC** by typing ***controlc*** at the computer's C:> prompt. Viscous damping levels range from 0 to 0.5 lbs/(in/s) for axes 1 and 2 and from 0 to 8 in-lbs/(rad/s) for axis 3. Turbulent damping levels range from 0 to 0.03 lbs/(in/s)^2 for axes 1 and 2 and from 0 to 1.5 in-lbs/(rad/s)^2 for axis 3. When this program is running you may decrease the damping level of any axis by typing the axis number repeatedly. You may increase the damping level of any axis by typing the axis number plus the shift key.

Step 8.
To set the damping levels to specific values, run the program **DVALC** by typing ***dvalc*** at the computer's C:> prompt. Enter the desired damping levels for the CEDO axes as the program asks for them.

Step 9.
To generate a target file for the pursuit tracking task, run any of the target-generating programs (**TAR1DOF**, **TAR2DOF**, **TAR2SIN**, **TARGETC**) by typing the program name at the computer's C:> prompt and following the program's directions. One of these programs must be run any time a new target pattern is desired for the pursuit tracking task. You may generate 10 different target files, each with a different file number, for use in a series of experiments.

Step 10.
To generate the mapping between the manipulator workspace and the computer screen for the pursuit tracking task, run the program **SCALEC** for a two-degree-of-freedom test or **SSCALE** for a one-degree-of-freedom test by typing ***scalec*** or ***sscale*** at the computer's C:> prompt.

Step 11.
To collect data during a 30 second pursuit tracking task, run the program **VCEDO** (viscous damping), **TCEDO** (turbulent damping), **CCEDO** (complete experimental program which allows damping values and damping types to changed without exiting the program), or **SCEDO** (one-degree-of-freedom test) by typing the program name at the computer's C:> prompt and following the program's directions. Programs **DVALC**, **SCALEC**, and one of the target generating programs must have been run prior to running one of these control programs.

Appendix F
CEDO 1 Model Details

This appendix contains detailed dimensions, calculations, and geometrical relationships used in deriving the CEDO model for estimating user force requirements outlined in Chapter 2. The notation for the links, joints, angles, and coordinates used in this analysis are shown schematically in Figure F-1, and link lengths, angles, and other relevant dimensions are listed in Table F-1.

Table F-1. Link lengths, angles, and other dimensions used in the CEDO model.

Variable	*Definition*	*Value*
d_1	length of link 1	21 in
d_2	length of link 2	14 in
d_3	length of link 3	14 in
d_4	length of link 4	7 in
d_5	length of link 5	7 in
d_6	distance from the midpoint of link 1 to joint c	3.5 in
d_7	$\sqrt{\left(\frac{d_5}{2}\right)^2 + \left(\frac{d_1}{2} + d_6\right)^2}$	14.43 in
d_8	$\sqrt{(d_5)^2 + \left(\frac{2d_1}{3}\right)^2}$	15.65 in
θ_1	angle of link 4 from Y axis (from input data files)	-
θ_2	angle of link 2 from X axis (from input data files)	-
γ	$\tan^{-1}\left(\frac{3d_5}{4d_1}\right)$	14.04°
φ	$\tan^{-1}\left(\frac{3d_5}{2d_1}\right)$	26.6°

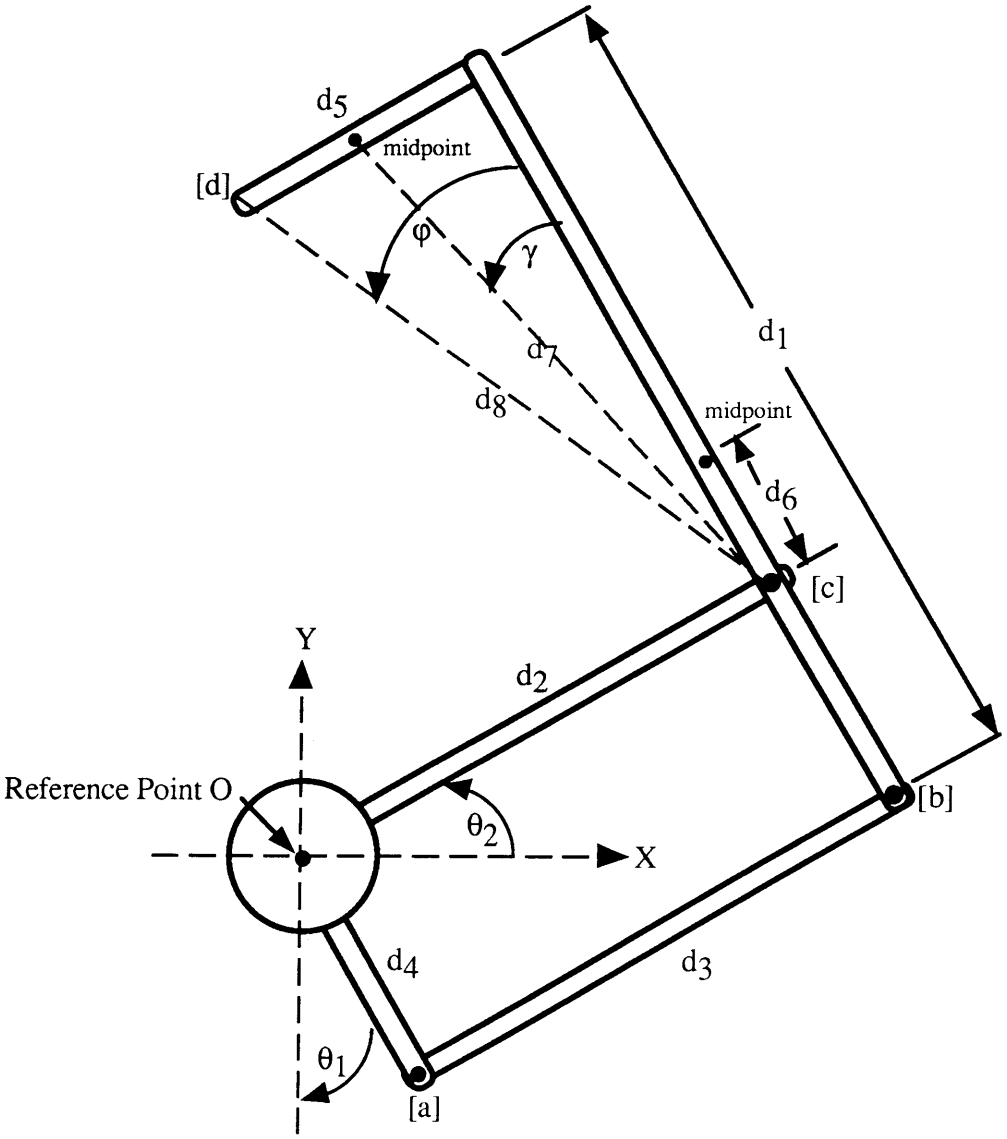

Figure F-1. Links, joints, angles, and coordinates used in the CEDO model.

As mentioned in Chapter 2, computing the rate of change of H_o, the total angular momentum of the system, requires calculating the masses and inertias of the five links, the masses of the four joints, and the position and velocity vectors of the centroids of the both the links and the joints. The masses of the five links, estimated from the link volume V (i.e. the outer and inner link radii R and r and the link length h) and the density of 6061 aluminum, ρ_a by:

$$m_{link} = \rho_a V = \rho_a \pi \left(R^2 - r^2\right) h \tag{F-1}$$

are listed in Table F-2. The moments of inertia of the five links about their centriods, estimated from:

$$I_c = \frac{m_{link}}{12}\left[3\left(R^2 - r^2\right) + h^2\right] \tag{F-2}$$

are listed in Table F-3. The masses of joints a, b, and c, estimated from summing the masses of the joint components -- two sets of roller bearings (measured), a steel shaft (estimated from the radius t, length s, and density ρ_s), and two aluminum plugs which couple the links to the shafts (estimated from the radii R and t, the lengths L and l, and density ρ_a) -- by:

$$m = m_{bearings} + \left(\rho_s \pi t^2 s\right)_{shaft} + \left(\rho_a\left[L^3 - \pi R^3 L\right]\right)_{plug1} + \left(\rho_a\left[l^3 - \pi t^3 l\right]\right)_{plug2} \tag{F-3}$$

are listed in Table F-4. The mass of joint d, measured using a balance scale after disassembling the joint from the CEDO, is also listed in Table F-4. Finally, the position vectors of the centroids of each of the links and joints in XY coordinates are listed in Table F-5. These position vectors were differentiated with respect to time to obtain the velocity vectors referred to in Chapter 2.

Table F-2. Link masses used in the CEDO 1 model.

Variable	*Definition*	*Value*
ρ_a	density of 6061 aluminum	0.1 lbm/in^3
R	outer link radius	0.75 in
r	inner link radius	0.685 in
m_1	mass of link 1	0.0615 lbm
m_2	mass of link 2	0.041 lbm
m_3	mass of link 3	0.041 lbm
m_4	mass of link 4	0.0205 lbm
m_5	mass of link 5	0.0205 lbm

Table F-3. Link inertias used in the CEDO 1 model.

Variable	*Definition*	*Value*
I_1	Moment of inertia of link 1	2.25 lbm-in^2
I_2	Moment of inertia of link 2	0.66 lbm-in^2
I_3	Moment of inertia of link 3	0.66 lbm-in^2
I_4	Moment of inertia of link 4	0.08 lbm-in^2
I_5	Moment of inertia of link 5	0.08 lbm-in^2

Table F-4. Joint masses used in the CEDO 1 model.

Variable	*Definition*	*Value*
$m_{bearings}$	mass of two sets of roller bearings	0.5 lbs
ρ_s	density of steel	0.284 lbm/in^3
s	shaft length	3.625 in
t	shaft radius	0.375 in
L	length of large aluminum plug (plug 1)	2.125 in
l	length of small aluminum plug (plug 2)	1.5 in
m_a	mass of joint a	1.05 lbm
m_b	mass of joint b	1.05 lbm
m_c	mass of joint c	1.05 lbm
m_d	mass of joint d	4.625 lbm

Table F-5. X and Y components of the position vectors to the centroids of the links and joints used in the CEDO 1 model.

Link/Joint	*X component*	*Y component*
1	$(d_2)\cos(\theta_2) - (d_6)\sin(\theta_1+\theta_2)$	$(d_2)\sin(\theta_2) + (d_6)\cos(\theta_1+\theta_2)$
2	$\left(\frac{d_2}{2}\right)\cos(\theta_2)$	$\left(\frac{d_2}{2}\right)\sin(\theta_2)$
3	$(d_4)\sin(\theta_1+\theta_2) + \left(\frac{d_3}{2}\right)\cos(\theta_2)$	$-(d_4)\cos(\theta_1+\theta_2) + \left(\frac{d_3}{2}\right)\sin(\theta_2)$
4	$\left(\frac{d_4}{2}\right)\sin(\theta_1+\theta_2)$	$-\left(\frac{d_4}{2}\right)\cos(\theta_1+\theta_2)$
5	$(d_2)\cos(\theta_2) - (d_7)\sin(\theta_1+\theta_2+\gamma)$	$(d_2)\sin(\theta_2) + (d_7)\cos(\theta_1+\theta_2+\gamma)$
a	$(d_4)\sin(\theta_1+\theta_2)$	$-(d_4)\cos(\theta_1+\theta_2)$
b	$(d_4)\sin(\theta_1+\theta_2) + (d_3)\cos(\theta_2)$	$-(d_4)\cos(\theta_1+\theta_2) + (d_3)\sin(\theta_2)$
c	$(d_2)\cos(\theta_2)$	$(d_2)\sin(\theta_2)$
d	$(d_2)\cos(\theta_2) - (d_8)\sin(\theta_1+\theta_2+\varphi)$	$(d_2)\sin(\theta_2) + (d_8)\cos(\theta_1+\theta_2+\varphi)$

Appendix G

Informed Consent Statement

Suppression of Abnormal Involuntary Movements by the Application of Mechanical Loads

We are interested in testing new methods of suppressing tremors and other unintentional movements in people who could use their limbs more effectively if these movements were reduced. We hope to determine whether such movements may be reduced by providing a brace for the affected limb which resists the muscles' "attempts" to move it in an undesirable way.

This experiment involves two tasks. For both tasks, your arm will be fitted comfortably in a splint attached to an apparatus which measures your arm position and in some trials resists your tremor. Surface sensors measuring electrical activity of your muscles may also be applied to your arm. In the first task you will be asked to view a computer screen. Two markers will appear on the screen. One will move as your limb moves. The other will serve as a target and may move in an unpredictable way. You will be asked to try to move your limb so that the response marker follows the target marker. The resistance, when present, may make it easier for you to perform this task. During the second part of the experiment you will be asked to perform various functional tasks such as writing, pouring water from cup to cup, eating, or drinking. The resistive apparatus may make it easier for you to perform these tasks.

Experimental trials will be done with different levels of "resistance" applied. Between trials you may rest as long and as frequently as necessary for your comfort. An experimental session will last approximately one hour. Further testing will be suited to your capacity and convenience.

Data from our experiments and other information obtained during experiments will be kept in a confidential file. If this information is used for education or published reports, your name will be withheld. Short sequences of video tape may be taken for our records if you consent, but this material will not be used for education or publication if you request that it be kept confidential.

Although much of the equipment we will be using is electronic in nature, no shock hazard is present. You may withdraw from participation in this study at any time. You are encouraged to ask questions and make comments or suggestions at any time. Your ideas will help us.

The goal of these studies is limited. We will not build a practical tremor-suppressing device for you to use in normal activities. If these experiments are successful, however, the design of such devices will have been helped by your participation. There are, at present, more conventional methods of treatment which might be appropriate for your movement disorder. It has not been conclusively demonstrated that the techniques to be tried in these experiments are useful alternatives to present methods of treatment.

Consent

Investigator:

I have fully explained to _____ the nature and purpose of the above procedure and will answer all questions to the best of my ability.

_____ _____

date investigator

Participant:

I have been satisfactorily informed of the above-described procedure and I agree to participate in these experiments. In the unlikely event of physical injury resulting from participation in this research, I understand that medical treatment will be available from the M.I.T. Medical Department, including first aid, emergency treatment, and follow-up care as needed, and that my insurance carrier may be billed for the cost of such treatment. However, no compensation can be provided for medical care apart from the foregoing. I further understand that making such medical treatment available, or providing it, does not imply that such injury is the investigator's fault. I also understand that by my participation in this study I am not waiving any of my legal rights.

I understand that I may also contact the Chairman of the Committee on the Use of Humans as Experimental Subjects, Dr. George Wolf (M.I.T. Room 56-213, 617-253-6781), if I feel I have been treated unfairly as a subject. (Further information may be obtained by calling the Institute's Insurance and Legal Affairs Office at 617-253-2822.)

_____ _____

date subject/parent/guardian

_____ _____

date witness to signature

Appendix H

Clinical Tremor Assessments

The Burke Rehabilitation Center Functional Tremor Assessment

NAME:_____ DATE:_____ AGE:_____ SEX:___
DIAGNOSIS:_____

1. Tremor Amplitude -- Upper Extremity
   Scoring: 0 -- none.
   1 -- slight (tremor amplitude <.5 cm); may be intermittent.
   2 -- moderate (tremor amplitude .5 cm - 1 cm).
   3 -- marked (tremor amplitude 1 cm - 2 cm).
   4 -- severe (tremor amplitude > 2 cm).

Tremor	Rest	Postural	Action	Total
RUE	_____	_____	_____	_____
LUE	_____	_____	_____	_____

2. Handwriting -- Name and Date _____
   Scoring: 0 -- normal.
   1 -- slightly untidy.
   2 -- legible but with significant tremor.
   3 -- illegible.
   4 -- unable to keep pencil on paper.

3. Drawing -- Archimedes Spiral _____
   Scoring: 0 -- normal.
   1 -- crosses lines occasionally/slightly tremulous.
   2 -- crosses lines frequently.
   3 -- great difficulty/many errors.
   4 -- unable.

4. Pouring -- Two 8cm cups, 1st filled to 1cm from top, pour from one cup to another _____
   Scoring: 0 -- normal.
   1 -- more careful than a person without tremor, but no water spilled.
   2 -- spills; 10% total water.
   3 -- spills; 10-50% total water.
   4 -- unable to perform without spilling most water.

5. Drinking/Eating Soup _____
   Scoring: 0 -- normal
   1 -- can use spoon, but will spill full spoon.
   2 -- cannot use spoon, can use cup/glass.
   3 -- needs two hands for cup.
   4 -- severely abnormal, must use straw.

6. Keyboard (10 keystrokes/min) _____
   Scoring: 0 -- normal
   1 -- 7-9 keys accurately.
   2 -- 4-6 keys accurately.
   3 -- more than 3 keys accurately.
   4 -- unable to perform.

The MIT CEDO Functional Tremor Assessment

NAME: _____ DATE: _____ AGE: _____ SEX: ___
DIAGNOSIS: _____

1. Tremor Amplitude -- Upper Extremity
   Scoring: 0 -- none
   1 -- slight (tremor amplitude <.5 cm); may be intermittent
   2 -- moderate (tremor amplitude .5 cm - 1 cm)
   3 -- marked (tremor amplitude 1 cm - 2 cm)
   4 -- severe (tremor amplitude > 2 cm)

Damping	Rest	Postural	Action	Total

2. Drawing -- Lines
   Scoring: 0 -- normal; can stay within .5 cm bounds
   1 -- crosses .5 cm bounds; can stay within 1 cm bounds
   2 -- crosses 1 cm bounds; can stay within 2 cm bounds
   3 -- accomplishes 2 cm bound task with difficulty; many errors
   4 -- unable to complete drawing

Damping	Vertical Task	Front-Back	Left-Right	Total

3. Drawing -- Archimedes Spiral
   Scoring: 0 -- normal
   1 -- crosses lines occasionally; slightly tremorous
   2 -- crosses lines frequently
   3 -- accomplishes task with great difficulty; many errors
   4 -- unable to complete drawing

Damping	Score

Appendix I
Muscular Fatigue and Exercise Physiology

Two concerns not addressed in the experimental work in this thesis are the relatively short-term effects that an energy-dissipating orthosis has on fatigue and the relatively longer-term effects that an energy-dissipating orthosis has related to its incidental function as an exercise device. This appendix contains background information on normal and pathological muscle control, muscle fatigue, muscle response to exercise, and fiber type conversion relevant to the conjectures made in Chapter 6 regarding long-term use of the CEDO.

Normal Muscle and Motor Control

Muscle and Motor Control Properties

Motor Unit: A motor unit consists of one alpha motoneuron and the muscle fibers it innervates. The muscle fibers of a motor unit are of the same type and share structural and functional properties. A muscle consists of a mixture of fiber types, and the fibers belonging to a single motor unit interspersed with fibers from other motor units throughout the muscle.

Types of Muscle Fibers: Histochemical procedures have identified three types of muscle fibers:

a). *Type I or SO "slow twitch oxidative"* -- are "red", "slow-twitch", "fatigue resistant", and have (compared to Type I fibers) aerobic metabolism, greater blood supply, greater mitochondrion density, more muscle cells per motor unit (i.e. smaller cells), smaller alpha motoneuron diameter, lower neuron discharge frequency at tetanus, lower excitation threshold, slower neuron conduction velocity, lower tetanic tension level, and lower force increment.

b). *Type IIa or FOG "fast twitch oxidative"* -- have properties between type I and type IIb fibers.

c). *Type IIb or FG "fast twitch glycolytic"* -- are "white", "fast-twitch", "fast fatiguing" and have greater storage of glycogen, greater force increment, more sensitivity to FES, high concentration of glycolytic enzymes [Binder 1989, Williams 1990].

Differences in Fiber Speeds: The speed at which a muscle fiber contracts is related to the rate at which the energy-releasing conversion of ATP to ADP occurs. The myosin molecules in fast fibers and slow fibers differ in the maximal rates at which they split ATP, which in turn determines the maximal rate at which cross bridges can cycle, and hence, determines the maximal velocity of shortening [Vander et al 1985, Williams 1990].

Net Muscle Force: The net force of a muscle at any time depends on the number of fibers active and on the force generated by each fiber. The force generated by each fiber depends on: motoneuron activation, reflex mechanisms, inhibition of antagonist muscles, muscle fiber cross-sectional area, muscle length, and contraction velocity [Klausen 1990].

Control of Muscle Force: The nervous system has 2 methods for controlling the force of a muscle: recruitment of motor units, and modulation of motor unit firing rates. EMG studies have shown that muscle force increases when additional motor units are recruited or when the firing rates of active motor units are increased. Small muscles, used for making precise movements requiring incremental changes in force, rely primarily on firing rate modulation to augment the force output between 50 and 100 percent MVC. Large muscles, in contrast, rely on motor unit recruitment up to 90 percent MVC. According to the size principle, large motor units require the greatest stimulus amplitude to become active. The smallest and most excitable neurons are turned on at low levels of stimulus strength, with the consequence that the muscle force may be finely tuned at low levels through the number of muscle fibers active. The larger motor units come in only at higher levels of force. Further increases in force come from increasing the frequency of the action potentials [Basmajian & DeLuca 1979].

Normal Use of Motoneurons: All available data suggest that during everyday life, the motoneurons with the lowest thresholds innervating slow muscle units fire at low rates for long periods of time while the neurons innervating fast fatiguing units fire in scarce and short high-frequency bursts. Intermediate neurons innervating fast, fatigue-resistant units have intermediate everyday firing. During long-lasting maximal performance, such as endurance training, all units fire at moderate rates, but as soon as the drive is not maximal, the neurons with the highest thresholds drop out. During short-lasting maximal performance, such as strength training, all units fire in long high-frequency bursts [Edstrom & Grimby 1986].

Asynchronous Activation: During most natural movements there is asynchronous activation of the participating motor units, a feature which helps produce a smooth movement even when motor units are firing at frequencies below their tetanic fusion rate. Synchronization is relatively uncommon under normal conditions, but is increased by factors such as fatigue, anxiety, and excess alcohol intake [Lee, 1987].

Muscle Fatigue

Working Definition of Fatigue: Exercise physiologists refer to fatigue as "failure to maintain required or expected force", while DeLuca refers to fatigue as time-dependent processes that begin at the onset of contraction and that lead eventually to "failure", the point at which the required or expected force can no longer be maintained.

Metabolic Causes of Fatigue: Metabolic and electrophysiological consequences of muscular activity which may cause fatigue include:

a) Depletion of energy for contractile mechanism

b) Impaired energy supply for membrane function (leads to impaired generation and propagation of sarcolemmal action potential or impaired calcium pumping by sarcoplasmic reticulum)

c) Accumulation of intercellular H+ (may inhibit activity of phosphofructokinase and phosphorylase; may reduce Ca2-activated actin/myosin interaction)

d) Accumulation of extracellular K+ (leads to impaired sarcoplasmic action potential generation and propagation or impaired action potential generation in transverse tubular system resulting in reduced efficiency of excitation-contraction coupling) [Edwards, 1981].

Details on the cellular mechanisms of muscle fatigue are given in Westerblad et al 1991.

Detection of Fatigue Using EMG: Metabolic muscle fatigue is a time-dependent process that begins at the onset of contraction. When a muscle contracts, its intramuscular pressure rises. This increase in pressure, over time, restricts blood flow to the muscle and allows metabolites such as lactic acid and H+ ions to accumulate. The accumulation of metabolites changes the muscle's electrochemical gradient and slows the propagation of action potentials. Eventually a failure point is reached at which the muscle's force output cannot be maintained at the desired level even when more motor units are recruited. The decrease in conduction velocity that occurs during muscle fatigue significantly alters and muscle's EMG signal. A decrease in conduction velocity "stretches" the EMG signal in the time domain and corresponds to a shift of the power density spectrum to lower frequencies in the frequency domain [Basmajian & DeLuca 1979].

Types of Muscle Fatigue: A muscle will fatigue fairly rapidly if stimulated at a high frequency, but it will also recover rapidly from this fatigue. This is the type of fatigue that accompanies short-duration, high-intensity types of exercise such as weight lifting. On the other hand, fatigue that develops more slowly with long-duration, low-intensity endurance exercise, such as long distance running, requires much longer periods of rest, often up to 24 hours before complete recovery is achieved [Vander et al, 1985].

Muscle Response to Exercise

Overview: The frequency with which a muscle is used and the duration and intensity of the activity affect the muscle properties. In general, the number of muscle fibers does not change with exercise but two other changes may occur:

a) alterations in the ATP-forming capacity of muscle fibers as a result of increased enzyme synthesis and increased blood flow to the muscle.

b) changes in the diameter of the muscle fibers as a result of the formation of additional myofibrils.

Low Intensity, Long Duration Exercise: Exercise that is of relatively low intensity but of long duration such as long distance running and swimming produces increases in the number of mitochondria in the oxidative fast and slow fibers that are recruited in this type of activity. There is also an increase in the number of capillaries around these fibers. All these changes lead to an increase in the capacity for endurance activity with a minimum of fatigue. There is little change in fiber diameter and thus little change in the strength of muscles as a result of endurance exercise [Vander et al 1985].

High Intensity, Short Duration Exercise: High-intensity, short-duration exercise such as weight lifting affects primarily the glycolytic fast fibers that are recruited only during very powerful contractions. These fibers undergo a great increase in fiber diameter as a result of the increased synthesis of actin and myosin filaments forming an increased number of myofibrils. The number of glycolytic enzymes also increases. The result of such high-intensity exercise is to increase the strength of the muscle. Such muscles, although powerful, have little capacity for endurance and fatigue rapidly [Vander et al 1985]. During a period of strength training, the typical sequence of improvement will include an initial period where the maximal external force is increased rapidly week by week, followed by a period with less increase towards an upper limit, set by the load used during training. If training is continued with the same load, no

further improvements is seen in muscle strength but endurance will increase continuously. If further strength is desired, the training load must be increased [Williams 1990].

A Mixed Program of Low and High Intensity Exercise: A mixed program of exercise can improve both strength and endurance but cannot achieve the maximal state of either strength or endurance that muscle is capable of with vigorous exercise training of one type [Vander et al 1985].

After Exercise is Stopped: If a regular pattern of exercise is stopped, the changes in the muscle that occurred as a result of the exercise will slowly return, over a period of months, to the condition before exercise began [Vander et al 1985].

The Current Word on Fiber Type Conversion

In Animals: In studies using lab animals the conversion of fiber populations has been shown to occur as a result of manipulating the thyroid status of the animals, training, prolonged electrical stimulation of selected skeletal muscles, and cross-innervation experiments [Edstrom & Grimby 1986].

In Humans: In humans, there are indications from cross-sectional biopsy studies that there is a difference between endurance-trained athletes and strength-trained subjects with reference to slow-twitch and fast-twitch fiber proportions. However, it must be emphasized that the inter-individual differences in fiber composition is considerable, even within a homogeneous group of athletes with a similar training profile and where the biopsy site is carefully standardized. If we assume that there are some differences in fiber composition related to differences in physical performance, are they training-induced or inherited? In muscle biopsies of twins, the fiber composition has been found to be identical in monozygotic twins but different dizygotic twins, which indicates that the genotype is highly significant for the

individual fiber type composition. *The studies on humans performed so far offer no conclusive proof for an interconversion between the two main groups of fibers,* although there is evidence for transformation between subgroups of fast-twitch fibers [Edstrom & Grimby 1986].

Fiber Type Conversion from Endurance Training in Humans: It is well known that endurance training causes an increased resistance to fatigue as well as an increase in the capillary supply of the trained muscle. The question of whether muscle fibers of one type can possibly be transformed into another type remains unsettled and there are as of yet no convincing data to substantiate the hypothesis that training might elicit interconversions between type II and type I fibers. However, endurance training has been found to elicit significant changes in the incidence of subtypes within the type II group; that is, there is an increase in type 2A fibers at the cost of type 2B, and this perhaps explains why endurance-trained individuals have a dominance of type 2A fibers [Hainaut et al 1981, Edstrom & Grimby 1986, Binder 1989].

Fiber Type Conversion from Strength Training in Humans: The result of interval training with high force levels produces little change in the histochemical profiles of the involved fibers but results in marked fiber hypertrophy. Again, there is no evidence of significant conversions of one type of fiber to another [Binder 1989].

Fiber Type Conversion from Electrical Stimulation in Humans: A change of muscle fiber contractile properties from fast-twitch to slow-twitch types as a result of increased activity has been conclusively demonstrated in artificial exercise induced by chronic nerve stimulation, but it is doubted that a corresponding change in contractile properties can be achieved during voluntary movements [Edstrom & Grimby 1986]. The result of low frequency electrical stimulation on Type II fibers is to produce, over a period of weeks to months, increased

activity levels in oxidative enzymes, an accompanying fatigue resistance, decreased fiber diameters, and the appearance of myosin with light-chain components characteristic of type I fibers [Binder 1989]. The result of short, high-frequency bursts of electrical stimulation on Type I fibers is to produce fiber conversion but the effects are less pronounced than those resulting from low-frequency stimulation [Binder 1989].

Muscle and Motor Control in People with Movement Disorders

What is Known

Fiber Type in Parkinson's Disease: Muscle biopsy material from patients with Parkinson's and upper motoneuron lesions have shown that the Type II fibers atrophy and the Type I fibers remain unchanged and sometimes hypertrophy. These changes are presumed to be related to the reduction of muscular power and the increase of tone seen in these patients [Edstrom 1970].

Motor Unit Behavior in Parkinson's Disease: Parkinson's Tremor shows discrete bursts which alternate in antagonistic muscles. Two distinct groups of motor units are recognized during the tremor at rest. The first consists of lower threshold, smaller amplitude motor units, and the second group consists of higher threshold, higher amplitude units. The order of recruitment is from low threshold to high threshold for each tremor burst according to the size principle [Shahini & Wierzbicka 1990].

Motor Unit Behavior in Spasticity: Spastic patients have 2 types of abnormal motor unit behavior when single motor unit discharge patterns are observed via EMG under isotonic conditions , the number of voluntarily activated motor units near any EMG electrode is significantly reduced, and the maximum firing rate of the units that can be recruited also is significantly reduced [Shahini & Wierzbicka 1990].

Motor Unit Behavior in ET:

The size principle does not hold for ET, as the slow twitch fibers are not always recruited before the large twitch fibers but in a seemingly random order as observed under isotonic conditions with EMG [Shahini & Wierzbicka 1990].

Motor Unit Behavior in Cerebellar Ataxia: Patients with cerebellar ataxia have an irregular pattern of SMU (single motor unit) firing as observed under isotonic conditions with EMG [Shahini & Wierzbicka 1990].

Questions Which Remain to be Answered:

1. What types of muscle fibers are active in intention tremor? Does it depend on the etiology? Do they change over time? Does it depend upon the intended movement and thus the fibers that are voluntarily contracted?
2. What types of muscle fibers will the CEDO (or other tremor suppressing device) exercise? What activities are people likely to do while using the CEDO?
3. Do individuals' tremors get worse with increased voluntary force?
4. Do individuals' tremors get worse with fatigue?
5. What is the nature of fatigue and weakness associated with the movement disorders of persons with tremor?
6. What is the mechanism by which damping reduces tremor?
7. How might damping influence fatigue?
8. Is there a chance that long-term use might decrease the CEDO's effectiveness?